FORM FINDING FOR CABLE-STAYED AND EXTRADOSED BRIDGES

vorgelegt von
Dipl.-Ing.
El Araby El Shenawy
aus Ägypten

Von der Fakultät VI – Planen Bauen Umwelt
der Technischen Universität Berlin
zur Erlangung des akademischen Grades

Doktor der Ingenieurwissenschaften
Dr.-Ing.

genehmigte Dissertation

Promotionsausschuss:

Prof.Dr.-Ing. Karsten Geißler
Gutachter: Prof. Dr. sc. techn. Mike Schlaich
Gutachter: Dr.-Ing. Akio Kasuga

Tag der wissenschaftlichen Aussprache: 05.12.2012

Berlin 2013
D 83

AKNOWLEDGMENTS

I would like to thank and express my profound gratitude to my supervisor Prof. Dr. sc. tech. Mike Schlaich from TU-Berlin “Technische Universität Berlin” for his encouragement, support and guidance.

I also take this opportunity to express my gratitude to Dr. Akio Kasuga for his kind advice and cordial support.

I am indebted to staff members of the “Conceptual and Structural Design Department” at TU-Berlin. I am grateful for their cooperation.

I wish also to express my thanks for all the great opportunities and professional development I have had at “Schlaich Bergerman und Partner”, "Campenon Bernard SGE" and “Dar Al-Handasah Consultants”.

I thank the ALMIGHTY, my parents and family.

El Araby El Shenawy

ABSTRACT

The form finding for cable supported structures (roof structures or bridge structures) means simply the definition of the cable forces under dead load. The form finding method for conventional cable-stayed bridges with concrete-only or steel-only deck cross sections is well established. In this research work the common methods used for the determination of the stay cable forces under dead load will be discussed. It will be shown that these methods will not lead to the desired stay cable forces or the desired bridge alignment in case of cable-stayed bridges with composite decks.

A new method will be presented for the form finding of cable-stayed bridges with composite (steel/concrete) or (concrete/concrete) deck cross sections if the composite section is planned to be constructed in two stages. For the establishment of the new method for the form finding of cable-stayed bridges with composite decks, the following effects will be investigated:

- The ratio between the moment of inertia of the first part of the composite section and the total moment of inertia of the composite section and the vertical shift between the center of gravity of the first part of the composite section and the center of gravity of the total composite section.
- The time dependent forces due to creep and shrinkage.

Further, the study carried out for the form finding of conventional cable-stayed bridges will be extended to additionally present a new method for the form finding of extradosed bridges. The extradosed bridges emerged in the last two decades as a promising structural system to effectively and economically bridge spans ranging between 100 and 200 m. For such spans the prestressed box girder bridges require deep and heavy deck cross section. Further, conventional cable-stayed bridges with spans less than 200m appear to be not economical. The researches and the survey of the extradosed bridges built so far, indicate that there is still a need to establish a consistent method for the definition of the stay cable forces under dead load. The method established in this research work for this purpose, includes also solutions to determine and handle the required internal and/or external prestressing within the deck cross section. The proposed method for the form finding of the extradosed bridges is suitable for use for bridges with concrete, steel or composite sections. For extradosed bridges with a concrete deck, a combination of the stay cable forces and the prestressing forces inside the deck section may be targeted to eliminate the bending moment along the entire length of the deck under dead load.

KURZFASSUNG

Die Formfindung für Seilkonstruktionen (Dachkonstruktionen oder Brückenbauwerke) bedeutet im vereinfachten Sinne die Definition der Seilkräfte für das Tragwerk unter Eigengewicht. Die gängigen Formfindungsverfahren für konventionelle Schrägseilbrücken mit Fahrbahnüberbauten aus Beton oder Stahl haben sich bereits etabliert. Die üblichen Methoden, die zur Ermittlung der Seilkräfte unter Eigengewicht verwendet werden, werden in dieser Forschungsarbeit diskutiert. Es wird gezeigt, dass für Brücken aus Verbundquerschnitten, diese Methoden weder zu den gewünschten Seilkräften noch zu der gewünschten Brückengeometrie führen. Für Schrägseilbrücken aus Verbundquerschnitten, die in zwei Bauabschnitten (BA) hergestellt werden, wird in dieser Forschungsarbeit ein neues Verfahren für die Berechnung der Seilkräfte unter Eigengewicht vorgestellt. Für diese neue Methode werden die folgenden Faktoren untersucht:

- Das Verhältnis zwischen dem Trägheitsmoment des Teilquerschnitts (erster BA) und dem Trägheitsmoment des Gesamtquerschnitts (zweiter BA) und der vertikale Abstand zwischen dem Schwerpunkt des Teilquerschnitts (erster BA) und dem Schwerpunkt des Gesamtquerschnitts (zweiter BA).
- Die Zeitabhängigen Kräfte infolge Kriechen und Schwinden.

In dieser Arbeit wird auch eine neue Methode zur Formfindung von Extradosed Brücken vorgestellt. Die Extradosed Brücken entstanden in den letzten zwei Jahrzehnten als ein effektives und wirtschaftliches Brückentragwerk für Spannweiten zwischen 100 und 200 m. Für solche Spannweiten erfordern die vorgespannten Hohlkastenbrücken sehr große Überbauhöhen. Darüber hinaus scheinen die konventionellen Schrägseilbrücken mit Spannweiten weniger als 200 m unwirtschaftlich zu sein. Die Forschungen und die Untersuchungen der bisher gebauten Extradosed Brücken zeigen, dass eine konsistente Methode zur Definition der Seilkräfte unter Eigengewicht noch nicht vorhanden ist. Die zu diesem Zweck in dieser Arbeit vorgestellte Methode eignet sich für Überbauten aus Beton-, Stahl- und Verbundquerschnitten. Außerdem werden Methoden zur Bestimmung der erforderlichen internen und externen Vorspannung empfohlen. Für Extradosed Brücken mit Fahrbahnüberbauten aus Beton können die Biegemomente unter Eigengewicht entlang der gesamten Brückenlänge, durch das aufeinander abstimmen der Seilkräfte und der Vorspannkräfte im Überbau eliminiert werden.

TABLE OF CONTENTS

1- INTRODUCTION 1
2- CABLE-STAYED BRIDGES IN GENERAL 5
2-1 Types of stay cables 5
2-1-1 Parallel-Bar Cables 6
2-1-2 Locked Coil Strand Cables 6
2-1-3 Parallel Wire Cables 7
2-1-4 Parallel Strand Cables 11
2-1-5 Anchorages of Stay Cables at Deck and Tower head Levels 16
2-2 Possible structural systems for conventional cable-stayed bridges (supporting system between the tower and the deck & between the deck and the end support) 22
3- PREVIOUS RESEARCH WORKS FOR CABLES-STAYED BRIDGES RELATED TO THE RECOMMENDED STAY CABLE FORCES UNDER DEAD LOAD 29
3-1 The continuous beam method 29
3-1-1 Effect of creep on a simple concrete beam 31
3-1-2 Effect of creep on a continuous concrete beam 34
3.2 The “bending moment envelope for live loads” method 42
3.3 The method of influence matrix for stay cable forces 44
4- CONSTRUCTION ANALYSIS OF BRIDGES WITH COMPOSITE DECKS 51
4-1 Time dependent effects on bridge structures with composite decks 52
4-1-1 Time dependent effect due to vertical loads (Type I) 52
4-1-2 Additional time dependent effect in case of a composite deck (Type II) 53
4-2 Construction stage analysis of cable-stayed bridges with concrete-only or steel-only deck section 57
4-3 Construction stage analysis for cable-stayed bridges with composite deck sections 58
4-3-1 Construction of the composite section in one single stage (Construction method no. 1) 58
4-3-2 Construction of the composite cross section in two stages (Construction methods nos. 2,3 and 4) 59
4-3-3 Application of the construction methods 2,3 and 4 on a simple cables supported beam 66

4-3-4 Proposed modification for the construction method no. 4 (construction method no. 5) 72
4-3-5 Application of the construction method no. (4) or (5) on cable-stayed bridges with composite deck sections 74
5- EXTRADOSED BRIDGES 77
5-1 Common configuration of previously constructed extradosed bridges 79
5-2 Design of stay cables for conventional cable-stayed bridges and extradosed bridges 80
5-3 Structural system for extradosed bridges 85
6- PROPOSED METHOD FOR THE DETERMINATION OF THE STAY CABLE FORCES UNDER DEAD LOAD FOR EXTRADOSED BRIDGES 89
6-1 Method of the calculation of the desired equivalent vertical stay cable forces W_C 90
6-2 Proposed method for handling the prestressing forces for extradosed bridges 100
6-2-1 Use of concordant prestressing cable profiles for continuous beams [Lin and Burns 1989] [Leonhardt 2004] 100
6-2-2 Possible use of concordant cable profiles for the extradosed bridges 103
6-2-3 Handling prestressing configurations other than concordant profiles 105
6-2-4 Preliminary design 113
6-3 Commercial consideration related to the use of the stay cables and the concordant prestressing cables 115
7- POSSIBLE CONSTRUCTION METHODS FOR THE EXTRADOSED BRIDGES 117
7-1 Fabrication of Precast Segments 118
7-2 Methods of erection of precast segments 120
7-2-1 Erection of deck with cross section consisting of three precast segments 123
7-3 Proposal for the construction of extradosed bridges 126
8- CONCLUSIONS AND RECOMMENDATIONS 131
8-1 Conclusions 131
8-2 Recommendations 132
REFERENCES 137
APPENDIX A 140
Application of the continuous beam method for the determination of the stay cable forces under dead load 140

APPENDIX B 146
Application of the proposed construction method no. (5) on a simple cable supported beam with composite cross section 146
APPENDIX C 155
Application of the proposed construction method no. (5) on a cable-stayed bridge with a composite deck cross section (steel/concrete) 155
APPENDIX D 160
Application of the proposed construction method no. (5) on a cable-stayed bridge with a composite deck cross section (concrete/concrete) 160
APPENDIX E 165
Stay cable forces under dead load for extradosed bridges 165

LIST OF SYMBOLS

A	Cross sectional area
A_s	Cross sectional area of a stay cable or a steel beam
B	Width of concrete slab
BMD	Bending moment diagram
C	Affinity factor for the concordant prestressing profile
C.G	Centre of gravity
e	Vertical distance between the centre of gravity of the steel section and the centre of gravity of the composite section
e_b	Eccentricity of the bottom straight prestressing tendons from the centre of gravity of the deck cross section
e_c	Vertical distance between the centre of gravity of the concrete slab and the centre of gravity of the composite section
e_t	Eccentricity of the top straight prestressing tendons from the centre of gravity of the deck cross section
E	Modulus of elasticity
E_0	Elastic modulus of the stay cable material in the absence of the sag effect
E_c	Elastic modulus of the concrete material
E_{eff}	Effective elastic modulus of the stay cable
E_s	Elastic modulus of the stay cable material
f_η	Supplementary factor depending only on η
F_1	First stage installation force for stay cables
F_{Di}	Desired force of stay cable no. i
F_i	Force of stay cable no. i
f_{ij}	Force of stay cable no. j due to tensioning the stay cable no. i by a force equal to 1
F_{max}	Maximum back stay force
F_{min}	Minimum back stay force
F_P	Prestressing force
F_{PTi}	Force in stay cable no. i resulting from the prestressing forces
I_s	Moment of inertia of the first part of the composite section
I_{comp}	Moment of inertia of the total composite section
I(x)	Moment of inertia of the deck cross section at any point
L	Span length
L_f	Partial length of the deck
L_h	Projected stay cable length in plan
L_i	Stressed length for stay cable no. i
L_m	Main span length
L_o	Partial length of the deck
L_s	Partial length of the deck
L_{ui}	Unstressed length for stay cable no. i
M	Bending moment
M_{Di}	Desired bending moment at the anchorage point of stay cable no. i
M_{DL}	Bending moment due to dead load
M_{LL}	Bending moment due to live load
M_{DL+LL}	Bending moment due to the combination of dead and live loads

M_{ij}	Bending moment at the anchorage point of stay cable no. j due to tensioning the stay cable no. i by a force equal to 1
M_m	Bending moment at the middle of the main span
M_r	Bending moment due to restraining the creep and shrinkage strains of concrete
M(x)	Bending moment at any point due to the combination of dead load and stay cable forces
$M_{m1}(x)$	Bending moment at any point due to a vertical unit load acting at point m_1
$M_{s1}(x)$	Bending moment at any point due to a vertical unit load acting at point s_1
M_{2s1}	Bending moment at the support no.2 under a unit vertical load at point s_1
M_{3s1}	Bending moment at the support no.3 under a unit vertical load at point s_1
M_{2m1}	Bending moment at the support no.2 under a unit vertical load at point m_1
M_{3m1}	Bending moment at the support no.3 under a unit vertical load at point m_1
NFD	Normal force diagram
N_r	Normal force due to restraining the creep and shrinkage strains of concrete
n	Total nos. of stay cables
P_{eq-i}	Equivalent nodal load of the prestressing forces at the support no. i
q	Uniform live load acting on the deck
Q_{2r}	The shear force on the right hand side of the support no. 2
Q_{2rs1}	The shear force on the right hand side of the support no. 2 under a unit vertical load at point s_1
Q_{2rm1}	The shear force on the right hand side of the support no. 2 under a unit vertical load at point m_1
Q_{3r}	The shear force on the right hand side of the support no. 3
Q_{3rs1}	The shear force on the right hand side of the support no. 3 under a unit vertical load at point s_1
Q_{3rm1}	The shear force on the right hand side of the support no. 3 under a unit vertical load at point m_1
R_{1s1}	The reaction force at the support no.1 due to a unit vertical load at point s_1
R_{2s1}	The reaction force at the support no.2 due to a unit vertical load at point s_1
R_{3s1}	The reaction force at the support no.3 due to a unit vertical load at point s_1
R_{4s1}	The reaction force at the support no.4 due to a unit vertical load at point s_1
R_{1m1}	The reaction force at the support no.1 due to a unit vertical load at point m_1
R_{2m1}	The reaction force at the support no.2 due to a unit vertical load at point m_1
R_{3m1}	The reaction force at the support no.3 due to a unit vertical load at point m_1
R_{4m1}	The reaction force at the support no.4 due to a unit vertical load at point m_1
R_i	Vertical reaction force at the support no. i
s	Spacing between two successive anchorage points of stay cables
S_i	Vertical reaction force at the spring no. i
SFD	Shear force diagram
SIDL	Superimposed dead load
t	thickness of concrete slab
W	Uniform dead load acting on the deck
W(x)	Dead load at any point
W_C	Equivalent uniform load of stay cable forces
W_{eq}	Equivalent uniform load of prestressing forces
W_{sc}	Weight of stay cables
z_b	Distance between the centre of gravity and the bottom fibre of the deck cross section

Z_{ij} Vertical deflection at the anchorage point of stay cable no. j due to tensioning the stay cable no. i by a force equal to 1

z_t Distance between the centre of gravity and the upper fibre of the deck cross section

Greek Letters

γ Specific weight

γ_1 The basic partial coefficient for steel for the fatigue test of the stay cables

γ_2 The partial coefficient taking into account the effect of grouping (fatigue tests carried out on separated wires or strands or the full size of the stay cable)

γ_3 The partial coefficient taking into account the conversion of the fatigue test values into characteristic values

ΔF_i Required re-stressing or de-stressing force for the stay cable no. i

$\Delta F_{i\text{-}\infty\text{-}0}$ Change of the stay cable force between the time infinity and the time of the construction completion.

ΔL_i Shortening length of stay cable no. i

ΔM_i Change of the bending moment at the anchorage point of stay cable no. i or at the intermediate support of a continuous beam

ΔZ_i Change of vertical deflection at the anchorage point of stay cable no. i

ΔZ_{11} Vertical deflection for construction method no. 1 in the first stage

ΔZ_{41} Vertical deflection for construction method no. 4 in the first stage

ΔZ_{12} Vertical deflection for construction method no. 1 in the second stage

ΔZ_{42} Vertical deflection for construction method no. 4 in the second stage

ΔZ_{m1} Vertical deflection at point m_1 due to the combination of the dead load and the stay cable forces

ΔZ_{s1} Vertical deflection at point s_1 due to the combination of the dead load and the stay cable forces

$\Delta\sigma_{per}$ Permissible stress variation

$\Delta\sigma_L$ Stress variation due to live load

$\Delta\sigma_{Test}$ Stress variation considered in the fatigue test

ε Strain

ε_{el} Elastic strain

$\varepsilon_{C\text{-}cr}$ Strain of concrete due to the creep effect

$\varepsilon_{C\text{-}sh}$ Strain of concrete due to the shrinkage effect

η Ratio between the side span and main span lengths

θ_i Angle of the stay cable no. i with the horizontal line

λ Ratio between the uniform live and dead loads acting on the deck

λL Partial length of the deck

ξ Ratio between the minimum and maximum back stay forces

σ Axial stress

σ_a Allowable stress in the stay cable under SLS loads

σ_w Axial stress in the stay cable due to dead load

σ_q Axial stress in the stay cable due to live load

σ_{UTS} Ultimate tensile stress of the stay cable material

ϕ_i Creep coefficient of the beam elements in span no. i

CHAPTER 1

1- INTRODUCTION

The stay cables for cable-stayed bridges with concrete or steel deck cross sections are generally installed in such a way that the deck under dead load, will not deflect vertically. Accordingly, the bending moment distribution along the deck length will be equal to the bending moment distribution of a continuous beam on rigid supports and, therefore, the effect of creep is eliminated and the achieved desired alignment does not change with time (fig. 1.1).

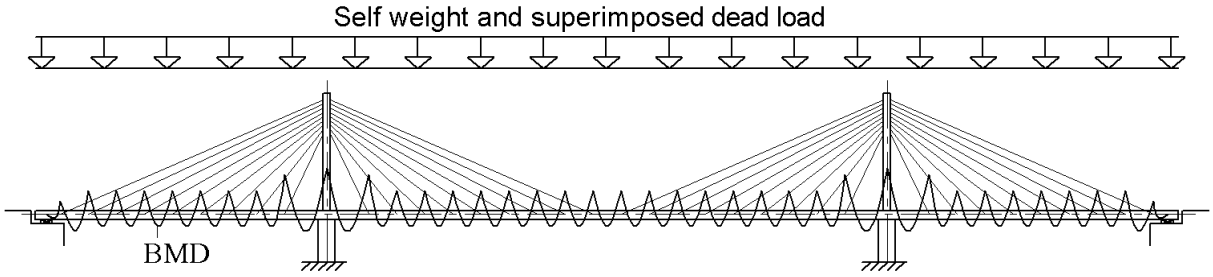

fig. 1.1: Desired bending moment distribution under dead load for conventional cable-stayed bridges

In case of a deck with concrete-only or steel-only cross section, each stay cable can be installed in one step to predetermined unstressed length to achieve the desired alignment and moment distribution under dead load, regardless of the selected construction method/sequence. For bridges with composite deck cross sections, (steel/concrete) or (concrete/concrete) figs. 1.2 and 1.3, the installation of the stay cables to predetermined lengths, does not lead necessarily to the desired forces and alignment under dead load at end of construction.

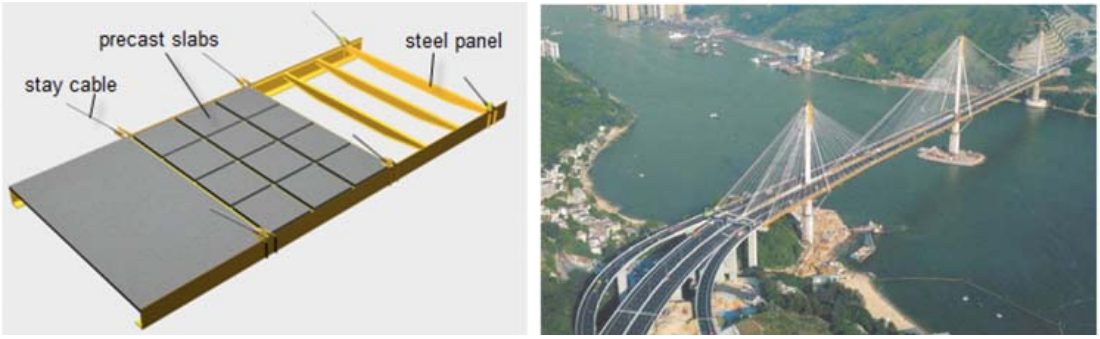

fig. 1.2: Composite deck steel/concrete used for the design of Ting Kau bridge in Hong Kong by "Schlaich Bergermann and Partner"

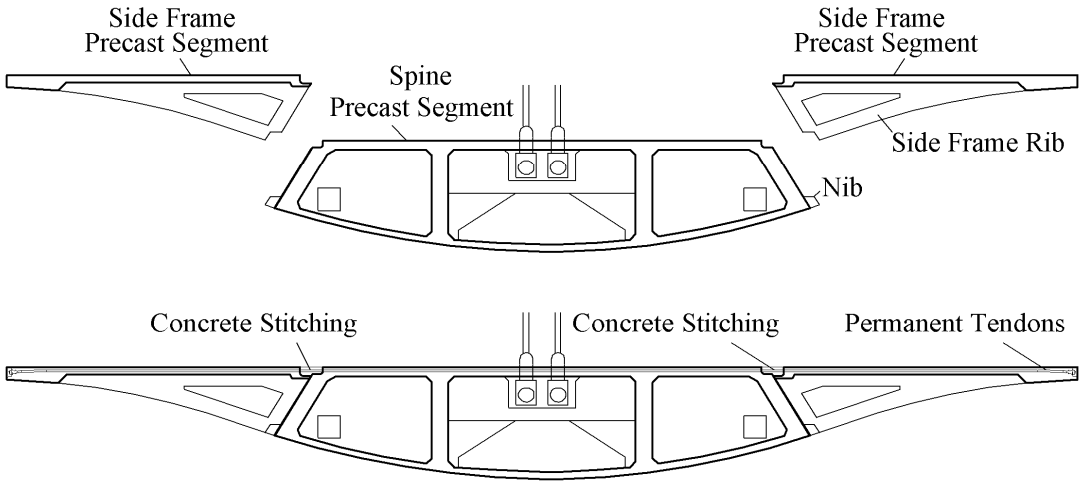

fig. 1.3: Composite deck concrete/concrete used for the design of Sungai Prai cable-stayed bridge in Penang/Malaysia by "Dar Consultants"

The achievement of the desired results will depend on the construction sequence of the deck elements, the ratio between the moment of inertia of the first part of the composite section to the moment of inertia of the total composite section and the vertical shift from the center of gravity of the first part of the composite section to the center of gravity of the total composite section. The desired results will be affected also by the time dependent forces due to shrinkage and creep.

In this research work a practical construction method will be proposed for cable-stayed bridges with composite decks, to ensure the achievement of the desired bending moment distribution similar to that shown in (fig. 1.1) taking into account the section properties of the composite section elements and the time dependent effects.

Whilst the desired bending moment distribution under dead load at end of construction for conventional cable-stayed bridges as that shown in (fig. 1.1) is targeted normally by bridge designers, it is noted that the bending moment distribution under dead load for extradosed bridges, with the common geometrical configuration shown in (fig. 1.4), is yet to be defined.

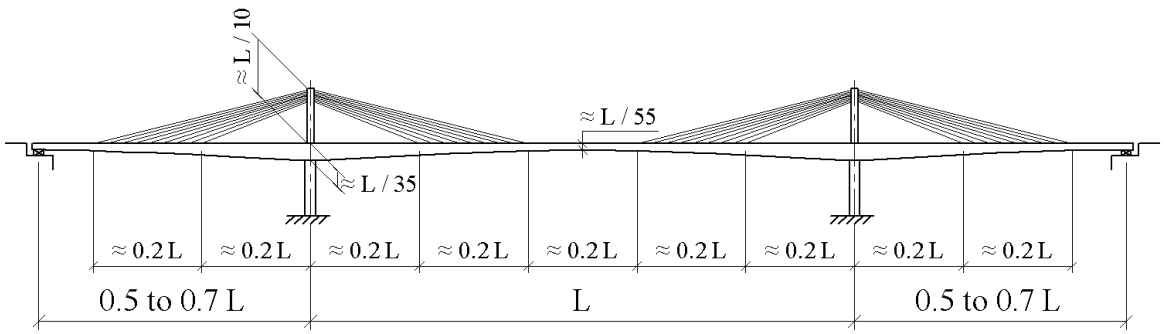

fig. 1.4: Common configuration of extradosed bridges

In this research work the proposed bending moment distribution under dead load shown in fig. 1.5, will be investigated for extradosed bridges.

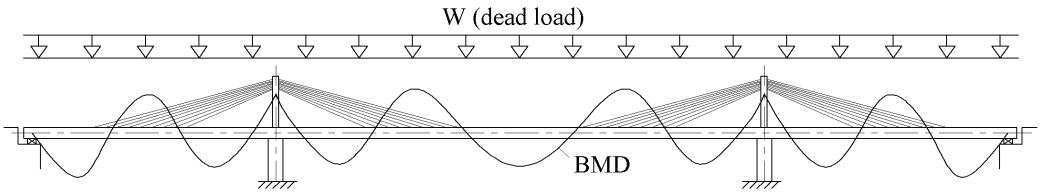

fig. 1.5: Proposed bending moment distribution under dead load for extradosed bridges

A composite deck cross section steel/concrete similar to that shown in fig. 1.2 has proven to be a successful choice for cable-stayed bridges, as far as the ease and speed of construction is concerned. The composite cross section concrete/concrete shown in fig. 1.3, consists of three pieces of precast segments. The central precast pieces are match cast spine segments which are erected first, with their relatively light weights, for the full length of the cable-stayed bridge and used subsequently as a platform for the erection of the precast side frames on both sides of the previously erected central segments. The said precast side frame segments are connected to the central precast spine segments by in-situ concrete stitching and transverse prestressing. The efficient and successful use of composite deck cross sections for cable-stayed bridges, should lead to an equal success for extradosed bridges as heavy temporary erection machines may be avoided. Practical construction methods will be presented in this research, which work for both of cable-stayed and extradosed bridges with composite decks. They will be a useful tool for bridge designers and contractors to achieve the desired alignment and forces within the structural elements for such types of bridges.

The research work will be arranged in the following chapters:

- Cable supported bridges in general (Chapter 2):

  The usual types of the stay cables used for cable-stayed and their methods of installation, will be presented. The structural systems and the behavior of cable-stayed bridges under external loads will be also briefly discussed.

- Previous research works for cable-stayed bridges related to the recommended stay cable forces under dead load (Chapter 3):

  The methods investigated previously for the determination of the stay cable forces under dead load for conventional cable-stayed bridges with concrete-only or steel-only deck sections will be explained.

- Construction analysis of cable-stayed bridges with composite decks (Chapter 4):

  The possible construction methods for cable-stayed bridges with composite decks will be presented. It will be shown that precautionary design and construction measures have to be taken in case the composite section is planned to be constructed in two stages. Further, a proposal will be made to ensure the achievement of the desired forces and alignment of the bridge elements under dead load, taking into account the section properties of the components of the composite section and the time dependant effects (creep and shrinkage).

- Extradosed bridges (Chapter 5):

  Based on the survey results of the extradosed bridges built so far, the common configuration of this type of bridges will be shown. The recommended methods for the design of the stay cables of extradosed bridges will be also discussed.

- Proposed method for the determination of the stay cable forces for extradosed bridges under dead load (Chapter 6):

  A new method will be developed to determine the stay cable forces under dead load for extradosed bridges. It will be shown that this method is suitable for use for extradosed bridges with concrete, steel or composite deck sections. For bridges with a concrete deck, the proposed method can be further optimised by using internal or external prestressing tendons inside the deck section. A combination of the stay cables and the prestressing forces may be targeted to considerably reduce the bending moments under dead load along the entire length of the bridge deck.

- Possible construction methods for extradosed bridges (Chapter 7):

  Taking into account the new proposed method for the definition of the stay cable forces under dead load as presented in Chapter 6, the possible methods for the construction of extradosed bridges will be discussed.

- Conclusions and recommendations (Chapter 8):

  A brief description for the outcome of this reseach work will be presented and recommendations for future researches will be made.

Finally**,** numerical examples are included in Appendices A to E to further clarify/ease the understanding of the contents of Chapters 3,4 and 6.

CHAPTER 2

2- CABLE-STAYED BRIDGES IN GENERAL

As implied by its name, the stay cables differentiate a cable-stayed bridge from other traditional bridges. The stay cables play a major structural role for cable-stayed bridges. They are designed normally to carry nearly 100 % of the dead load and serve in addition as elastic supports for the deck to allow for the safe transfer of the traffic loads to the foundations through the pylons. To ease the understanding of the next Chapters, the types of stay cables usually used for the construction of cable- stayed bridges and their methods of installation will be discussed in Section 2-1. In addition, the common structural systems of the modern cable-stayed bridges will be briefly presented in Section 2-2. For the readers who are familiar with the design and construction of cable-stayed bridges, they can go directly to Chapter 3.

2-1 Types of stay cables

In general the steel material used for the stay cables is characterized by its higher carbon content compared to that of the structural steel. Whilst the carbon content of the structural steel material is equal to 0.15 to 0.20%, the carbon content of the material used for the stay cables is equal to 0.80% [Gimsing and Georgakis 2011]. Due to its higher carbon content, the tensile strength of the stay cable material being equal to approximately 1800 MPA is almost equal to more than four times that of the mild structural steel (=370 MPA). Its tensile strength is also more than twice that of the high strength structural steel (=790 MPA). The increase in the tensile strength is paid for by a noticeable decrease of the ductility. The elongation at the breaking point for the stay cable material is equal to 4%. For the mild structural steel and the high strength structural steel, the elongation at the breaking point reach values of 24% and 18% respectively [Gimsing and Georgakis 2011].

The types of cables usually used for cable supported bridges are:

a- Parallel-bar cables.

b- Locked coil strand cables.

c- Parallel-wire cables.

d- Parallel strand cables.

2-1-1 Parallel-Bar Cables

Parallel-bar cables are steel threaded bars (fig. 2.1) usually manufactured with diameters 16, 19, 25, 32, 36, 43 and 57mm. The bars with diameters 16mm may be delivered in reels and those with diameters greater than 16mm are delivered with straight lengths 15 or 20m [Walter et al. 1999]. The continuity of the bars with diameters greater than 16mm may be achieved by using couplers. The ultimate strength of these types of cables varies between 1030 and 1470 N/mm^2 and they have an elastic modulus equal to 210000 N/mm^2. As the ultimate strength of the stressing bars is generally less than the ultimate strength of the wires used for the fabrication of other types of stay cables, the cross section of stay cables made out of stressing bars are normally larger. On the other hand, the use of bigger cross section leads to a reduction in the stresses variations and enhances the fatigue strength of the stay cables. As shown in fig. 2.1, the stressing bars are installed normally in metal ducts kept in position by polyethylene spacers and parallel to each other. The bars can slide in the longitudinal direction which allows the individual stressing of the steel bars. Upon tensioning all bars, the voids inside the metal ducts around the steel bars are normally injected with cement grout. The cement grout injection does not only provide the necessary corrosion protection for the steel bars but contribute in carrying part of the live loads as well.

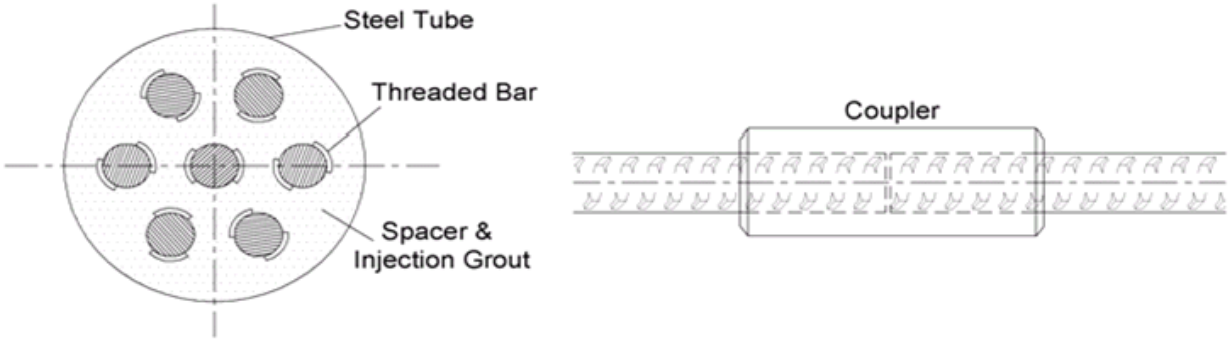

fig. 2.1: Parallel bar cables [Walter et al. 1999]

2-1-2 Locked Coil Strand Cables

In the locked coil strand a number of different shapes of wires cross sections are used to form a strand with a smoother and tighter surface. Typically, the locked coil strand will have a core of a normal helical strand composed of round wires. Around this core is one to several layers of wedge shaped wires and the outer layers are of wires with a special S-shape (fig. 2.2). The S-shape layer forms an envelope which is more or less water tight (hence the name “Locked Coil

Cables") [PFEIFER 2010]. These strands are fabricated by successive spinning of wire layers generally with opposite direction of helix. As a smaller pitch is used in the multi-wire strands, the decrease of the stiffness is more than that of the seven wire strands. The nominal elastic modulus for the multi wire helical strand is about 15-25% less than the value for straight wires [Gimsing and Georgakis 2011]. The elastic modulus of these types of strands is typically equal to 170000 N/mm^2. When the first loading is applied to a helical strand, the elongation will be due not only to the elastic strain in the wires, but also to an irreversible elongation caused by the compaction of the strand. To remove this non-elastic elongation, a pre-stressing is applied to make the strand behave in a nearly ideal elastic manner in the final structure. The locked coil strands are fabricated generally with diameters ranging from 30mm to 150mm. The largest diameters of locked coil strands are used for cable-stayed bridges in which a stay cable may be made of one single strand. The smaller diameters (60 to 80mm) are used in cases where the final cable is composed of several strands. As opposed to other types of stay cables, stay cables with locked coil strands are installed without external ducts or grouting and for this reason, they have to be fabricated with care as far as the corrosion protection of all of their wires, is concerned.

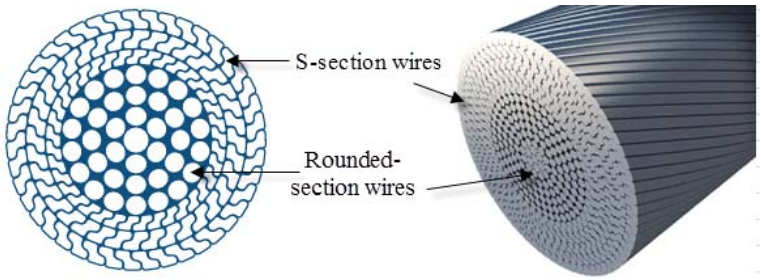

fig. 2.2: Locked coil strand

2-1-3 Parallel Wire Cables

They consist of bundles of 7mm diameter wires (figs. 2.3 to 2.5). The number of wires in each bundle is varying between 50 and 350. The ultimate strength of the wires of these types of cables is equal to 1670 N/mm^2. This means that the ultimate load capacity of one wire can reach a value of 6.5 tons and the ultimate load capacity of a bundle with 300 wires will be equal to 1950 tons. The elastic modulus of these types of cables is about 205000 N/mm^2 which is a little less than that of the parallel bar cables. The results of the tests carried out on stay cables system with parallel wires, have shown that they can withstand stress variations of 350-400 N/mm^2 over two million cycles with a maximum stress of 750 N/mm^2 which is nearly equal to 45% of the ultimate tensile stress of the wires material [Walter et al. 1999]. Fig. 2.6 shows testing the fabricated stay

cable with its full length prior to its delivery to the erection site. The jacking load in the test is normally equal to 1.5 times the maximum expected load during the service live of the stay cable. Fig. 2.7 shows that the stay cables with parallel wires are manufactured with its full length in the factory and delivered to the erection site with special coils. As it is the case for BBR-HiAm stay cable system, all of the individual parallel wires are galvanized by immersing the wires in a bath of melted zinc. The wires are covered by internal black HDPE-layer and external white HDPE-layer. The external HDPE-layer can be made of any desired color which has normally to be anti-violet. Figs. 2.4 and 2.5 show the method of anchoring the stay cable wires inside the stay cable head. The ends of the wires are swaged to allow the wires to be anchored to the outer face of a perforated steel plate. Subsequently the stay cable head under the perforated steel plate is grouted by a mix of epoxy resin, zinc powder and steel balls. It is also to be noted that the stay cable head is threaded from inside and outside. The inside threading allows pulling the stay cable by a pulling rod during installation and the outside threading helps to anchor the stay cable head to a bearing plate using a special nut (figs. 2.7 to 2.9). The fabrication length of the stay cable has to be determined with care allowing appropriate tolerances. In case the stay cable is found at the erection site too long, additional steel shims fabricated in two half, will have to be inserted between the permanent nuts and the bearing plates. These shims may have to be placed at both ends of the stay cables. In case the stay cable is found too short, it may have to be re-fabricated to avoid the overstressing of the stay cable or breaking and recasting the concrete at the anchorage locations. Breaking and recasting the concrete to shorten the distance between the stay cable ends is very tedious and time consuming due to the common reinforcement congestion at the anchorage zones.

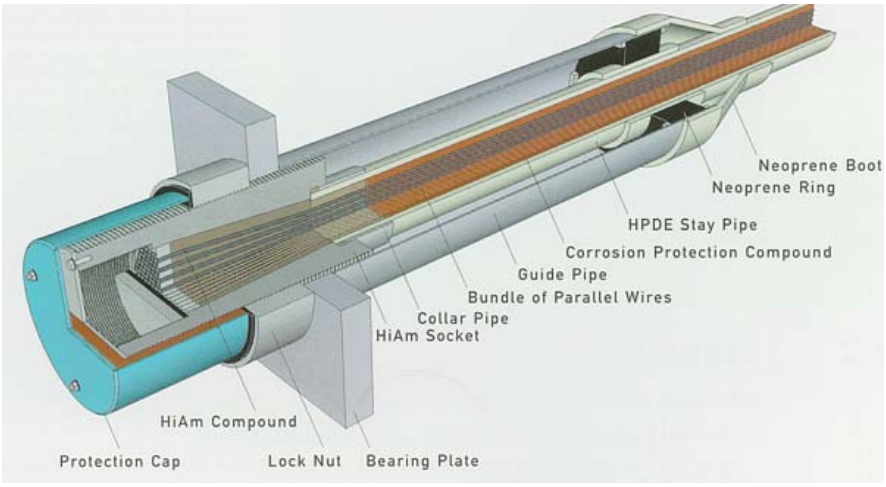

fig. 2.3: Stay cables with parallel wires cables/ BBR-HiAm system [www.bbrnetwork.com]

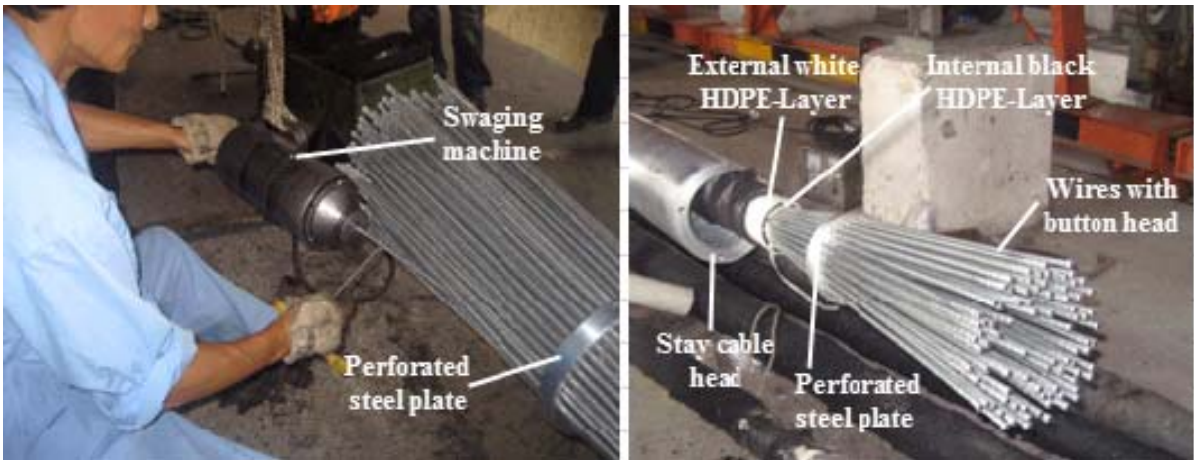

fig. 2.4: Swaging the wires prior to grouting the stay cable head

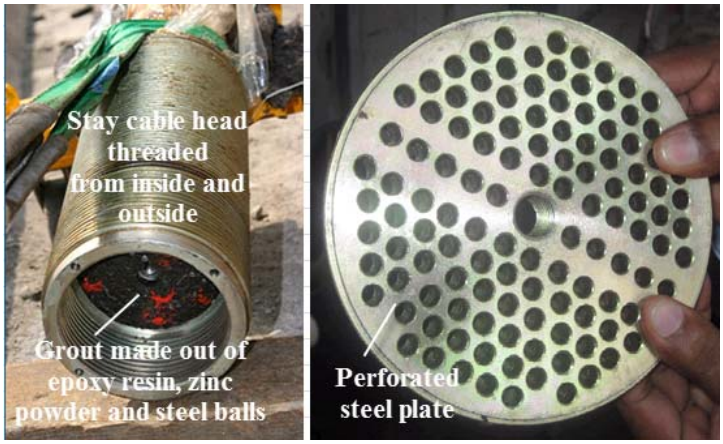

fig. 2.5: Anchorage of the wires at the stay cable head

fig. 2.6: Testing of the fabricated stay cable with its full length prior to its delivery to the erection site

fig. 2.7: Uncoiling and pulling the stay cable ends to the pylon head and along the deck level

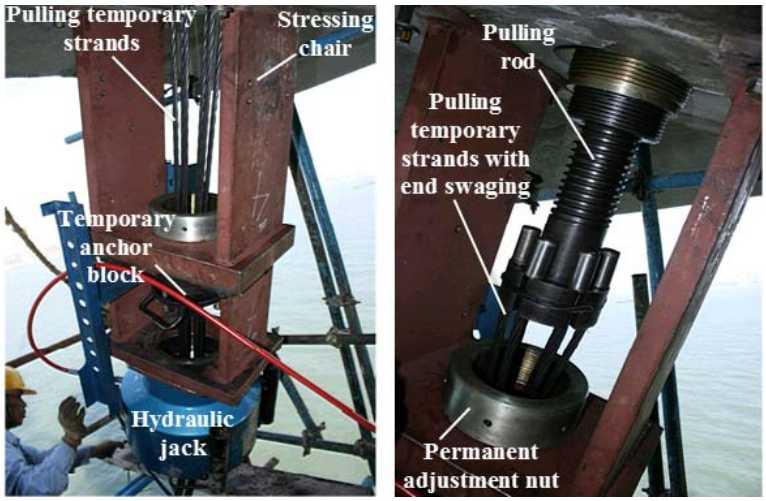

fig. 2.8: Pulling the stay cable to the deck soffit using pulling rods and temporary strands anchored at the pulling rod head

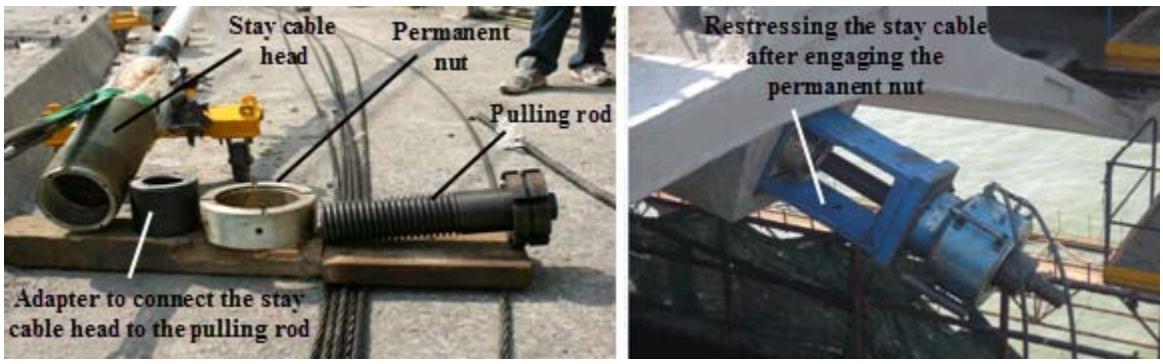

fig. 2.9: Equipments used for installation and stressing of stay cables (parallel wire cables system)

2-1-4 Parallel Strand Cables

They consist of bundles of strands. The strand is normally made from seven wires with 5mm diameter each. These strands are the simplest to be found within the cable supported bridges. At present they are widely used as tendons of pre-stressed concrete structures. The seven-wire strand consists of a single straight 5mm diameter wire core surrounded by a single layer of six wires giving the strand a nominal diameter of 15mm and a nominal cross sectional area equal to 150mm^2 (figs. 2.10 and 2.11). All of the six wires, surrounding the said core wire, have the same pitch and direction of helix. As the pitch is relatively large, the inclination of the wire axis in respect to the strand axis is small. This means that the stiffness of the seven-wire strand is nearly equal to that of the straight wires. Typically, the nominal elastic modulus for the seven–wire strand will be 5-6% less than that of the wires. The typical elastic modulus of these types of cables is equal to 195000 N/mm^2 [Gimsing and Georgakis 2011]. Figs. 2.12 and 2.13 show the components of the stay cable head and the special wedges used for the anchorage of the individual strands at the outer face of the anchorage block [Freyssinet 1999]. The international codes and specifications recommend to test the stay cable system of this type for fatigue strength. The stay cables have to prove a fatigue strength of about 200 N/mm^2 at a maximum stress of 750 N/mm^2 with two million cycles. The bites/pinches applied by the wedges on the strands are normally the reasons for the low fatigue strength of the stay cable with parallel strands when compared with the stay cables made of parallel wires. As shown within figs. 2-10 and 2.11, the individual strands of Freyssinet stay cable system are galvanized and coated with a thin black HDPE-layer after filling the interstices of its 7-wires with special petroleum wax. The strand bundle is placed inside a colored external HDPE-layer. Fig. 2-10 shows also that the external HDPE-layer is provided with helical ribs which enhance the stay cables behavior under the effect of wind and/or rain.

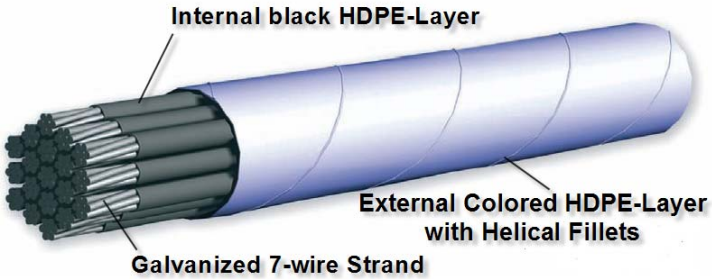

fig. 2.10: Components of parallel strand cables [www.freyssinetusa.com]

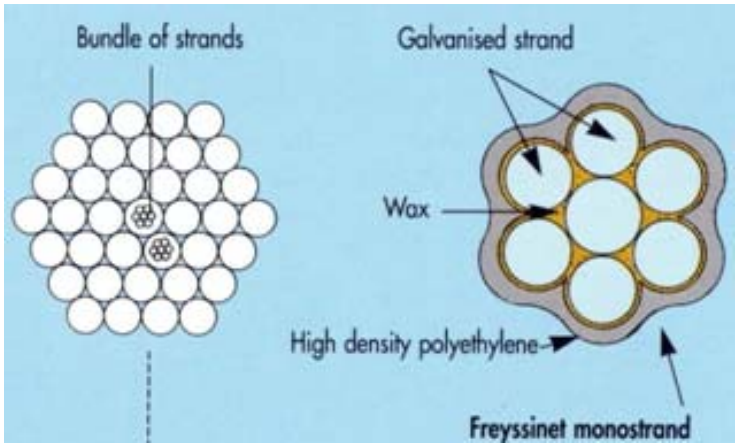

fig. 2.11: Cross sections through the strand bundle and the mono-strand used for Freyssinet stay cable system [Freyssinet 1999]

The parallel strands stay cables are installed normally strand by strand. Due to the flexibility of deck and tower, the force of the individual strands of a stay cable varies during the stressing operation. To ensure uniformity of force in all strands of a stay at the end of the stressing operation, a patented method has been developed by Freyssinet, called Isotension [Freyssinet 1999]. The principle of the Isotension may be described as follows (figs. 2.14 and 2.15):

- The first strand ("the master strand") is fixed to one of the stay cable two anchorages and its other end is threaded into the other anchorage and then cut and stressed to a calculated force, using the theoretical numerical model of the bridge structure. Due to the flexibility of the structure, the calculated force of the master strand, has to be higher than the desired strand force when all strands of the stay cables are stressed.
- The wedge of the master strand is not yet engaged to the stay cable anchor block. The master strand is instead wedged to a special single anchoring device provided with a load cell which gives the reading of the current master strand force.
- The second strand is then installed in a similar manner, cut and stressed. The stressing is done, as for the master strand, with a mono-strand jack equipped with a load cell identical to the one indicating the force of the master strand. As the second strand is stressed, the force in the first strand decreases and the stressing operation is stopped when the readings of the two load cells are identical. The second strand is then anchored/wedged to the permanent anchor block. The two strands are equally stressed.

- The third strand is then installed and stressed until its force reaches the force of the master strand (which decreases jointly with the force of the second strand). The three strands are identically stressed.
- The same operation is repeated until the last strand of the stay cable. The last reading of the stay is then to be compared with the expected theoretical force. The stay cable force may then be adjusted by the multi-strand jack if necessary.

Figs. 2-16 to 2.18 show the installation for the stay cables of Sungai Prai Bridge in Penang/Malaysia. Fig. 2.16 shows a schematic for the method used for threading the strands using 4-winches noting that the stay cables for this bridge are anchored to the tower head by using the saddle system.

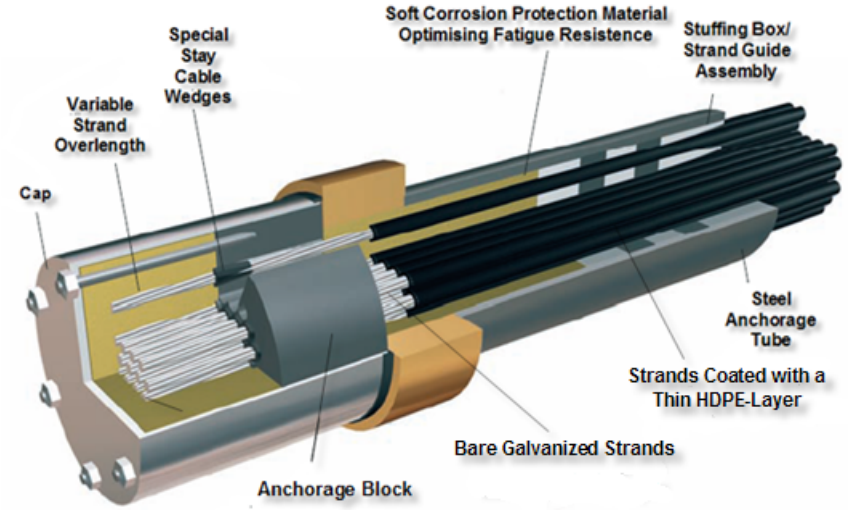

fig. 2.12: Anchorage components of parallel strand stay cable [www.freyssinetusa.com]

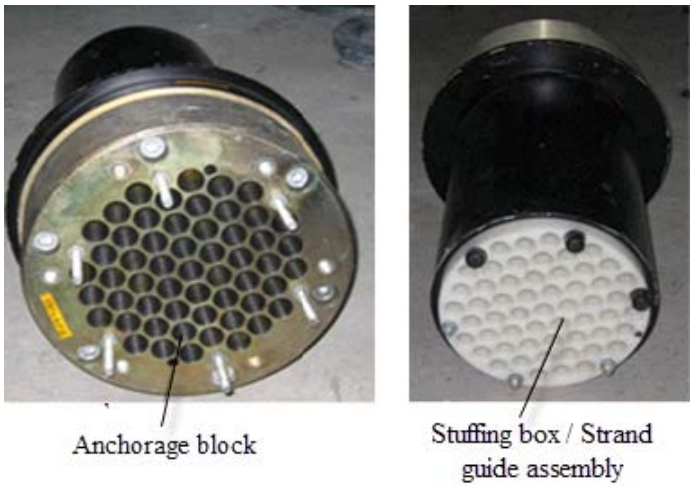

fig. 2.13: Anchorage block used for Freyssinet stay cable system

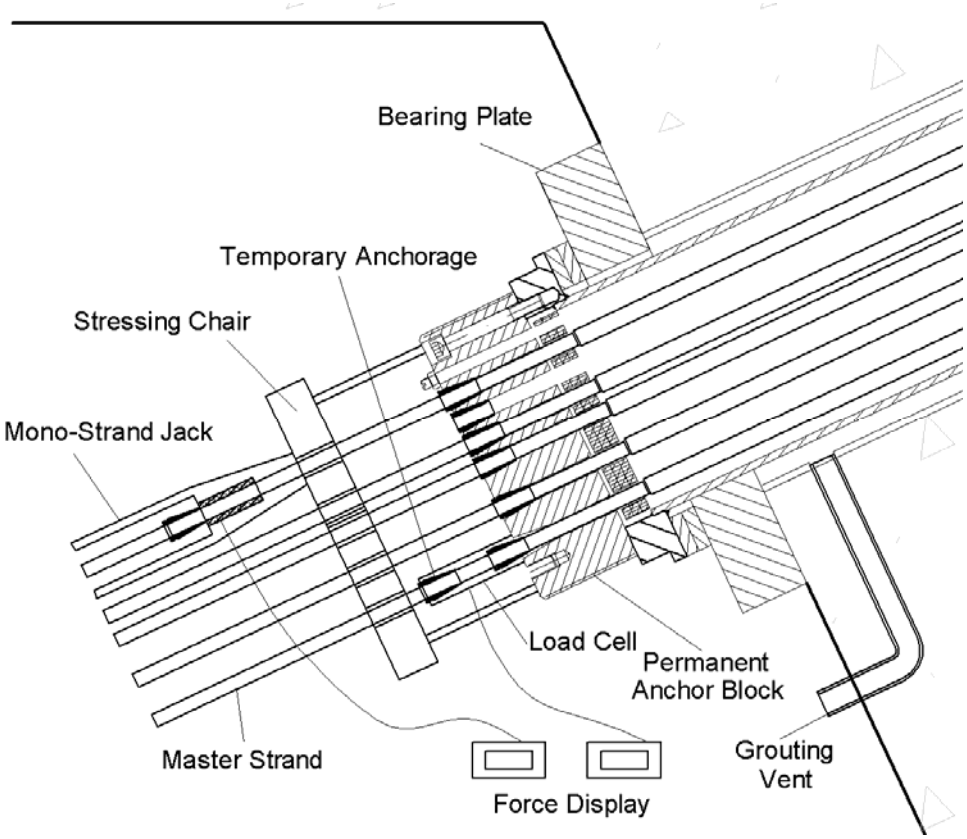

fig. 2: 14: Installation of the parallel strand cables with the isotension method (schematic)

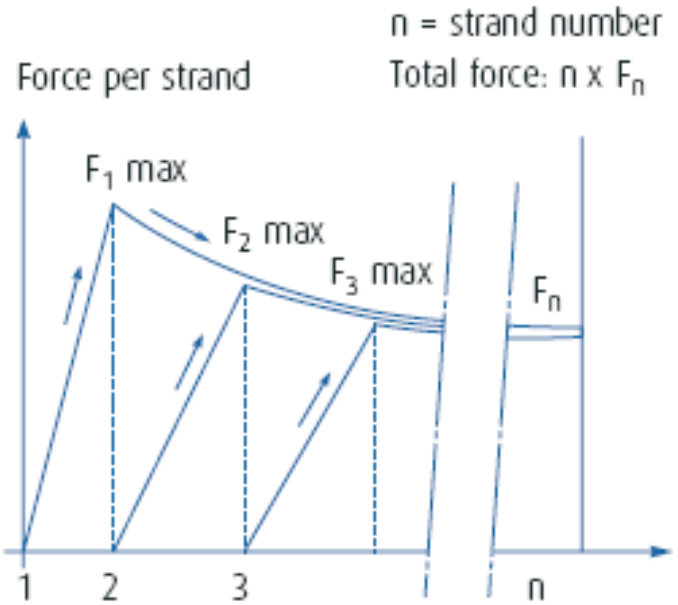

fig. 2.15: Isotension principle diagram [Freyssinet 1999]

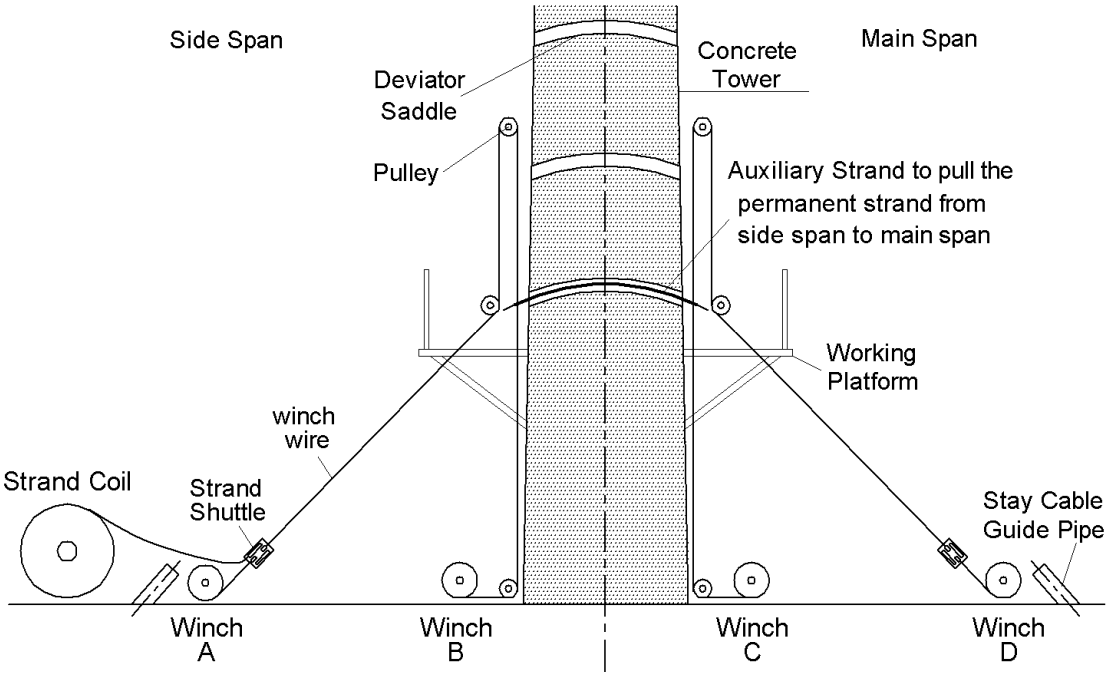

fig. 2.16: Threading the strands from the anchorage location on the side span side to the anchorage location on the main span side through the deviator saddle (schematic)

fig. 2.17: Threading the stay cables strands for Sungai Prai cable-stayed bridge in Penang/Malaysia

fig. 2.18: Installation of the parallel strand cable by the "strand by strand" method

2-1-5 Anchorages of Stay Cables at Deck and Tower head Levels

The stay cables are manufactured normally with one active end and one passive end during the installation/stressing operation. The stay cable may be stressed at the deck level or at the pylon head level. Figs. 2.19 and 2.20 show two types of passive and active stay cable anchorages at deck level.

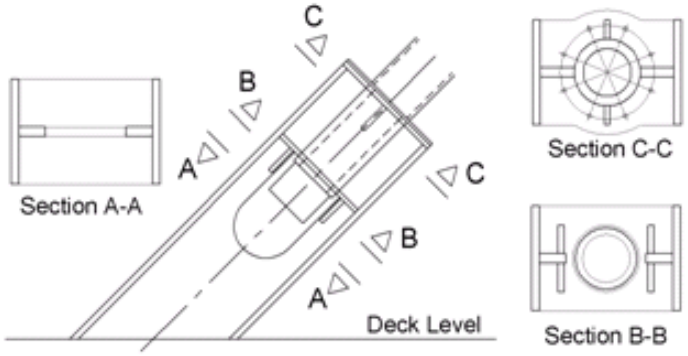

fig. 2.19: Passive anchorage at deck level

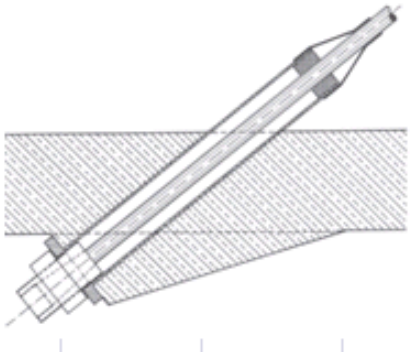

fig. 2.20: Active anchorage at deck level [Leonhardt and Zellner 1980]

Figs. 2.21 to 2.28 show different possibilities for the stay cable anchorages at the tower head. In case the dimensions of the tower head allow the arrangement of a central chamber, a solution

similar to that shown within fig. 2.21 may be followed. The central chamber should normally be sufficiently large to handle the equipment necessary for pulling and stressing the stay cables. In case the dimensions of the tower head are too small to accommodate the anchorages of the stay cables and/or the provision of a central chamber, one of the anchorage systems similar to that shown within figs. 2.22 and 2.24 may be adopted. Figs. 2-22 and 2.23 show the tower head for Ting Kau bridge in Hong King. The width and the length of the slender concrete tower head cross section, being equal to 5 and 10m respectively, were not adequate to anchor 8-stay cables in one level. Accordingly additional two external steel boxes had to be connected to the concrete tower head section to allow the anchorage of the stay cables in the manner shown within fig. 2.22. The overcrossing of stay cables may be chosen in case the arrangements of the stay cables anchorages are made in such a way that the torsion/twist of the tower head are to be avoided as it is the case for the configuration shown within fig. 2.24. For the towers of Worli cable-stayed bridge in Mumbai/India (fig. 2.25) a cross beam connecting the top of the tower heads has been constructed to carry/reduce the twist of the tower heads resulting from the arrangement of the stay cable anchorages shown within sections 1-1 and 2-2. The use of deviation saddles at the tower head as that shown within figs. 2.26 and 2.27 helps to save the anchorages at the tower head, simplify the design and construction of the tower head and helps also to achieve a slender tower head as the saddle normally does not occupy big space of the tower head section. For Sungai Prai Bridge in Malaysia, each stay cable consists of strands of the type shown within fig. 2.11. Each strand is continuous from the deck anchorage in the side span to the deck anchorage in the main span. As shown within sections A-A, B-B and C-C of fig. 2.26, the black HDPE-layer covering every single strand outside the steel saddle are removed inside the saddle. To avoid the slippage of the strands inside the saddle resulting from the possible unsymmetrical live loads on both sides of the tower head, the saddle tube was injected with cement grout upon the installation of all strands. Despite of the said injection of the saddle with cement grout, the removal of the black HDPE-layer around the individual strands inside the saddle, may be problematic with respect to the corrosion protection, fatigue resistance and the possibility to replace the stay cables when necessary. To avoid these disadvantages, Freyssinet developed a high performance deviation saddle, called the multi tube saddle and used what is called Cohestrand [Lecinq et al. 2005]. The Cohestrand is similar to the strand shown within figure 2.11 except for the petroleum wax which is replaced by a special resin which is a compound of polybutadiene (PolyBd) resin

wrapping all the wires including the core wire and adhesion element (Orevac) on polyethelene. The key aspect of the Cohestrand manufacturing is the co-extrusion of the PolyBd, the Orevac and the polyethylene onto the strand to obtain a sufficient bond. The minimum shear resistance of the compound shall be 4.0 N/mm^2 at $20C^0$ between the outer sheath and the 7-wire strand. The triple anticorrosion barrier of the Cohestrand can be maintained also inside the deviation saddle without any discontinuity. This is the key to avoid any weak point in the corrosion protection of the cables. The saddle is made of a bundle of individual deviation tubes placed inside a large steel saddle tube. The space between the individual tubes is filled in factory with a special high strength cement grout (compression strength at 28-days > 130 N/mm^2). The saddle is delivered to the site fully assembled and grouted. Upon the installation of the saddle in the tower head, the strands are threaded one by one through the individual tubes. The saddle provides an individual deviation of each strand by a small tube and the fix point of the cable is obtained from friction of each strand on its individual deviation tube. Using Cohestrand, the friction can be transferred through the sheath, hence the HDPE sheath of the strand is continuous through the saddle and the corrosion protection of the free length is not interrupted in the saddle. A special surface treatment of the tubes ensures that the friction coefficient between the strand and the saddle is greater than 0.5 which is normally enough to block unsymmetrical forces in most bridges. As the radial forces are not transmitted between the strands, the fatigue performance of the multi-tube saddle is improved. It has been tested successfully for two million cycles of 200 N/mm^2 axial fatigue loading. The saddle enables also the replacement of each strand. The deviation saddle with the Cohestrand was implemented for the first time for Sungai Muar cable-stayed bridge in Johor/Malaysia (fig. 2.28 and 2.29). The bridge was designed by “Jean-Muller International”. Its total length is equal to 632m with main span of 132m. The multi tube saddles were manufactured and grouted in France, then delivered to Malaysia. The stay cable sizes range from 37 to 73 strands. The stays were installed strand by strand and stressed simultaneously from both of its ends with the Iso-tension system.

VSL developed also a saddle system allowing “strand by strand” installation and replacement. The saddle in this system is composed of a steel box filled with a high strength ductal type cement grout. Each strand is installed without the black HDPE-sheating in individual slightly ovalised V-shape hole and special grout is used when the strand installation is completed [VSL 2008]. This saddle system was intensively tested at the TU-Berlin [Schlaich et al. 2012].

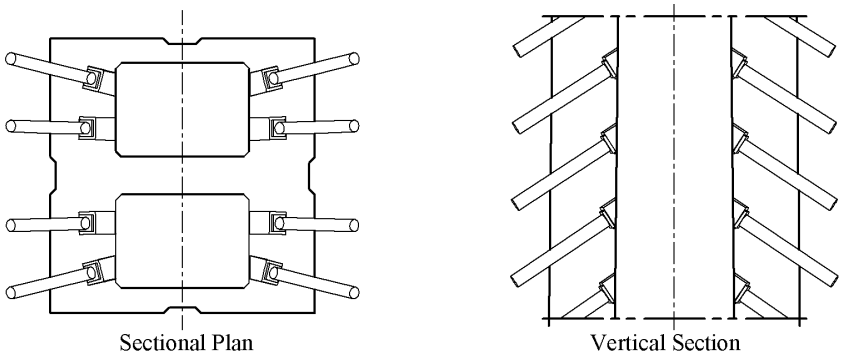

fig. 2.21: Stay cable anchorages inside the tower head

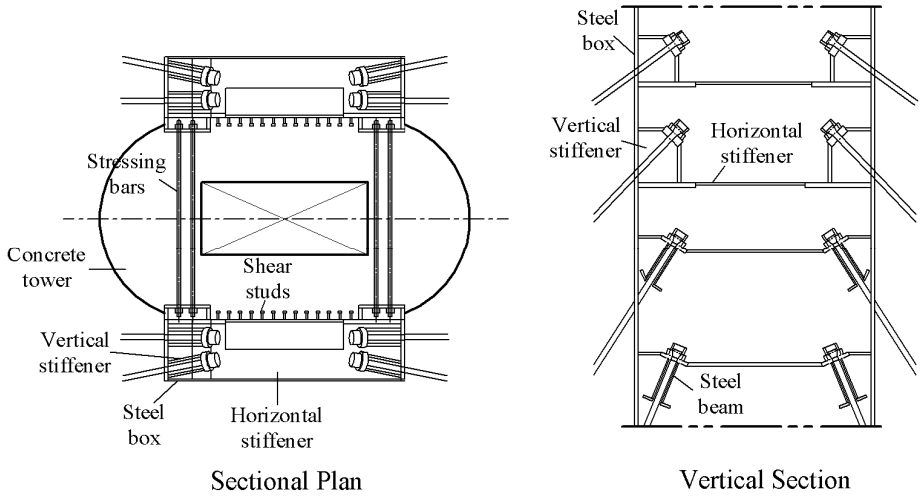

fig. 2:22: Anchorage of stay cables using external steel box

fig. 2.23: Tower head of Ting Kau bridge

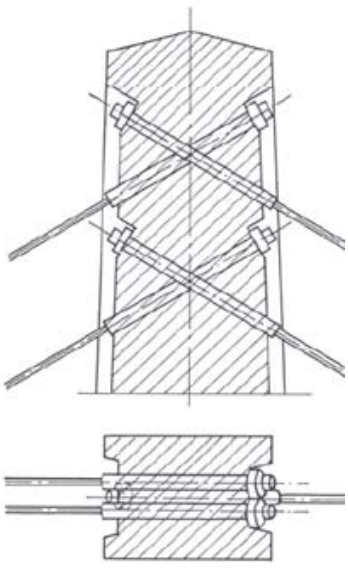

fig. 2.24: Overcrossing of stay cables [Leonhardt and Zellner 1980]

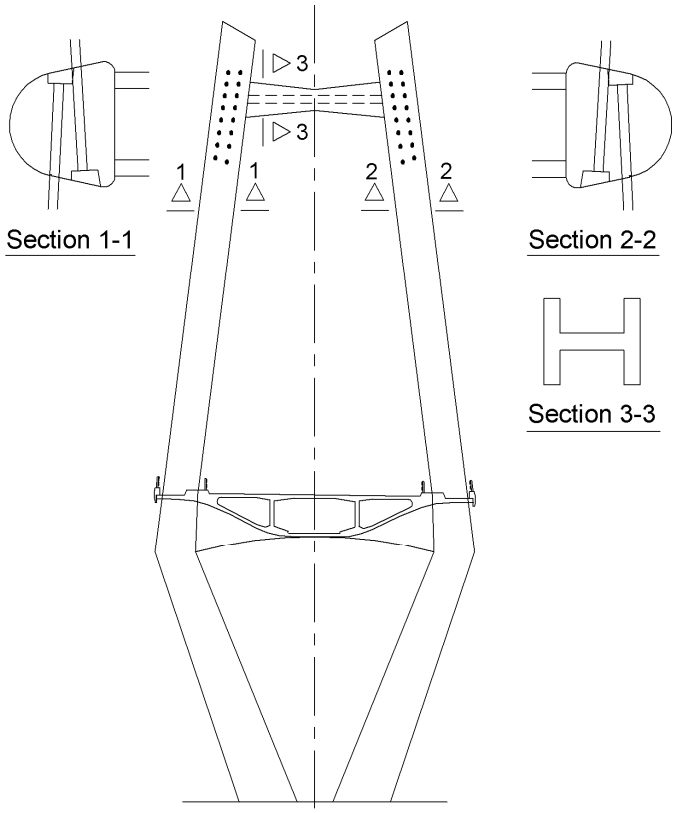

fig. 2.25: Anchorage of the stay cables at the tower head of Worli cable-stayed bridge in Mumbai/India

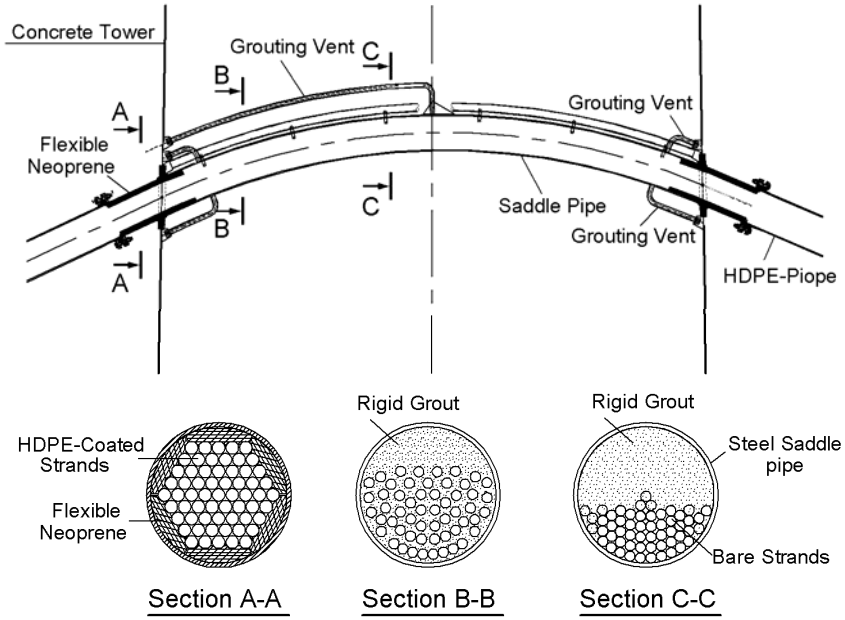

fig. 2.26: Anchorage of stay cable at the tower head using a steel saddle and rigid cement grout

fig. 2.27: Placement of steel saddles within the tower head before concreting

fig. 2.28: The prefabricated saddles used for Sungai Muar cable-stayed bridge in Johor/Malaysia [Lecinq et al. 2005]

fig. 2.29: Sungai Muar cable-stayed bridge in Johor/Malaysia [Lecinq et al. 2005]

2-2 Possible structural systems for conventional cable-stayed bridges (supporting system between the tower and the deck & between the deck and the end support)

The contribution of each bearing element of a conventional cable-stayed bridge (towers, stay cables and deck) in carrying the self weights and/or the external loads depends to a great extent on the chosen supporting system. Cable-stayed bridges may have one of the configurations shown in fig. 2.30. The modern form of cable-stayed bridges started first with the use of few numbers of stay cables acting as elastic supports for a relatively stiff deck fig. 2.30 (a) [Leonhardt and Zellner 1980]. In this system only slender towers over the deck level are required as they will carry the vertical component forces of the said few numbers of stay cables, and may also carry small bending moments. Similar to the extradosed bridges, which will be dealt with in Chapters 5 and 6, the bridge configuration shown in fig. 2.30 (a), does not have backstays connecting the tower tip to the rigid end support. The stability of this bridge configuration is achieved mainly by its stiff deck.

As opposed to the structural system of the bridge shown in fig. 2.30 (a), the bridge in fig. 2.30 (b) has a slender deck and is provided with back stays connecting the tip of the tower to the rigid end supports, serving to stabilize the towers in the longitudinal direction. The rocker bearings are connected at their top ends to the deck by hinges. They have also hinges at their bottom ends. The main function of these rocker bearing is to carry the vertical component forces of the backstays while allowing the horizontal movement of the deck. The horizontal component forces of the back stays, in this particular structural system, will be carried by the deck and they will balance the horizontal component of the stay forces of the main span side. As the deck moves longitudinally under the effect of temperature changes, shrinkage, creep or live loads, the rocker bearings will move with the deck at their top ends and will therefore rotate around their bottom hinges. According to the extent of these movements, the height of the rocker bearings should be chosen so that no restraining actions between the deck and the rocker bearing will be introduced. The bridge shown in fig. 2.30 (c) is characterized by its stiff tower. This type of tower will not be in need of back stays as in the case of the bridge shown in fig. 2.30 (b). The bridge configuration shown in fig. 2.30 (d) is not common in that it has an expansion joint at the center of its main span and not at the bridge ends. The backstays are anchored outside the bridge deck and the deck is fixed to the end supports. The supporting system configuration shown in fig. 2.30 (d) was adopted for Barrios de Luna bridge in Spain [Walter et al. 1999]. The structural system of the

bridge shown in fig. 2.30 (e) is similar to that shown in fig. 2.30 (d), but the deck in this configuration has two expansion joints arranged near the towers. For the bridge configurations shown in figs. 2.30 (b) and (c), the deck may be rigidly connected to one of the towers or left swimming in the longitudinal direction. The deck of the bridges in fig. 2.30 (d) and (e) may be connected to the towers in the longitudinal direction only in case of relatively short side spans and/or flexible tall towers above the ground to avoid high restraining forces between the towers and the deck. Under dead load, the decks of the bridges shown in figs. 2.30 (a) to (d) are under compression normal forces, and the deck of the bridge shown in fig. 2.30 (e) is under tension normal force. In this connection, it should be noted that the choice of a steel deck is best suitable for the configuration of fig. 2.30 (e). This configuration was selected by F. de Miranda for the design of the bridge over the Arno [Walter et al. 1999].

If there is no need for large free side span and the site conditions permit, one or more additional piers in the side span as shown in fig. 2.30 (f) may be introduced. This will help to reduce the uplift force which has to be carried by the rocker bearings at the end of the side span.

It can also be understood that each half of the cable-stayed bridges shown in figs. 2.30 (b) to (d) and (f), from the middle of the main span to the end support, is statically stable. This is not valid for the bridge configuration shown in fig. 2.30 (e). Each half of this bridge configuration cannot stand alone similar to the case of the common suspension bridge configuration.

To resist the transverse wind loads acting on the deck and cables, the deck is normally supported in the transverse direction in all configurations shown in (fig. 2.30) at the towers and at the end supports at both bridge ends.

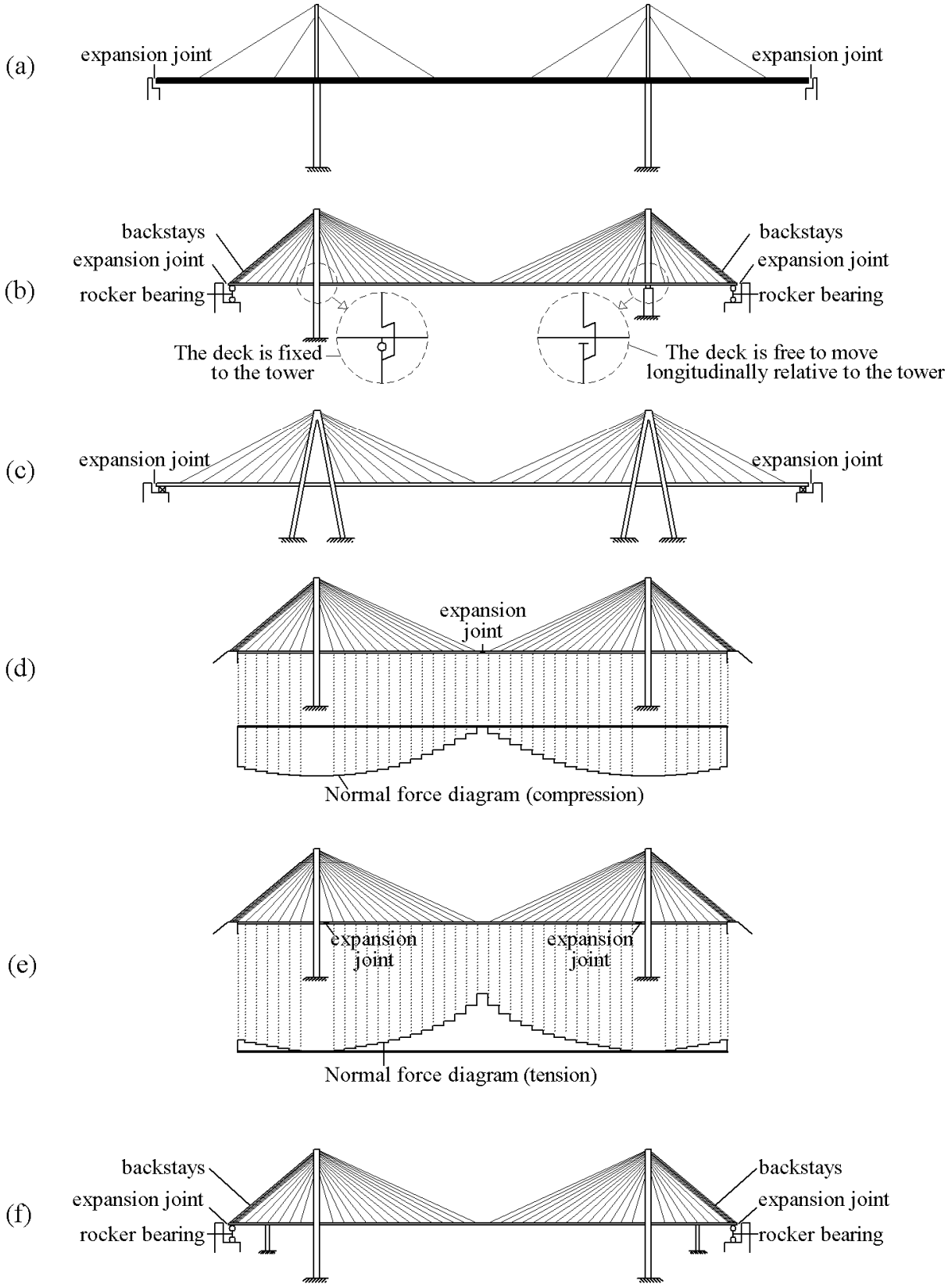

fig. 2.30: Possible structural systems for conventional cable-stayed bridges

Ratio between the side span and the main span length:

The backstays of the modern cable-stayed bridges play a dominant role to ensure the overall stability of the structural system. They help to stabilize the tip of the tower as they hold the tower back towards the side span when the main span carries live load. The live load q on the main span increase the backstay forces fig. 2.31. The backstay forces are reduced to their minimum level when the live load q occupy only the side span fig. 2.32. The backstays get normally the largest stress variations/amplitudes compared to all other cables. They have to be dimensioned in such a way that the said stress variations are kept safely below their fatigue strength.

From figures 2.31 and 2.32 and by ignoring the bending stiffness of deck and assuming that all stay cables intersect at the top of the tower head, the following equations may be written [Gimsing and Georgakis 2011]:

$$F_{max}\, L_s \sin(\theta) = (q+w)\, \frac{\left(\frac{L_m}{2}\right)^2}{2} - w\, \frac{{L_s}^2}{2} \tag{2.1}$$

$$F_{min}\, L_s \sin(\theta) = w\, \frac{\left(\frac{L_m}{2}\right)^2}{2} - (q+w)\, \frac{{L_s}^2}{2} \tag{2.2}$$

By dividing both sides of equation 2.2 over the corresponding sides of equation 2.1, the following equation can be obtained:

$$\frac{F_{min}}{F_{max}} = \frac{w\,{L_m}^2 - 4\,(w+q)\,{L_s}^2}{(w+q)\,{L_m}^2 - 4\,w\,{L_s}^2} \tag{2.3}$$

Assuming that $\zeta = \frac{F_{min}}{F_{max}}$, $\lambda = \frac{q}{w}$, $\eta = \frac{L_s}{L_m}$

The ratio between the minimum and maximum backstay forces ζ can be determined from the following equation:

$$\eta = \frac{1 - 4\,(1+\lambda)\,\eta^2}{(1+\lambda) - 4\,\eta^2} \tag{2.4}$$

By rearrangement, the following equation can also be obtained:

$$\eta = \frac{1}{2}\sqrt{\frac{\zeta(1+\lambda)-1}{\zeta-1-\lambda}} = \frac{1}{2}\sqrt{\frac{1-\zeta(1+\lambda)}{1-\zeta+\lambda}} \tag{2.5}$$

Equation (2.5) can be presented graphically as shown within fig. 2.33.

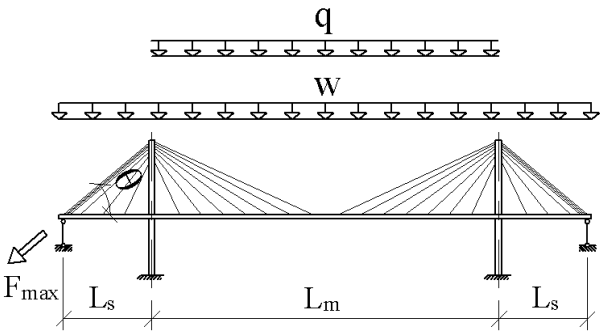

fig. 2.31: Load case for maximum back stay forces

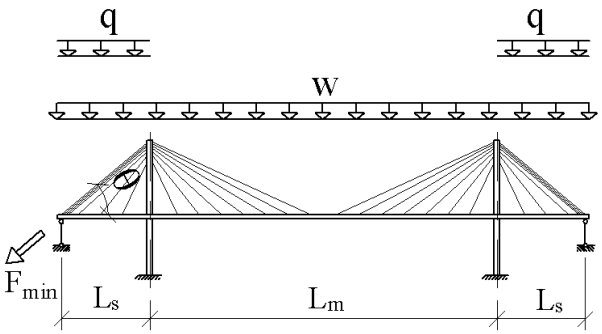

fig. 2.32: Load case for minimum back stay forces

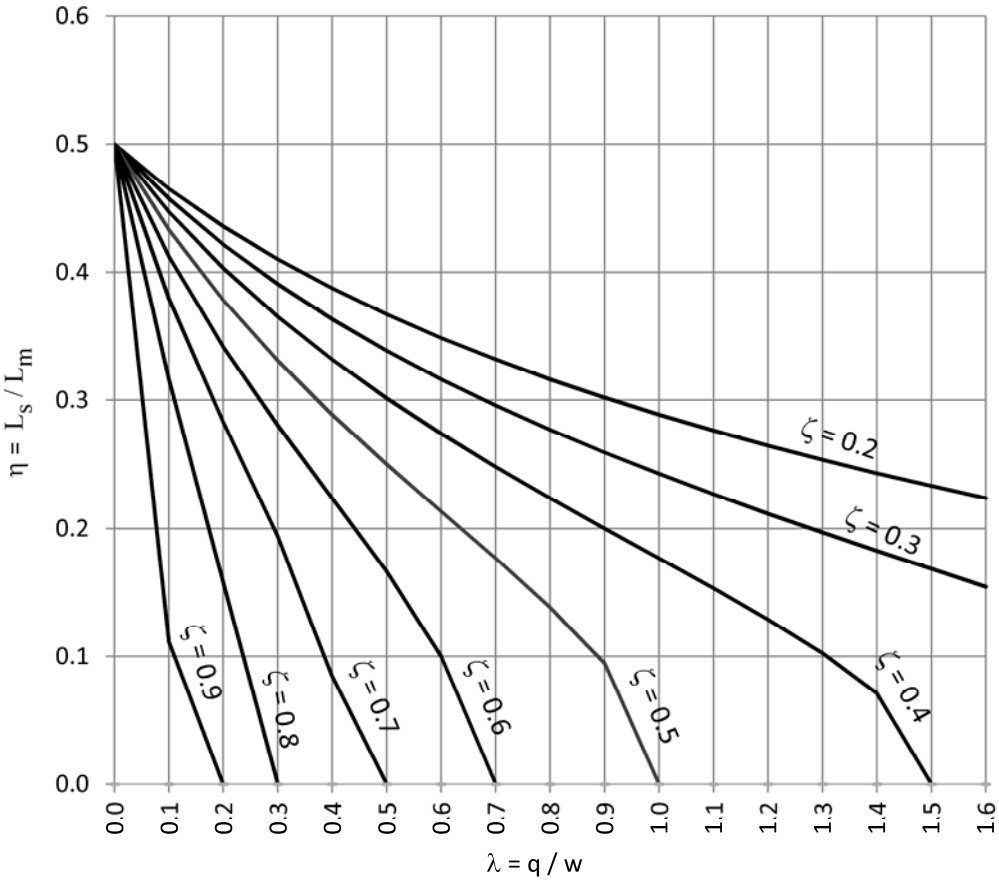

fig. 2.33: Relationship between the ratio of the side span and the main span η & the ratio between the live load and the dead load λ [Gimsing and Georgakis 2011]

From the above equations and diagram the following can be observed:

- For a specific ratio between the side span and the main span length η, the ratio between the minimum and maximum backstay forces decreases with the increase of the ratio between the live load and the dead load. The above diagram shows that for $\eta = 0.3$, ζ decreases from approximately 0.8 to 0.2, if λ increases from 0.1 to 0.9.
- For a specific ratio of λ, ζ decreases with the increase of η. In case λ is equal to 0.3 for example and it is not desired to reduce ζ below 0.3, η can not be made greater than 0.4.
- As it is known from the previous experience that λ for cable-stayed bridges with concrete and steel deck is equal to approximately 0.2 and 0.4 respectively, therefore, if it is desired to ensure that ζ will not be less than 0.25, it will be necessary to ensure that η will not be more than 0.42 for a bridge with a concrete deck and not more than 0.37 for a bridge with a steel deck.

It has to be noted further that it is generally desired by the bridge designer to ensure that the backstay forces/stresses will not be reduced below a specific value as the stay cable stress reduction will lead to higher sag and consequently undesired reduction of the stay cable elastic modulus as will be explained later in this Section. It should also be kept in mind that the above equations 2.1 to 2.5 and fig. 2.33 have been derived with the assumptions that the dead and live loads are uniformly distributed along the main span and the side span lengths. It was assumed also that the stay cables have the fan shape and the deck of the side span is not supported at any intermediate supports. In case one or more of the assumptions made are not applicable, the above equations and diagram will not be valid and it may be necessary to derive similar equations for the bridge under consideration.

Stiffness of Stay Cables:

The stay cables under dead load take a catenary form. Due to the sag of the stay cables under dead load, the effective elastic modulus E_{eff} will be less than the elastic modulus for the stay cables steel material E_0. If the cables are simulated as straight elements in a computer model, say with truss elements, a modulus of elasticity $E_{eff} < E_0$, should be used especially in case the cable is too long (refer to fig. 2.34). E_{eff} is influenced by the self weight of cable in addition to its length and force. The effective elastic modulus E_{eff} can be calculated from the following equation known as Ernst formula [Walter et al. 1999]:

$$E_{eff} = E_0 \frac{1}{1 + \frac{\gamma^2 L_h^2 E_0}{12 \sigma^3}} \qquad (2.6)$$

where:

E_{eff} = the effective elastic modulus in [N/mm^2]

E_0 = the elastic modulus of the stay cable material in the absence of the sag effect [N/mm^2]

γ = the specific weight of the stay cable material in [N/mm^3]

L_h = the projected stay cable length in plan in [mm]

σ = the axial stress of the cable in [N/mm^2]

The above equation shows that the stay cable stiffness increases with the third power of the steel stress and decreases with the second power of the projected stay cable length in plan due to the sag effect. Fig. 2.34 presents equation 2.6 graphically assuming that the values of E_0 and γ are equal to 195000 N/mm^2 and 0.00008 N/mm^3 respectively.

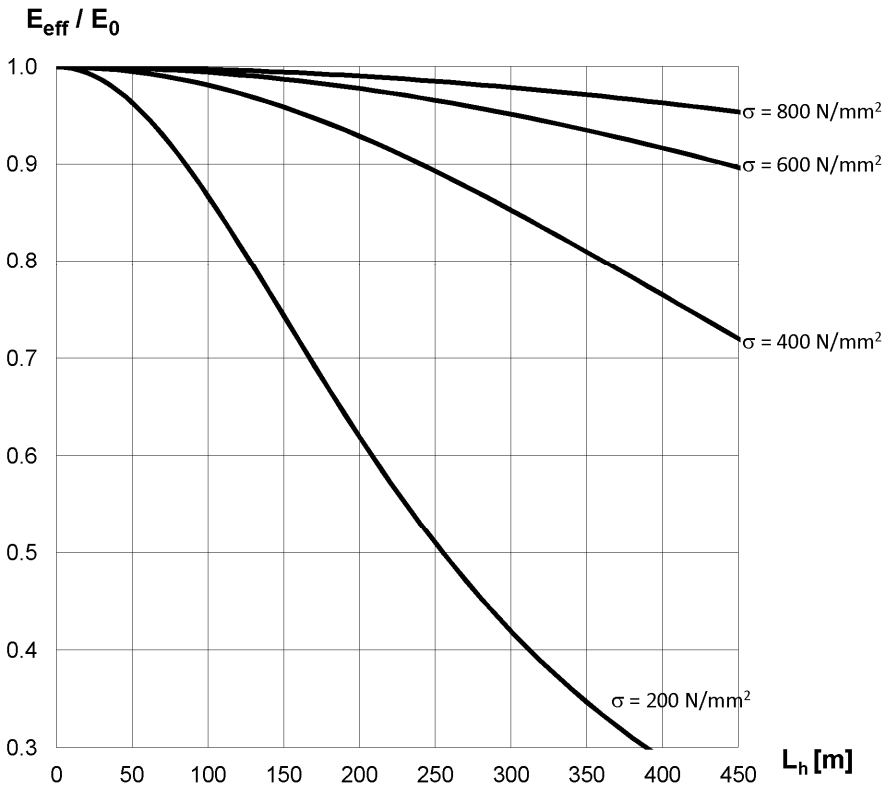

fig. 2.34: Effect of the stay cable sag on its effective elastic modulus [Walter et al. 1999] [Freyssinet 1999]

CHAPTER 3

3- PREVIOUS RESEARCH WORKS FOR CABLES-STAYED BRIDGES RELATED TO THE RECOMMENDED STAY CABLE FORCES UNDER DEAD LOAD

Several research works and scientific papers have dealt with the optimum method for the determination of the stay cable forces under dead load. The outcome of these research works may be summarized by the following three methods:

- The continuous beam method:

  This method is suitable for use for cable-stayed bridges with concrete decks. It will be explained within Section 3-1 that the use of this method will help to eliminate the creep effect of the concrete material, on the stay cable forces.

- The "bending moment envelope for live loads" method:

  This method is recommended for cable-stayed bridges with steel decks as the steel material does not creep [Svensson 2012]. It will be presented within Section 3-2.

- The "influence matrix for stay cable forces" method:

  This is a general method used basically to achieve any desired stay cable forces, specific desired bending moment distribution along the deck length or specific desired profile for the deck elements as will be explained in Section 3-3. The new proposed approach in Chapter 6 for the determination of the stay cable forces under dead load for extradosed bridges, is based on this method.

3-1 The continuous beam method

The stay cable forces for the completed structure of the cable-stayed bridges with concrete decks, under uniform or variable dead load, can be determined by the continuous beam method [Schlaich 2001] [Svensson 2012]. The dead load is applied on an imaginary continuous beam resting on rigid supports at the locations of the stay cable anchorages (fig. 3.1). The vertical reaction force R_i at the imaginary rigid support is calculated and used to determine the desired stay cable forces for the completed bridge under dead load F_{Di} , from the following formula:

$$F_{Di} = \frac{R_i}{\sin(\theta_i)} \tag{3.1}$$

The back stay forces should be determined in such a way that they will indirectly support the central part of the main span which is not balanced by the side span. The stay cable forces at the central part of the main span should be calculated from equation (3.1) and the back stay forces should be determined with the condition that their horizontal components will be equal to the horizontal components of the corresponding stay cable forces of the main span. By following this method of calculation, the bending moments in the pylons can be avoided.

The achievement of such stay cable forces will lead to the bending moment, shear and normal forces distributions shown in fig. 3.1 (in case the dead load is assumed to be uniform along the entire bridge length). The bending moment distribution shown in fig. 3.1 helps to eliminate the effect of creep and therefore the achieved desired alignment will remain unchanged with the passage of time. This will be clarified further in Section 3-1-1 by studying the effect of creep on a simple beam subjected to a uniformly distributed load and end nodal bending moments. In addition the effect of creep on a continuous beam subject to uniformly distributed loads will be discussed under section 3-1-2.

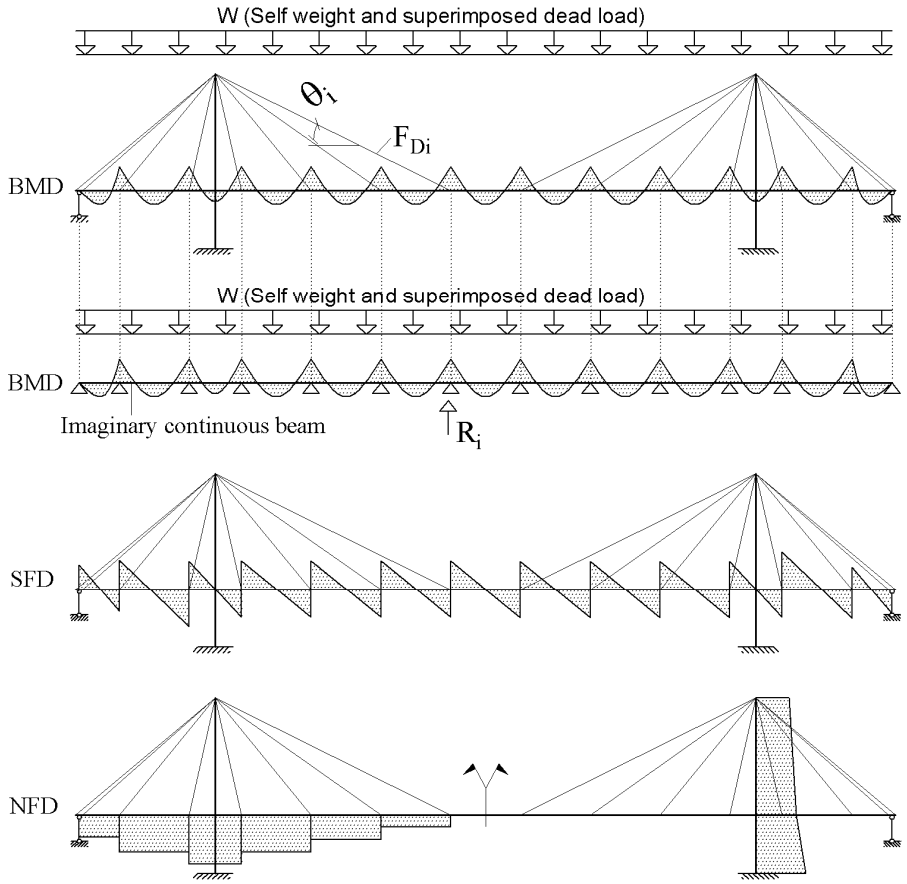

fig. 3.1: Desired bending moments, shear and normal force distributions under dead load, for cable-stayed bridges with concrete deck sections

As an alternative to the use of equation (3.1) the desired stay cable forces F_{Di} may be also obtained by modeling the whole structure including the stay cables. By the assignment of imaginary high values of the cross sectional areas for the beam elements of the pylon, deck and the truss elements of the stay cables (i.e. by making them very stiff), the stay cable forces resulting from the application of the dead load W, will be equal to the desired stay cable forces F_{Di} directly.

3-1-1 Effect of creep on a simple concrete beam

Creep of the concrete material occurs normally due to a constant load/stress introduced at time t_1 and sustained for a time period (t_2-t_1) [fig. 3.2 (a) and (b)]. As shown in fig. 3.2(b), the instantaneous elastic shortening ε_{el} takes place due to the applied stress σ at time t_1. If the applied stress σ is sustained for a period of time (t_2-t_1), the concrete material will suffer additional creep strain ε_{cr} .

The effect of creep on a simple concrete beam subject to "permanent" uniform distributed load W and "permanent" nodal end bending moments M, is shown in fig. 3.2 (c) to (l). The uniform load W shown in fig. 3.2 (c) leads to the bending moment distribution and the elastic deflection line shown in figs. 3.2 (d) and (e) respectively. If the uniform load W remains acting on the beam, the deflection line of the beam will move downwards with the passage of time due to creep of the concrete material as shown with the dotted line in fig. 3.2 (e). Similarly, the beam under the permanent nodal loads M will deflect upwards elastically first and the deflection line will move upwards with the passage of time due to creep of the concrete material [refer to figs. 3.2 (f) to (h)]. The absolute values for the angle of rotations $|\theta_w|$ and $|\theta_m|$ of the elastic deflection lines at the supports due to the uniform and the nodal loads W and M, may be calculated from the following equations:

$$\theta_w = \frac{W L^3}{24 E_c I} \tag{3.2}$$

$$\theta_m = \frac{M L}{2 E_c I} \tag{3.3}$$

where E_c is the elastic modulus of the concrete material and I is the moment of inertia of the beam cross section.

Now, if the permanent uniform and nodal loads W and M are applied on the concrete beam simultaneously as shown in fig. 3.2 (i), the resulting elastic deflection line will be the sum of the elastic lines shown in figs. 3.2 (e) and (h) and its final shape will be dependent on the magnitudes of W and M. It can easily be concluded that in case the absolute value of |M| is less than the absolute value of $|WL^2/12|$ (i.e. in case $|\theta_w| > |\theta_m|$), the beam will tend to creep downwards as shown in fig. 3.2(j) and will creep upwards in case |M| is greater than $|WL^2/12|$ (i.e. in case $|\theta_w| < |\theta_m|$) as shown in fig. 3.2(l). In case $|M| = |WL^2/12|$ (i.e. case $|\theta_w| = |\theta_m|$), the resultant elastic rotation at the supports will be equal to zero and will not be affected by creep. However, the beam elements between the end supports will continue to creep and the sum of the elastic and creep deflection at the middle of the beam will be equal to:

$$\Delta Z_{el+cr} = \frac{(1+\phi)}{E_c I}\left(\frac{1}{8} M L^2 - \frac{5}{384} W L^4\right) \tag{3.4}$$

where ϕ is the creep coefficient.

As the simple beam is a determinate structure, the rotation of the beam will not be restrained and the bending moment distribution due to the uniform load W in fig. 3.2 (d) or due to the nodal bending moment M in fig 3.2 (g) will not be affected by creep.

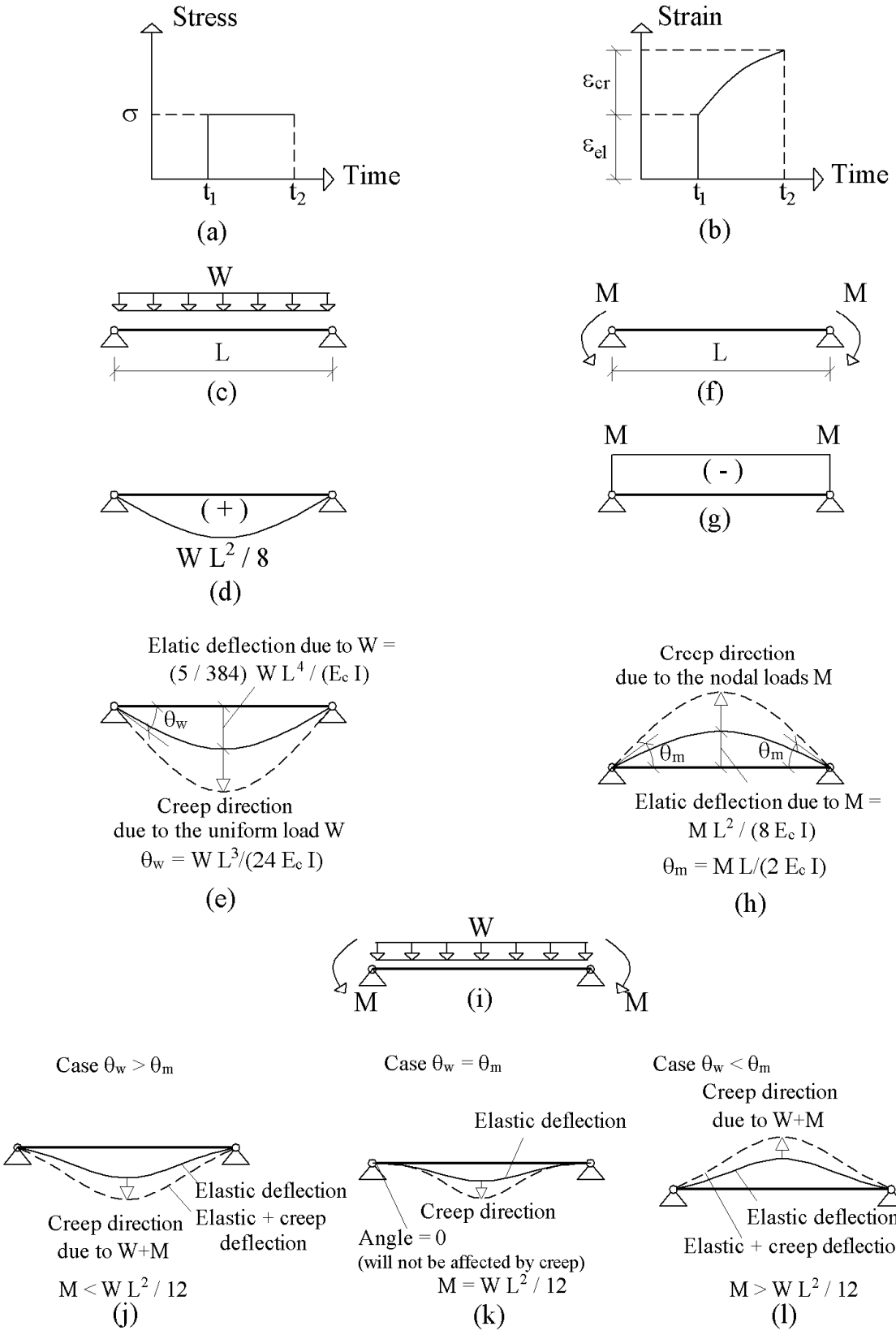

fig. 3.2: Creep effect on a simple concrete beam

3-1-2 Effect of creep on a continuous concrete beam

The effect of creep on a simple beam under the uniform dead load W and the end nodal bending moments M as explained under Section 3-1-1 will ease the understanding of the creep effect on a continuous beam under uniform dead loads which will be explained in this Section. Further, the creep effect on a continuous beam will help to understand the creep effect on a cable-stayed bridge.

The method of calculations of the bending moments and deflections of a continuous beam due to the creep effect, will be explained in this Section.

Fig. 3.3(a) shows a continuous beam with "n+1" nos. of spans under permanent uniform dead loads equal to W_1, W_2, …., W_{n+1} . The moment of inertias of the beam cross sections are assumed to be equal to I_1, I_2, …., I_{n+1} . For the calculations of the bending moments M_1 to M_n at the internal supports "i to n" shown in fig. 3.3(b), the beam segments nos. i and "i+1" are first separated as shown in fig. 3.3 (c) where the continuity of the beam segment is replaced by couples of hog bending moments at their ends. The achievement of the compatibility condition between the beam segment no. i and the beam segment no. i+1, under the dead loads W_i and W_{i+1}, requires that the angle of rotation of the elastic deflection line on both sides of the internal support no. i, must be equal (i.e. $\theta_{iL} = \theta_{iR}$). Accordingly, the following equations may be written:

$$\theta_{iL} = \frac{-W_i L_i^3}{24 E_c I_i} + \frac{-M_{i-1} L_i}{6 E_c I_i} + \frac{-M_i L_i}{3 E_c I_i}$$

$$\theta_{iR} = \frac{W_{i+1} L_{i+1}^3}{24 E_c I_{i+1}} - \frac{-M_i L_{i+1}}{3 E_c I_{i+1}} - \frac{-M_{i+1} L_{i+1}}{6 E_c I_{i+1}}$$

$$\frac{-W_i L_i^3}{24 E_c I_i} - \frac{M_{i-1} L_i}{6 E_c I_i} - \frac{M_i L_i}{3 E_c I_i} = \frac{W_{i+1} L_{i+1}^3}{24 E_c I_{i+1}} + \frac{M_i L_{i+1}}{3 E_c I_{i+1}} + \frac{M_{i+1} L_{i+1}}{6 E_c I_{i+1}} \qquad (3.5)$$

Note: The above equations have been written based on the assumption that the hog bending moments have negative values and that the angles of rotation of the beam axis are positive in the clockwise direction.

The rearrangement of equation (3.5) leads to the following equation:

$$-\left(\frac{M_{i-1} L_i}{6 I_i} + \frac{M_i L_i}{3 I_i} + \frac{M_i L_{i+1}}{3 I_{i+1}} + \frac{M_i L_{i+1}}{6 I_{i+1}} \right) = \frac{W_i L_i^3}{24 I_i} + \frac{W_{i+1} L_{i+1}^3}{24 I_{i+1}} \qquad (3.6)$$

Equation 3.6 may be translated into a matrix form for the entire continuous beam as follows:

$$\begin{pmatrix} \frac{L_1}{3I_1}+\frac{L_2}{3I_2} & \frac{L_2}{6I_2} & 0 & 0 & 0 & 0 & 0 \\ \frac{L_2}{6I_2} & \frac{L_2}{3I_2}+\frac{L_3}{3I_3} & \frac{L_3}{6I_3} & 0 & 0 & 0 & 0 \\ .... & .... & .... & .... & .... & .... & .... \\ 0 & 0 & \frac{L_i}{6I_i} & \frac{L_i}{3I_i}+\frac{L_{i+1}}{3I_{i+1}} & \frac{L_{i+1}}{6I_{i+1}} & 0 & 0 \\ .... & .... & .... & .... & .... & .... & .... \\ 0 & 0 & 0 & 0 & \frac{L_{n-1}}{6I_{n-1}} & \frac{L_{n-1}}{3I_{n-1}}+\frac{L_n}{3I_n} & \frac{L_n}{6I_n} \\ 0 & 0 & 0 & 0 & 0 & \frac{L_n}{6I_n} & \frac{L_n}{3I_n}+\frac{L_{n+1}}{3I_{n+1}} \end{pmatrix} \begin{pmatrix} M_1 \\ M_2 \\ .... \\ M_i \\ ... \\ M_{n-1} \\ M_n \end{pmatrix} = - \begin{pmatrix} \frac{W_1 L_1^3}{24I_1}+\frac{W_2 L_2^3}{24I_2} \\ \frac{W_2 L_2^3}{24I_2}+\frac{W_3 L_3^3}{24I_3} \\ .... \\ \frac{W_i L_i^3}{24I_i}+\frac{W_{i+1} L_{i+1}^3}{24I_{i+1}} \\ ... \\ \frac{W_{n-1} L_{n-1}^3}{24I_{n-1}}+\frac{W_n L_n^3}{24I_n} \\ \frac{W_n L_n^3}{24I_n}+\frac{W_{n+1} L_{n+1}^3}{24I_{n+1}} \end{pmatrix} \tag{3.7}$$

The solution of equation (3.7) provides the bending moments at the internal supports M_1, M_2, …, M_n shown in fig. 3.3 (b). Accordingly, the angles of rotations θ_1 to θ_n at the internal supports 1 to n for the elastic deflection line shown in fig. 3.3(d) can be determined from the following equation:

$$\theta_{1\ldots n} = \begin{pmatrix} \frac{-W_1 L_1^3}{24 E_c I_1}-\frac{M_1 L_1}{3 E_c I_1} \\ \frac{-W_2 L_2^3}{24 E_c I_2}-\frac{M_1 L_2}{6 E_c I_2}-\frac{M_2 L_2}{3 E_c I_2} \\ .... \\ \frac{-W_i L_i^3}{24 E_c I_i}-\frac{M_{i-1} L_i}{6 E_c I_i}-\frac{M_i L_i}{3 E_c I_i} \\ ... \\ \frac{-W_{n-1} L_{n-1}^3}{24 E_c I_{n-1}}-\frac{M_{n-2} L_{n-1}}{6 E_c I_{n-1}}-\frac{M_n L_{n-1}}{3 E_c I_{n-1}} \\ \frac{-W_n L_n^3}{24 E_c I_n}-\frac{M_{n-1} L_n}{6 E_c I_n}-\frac{M_n L_n}{3 E_c I_n} \end{pmatrix} \tag{3.8}$$

Further, the elastic vertical deflection at the middle of each beam segment z_{c1} to $z_{c(n+1)}$ can be calculated from the following equation (noting that the downward deflection is considered negative):

$$z_{c1\ldots c(n+1)} = \begin{pmatrix} \dfrac{-5\,W_1\,L_1^4}{384\,E_c\,I_1} - \dfrac{M_1\,L_1^2}{16\,E_c\,I_1} \\ \dfrac{-5\,W_2\,L_2^4}{384\,E_c\,I_2} - \dfrac{M_1\,L_2^2}{16\,E_c\,I_2} - \dfrac{M_2\,L_2^2}{16\,E_c\,I_2} \\ .... \\ \dfrac{-5\,W_i\,L_i^4}{384\,E_c\,I_i} - \dfrac{M_{i-1}\,L_i^2}{16\,E_c\,I_i} - \dfrac{M_i\,L_i^2}{16\,E_c\,I_i} \\ ... \\ \dfrac{-5\,W_n\,L_n^4}{384\,E_c\,I_n} - \dfrac{M_{n-1}\,L_n^2}{16\,E_c\,I_n} - \dfrac{M_n\,L_n^2}{16\,E_c\,I_n} \\ \dfrac{-5W_{n+1}\,L_{n+1}^4}{384\,E_c\,I_{n+1}} - \dfrac{M_n\,L_{n+1}^2}{16\,E_c\,I_{n+1}} \end{pmatrix} \qquad (3.9)$$

In fig. 3.3, it is assumed that the dead loads W_1 to W_{n+1} are applied simultaneously on the continuous beam segments. The instantaneous elastic deflection of the continuous beam will take the shape shown in fig. 3.3(d). Assuming now that the creep coefficients for the beam segments are equal to ϕ_1 to ϕ_{n+1}, the effect of creep can be determined by separating the beam segments as shown in fig. 3.3 (e). The separation of the beam segments to statically determinate simple beams means that they can rotate freely at the internal supports without being restrained. The compatibility condition requires however that the bending moments ΔM_{i-1} , ΔM_i , ΔM_{i+1} at the internal supports (i-1), (i) and (i+1) should be applied to ensure that the angles of rotation on both side of any internal support i remain equal (i.e. $\phi_i\ \theta_i + \Delta\theta_{iL} = \phi_i\ \theta_i - \Delta\theta_{iR}$) [refer to fig. 3.3(e)]. Accordingly, the following equation may be written:

$$\Delta\theta_{iL} = \frac{-\Delta M_{i-1}\,L_i}{6\,E_c\,I_i} + \frac{-\Delta M_i\,L_i}{3\,E_c\,I_i} \quad , \quad \Delta\theta_{iR} = -\frac{-\Delta M_i\,L_{i+1}}{3\,E_c\,I_{i+1}} - \frac{-\Delta M_{i+1}\,L_{i+1}}{6\,E_c\,I_{i+1}}$$

$$\phi_i\,\theta_i - \frac{\Delta M_{i-1}\,L_i}{6\,E_c\,I_i} - \frac{\Delta M_i\,L_i}{3\,E_c\,I_i} = \phi_{i+1}\,\theta_i + \frac{\Delta M_i\,L_{i+1}}{3\,E_c\,I_{i+1}} + \frac{\Delta M_{i+1}\,L_{i+1}}{6\,E_c\,I_{i+1}} \qquad (3.10)$$

where:

$\Delta\theta_{iL}$ = the change in the angle θ_i (calculated by using equation 3.8) due to ΔM_{i-1} and ΔM_i [refer to fig. 3.3 (e)]

$\Delta\theta_{iR}$ = the change in the angle θ_i due to ΔM_i and ΔM_{i+1} [refer to fig. 3.3 (e)]

The rearrangement of equation (3.10) leads to the following equation:

$$-\left(\frac{L_i}{6\,E_c\,I_i}\Delta M_{i-1}+\left(\frac{L_i}{3\,E_c\,I_i}+\frac{L_{i+1}}{3\,I_{i+1}}\right)\Delta M_i+\frac{L_{i+1}}{6\,E_c\,I_{i+1}}\Delta M_{i+1}\right)=\phi_{i+1}\,\theta_i-\phi_i\,\theta_i \tag{3.11}$$

Equation 3.11 may be translated into a matrix form for the entire continuous beam as follows:

$$\begin{pmatrix}
\frac{L_1}{3E_cI_1}+\frac{L_2}{3E_cI_2} & \frac{L_2}{6E_cI_2} & 0 & 0 & 0 & 0 & 0\\
\frac{L_2}{6E_cI_2} & \frac{L_2}{3E_cI_2}+\frac{L_3}{3E_cI_3} & \frac{L_3}{6E_cI_3} & 0 & 0 & 0 & 0\\
.... & .... & .... & .... & .... & .... & ....\\
0 & 0 & \frac{L_i}{6E_cI_i} & \frac{L_i}{3E_cI_i}+\frac{L_{i+1}}{3E_cI_{i+1}} & \frac{L_{i+1}}{6E_cI_{i+1}} & 0 & 0\\
.... & .... & .... & .... & .... & .... & ....\\
0 & 0 & 0 & 0 & \frac{L_{n-1}}{6E_cI_{n-1}} & \frac{L_{n-1}}{3E_cI_{n-1}}+\frac{L_n}{3E_cI_n} & \frac{L_n}{6E_cI_n}\\
0 & 0 & 0 & 0 & 0 & \frac{L_n}{6E_cI_n} & \frac{L_n}{3E_cI_n}+\frac{L_{n+1}}{3E_cI_{n+1}}
\end{pmatrix}
\begin{pmatrix}\Delta M_1\\ \Delta M_2\\ ....\\ \Delta M_i\\ ...\\ M_{n-1}\\ \Delta M_n\end{pmatrix}=-\begin{pmatrix}\phi_2\theta_1-\phi_1\theta_1\\ \phi_3\theta_2-\phi_2\theta_2\\ ....\\ \phi_{i+1}\theta_i-\phi_i\theta_i\\ ...\\ \phi_n\theta_{n-1}-\phi_{n-1}\theta_{n-1}\\ \phi_{n+1}\theta_n+\phi_n\theta_n\end{pmatrix} \tag{3.12}$$

The solution of equation (3.12) provides the <u>additional</u> bending moment at the internal supports ΔM_1, ΔM_2, …, ΔM_n [refer to fig. 3.3 (e)] due to the creep effect.

Accordingly, the <u>additional</u> angles of rotations $\Delta\theta_1$ to $\Delta\theta_n$ at the internal supports 1 to n and the <u>additional</u> vertical deflections Δz_{c1} to $\Delta z_{c(n+1)}$ at the middle of the span segments 1 to n+1 due to the creep effect, can be determined from the following equations:

$$\Delta\theta_{1\ldots n}=\begin{pmatrix}
\phi_1\,\theta_1-\frac{\Delta M_1\,L_1}{3\,E_c\,I_1}\\
\phi_2\,\theta_2-\frac{\Delta M_1\,L_2}{6\,E_c\,I_2}-\frac{\Delta M_2\,L_2}{3\,E_c\,I_2}\\
....\\
\phi_i\,\theta_i-\frac{\Delta M_{i-1}\,L_i}{6\,E_c\,I_i}-\frac{\Delta M_i\,L_i}{3\,E_c\,I_i}\\
...\\
\phi_{n-1}\,\theta_{n-1}-\frac{\Delta M_{n-2}\,L_{n-1}}{6\,E_c\,I_{n-1}}-\frac{\Delta M_n\,L_{n-1}}{3\,E_c\,I_{n-1}}\\
\phi_n\,\theta_n-\frac{\Delta M_{n-1}\,L_n}{6\,E_c\,I_n}-\frac{\Delta M_n\,L_n}{3\,E_c\,I_n}
\end{pmatrix} \tag{3.13}$$

Note: θ_1 to θ_n are to be determined from equation (3.8)

$$\Delta z_{c1\ldots c(n+1)} = \begin{pmatrix} \phi_1 Z_{c1} - \dfrac{\Delta M_1 L_1^2}{16 E_c I_1} \\ \phi_2 Z_{c2} - \dfrac{\Delta M_1 L_2^2}{16 E_c I_2} - \dfrac{\Delta M_1 L_2^2}{16 E_c I_2} \\ .... \\ \phi_i Z_{ci} - \dfrac{\Delta M_{i-1} L_i^2}{16 E_c I_i} - \dfrac{\Delta M_i L_i^2}{16 E_c I_i} \\ ... \\ \phi_n Z_{cn} - \dfrac{\Delta M_{n-1} L_n^2}{16 E_c I_n} - \dfrac{\Delta M_n L_n^2}{16 E_c I_n} \\ \phi_{n+1} Z_{c(n+1)} - \dfrac{\Delta M_n L_{n+1}^2}{16 E_c I_{n+1}} \end{pmatrix} \quad (3.14)$$

Note: z_{c1} to $z_{c(n+1)}$ are to be determined from equation (3.9)

Case of a continuous beam with constant creep coefficient:

In the special case where the creep coefficient for all beam segments are equal, the values of all elements of the matrix on the right hand side of equation (3.12) will be equal to zero. Accordingly, the solution of equation (3.12) in this particular case will require that ΔM_1 to ΔM_n must be equal to zero. This means that the creep will not lead to any change of the bending moments. From equations (3.13) and (3.14), the additional deflection line of the beam due to creep will be affine with the elastic deflection line and the affinity factor will be equal to the creep coefficient. This case is comparable with the results of the bending moment calculations for the continuous beam shown in fig. 3.3(a) if the moment of inertias of the beam cross section are reduced by a constant factor. The bending moments shown in fig. 3.3(b) will remain unchanged but the elastic deflection line shown in fig. 3.3(d) will be scaled up based on the said reduction factor of the moment of inertias. A further study for the effect of creep on continuous beams leads to the conclusion that in case only one span of the continuous beam creeps, bending moments will be induced in the entire length of the continuous beam. Fig. 3.3(f) shows the bending moment distribution resulting from the creep of the beam segment between the internal supports (i) and (i+1) only. This case may be experienced in practice if for example one span of the continuous beam is built out of concrete while all other spans are built with steel or if one

span is built with in-situ concrete while all other spans are built with relatively old precast concrete segments.

The above study of the effect of creep on continuous beam highlights the benefit of selecting the stay cable forces to get the deck to behave as a continuous beam as if there were rigid supports at the anchorage points of each stay cable at the deck level. The benefit of using precast segmental construction with low uniform creep coefficients and uniform elastic modulus, can be also understood from the above explanation.

Going back to fig. 3.1, it can be understood that the downward creep which would have taken place for each deck segment due to the dead load W is counterbalanced by the upward creep due to the selected stay cable forces using the continuous beam method. It should be further noted that the desired results shown in fig. 3.1, will be more accurately obtained if the compression elements of the deck and the pylons are built longer to compensate the axial elastic shortening due to the normal forces and to compensate in addition the axial shortening resulting from the time dependent creep and shrinkage effects. For further clarifications on the use of the continuous beam method for the determination of the desired stay cable forces under dead load, refer to the numerical example under Appendix A.

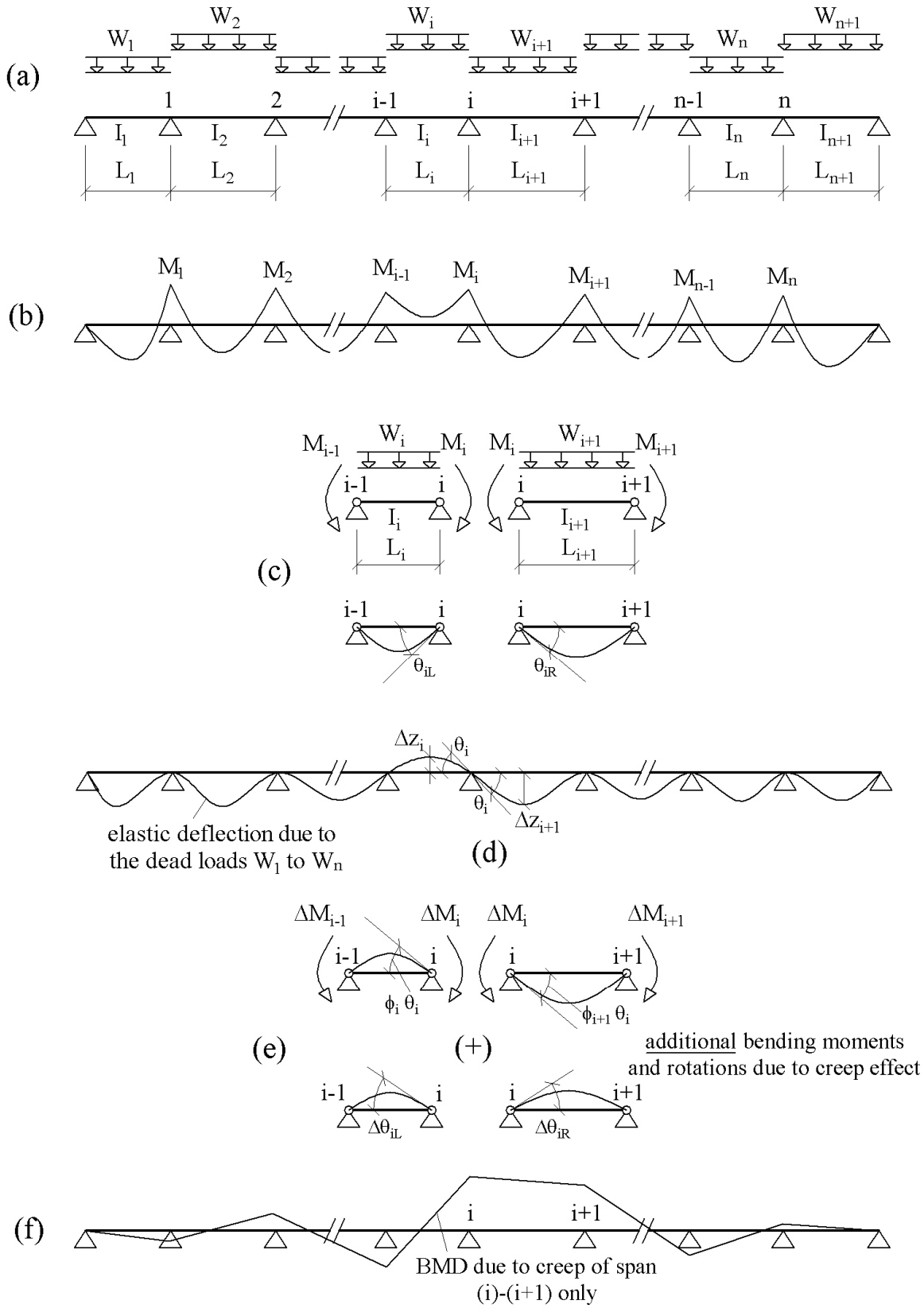

fig. 3.3: Creep effect on a continuous concrete beam

After the calculation of the theoretical desired stay cable forces by the continuous beam method, it will be explained hereafter how to achieve these desired forces in reality. At the time of the stay cable installation during construction, the structural system will be different from the structural system of the completed bridge and the acting loads are different from the dead load at end of construction. Therefore, it is necessary for the achievement of the desired end results for the completed structure under dead load, to install the stay cables "to length". This means that the unstressed length of the stay cable at the time of installation should be equal to the unstressed length of the stay cable for the completed structure. From fig. 3.1, the unstressed length L_{ui} for any cable may be calculated by using the following formula:

$$L_{ui} = \frac{L_i}{(1+\varepsilon_i)} = \frac{L_i}{\left(1+\frac{F_{Di}}{E_s\ A_{si}}\right)} \qquad (3.15)$$

where:

L_i = the stressed length of the stay cable i, in the completed structure configuration, at time infinity (when all creep and shrinkage effects have taken place)

F_{Di} = the desired stay cable force under dead load at time infinity

ε_i = is the elastic strain of the stay cable under the effect of the cable force F_{Di}

A_{si} = the cross sectional area of the stay cable i.

The installation of the stay cable "to length" as per formula 3.15 will help to achieve the desired stay cable forces at time infinity under dead load and the bending moment distribution shown in fig. 3.1. Further, the installation of the stay cables "to length" provides the contractor with the flexibility to:

- Select any of the construction methods shown in fig. 3.4 which would suit the prevailing site conditions, the available construction tools/equipments and the available labor expertise.
- Adopt any construction sequence for the deck, pylon elements and stay cables installation as long as the adopted sequence would have no adverse effect on the integrity of the structure. The contractor would also be able to change the previously planned construction sequence at a later stage during construction due to any unforeseen reasons, if the need arises.
- Change the temporary construction loads, like weights of cranes, erection machines, cable coils etc. if deemed necessary provided that the adequacy of the structural elements will be checked at all construction stages.
- Introduce and remove of temporary trestles and/or temporary stay cables wherever required.

(a) Balanced cantilever method - Rion Antirion bridge in Greece [http://en.structurae.de]

(b) Progressive placement method (Sungai Prai bridge in Malaysia)

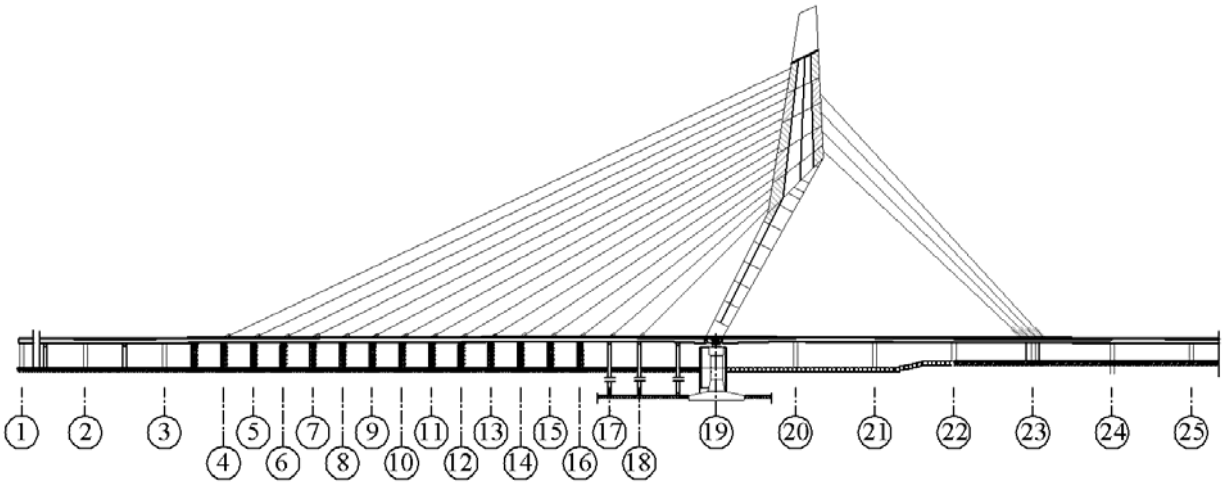

(c) Deck construction on scaffolding (Wazirabad bridge in India)

fig 3.4: Common construction methods for cable-stayed bridges

3.2 The "bending moment envelope for live loads" method

The continuous beam method explained above for the determination of the stay cable forces at time infinity under dead load, is considered by many bridge designers as the best method for cable-stayed bridges with concrete deck cross sections. This is because the achieved bending moment distribution, as mentioned above, helps to reduce the creep effect and the related change in the bridge alignment. For cable-stayed bridges with steel deck cross sections, the continuous beam method may not be the best method from the economic point of view as stated by H. Svensson [Svensson 2012]. Fig. 3.5 (a) shows the typical envelope of bending moment distribution due to live loads for the conventional cable-stayed-bridges. H. Svensson

recommended to use the continuous beam method only in case of concrete deck section. Accordingly, the behavior of the concrete deck under the dead and live loads would follow fig. 3.5 (b). In case the deck is made of steel section and because the steel deck does not creep, the behavior of the deck under the dead and live loads should follow fig. 3.5 (c).

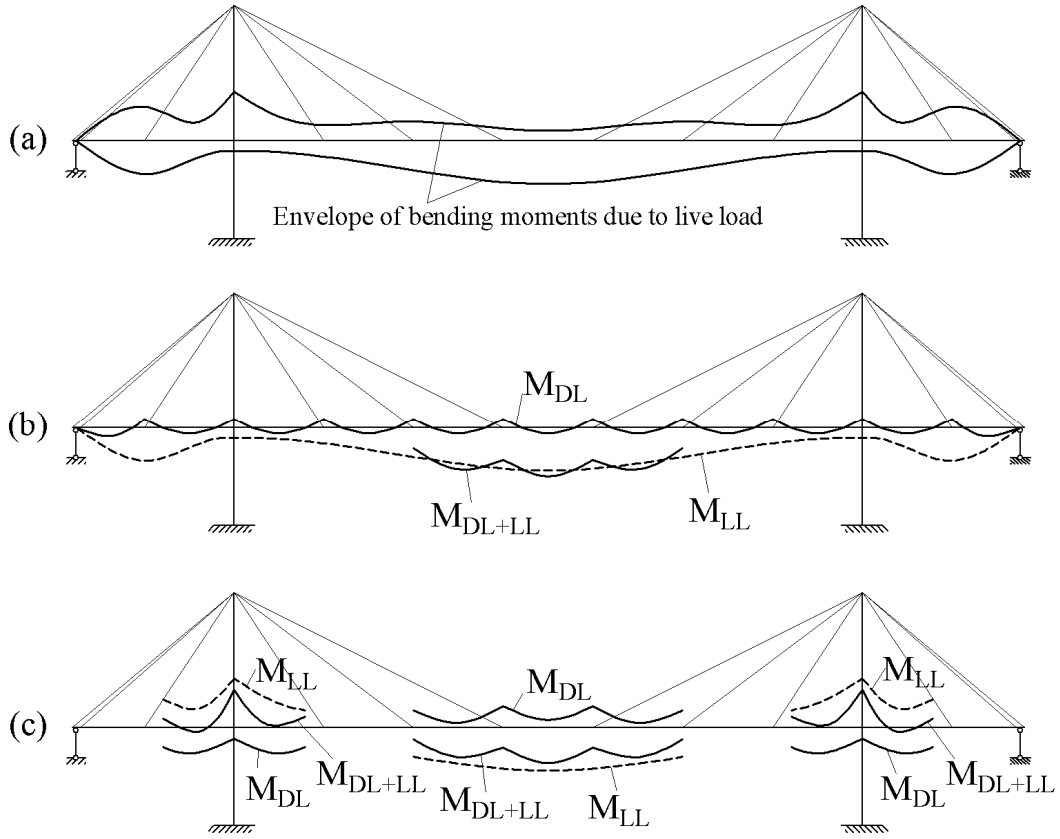

fig 3.5: Effect of the live load on the selection of the stay cable forces under dead load [Svensson 2012]

By comparing figs. 3.5 (b) and (c), it can be concluded that the approach proposed by H. Svensson leads to an economical solution for the steel deck as the required bending moment capacity of the steel deck section will be less than the maximum bending moment resulting from the live loads. It should however be noted that the deck elements will have to precambered to counter the deflection associated with the creation of M_{DL} shown in fig. 3.5(c). Further, this method leads to higher stay cable forces and consequently higher stay cable quantities as compared with the corresponding stay cable forces and quantities resulting from the method of the continuous beam method [fig. 3.5(b)]. The achieved saving in the deck material cost should, therefore, be compared with the extra cost of the stay cable material, if the method proposed by H. Svensson is followed.

3.3 The method of influence matrix for stay cable forces

The modern versions of the commercial computer soft-ware for bridges analysis/design, may be used to target specific desired stay cable forces, specific bending moment distribution or to eliminate the deflection of the deck under dead load at the anchorage points of the stay cables [Gabrow 2004] [Pedrozzi 2004].

The stay cable force [fig 3.6 (a)] of cable no. i under dead load is assumed to be equal to F_i (as calculated by the computer model prior to the application of any shortening of the stay cables). The desired stay cable force [fig. 3-6 (b)] under dead load is assumed to be equal to F_{Di} which may simply desired to be equal to [Ws / sin (θ_i)]. By using the computer model, it is possible to calculate the force in any stay cable resulting from tensioning the stay cable no. i by a force equal to 1. By repeating this exercise for all of the n-nos. of cables, the following equation can be written (noting that the square matrix on the left hand side of this equation with its size n x n is called the influence matrix for stay cable forces):

$$\begin{pmatrix} f_{11} & f_{12} & \dots & f_{1i} & \dots & f_{1(n-1)} & f_{1n} \\ f_{21} & f_{22} & \dots & f_{2i} & \dots & f_{2(n-1)} & f_{2n} \\ \dots & \dots & \dots & \dots & \dots & \dots & \dots \\ f_{j1} & f_{j2} & \dots & f_{ji} & \dots & f_{j(n-1)} & f_{jn} \\ \dots & \dots & \dots & \dots & \dots & \dots & \dots \\ f_{(n-1)1} & f_{(n-1)2} & \dots & f_{(n-1)i} & \dots & f_{(n-1)(n-1)} & f_{(n-1)n} \\ f_{n1} & f_{n2} & \dots & f_{nj} & \dots & f_{n(n-1)} & f_{nn} \end{pmatrix} \begin{pmatrix} \Delta F_1 \\ \Delta F_2 \\ \dots \\ \Delta F_j \\ \dots \\ \Delta F_{(n-1)} \\ \Delta F_n \end{pmatrix} = \begin{pmatrix} F_{D1} - F_1 \\ F_{D2} - F_2 \\ \dots \\ F_{Dj} - F_j \\ \dots \\ F_{D(n-1)} - F_{(n-1)} \\ F_{Dn} - F_n \end{pmatrix} \qquad (3.16)$$

where (refer also to fig. 3.6):

n = total nos. of stay cables

F_{Di} = desired stay cable force for the cable no. i under dead load

F_i = stay cable force of the cable no. i under dead load prior to the shortening /re-stressing of any stay cable by the forces ΔF_i

F_{ji} = force in stay cable no. j due to tensioning the stay cable no. i by a force equal to 1 [fig. 3.6 (c)]

ΔF_i = required re-stressing force for the stay cable no. i

The solution of equation (3.16) provides the necessary re-stressing or de-sstressing forces ΔF_1 to ΔF_n. Upon the completion of the re-stressing or de-stressing of all stay cables by the forces ΔF_1 to ΔF_n, the stay cable force in cable no. i, for example, will be equal to the desired force F_{Di}.

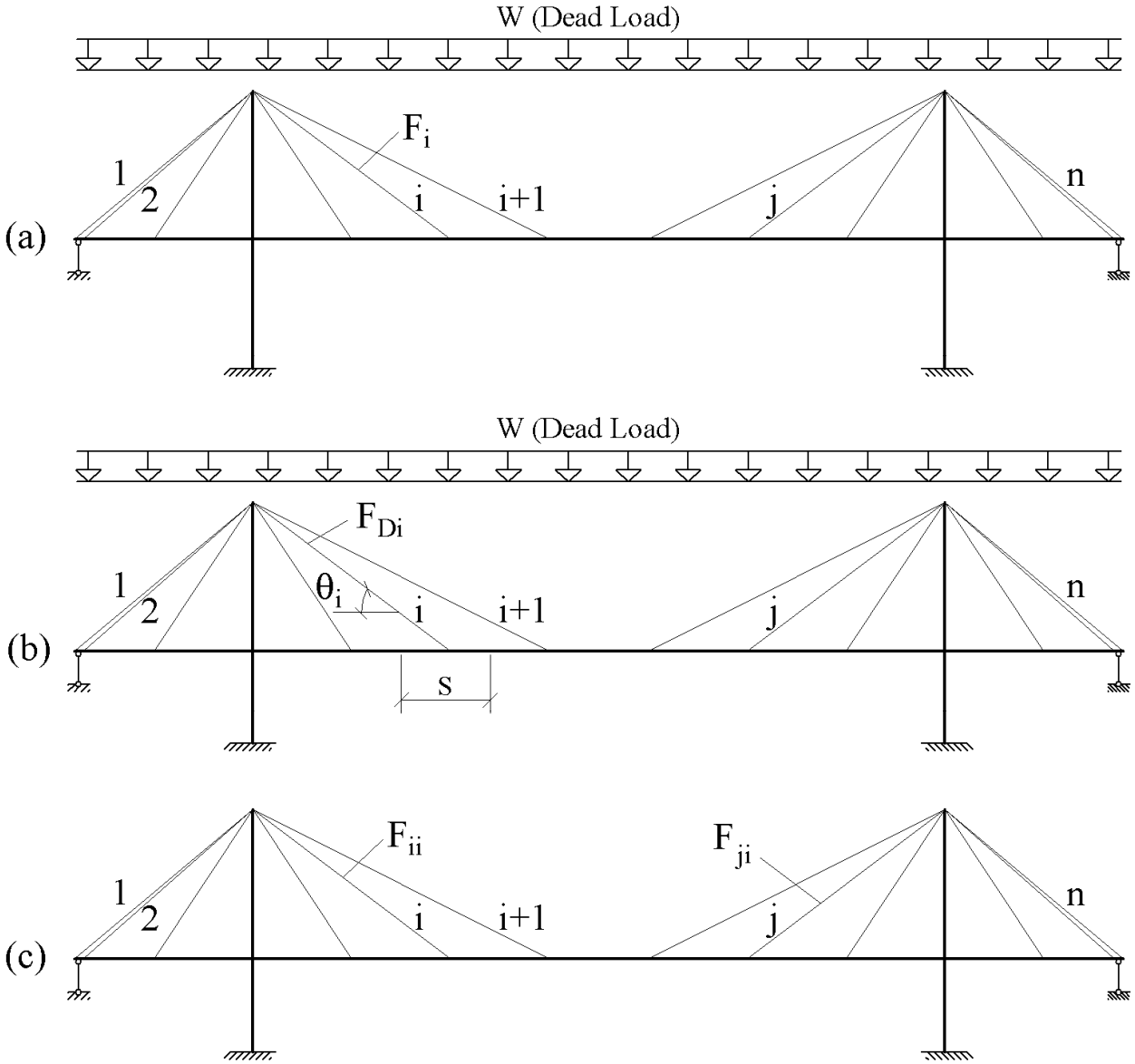

fig 3.6: Application of the "influence matrix for stay cable forces" method to achieve specific desired stay cable forces under dead load

The "influence matrix for stay cable forces" method can also be used to achieve specific desired bending moment distribution. In fig 3.7 (a), the bending moment distribution under dead load is calculated by the computer (prior to the application of any shortening of the stay cables). The

desired bending moment M_{Di} at the anchorage point of stay cable no. i, for example, may be calculated by hand from the following simple formula [refer also to fig. 3.7(b)]:

$$M_{Di} = \frac{W s^2}{12} \tag{3.17}$$

To allow the bending moment distribution shown in fig 3.7 (a) to be changed to the desired bending moment distribution shown in fig. 3.7 (b), the stay cables should be re-stressed or de-stressed by the forces ΔF_1 to ΔF_n, which may be determined by the following equation:

$$\begin{pmatrix} M_{11} & M_{12} & \dots & M_{1i} & \dots & M_{1(n-1)} & M_{1n} \\ M_{21} & M_{22} & \dots & M_{2i} & \dots & M_{2(n-1)} & M_{2n} \\ \dots & \dots & \dots & \dots & \dots & \dots & \dots \\ M_{j1} & M_{j2} & \dots & M_{ji} & \dots & M_{j(n-1)} & M_{jn} \\ \dots & \dots & \dots & \dots & \dots & \dots & \dots \\ M_{(n-1)1} & M_{(n-1)2} & \dots & M_{(n-1)i} & \dots & M_{(n-1)(n-1)} & M_{(n-1)n} \\ M_{n1} & M_{n2} & \dots & M_{ni} & \dots & M_{n(n-1)} & M_{nn} \end{pmatrix} \begin{pmatrix} \Delta F_1 \\ \Delta F_2 \\ \dots \\ \Delta F_j \\ \dots \\ \Delta F_{(n-1)} \\ \Delta F_n \end{pmatrix} = \begin{pmatrix} M_{D1} - M_1 \\ M_{D2} - M_2 \\ \dots \\ M_{Dj} - M_j \\ \dots \\ M_{D(n-1)} - M_{(n-1)} \\ M_{Dn} - M_n \end{pmatrix} \tag{3.18}$$

where:

M_{ji} = the bending moment at the anchorage point of stay cable no. j due to tensioning the stay cable no. i by a force equal to 1 [fig. 3.7 (c)]

F_i = stay cable force for the cable no. i due to dead load [loading configuration of fig. 3.7 (a)]

ΔF_i = required re-stressing or de-stressing force for the stay cable no. i, to achieve the desired bending moment distribution shown in fig. 3.7 (b) (upon the completion of the re-stressing or de-stressing of all stay cables by the forces ΔF_1 to ΔF_n the bending moment at the anchorage point of stay cable no. i, for example, will be equal to the desired bending moment M_{Di})

M_i = bending moment at the anchorage point of stay cable no. i due to dead load [loading configuration of fig. 3.7 (a)]

M_{Di} = desired bending moment at the anchorage point of stay cable no. i due to dead load [fig. 3.7 (b)]

The "influence matrix for stay cable forces" method can also be used to target a specific vertical profile for the deck. Fig. 3.8 (a) shows the deflection line of the deck under dead load as calculated by the computer (prior to the application of any shortening of the stay cables). The

desired vertical profile of the deck under dead load is shown in fig 3.8 (b) where the vertical deflection at the anchorage points of the stay cables are equal to zero.

To allow the vertical profile shown in fig 3.8 (a) to be changed to the desired vertical profile shown in fig. 3.8 (b), the stay cable forces should be re-stressed or de-stressed by the forces ΔF_1 to ΔF_n, which may be determined by the following equation:

$$\begin{pmatrix} Z_{11} & Z_{12} & \cdots & Z_{1i} & \cdots & Z_{1(n-1)} & Z_{1n} \\ Z_{21} & Z_{22} & \cdots & Z_{2i} & \cdots & Z_{2(n-1)} & Z_{2n} \\ \cdots & \cdots & \cdots & \cdots & \cdots & \cdots & \cdots \\ Z_{j1} & Z_{j2} & \cdots & Z_{ji} & \cdots & Z_{j(n-1)} & Z_{jn} \\ \cdots & \cdots & \cdots & \cdots & \cdots & \cdots & \cdots \\ Z_{(n-1)1} & Z_{(n-1)2} & \cdots & Z_{(n-1)i} & \cdots & Z_{(n-1)(n-1)} & Z_{(n-1)n} \\ Z_{n1} & Z_{n2} & \cdots & Z_{ni} & \cdots & Z_{n(n-1)} & Z_{n\,n} \end{pmatrix} \begin{pmatrix} \Delta F_1 \\ \Delta F_2 \\ \cdots \\ \Delta F_j \\ \cdots \\ \Delta F_{(n-1)} \\ \Delta F_n \end{pmatrix} = \begin{pmatrix} \Delta Z_1 \\ \Delta Z_2 \\ \cdots \\ \Delta Z_j \\ \cdots \\ \Delta Z_{(n-1)} \\ \Delta Z_n \end{pmatrix} \qquad (3.19)$$

where:

Z_{ji} = the vertical deflection at the anchorage point of stay cable no. j due to tensioning the stay cable no. i by a force equal to 1 [fig. 3.8 (c)]

F_i = stay cable force for the cable no. i due to dead load [loading configuration of fig. 3.8 (a)]

Z_i = the vertical deflection at the anchorage point i due to dead load [loading configuration of fig. 3.8 (a)]

ΔZ_i = $0.0 - Z_i$

ΔF_i = required re-stressing or de-stressing force for stay cable i, to achieve the desired vertical profile shown in fig. 3.8 (b) (upon the completion of the re-stressing or de-stressing of all stay cables by the forces ΔF_1 to ΔF_n, the deflection of the deck at the anchorage points of the stay cables will be equal to 0.0 as shown in fig. 3.8(b)

From the above explanation, it can be concluded that “influence matrix for stay cable forces” method may be used to achieve combinations of desired stay cable forces, desired bending moments and desired deformations at specific locations. The nos. of the desired stay cable forces, bending moments and deflections (i.e. the nos. of the unknowns), should however be equal to the nos. of the stay cables n.

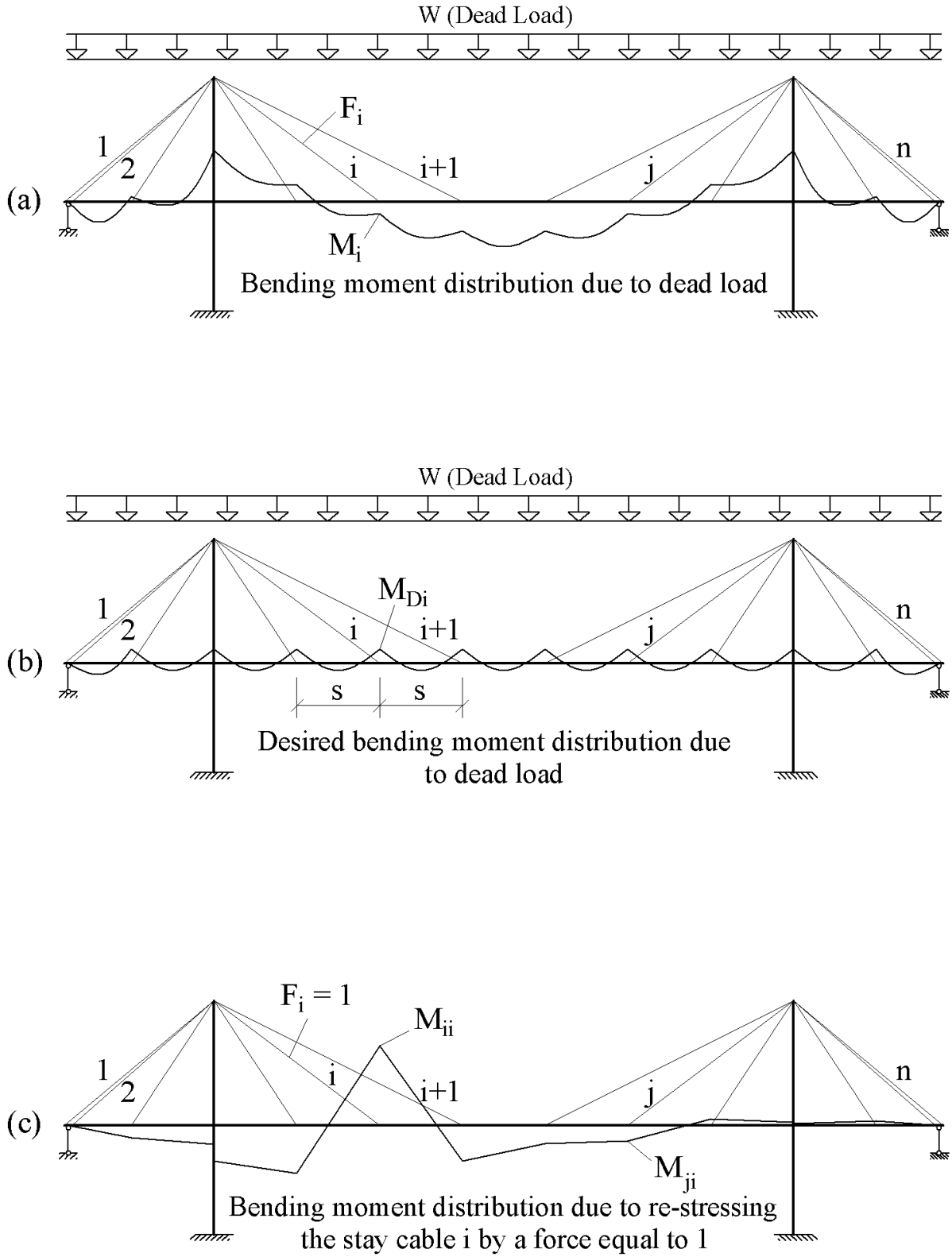

fig 3.7: Application of the "influence matrix for stay cable forces" method to achieve a specific desired bending moment distribution along the deck length under dead load

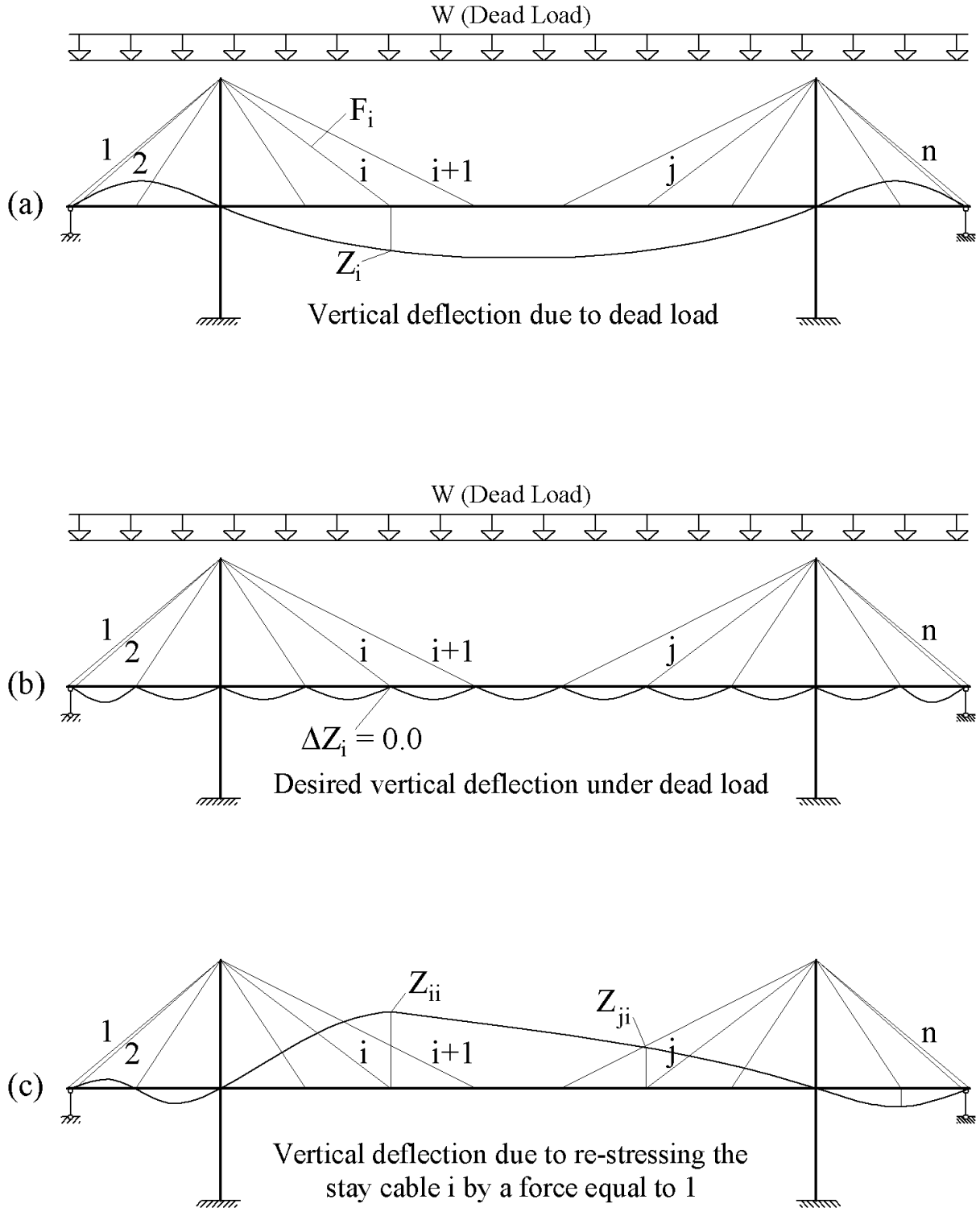

fig 3.8: Application of the "influence matrix for stay cable forces" method to achieve a specific desired vertical profile for the deck under dead load

CHAPTER 4

4- CONSTRUCTION ANALYSIS OF BRIDGES WITH COMPOSITE DECKS

As explained in Chapter 3 the stay cables for conventional cable-stayed bridges with concrete decks are normally installed in such a way that the deck under dead load will not deflect vertically. Accordingly, the bending moment distribution along the deck length will be similar to the bending moment distribution of a continuous beam on rigid supports and, therefore, the effect of creep is eliminated and the achieved desired alignment does not change with time. The stay cables may then be installed to predetermined unstressed lengths L_u to achieve the desired alignment and the desired bending moment distribution under dead load regardless of the construction method/sequence.

For bridges with composite deck cross sections (concrete/concrete or steel/concrete), the installation of the cables to predetermined lengths, similar to the case of conventional cable-stayed bridges with concrete-only sections or steel-only sections, does not lead necessarily to the desired forces and alignment under dead load. The achievement of the desired results will be influenced by the time dependant forces due to the creep and shrinkage effects of the concrete parts of the composite section as will be explained in Section 4-1.

It will be also illustrated within sections 4-2 and 4-3 that the desired results will be dependent on the method of construction of the composite section (i.e. whether the components of the composite section will be constructed in a single stage or two stages) and the ratio of the moment of inertia of the first part of the composite section I_s to the moment of inertia of the total composite section I_{comp}. Further, the desired results will depend on the vertical shift "e" between the center of gravity of the first part of the composite section and the center of gravity of the total composite section.

A practical method will be proposed in Section 4-3, which may be followed during the design stage and during construction, to ensure the achievement of the desired results for the completed bridge at time infinity taking into account the effects of the ratio "I_s / I_{comp}", the vertical shift e and the time dependant forces due to creep and shrinkage of the concrete material.

4-1 Time dependent effects on bridge structures with composite decks

For bridge structures with composite decks, the following two types of the time dependent effects should be studied to achieve the desired forces and alignment under dead load for the completed bridge:

- Time dependent forces and deformations due to the creep effect resulting from the vertical dead load and the vertical components of the stay cable forces (Type I).
- Additional time dependent effect resulting from the creep and shrinkage of the concrete elements of the composite section. Restraining this type of creep and shrinkage by the non-concrete elements of the composite section, leads to internal eccentric horizontal forces within the composite section elements and consequently result in a change in the stay cable forces and leads also to vertical deformation of the bridge structure. This type of creep and shrinkage effect will be referred to as time dependant effect (Type II).

The extent/magnitudes of the creep and shrinkage strains for any time interval Δt depend mainly on the following parameters [Ghali and Favre 1994]:

- The characteristic compressive strength of concrete at the age of 28-days.
- The relative humidity of the ambient environment.
- The notional size of the deck section which is equal to twice the cross sectional area of the deck section divided by the perimeter in contact with atmosphere.
- Type of cement used for the concrete mix.
- Age of concrete at the beginning of shrinkage.
- Age of concrete at the time of first loading.

4-1-1 Time dependent effect due to vertical loads (Type I)

If the stay cable forces under dead load F_{Di} [fig. 4.1 (a)] are selected in such a way that the vertical component of each stay cable force [$F_{Di} \sin(\theta_i)$] is equal to the corresponding vertical reaction force R_i for an equivalent imaginary continuous beam fig. 4.1 (b), the creep effect due to the combination of the dead load and the vertical components of the selected stay cable forces, at the anchorage points of the stay cables will be eliminated [refer to the deck profile shown in fig. 4.1 (c)]. In case [$F_{Di} \sin(\theta_i)$] is selected higher than the reaction force R_i , the deck profile for the completed bridge will be similar to that shown in fig. 4.1 (d) and the level of the anchorage points

of the stay cables will change with time. Fig. 4.1 (e) shows the deck profile and the direction of the creep effect in case [F_{Di} sin (θ_i)] is selected less than R_i.

4-1-2 Additional time dependent effect in case of a composite deck (Type II)

In case of a steel/concrete composite section, the creep and shrinkage of the concrete part of the composite section will be restrained by the steel part and internal eccentric horizontal forces will, therefore, be induced in the composite section. The internal restraint will also take place in case of concrete/concrete composite section if the concrete components are of different ages and different loading histories.

For a composite deck cross section consisting of a steel beam and a concrete slab as that shown in fig. 4.2 (a) and if the normal force distribution "NFD" acting on the deck is similar to that shown in fig. 4.2 (b), the concrete slab will tend to creep and shrink and internal eccentric horizontal forces will be induced between the elements of the composite section accordingly. The creep and shrinkage strains of the concrete material ($\varepsilon_{C\text{-}cr}$ and $\varepsilon_{C\text{-}sh}$) for each deck element can be estimated from the normal force distribution shown in fig. 4.2 (b) and also from the above mentioned factors affecting the extent of creep and shrinkage.

Based on the estimated values of ($\varepsilon_{C\text{-}cr}$ and $\varepsilon_{C\text{-}sh}$)$_i$ for each deck element, the creep and shrinkage effects of the concrete elements of the composite section may be replaced by a normal compression force N_{ri} acting at the centre of gravity of the concrete section. The value of N_{ri} may be determined from the following equation:

$$N_{ri} = \left(\varepsilon_{C-cr} + \varepsilon_{C-sh}\right)_i E_C \, B \, t \qquad (4.1)$$

where B and t are the width and the thickness of the concrete slab and E_c is the elastic modulus of the concrete material.

If the bridge ends are assumed to be fully restrained against the movement and rotation as shown in fig. 4.2 (c) and the internal compression force N_{ri} is applied on the deck elements at the center of gravity of the concrete slab, the reaction forces at the imaginary end supports at the level of the center of gravity of the composite section will be equal to N_r (tension force) and M_r (hog bending moment), noting that M_r can be calculated from the following equation [Iles 1989]:

$$M_r = N_r \, e_C \qquad (4.2)$$

where e_C is the vertical distance between the centre of gravity of the concrete slab and the centre of gravity of the composite section.

Consequently, the reaction forces N_r and M_r are to be applied as nodal loads in a reversed direction at the ends of the real structure. Fig 4.2 (d) shows the expected bending moment distribution along the deck length resulting from the reversed forces N_r and M_r in case the stay cables are assumed very stiff (act as rigid supports and do not allow the deck to deflect vertically at the anchorage points). In case the stay cables are assumed very soft, the bending moment distribution resulting from the reversed forces N_r and M_r will follow the diagram shown in fig. 4-2 (e). In reality the bending moment distribution will lie between the diagrams shown in figs. 4.2 (d) and 4-2 (e) depending on the actual stiffness of the stay cables. For the BMDs. shown in figs. 4.2(d) and (e), it is important to note that the actual values of the bending moments which the deck will suffer, are the moments measured from the dotted lines as a datum.

It can be understood from the above explanation that the time dependent effect (type II) lead to additional bending moments along the full length of the bridge deck. Consequently, the deck profile and the stay cable forces will be affected. If the stay cable forces and the structure deformations, due to the time dependant effect type II, can be accurately estimated/calculated, they should be counterbalanced by additional re-stressing or des-stressing of the cables and precambering the deck elements during the form finding process in the design stage (refer to the numerical example in Appendix B for further clarification).

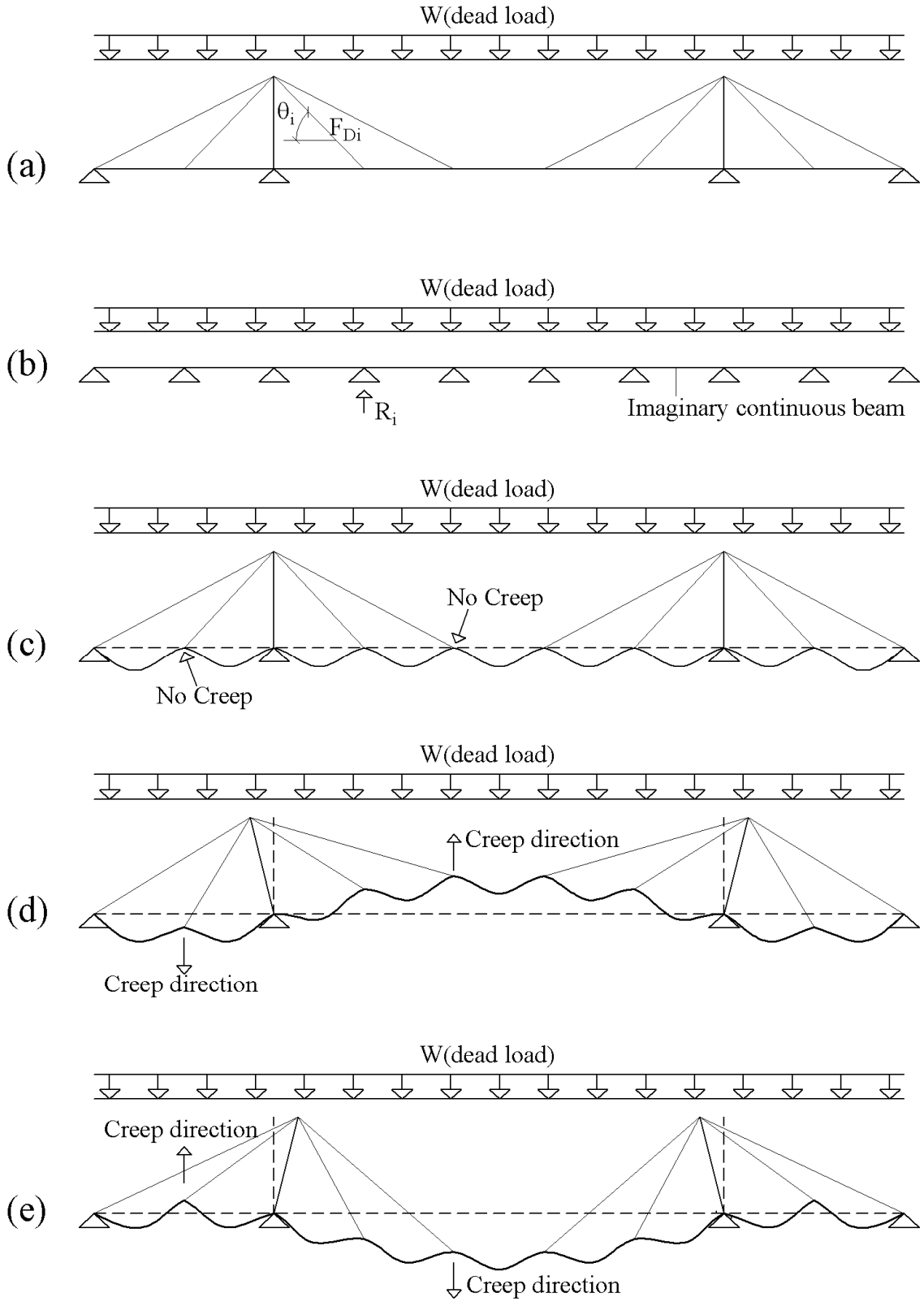

fig. 4.1: Time dependent effect due to vertical loads (Type I)

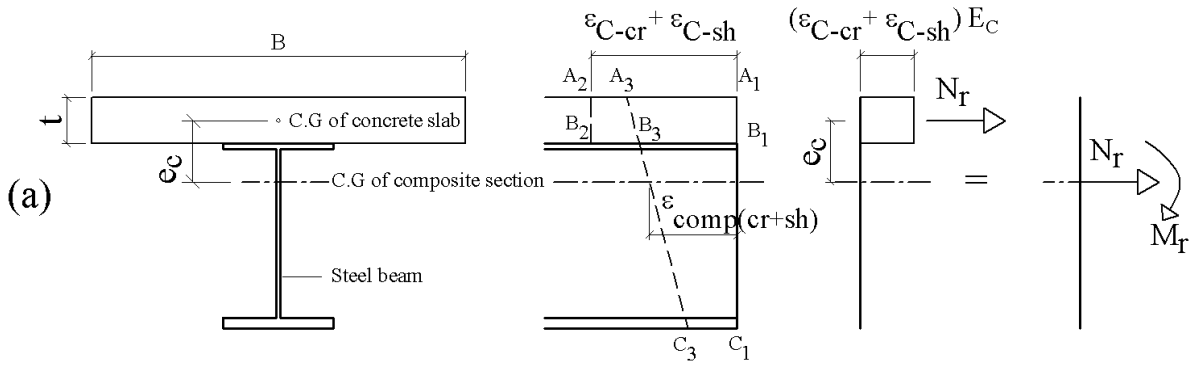

Note: $A_1 B_1$ would move to $A_2 B_2$ if the concrete slab is not restrained by the steel element. Due to the composite action between the concrete slab and the steel element, $A_1 B_1 C_1$ will move to $A_3 B_3 C_3$ under the effect of shrinkage and creep of the concrete slab.

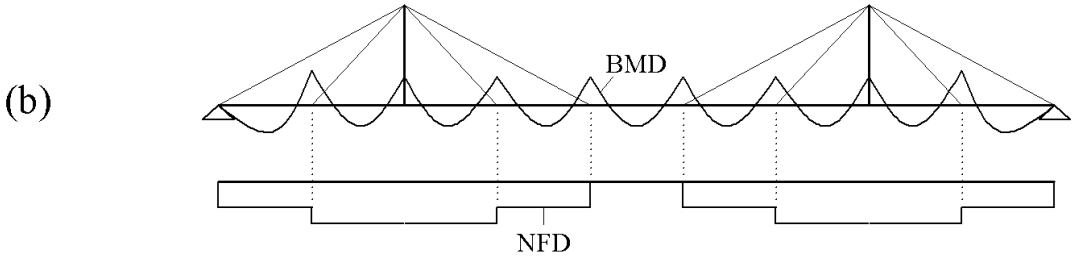

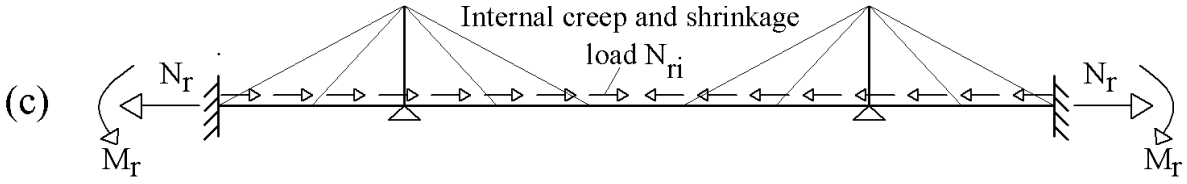

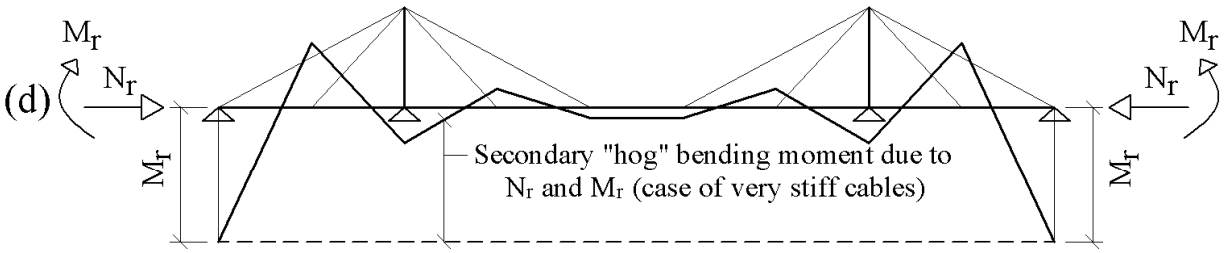

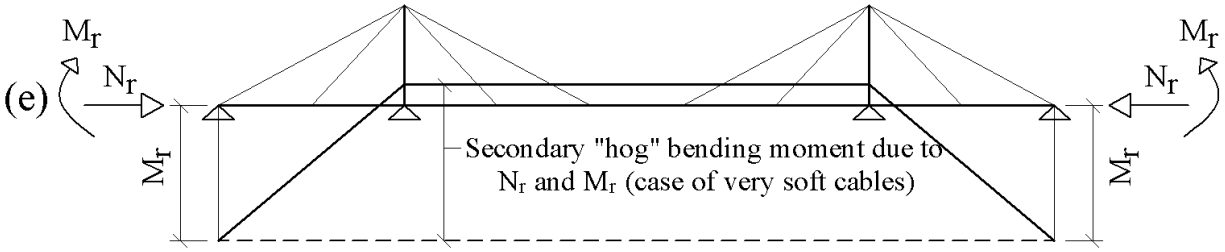

fig. 4.2: Additional time dependent effect in case of composite deck (Type II)

4-2 Construction stage analysis of cable-stayed bridges with concrete-only or steel-only deck section

For cable-stayed bridges with deck cross sections made of concrete-only, it is normally recommended to install the stay cables to specific predetermined unstressed lengths L_{ui} (fig. 4.3) so that a bending moment distribution is achieved, similar to that shown within fig. 3.1. By installing the individual stay cables to the calculated "unstressed length" L_{ui} as per the formula shown in fig. 4.3 (c) and by constructing every new deck and pylon segment tangential to the previously constructed segment, the desired alignment and forces for the completed structure under dead load can be obtained provided that the integrity of the structure is examined at each construction stage. It is also to note that the deck and pylon elements/segments have to be built longer to compensate the elastic axial shortening due to the normal forces shown within fig. 3.1 and to compensate also the axial shortening due to the time dependant forces resulting from the shrinkage and creep effects.

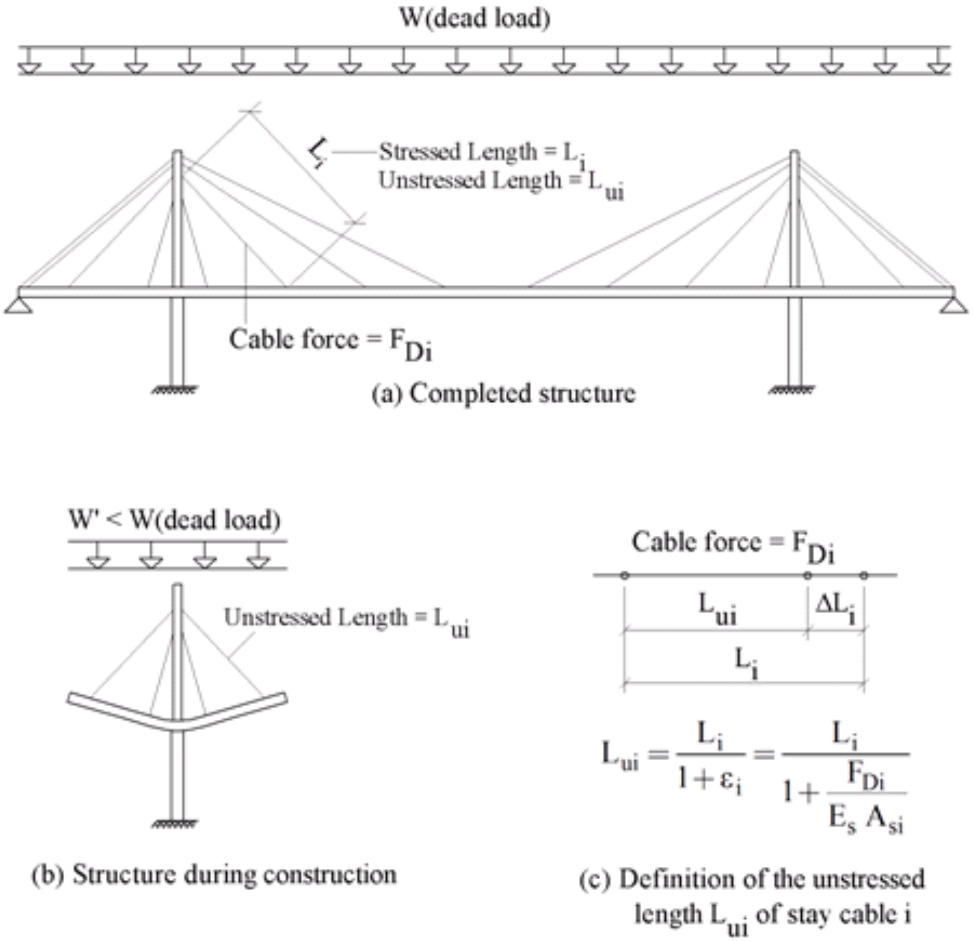

fig. 4.3: Installation of stay cables to "length"

4-3 Construction stage analysis for cable-stayed bridges with composite deck sections

Four construction methods for cable-stayed bridges with composite decks will be discussed in sections 4-3-1 and 4-3-2

4-3-1 Construction of the composite section in one single stage (Construction method no. 1)

In this method the composite section properties of the deck elements/segments are achieved on the ground before erection. This method was implemented for the multi-span Rion Antirion cable-stayed bridge in Greece (figs. 4.4 and 4.5).

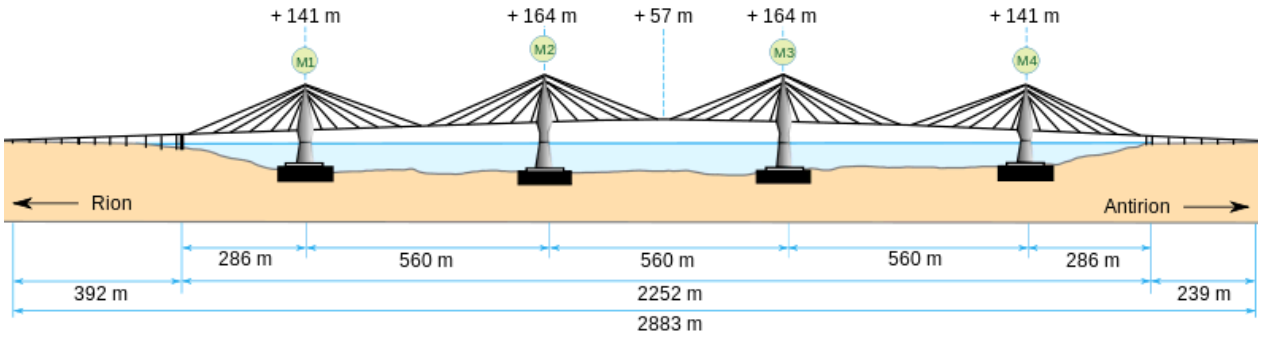

fig. 4.4: Rion Antirion bridge in Greece (completed in 2004) [http://en.wikipedia.org]

fig. 4.5: Rion Antirion bridge during construction [http://en.structurae.de]

If the construction method no. 1 for the composite deck cross section is implemented and the stay cables are installed to the unstressed length L_{ui} [refer to fig. 4.3 (c)], which is based on the desired stay cable forces F_{Di} obtained by the continuous beam method, only the time dependent effect (Type I) will be avoided. To achieve the desired stay cable forces and the desired bending

moment distribution, similar to that shown within fig. 3.1, the time dependent effect (Type II) has to be taken into account (refer to Section 4.1). The stay cable forces will have to be re-stressed or de-stressed to eliminate the changes resulting from the time dependent effect (Type II). The deformations resulting from the time dependant effect (type II) should also be accounted for during the calculations of the required precamber for the deck and the pylon elements (refer also to Appendix B).

The construction method no. 1 described above, cannot always be implemented as they require cranes with heavy lifting capacities which are very often not available. Many contractors prefer to handle the components of the composite sections (steel + concrete) or (concrete + concrete) separately as shown in figs. 1.2 and 1.3.

If the components of the composite section are to be constructed in two stages, three construction methods may be investigated which will be referred to as construction methods 2, 3 and 4 to differentiate them from the above described construction method no. 1.

4-3-2 Construction of the composite cross section in two stages (Construction methods nos. 2,3 and 4)

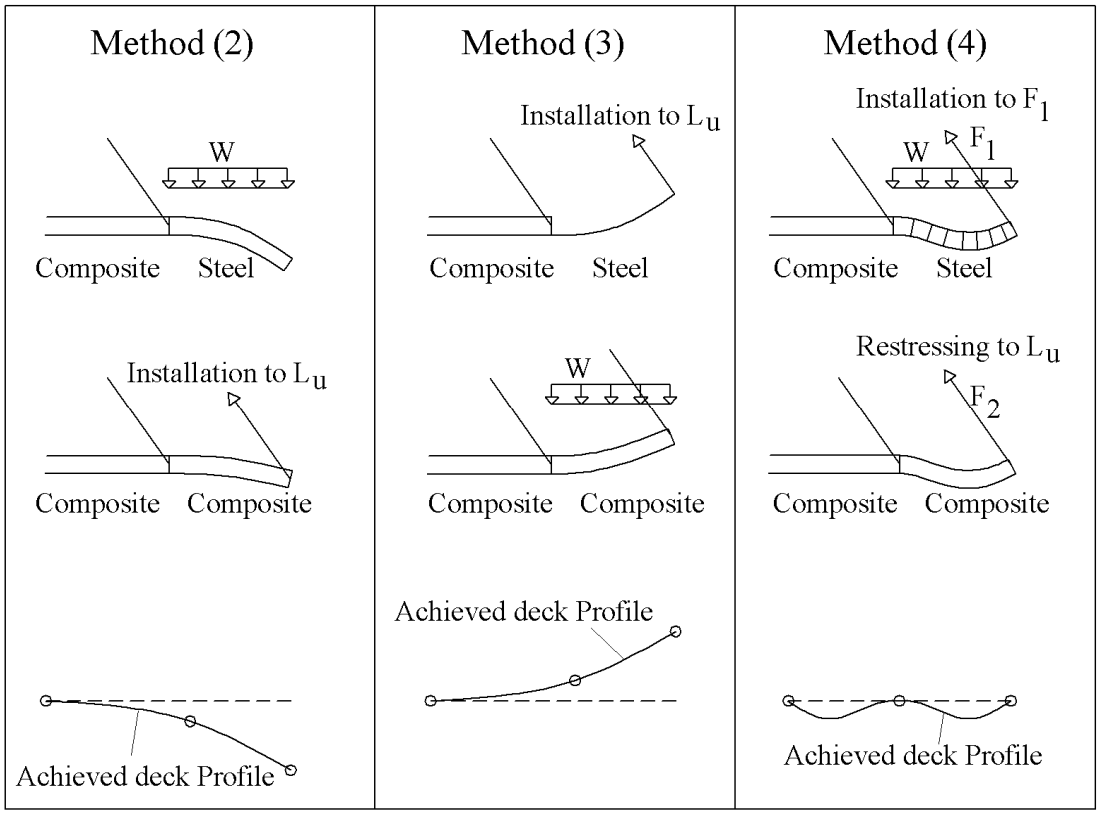

fig. 4.6: Construction methods for composite section in two stages (schematic) [Schlaich 2001]

The methods nos. 2, 3 and 4, shown in fig. 4.6. for the construction of a steel/concrete composite section in two stages, have been discussed in [Schlaich 2001], noting that only the time dependent effect (type I) was taken into account.

In the construction method no. 2, the deck segment is installed first with its steel cross section, tangential to the previously constructed deck segment. The newly erected deck segment, with its steel cross section only, is then loaded with the weight of the concrete slab W and the composite section properties is achieved prior to the installation of the stay cable at the far end of the new deck segment. Accordingly undesired downward curvature and hog bending moments will be "frozen" in the steel section of the deck segment and the desired geometry and stay cable forces will not be achieved for the completed structure if the stay cables are installed to the unstressed lengths L_{ui} calculated in accordance with the formula shown in fig. 4.3(c). The final profile of the deck will be lower than the desired geometry as shown schematically in fig. 4.6.

The construction method no. 3 is the extreme opposite of construction method no. 2. The new deck segment is erected first with its steel section tangential to the previously constructed segment and the stay cable is installed to the unstressed length L_{ui} in accordance with the formula shown in fig. 4.3(c). If, theoretically, the composite section properties are achieved prior to the application of the load W, undesired upward curvature and sag bending moment will be "frozen" in the steel section of the deck segment. Accordingly, the desired geometry and stay cable forces will not be achieved for the completed structure. The final profile of the deck will be higher than the desired geometry.

To avoid the shortcomings of the construction methods nos. 2 and 3 described above, the construction method no. 4 shown in fig. 4.6, was proposed [Schlaich 2001]. As opposed to the construction methods nos. 2 and 3, two opposite curvatures will be "frozen" in the steel only section of the deck segment under erection to avoid the undesired downward or upward "frozen" curvatures associated with the construction methods 2 and 3 respectively. As such, the far end of the newly erected deck segment would not deviate from the desired geometry as shown in fig. 4.6. The procedure of the construction method no. 4 as described in [Schlaich 2001], may be summarized as follows:

A- The desired stay cable force F_{Di} for the completed structure is to be determined from the final bridge configuration under dead load with the composite deck cross section properties. The

continuous beam method may be used to calculate the desired stay cable forces under dead load F_{Di} and the unstressed length L_{ui} for each individual cable is to be determined as per the formula shown in fig. 4.3 (c).

B- As shown in fig. 4.7, the typical erection cycle for a deck segment starts with the construction of the first part of the composite section (steel only section), tangential to the previously constructed deck segment (Note: the deck segments are shown horizontal for simplicity). Further, each stay cable will have to be installed in two stages as will be explained below.

C- The steel cross section of the deck segment under erection is to be loaded with the weight of the second part of the composite section (i.e. the weight of the concrete slab). The first stage installation force of the stay cable, prior to the achievement of the composite cross section properties, should be determined in such a way that the bending moment distribution along the new deck segment with its steel only cross section, will be similar in shape to that shown in fig. 4.7 (the "frozen" bending moment), noting that "e" is equal to the vertical distance between the center of gravity of the steel only section and the center of gravity of the total composite section. The "frozen" bending moment distribution shown in fig. 4.7, will lead to two opposite "frozen" curvatures in the steel section of the deck segment prior to the achievement of the composite section properties.

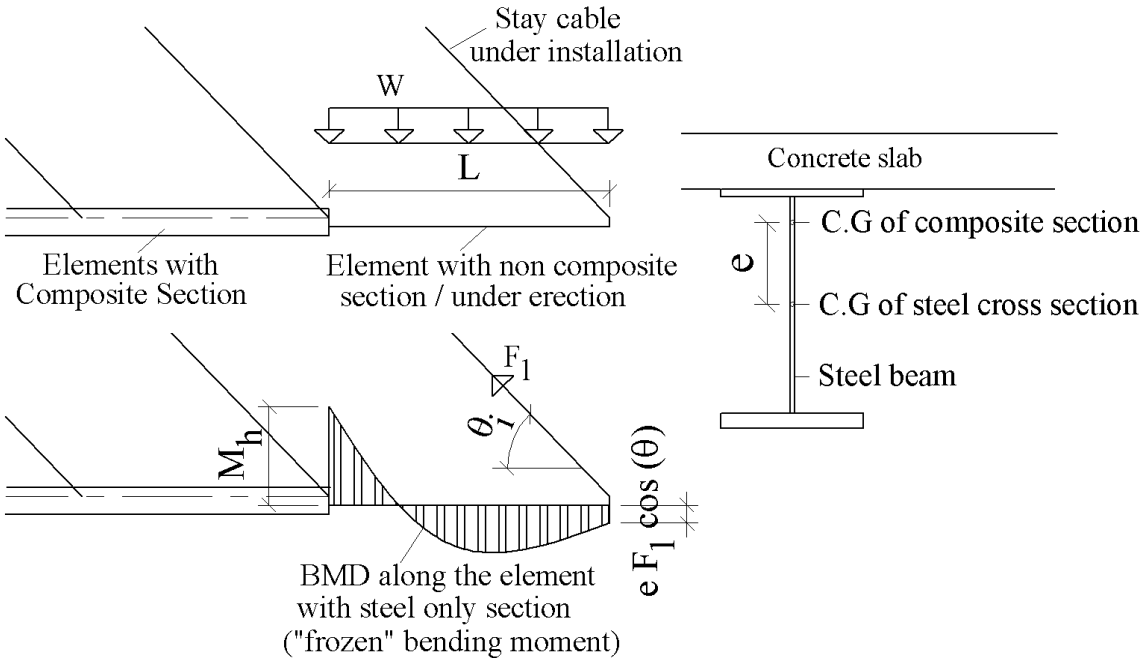

fig. 4.7: Bending moment distribution along the deck segment under erection prior to the achievement of the composite section properties [Schlaich 2001]

D- Upon the achievement of the composite section properties, the stay cables are to be re-stressed "to length" so that the unstressed length of the stay cable will be equal to the unstressed length L_{ui} calculated under point "A" above.

Further investigations for the construction method no. 4 described above, have been carried out and it was found that the desired stay cable forces and the desired geometry for the completed structure under dead load, will be achieved provided that:

- The time dependent effect (Type II) may be ignored (if, for example, very old precast segments are planned to be used).
- The ratio between the moment of inertia of the first part of the composite section I_s and the moment of inertia of the total composite section I_{comp} , is relatively high (refer to Appendices C and D).
- The vertical shift between the center of gravity of the first part of the composite section and the center of gravity of the total composite section "e" is negligible.

To understand the influence of the parameters I_s / I_{comp} and "e" on the desired forces and geometry for the completed structure under dead load, two models for the typical erection cycle of construction methods nos. 1 and 4 are investigated and compared as shown in fig. 4.8.

In this study it will be shown that the achievement of the same stay cable force at the end of the typical erection cycle of construction methods (1) and (4), will not lead to the same relative vertical deflection between the two ends of the deck segment under erection. Further the angles of rotations of the deck profiles at the far end of the deck segments under erection, will not be equal for both of the construction methods (1) and (4). In other words, it will be concluded from this study that it is impossible to achieve the same stay cable forces at the end of the erection cycle of construction methods nos. (1) and (4), if the stay cables are installed to the same unstressed length L_{ui}.

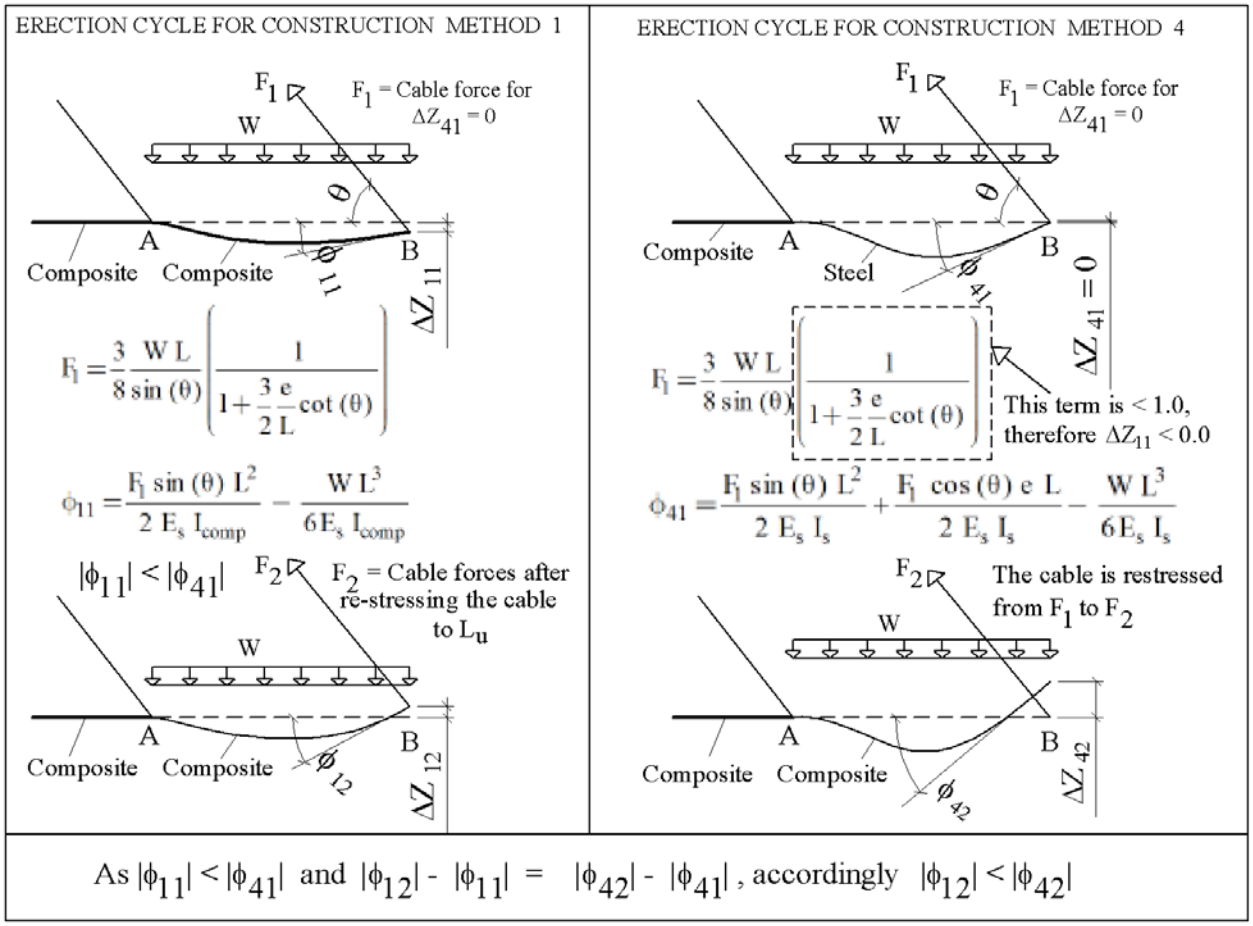

fig. 4.8: Comparison between the erection cycle of construction methods nos. (1) and (4)

The following points should be noted concerning the content of fig. 4.8:

- The time dependent effect (type II) is ignored for both of construction methods (1) and (4).
- E_s is the elastic modulus of the idealized section of the two parts of the composite section (the area and the moment of inertia of the concrete section are transferred to equivalent steel area and moment of inertia based on the ratio between the elastic modulus of the concrete to the elastic modulus of steel).
- I_s and I_{comp} are the moment of inertia of the first part of the composite section and the moment of inertia of the total composite section respectively (expressed in the idealized steel unit).
- In construction method no. (1), the composite section properties are achieved before the erection of the segment AB (similar to the erection method used for Rion Antirion bridge fig. 4.5). As such, the desired geometry and the desired cable forces will be achieved for the completed structure if the cables are installed to the unstressed length L_{ui} [fig. 4.3(c)], noting that the time dependent effect type II is ignored.

- In Method no. (4), the composite section properties are achieved after the erection of the segment AB.
- F_1 is the force required in construction method (4) to get the relative vertical deflection between points A and B to be equal to zero, noting that the structural system between points A and B at the time of the application of the force F_1, is a determinate structural system.

The relative vertical deflection between the two ends A and B of the segment under erection is caused by the external load W and the cable force F_1. From the above mentioned definition of the force F_1, it may be calculated by solving the following equation:

$$\frac{W L^4}{8 E_s I_s} = \frac{F_1 \sin(\theta) L^3}{3 E_s I_s} + \frac{F_1 \cos(\theta) e L^2}{2 E_s I_s} \qquad (4.3)$$

By rearrangement of equation (4-3)

$$F_1 = \frac{3 W L}{8 \sin(\theta)} \frac{1}{\left(1 + \frac{3}{2} \frac{e}{L} \cot(\theta)\right)} \qquad (4.4)$$

- The force F_1 is dependent on the eccentricity "e" [refer to equation (4.4] and fig. 4.7).
- If the cable in construction method (1) is installed also in two stages and the first installation force is made also equal to the value of the force F_1 as defined above , the point B in the case of construction method (1) will be lower than the point B in case of construction method (4). This can be concluded by studying the above equation (4.4) of F_1, noting that the eccentricity “e” in the case of construction method no. (1) is equal to zero and therefore the cable force required to eliminate the relative vertical deflection between the points B and A would be equal to 3/8 W L / sin (θ) which is higher than the force F_1 in equation no. (4.4).
- After the first stage installation of the cable in construction methods (4) and (1) to the same cable force F_1 calculated from equation (4.4), the absolute value of the angle of rotation of the deck profile at point B “ $|\phi_{41}|$ “ in case of construction method (4) will be higher than the absolute value of the corresponding angle at point B “ $|\phi_{11}|$ “ in the case of construction method (1). This can be concluded by studying the equations of the angles of rotations $|\phi_{41}|$ and $|\phi_{11}|$ shown in fig. 4.8, noting that the moment of inertia for the composite section I_{comp} (expressed in the idealized steel units) is higher than the moment of inertia of the steel section I_s (expressed also in steel units). It is also to be noted that E_s is the elastic modulus of the steel material.

- After the cable installation in construction method (4) to the force F_1, the deck segment under erection will get the composite section properties and the "frozen" bending moment distribution in the deck segment under erection will be similar in shape to that shown within fig. 4.7.
- The force F_2 is defined from construction method no. (1) which is the cable force after being re-stressed to the unstressed length L_{ui} [calculated in accordance with the formula shown in fig. 4.3 (c)].
- Upon the achievement of the composite section properties in construction method no. (4), the effect of the re-stressing of the cable from F_1 to F_2 on the deck segment AB will be the same in both of construction methods (4) and (1). This means that at the end of the erection cycle, point B in case of construction method (4) will remain higher than Point B in case of construction method (1) and the absolute angle of rotation for the deck profile $|\phi_{42}|$ at point B in case of construction method (4) will be higher than the corresponding angle of rotation $|\phi_{12}|$ in case of construction method (1). Accordingly, construction method (4) will lead ultimately to a deck profile higher than the desired deck profile which would be obtained if construction method (1) is followed. It can also be concluded that it is impossible to achieve the same stay cable forces at the end of the erection cycle of construction methods nos. 1 and 4, if the stay cables are installed to the same unstressed length L_{ui}. Accordingly construction method (4) cannot be followed, without modification, if both of the desired stay cable forces and the desired geometry are required to be achieved for the completed structure under dead load.

4-3-3 Application of the construction methods 2,3 and 4 on a simple cables supported beam

In this section the construction methods nos. 2, 3 and 4 described above under Section 4-3-2 will be applied on the cables supported beam shown in fig. 4.9. It will be explained in this study that the installation of stay cables to the unstressed length L_{ui}, in accordance with the formula shown in fig. 4.3 (c), will not lead to the desired forces and the desired geometry for the completed structure if any of the construction methods 2,3 or 4 is followed. In Section 4-3-4, a new method will be proposed (construction method no. 5) to achieve the desired forces and geometry.

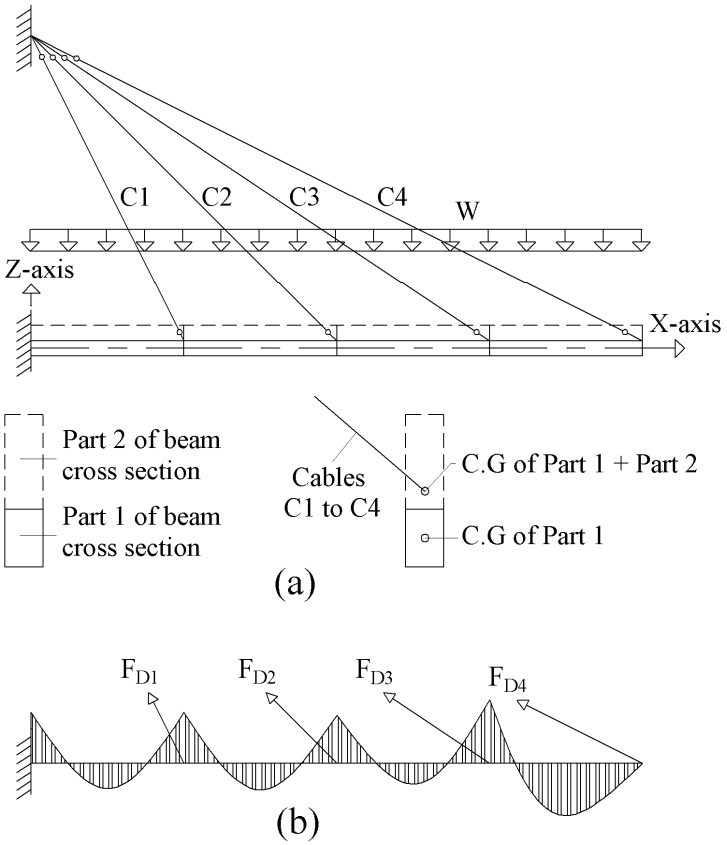

fig. 4.9: Cable supported beam with a rectangular cross section constructed in two stages

The desired bending moment distribution under dead load is shown in fig. 4.9 (b). The cable forces leading to this bending moment distribution are assumed to be equal to F_{D1} to F_{D4} and the corresponding unstressed lengths of the cables are assumed to be equal to L_{u1} to L_{u4} (noting that the time dependent effect type (II) will be ignored in this study) .

Fig. 4.10 shows the erection stages for the two extreme construction methods nos. 2 and 3 described above. In construction method no. 2, fig. 4.10 (a to c), the beam is constructed in 4-stages with four equal lengths. All the segments are constructed tangential to the previously constructed segments. Each beam segment is constructed first with its "part 1" shown within fig.

4.9(a). By casting the remaining part of the beam section (part 2 of the cross section), part 1 of the cross section will have to carry its own weight and in addition the concrete weight of part 2. Accordingly, a relatively big downward deflection and hog bending moment will be "frozen" within part 1 of the beam cross section. Upon the hardening of the newly cast concrete of part 2 of the cross section, the cables are installed with the unstressed lengths L_{u1} to L_{u4}.

In construction method no. 3, fig. 4.10 (f to h), the beam is constructed also in 4-stages with 4-segments equal in length. Each segment is constructed first with its first part of the composite section [refer to part 1 of the cross section shown within fig. 4.9(a)] tangential to the previously constructed segments. The cables are then installed to the unstressed lengths L_{u1} to $L_{u4,}$ prior to the application of the external uniform load W. If it is assumed theoretically that the composite section properties are achieved in the absence of the weight W, a relatively big upward deflection and sag bending moment will be "frozen" within part 1 of the beam cross section before the achievement of the composite section properties.

Computer models have been established to study the results for both of the construction methods nos. 2 and 3. The computer results show, as expected, that the cable forces for the completed structure for construction method no. 2, are higher than the corresponding desired forces F_{D1} to F_{D4}. For construction method no. 3, the cable forces for the completed structure are less than the desired forces F_{D1} to F_{D4}.

Fig. 4.10 (d , e, i and j) show also the resulting vertical deflection and bending moment diagrams for both of the construction methods nos. 2 and 3 for the completed structure (when all cables are already installed to the unstressed lengths L_{u1} to L_{u4}), which are not similar to the desired results (refer to fig. 4.9(b)). Accordingly it can be concluded that if the beam cross section is constructed in two stages [as it is the case for both of construction methods (2) and (3)], the installations of the cables to the unstressed lengths L_{u1} to $L_{u4,}$ do not lead to the desired alignment and the desired forces within the structural elements for the completed structure.

Further, it can be seen from fig. 4.10(e) that the beam elements in construction method no. (2) have to carry excessive sag bending moment due to the following reason:

- The beam elements get extra downward deflection due to the fact that their "part 1" of the composite section shown in fig. 4.9 (a), carried the external uniform load prior to the cable installation.
- Due to the extra downward deflection of the beam elements, extra cable forces have to be

carried by the beam as the cables are installed to the predetermined unstressed lengths L_{u1} to L_{u4}. The extra cable forces lead to the above mentioned excessive sag bending moment.

Similarly, the excessive hog bending moment shown within fig. 4.10 (j) for construction method no. 3, can be justified as follows:

- The beam elements get extra upward deflection due to the fact that their "part 1" of the composite section carried the vertical component of the installation cable force prior to the achievement of the composite section properties.
- Due to the extra upward deflection of the beam elements, less cable forces will be introduced to the structure when the cables are installed to the predetermined unstressed lengths L_{u1} to L_{u4} and, therefore, the hog bending moment acting on the beam elements due to the external uniform load W will be higher.

It should now be noted that the bending moment shown within fig. 4.10 (e) for construction method no. 2 may be corrected to be similar to the desired bending moment diagram shown within fig. 4.9 (b) provided that the cable forces are de-stressed to "F_{D1} to F_{D4}". By de-stressing the cable forces this way, both of the desired bending moment diagram and the cable forces are achieved but the desired vertical profile of the beam elements will not be achieved noting that extra downward deflection will be added to the vertical deflection shown within fig. 4.10(d). This problem would however be solved by pre-cambering the beam segments in accordance with the final vertical deflection line (with opposite sign) upon carrying out the above described de-stressing of the cable forces.

Similarly, the bending moment shown within fig. 4.10 (j) for construction method no. 3 may be corrected to be similar to the desired bending moment diagram shown within fig. 4.9 (b) provided that the cable forces are re-stressed to "F_{D1} to F_{D4}". By re-stressing the cable forces this way, both of the desired bending moment diagram and the cable forces are achieved but the desired vertical profile of the beam elements will not be achieved noting that extra upward deflection will be added to the vertical deflection shown within fig. 4.10 (i). This problem would however be solved by pre-cambering the beam segments in accordance with the final vertical deflection line (with opposite sign) upon carrying out the above described re-stressing of the cable forces.

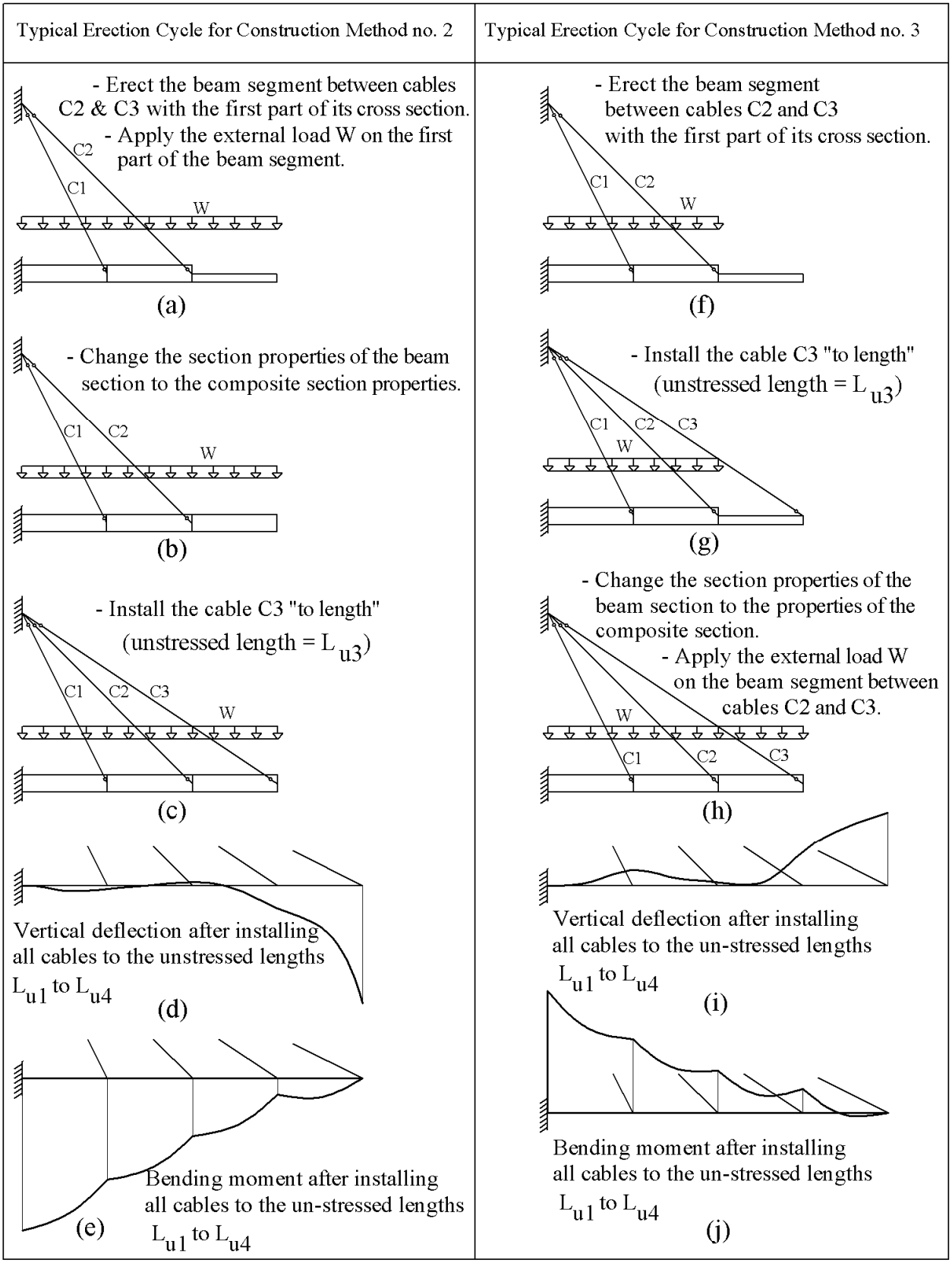

fig. 4.10: Application of the construction methods nos. 2 and 3 on a cables supported beam

Further to the above, it should be emphasized that although de-stressing or re-stressing of the cables help to ultimately achieve the desired forces within the beam elements, the problem of the interim high level of forces/stresses within the beam elements prior to the above mentioned de-stressing or re-stressing of cables for construction methods nos. 2 and 3 respectively [refer to the bending moment diagrams of figs. 4.10 (e) and 4.10 (j)], remained unresolved. Following any of the two extreme construction methods 2 and 3 described above is, therefore, practically not possible.

The application of construction method no. 4 on the cables supported beam shown in fig. 4.9 (a), requires the installation of each of the 4-cables in two stages. In the first stage of the cable installation, the cable is to be tensioned to an initial force F_1 to create a bending moment distribution, similar in shape to that shown within fig. 4.7 which has to be within the capacity of part 1 of the beam cross section. The initial installation force F_1 is dependent on the external uniform load W and the vertical shift "e" between the C.G of the first part of the beam section and the C.G of the total composite section [refer to equation (4.4)]. Upon the achievement of the composite section properties, the second stage of the cable installation (to the unstressed lengths L_{u1} to L_{u4}) may be carried out. As explained under Section 4.3.2, the results of the computer model for the cables supported beam shown in fig. 4.9, confirmed that the installations of the cables to the unstressed lengths L_{u1} to L_{u4}, do not lead to the achievement of the desired alignments or the desired cable forces at end of construction. The resulting geometry and forces will be dependent on the ratio I_s / I_{comp}. Computer models have been established to study the effect of the ratio I_s / I_{comp} on the vertical deflection of the beam, the bending moment distribution and the cable forces for the completed structure assuming that the cables are installed in two stages and the final unstressed lengths for the cables are equal to L_{u1} to L_{u4} [calculated in accordance with the formula of fig. 4.3(c)]. Figs. 4.11 and 4.12 show, for the particular structure under investigation, that the high values of the ratio I_s / I_{comp} (above 40%), lead almost to the desired vertical profile and the desired bending moment distribution for the completed structure. For I_s / I_{comp} (above 40%) the stay cable forces for the completed structure deviate slightly from the desired cable forces F_{D1} to F_{D4} by about ±5%. The stay cable forces would however deviate by up to ± 25% in case the ratio I_s/I_{comp} is as low as 5%. Accordingly, it can be concluded that in case the cables are installed in two stages and the total unstressed lengths of the cables are equal to L_{u1} to L_{u4} (after carrying out the two installation stages), the cables may be required to be re-

stressed or de-stressed at end of construction to the desired forces F_{D1} to F_{D4}, in particular when the ratio I_s/I_{comp} is relatively low. The re-stressing or the de-stressing of the cable forces will help to achieve the desired cable forces and the desired bending moment for the completed structure. Further, the beam segments will have to be pre-cambered to achieve the desired alignment for the completed structure in addition to the achieved desired forces.

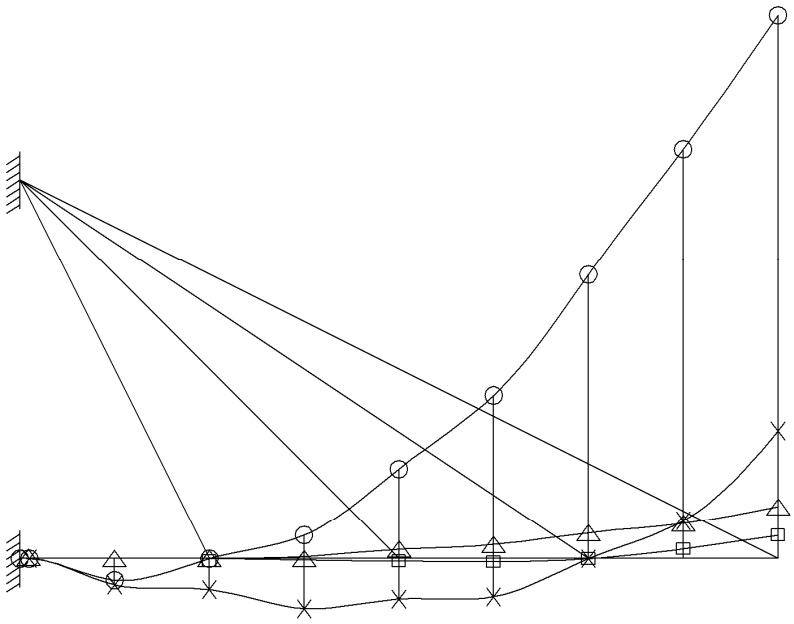

○ I_S / I_{comp}= 5% after re-stressing/de-stressing of cables to the desired force F_{Di}
× I_S / I_{comp}= 5% before re-stressing/de-stressing of cables to the desired forces F_{Di}
△ I_S / I_{comp}= 40% after re-stressing/de-stressing of cables to the desired forces F_{Di}
□ I_S / I_{comp}= 40% before re-stressing/de-stressing of cables to the desired forces F_{Di}

fig. 4.11: Effect of the ratio I_s / I_{comp} on the vertical deflection profile for the completed structure in case the cables are installed "to length" with construction method no. 4

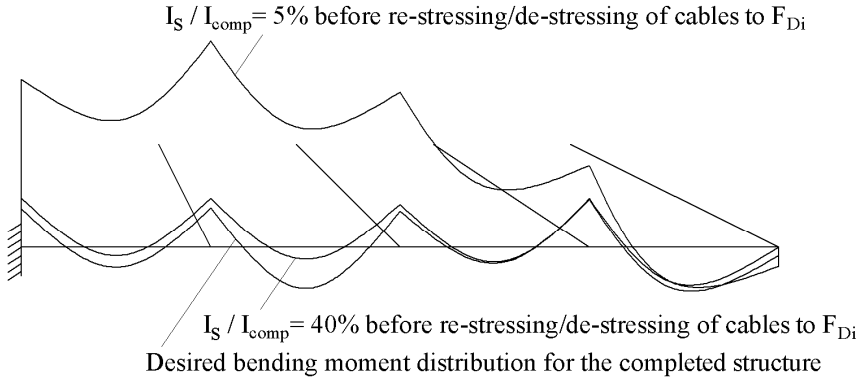

Note: for the cases of I_S / I_{comp} = 5% and 40%, the BMD will be the same as the desired BMD after re-stressing/de-stressing of cables to F_{Di}

fig.4.12: Effect of the ratio I_s / I_{comp} on the bending moment distribution for the completed structure in case the cables are installed "to length" with construction method no. 4

4-3-4 Proposed modification for the construction method no. 4 (construction method no. 5)

Based on the discussions made under 4-3-1 to 4-3-3, the proposed procedure for the construction of the cable-stayed bridges with composite decks, may be summarized as follows: (taking into account the effects of the ratio between the moment of inertia of the first part of the composite section to the moment of inertia of the total composite section I_s / I_{comp} , the vertical shift "e" between the center of gravity of the first part of the composite section and the center of gravity of the total composite section and the time dependant forces due to shrinkage and creep):

a- The desired cable forces F_{Di} under dead load at time infinity (when all time dependant effects have taken place) are to be determined in such a way that the vertical components of the cables would be equal to the vertical reaction forces for an equivalent continuous beam on rigid supports.

b- A computer model is to be established to carry out the "step by step construction stage analysis" using the actual cross section properties of the deck elements at any particular construction stage (refer to Section 3-1).

c- Each deck element is to be introduced in the computer model initially with the properties of the first part of the composite section. The new deck and pylon elements are to be introduced in the model with initial longer lengths to balance the elastic shortening due to the normal forces resulting from the horizontal components of the stay cable forces and the normal forces in the pylon elements at time infinity (this initial length should be taken into account for the definition of the precamber as will be clarified below). Each stay cable is to be installed to an initial force in accordance with equation no. (4.4). The use of equation no. (4.4) leads to "frozen" bending moments distribution for the deck segments under erection, similar in shape to that shown within fig. (4.7). Subsequently, the properties of the deck cross section are to be changed to the properties of the composite section. The stay cable is then to be re-stressed "to length" as explained in construction method no. (4) under Section 4-3-1.

d- Point "c" is to be repeated for all deck segments/cables.

e- The stay cable forces and the structure deformations due to the time dependent effects will be determined in the computer model (refer to Section 4-1) during construction and till time infinity. The creep and shrinkage effects are calculated in the computer model in small time intervals. Partial creep and shrinkage factors for each time interval are considered in the computer model based on the factors mentioned within Section 4-1. In this connection

reference is made to [Ghali and Favre 1994] for more details. The relaxation effect of the stay cable material may be taken into account in small time intervals as well.

f- The stay cable forces are to be calculated by the computer model upon the erection of all structural elements and the application of all external loads and after all time dependent effects have taken place (at time infinity). The calculated stay cable forces at time infinity, using the "step by step construction stage analysis" by the computer model, will not be equal to the desired stay cable forces F_{Di} calculated earlier under point "a" above. The reasons of the difference between the stay cable forces calculated under point "a" and the stay cable forces calculated by the "step by step computer model analysis", are explained under sections"4-2" and "4-3".

g- Assuming that the change in each cable force between the time infinity and the time of the construction completion as calculated with the computer model is equal to $\Delta F_{i-\infty-0}$, the design force for each stay cable at end of construction should be equal to $F_{Di} - \Delta F_{i-\infty-0}$. Accordingly, the stay cable forces at end of construction are to be re-stressed or de-stressed to the force: $(F_{Di} - \Delta F_{i-\infty-0})$.

h- During the design stage, the stay cables are to be re-stressed or de-stressed at time infinity, in the computer model) to F_{Di}. The vertical and horizontal deflections of the structure elements should then be calculated at time infinity and precambered accordingly (the initial length of the deck and pylon segments, as indicated above under point c, should be taken into account during the definition of the required fabrication length of each element).

To illustrate further the proposed construction method no. (5), refer to the numerical example under Appendix B.

4-3-5 Application of the construction method no. (4) or (5) on cable-stayed bridges with composite deck sections

The construction method no. (4), as proposed in [Schlaich 2001], was applied previously on a simple cables supported beam in Section 4-3-3. The same construction method will be applied in this section on a complete cable-stayed bridge to highlight/resolve additional problems not covered in the case of the above mentioned cables supported beam.

If the composite deck segments of a cable-stayed bridge are built with the balanced cantilever method starting from the pylon and the construction method no. (4) is followed, special attention should be paid in the design stage, during the activation of the end supports and also during the activation of the closure joint between the two cantilevers of the main span.

As explained under Section 4-3-2, the erection of the deck segments with the construction method no. (4), does not lead to the same deck profile when compared to the construction method no. 1. Accordingly, and as shown in fig. 4.13 (a), the deck profile prior to the activation of the end supports in case the construction method no. (4) is followed, will deviate from the deck profile of construction method no. 1.

If construction method no. (4) is followed, the tip of the deck at the end supports should be jacked down in accordance with the vertical deflection ΔZ_1 and not $(\Delta Z_1 + \Delta Z_2)$, otherwise additional forces will be locked-in between the deck and the end supports and the desired stay cable forces and bending moment distribution at time infinity will not be achieved.

Similarly, the temporary forces P required to connect the two half of the cable-stayed bridge tangentially at the closure joint [fig 4.13 (b) and (c)], should be determined from a computer model assuming that the construction method no. (1) is followed. The choice of the jacking force at the end supports or the temporary loads at the closure joint in accordance with construction method no. (1), would lead to the deck profile shown in fig. 4.13 (d) for the completed structure. By selecting an appropriate pre-camber for the deck, the end supports will be constructed at the right desired levels and the deck segments at the closure joint will be constructed without a kink.

The above explanation implies that the “step by step construction stage analysis” for a cable-stayed bridge with composite deck, requires the establishment of two computer models. The first computer model will consider the erection of the deck segments with the construction method no. 4 and the erection of the deck segments will follow construction method no. 1 in the second computer model. The first computer model will be used for the determination of the required

precamber and also for monitoring the bridge behavior during construction. The second model will be used to determine the required jacking forces at the end supports or the temporary forces at the closure joint at the middle of the main span, as explained above.

In Appendix C and Appendix D, the results of the application of the proposed construction method no. (5) on cable-stayed bridges with composite deck cross sections (steel/concrete) and (concrete/concrete), are shown.

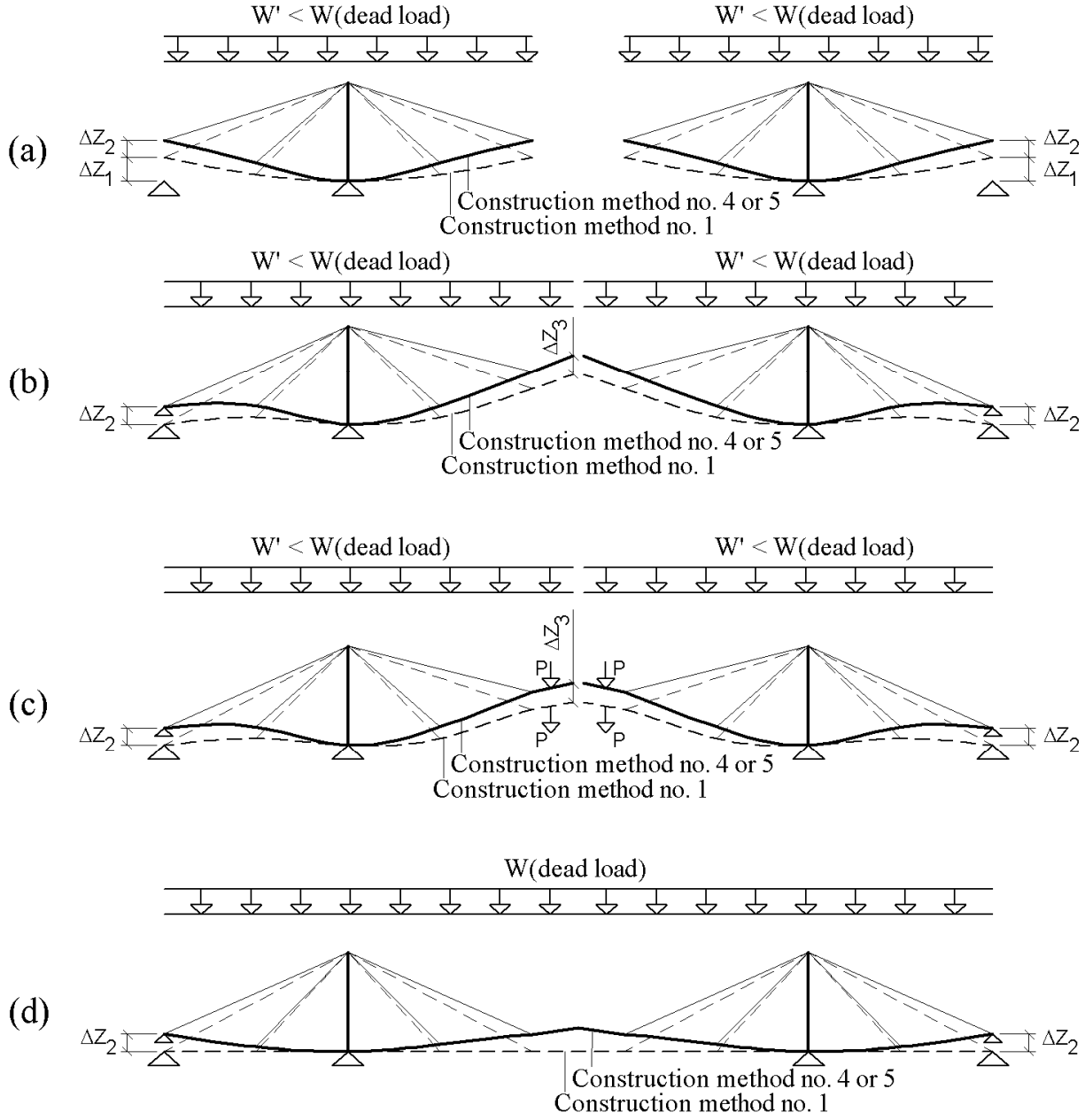

fig. 4.13: Comparison between construction methods 4 or 5 with construction method 1

CHAPTER 5

5- EXTRADOSED BRIDGES

Cantilever constructed prestressed box girder bridges (fig. 5.1) have been built successfully in the last 50-years for spans varying between 30 and 100m. Prestressed box girder bridges with spans between 50 and 100m are constructed normally with the balanced cantilever methods and the pertinent method of analysis is well established [Mathivat 1983]. Few of them have been constructed with spans over 100m noting that such types of bridges require deep and heavy deck cross sections. As the conventional cable-stayed bridges appear to be not economical for spans less than 200m (fig. 5.1), bridge designers have been investigating a suitable structural system to "close the gap" for bridges with spans ranging from 100 to 200m.

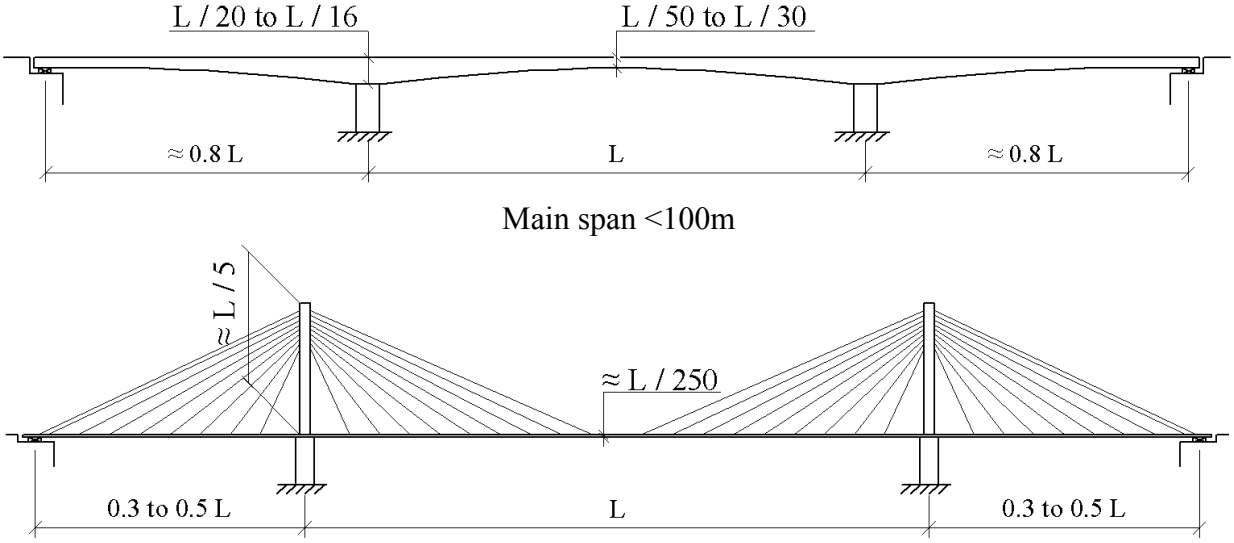

fig. 5.1: Common configurations of prestressed box girder bridges and conventional cable-stayed bridges

The extradosed bridge (fig. 5.2) may be considered as the optimum structural system to close the above mentioned "gap". Benefitting from the experiences gathered previously for the design and construction of both of the prestressed box girder bridges and conventional cable-stayed bridges, extradosed bridges emerged in the last twenty years in some countries, specially in Japan, as the preferred option to bridge spans of 100 to 200m [Kasuga 2006] [Meiss 2007].

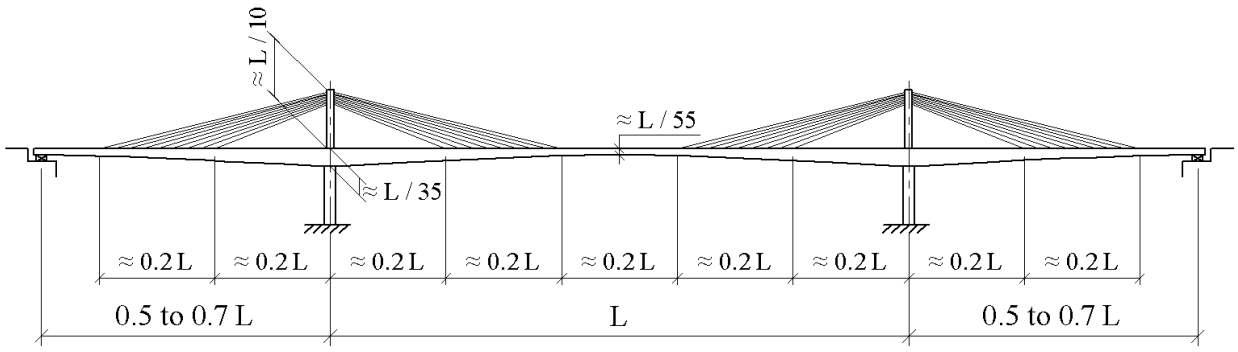

Main span 100-200m

fig. 5.2: Common configuration of extradosed bridges

The deck depth for extradosed bridges, can be effectively reduced, when compared with the prestressed box girder bridges, leading to ease of the construction of the foundations, substructure, superstructure, enhancement of the bridge aesthetic and an overall cost advantages. Further, the reduction of the girder height facilitates the compliance imposed very often on the bridge designer to keep a minimum clearance height under the main bridge span and therefore, the bridge deck would not be required to be excessively raised. As such, the costly required ramps associated with the said raising of the bridge deck may be avoided.

The word extrados comes from the French word extradossé which is defined as the exterior curve or surface of an arch. In 1988 the French engineer Jacques Mathivat used the term “extradosed” to describe an innovative cabling concept proposed by him for the Arrêt-Darré viaduct (fig 5.3). As shown in fig. 5.3, it was proposed that the external prestressing tendons protrude outside the deck and to be deviated over the pier by a short pylon. The proposal was not selected for construction and a conventional cantilever post tensioned structure was used instead [Mermigas 2008]. Professor Christian Menn used for the design of Ganter bridge in Switzerland (fig. 5.4) prestressing tendons encased in concrete walls above the deck level. The proposal made by Professor Jacques Mathivat for the Arrêt-Darré viaduct (fig. 5.3) and the design of Ganter bridge by Professor Christian Menn (fig. 5.4) are considered to be the inspiration of the design of the modern extradosed bridges constructed in the years 1990s and 2000s.

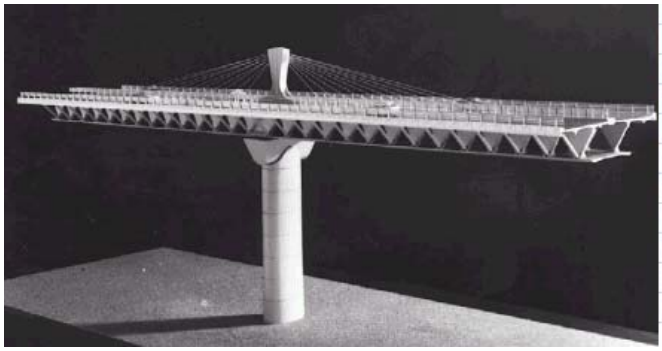

fig 5.3**:** Arrêt-Darré viaduct as proposed by J. Mathivat in 1988 [Mermigas 2008]

fig. 5.4: Ganter bridge, Switzerland completed in1980 [www.highestbridges.com]

5-1 Common configuration of previously constructed extradosed bridges

Several extradosed bridges have been successfully built in the last two decades with differing spans, tower heights and stay cable arrangements.

As explained within Chapter 3, the method for the form finding of conventional cable-stayed bridges is well defined with regard to the definition of the desired stay cable forces and the distribution of the forces within the bridge deck elements (bending moments, shear and normal forces) under dead load (refer to fig. 3.1). It is, however, noted that the method of the form finding for the extradosed bridges is yet to be established. Therefore, in Chapter 6 of this research work, a method for extradosed bridges will be presented which can be followed by bridge designers to determine the stay cable forces under dead load.

A survey carried out for the extradosed bridges built so far, show that they follow in general the geometry configuration shown within fig. 5.2 and that most of the extradosed bridges were built with side span to main span length ratio varying between 0.5 to 0.7 [Kasuga 2006].

Zone 1 shown within fig. 5.5 (a) is left unsupported by stay cables. The same approach was also adopted by bridge designers for many conventional cable-stayed bridges. Leaving zone 1 unsupported by stay cables is justified in that the vertical loads in this zone are preferred to be transferred directly to the piers rather than carrying the loads upwards to the pylon head by stay cables and transferring the same load back to the pier. In fig. 5.5 (b), it is logic to transfer the vertical load at point P1 through the bending/shear stiffness of deck directly to the point P2 rather than transferring it upwards to the tower head at the point P3, through stay cables, and transferring the same load back to point P2 through the pylon. To ensure the transfer of the vertical load in zone 1 through the shorter path (P1-P2), it may be prudent to increase the deck

thickness in this zone (by providing deck haunch) as shown within fig. 5.5 (c). Fig. 5.2 shows also that the extradosed bridges have been built with stay cable angles to the horizontal as low as 15-degress. To ensure the effectiveness of the stay cables, this angle cannot be less than the said 15-degrees. The central part of the main span (zone 3) is not supported by stay cables and, therefore, the deck transfers the vertical loads in this zone through its bending stiffness to the stay cables in zones 2. It can also be noted that the common configuration of extradosed bridges does not have backstays contrary to the cable-stayed bridges (refer to fig. 5.1 and Section 2-2).

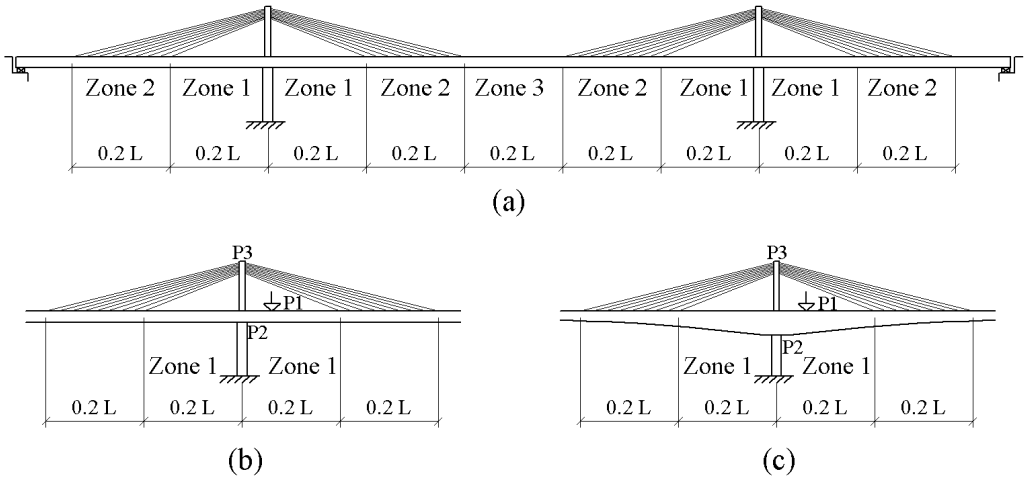

fig. 5.5: Cables configuration for extradosed bridges

5-2 Design of stay cables for conventional cable-stayed bridges and extradosed bridges

Similar to the conventional cable-stayed bridges, the stay cable forces for the extradosed bridges under dead load, can be controlled by shortening the cables to predetermined lengths to achieve specific desired bending moment distribution. A proposal for the determination of the desired stay cable forces under dead load for extradosed bridges will be presented in Chapter 6. Upon the selection of the stay cable forces under dead load, the stay cable forces under live load may be estimated as a percentage of the stay cable forces under dead load and the size of the stay cables may be calculated accordingly based on the allowable stresses in the Service Limit State as per the respective specification. The estimated sizes of the stay cables should then be checked for compliance with the requirements of the fatigue limit state and the strength limit state. This process should be repeated ("iteration process") until an economical design is reached (i.e. until the minimum size/weight of stay cables is reached).

The compliance with the fatigue limit state will depend mainly on the ratio between the live load q corresponding to the type of traffic the bridge is subjected, and the dead load w [Walter et al.

1999]. If the ratio q/w is small (case of concrete cable-stayed bridges), the axial stress variation due to live load σ_q in the stay cables will be smaller than the permissible limit of the stress variation $\Delta\sigma_{per}$ (guaranteed by the manufacturer of the cable based on tests carried out over two million cycles) and the load bearing capacity of the selected stay cable cross section will be fully utilized (refer to fig. 5-6 / Strength criterion):

$\sigma_q < \Delta\sigma_{per}$ and $\sigma_w + \sigma_q = \sigma_a$

The load bearing capacity is defined as the multiplication of the allowable axial stress at the service limit state σ_a times the cross sectional area of the stay cable and σ_a at SLS is taken normally by several international specifications equal to 0.45 times the ultimate tensile strength of the stay cable material σ_{UTS}.

On the other hand, if the ratio q/w is high as it is the case for steel railway bridges for example, the stress variation due to live load σ_q will be high and the load bearing capacity of the selected stay cable cross section will not be fully utilized (refer to fig. 5-6/Fatigue criterion):

$\sigma_q = \Delta\sigma_{per}$ and $\sigma_w + \sigma_q < \sigma_a$

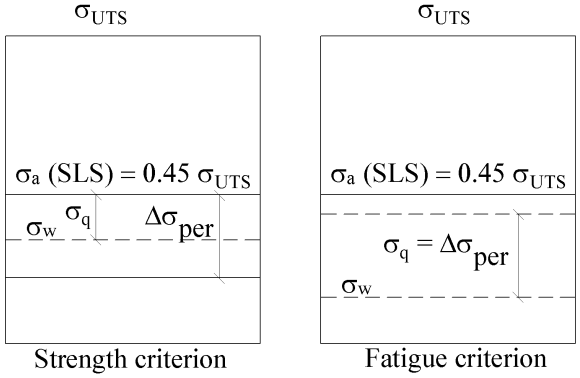

fig. 5.6: Strength criterion and fatigue criterion for the design of stay cables [Walter et al. 1999]

Further to fig. 5.6, the strength and fatigue criterions may be represented by equations (5.1) and (5.2) and fig. 5.7 [Walter et al. 1999]:

$$\sigma_w = \frac{w}{w+q}\sigma_a = \left(1+\frac{q}{w}\right)^{-1}\sigma_a = 0.45 \text{ x } 1770 \text{ MPa x } \left(1+\frac{q}{w}\right)^{-1} = 797\left(1+\frac{q}{w}\right)^{-1} \text{ MPa} \qquad (5.1)$$

For a stay cable system with a permissible stress variation $\Delta\sigma_{per}$ equal to say 200 MPa:

$$\sigma_w = \frac{w}{q}\Delta\sigma_{per} = \left(\frac{q}{w}\right)^{-1}\Delta\sigma_{per} = 200\left(\frac{q}{w}\right)^{-1} \text{ MPa} \qquad (5.2)$$

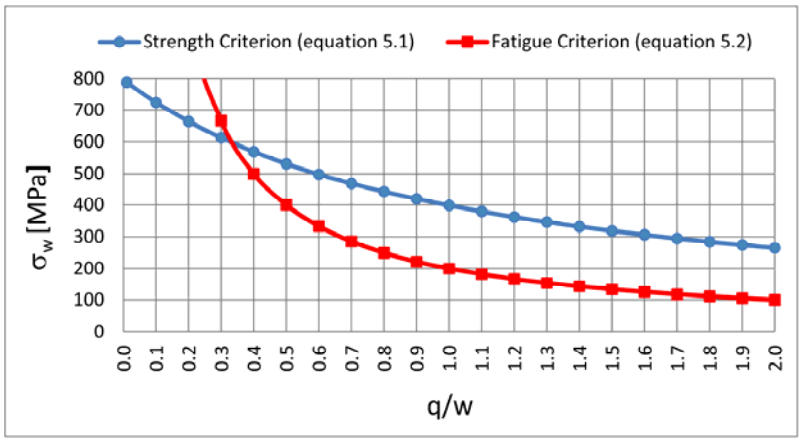

fig. 5.7: Relationship between the dead load permissible stress σ_w and the ratio q/w [Walter et al. 1999]

From fig. 5.7, it can be understood that the fatigue criterion governs the design of the stay cables for a ratio of q/w exceeding 0.30 at $\sigma_w \approx 600$ Mpa (Note: this is valid only if $\Delta\sigma_{per} = 200$ MPa). The pylon height for the extradosed bridges built so far are equal to approximately one tenth of the main span length which is equal to half of the corresponding pylon height for conventional cable-stayed bridges. The short pylon, the relatively stiff deck and in addition the absence of the back stays in the case of the extradosed bridges (as compared to the conventional cable-stayed bridges), limit the variation of the stresses in the stay cables due to live loads. The stress variations due to live loads, remain generally less than the corresponding stress variations for conventional cable-stayed bridges. Accordingly the restrictions of limiting the stresses in all stay cables to 0.45 x the ultimate tensile strength of the stay cable material σ_{UTS} as required by several international design codes, may be relaxed.

The SETRA recommendations link the allowable axial stress σ_a at SLS for the stay cables with the stress variation $\Delta\sigma_L$ due to SLS live loads and can be determined from the following equation (refer also to fig. 5.8). The allowable axial stress σ_a is applicable for the entire stay cable system [SETRA 2002] [Mermigas 2008].

$$\sigma_a = \begin{cases} 0.6\,\sigma_{UTS} & \text{if } \Delta\sigma_L \le 50\,\text{MPa} \\ \sigma_a \le 0.46\left(\dfrac{\Delta\sigma_L}{140}\right)^{-0.25}\sigma_{UTS} & \text{if } 50 < \Delta\sigma_L \le 140\ \text{MPa} \\ 0.46\,\sigma_{UTS} & \text{if } \Delta\sigma_L > 140\,\text{MPa} \end{cases} \qquad (5.3)$$

The allowable stress σ_a at SLS as per the Japan Prestressed Concrete Engineering Association's Specifications, may be determined from the following equations, noting that these two equations are applicable for the individual stay cables and not for the entire stay cable system as it is the case of equation 5.3 (refer also to fig. 5.8) [Ogawa and Kasuga 1998] [Kasuga 2006].

For a strand stay cable system fabricated on site (refer also to 2-1-4)

$$\sigma_a = \begin{cases} 0.6\,\sigma_{UTS} & \text{if } \Delta\sigma_L \le 70\ \text{MPa} \\ (-0.00667\,\Delta\sigma + 1.0667)\,\sigma_{UTS} & \text{if } 70 < \Delta\sigma_L \le 100\ \text{MPa} \\ 0.4\,\sigma_{UTS} & \text{if } \Delta\sigma_L > 100\ \text{MPa} \end{cases} \tag{5.4}$$

and for a stay cable wire system fabricated in the factory (refer also to 2-1-3)

$$\sigma_a = \begin{cases} 0.6\,\sigma_{UTS} & \text{if } \Delta\sigma_L \le 100\ \text{MPa} \\ (-0.00667\,\Delta\sigma + 1.2667)\,\sigma_{UTS} & \text{if } 100 < \Delta\sigma_L \le 130\ \text{MPa} \\ 0.4\,\sigma_{UTS} & \text{if } \Delta\sigma_L > 130\ \text{MPa} \end{cases} \tag{5.5}$$

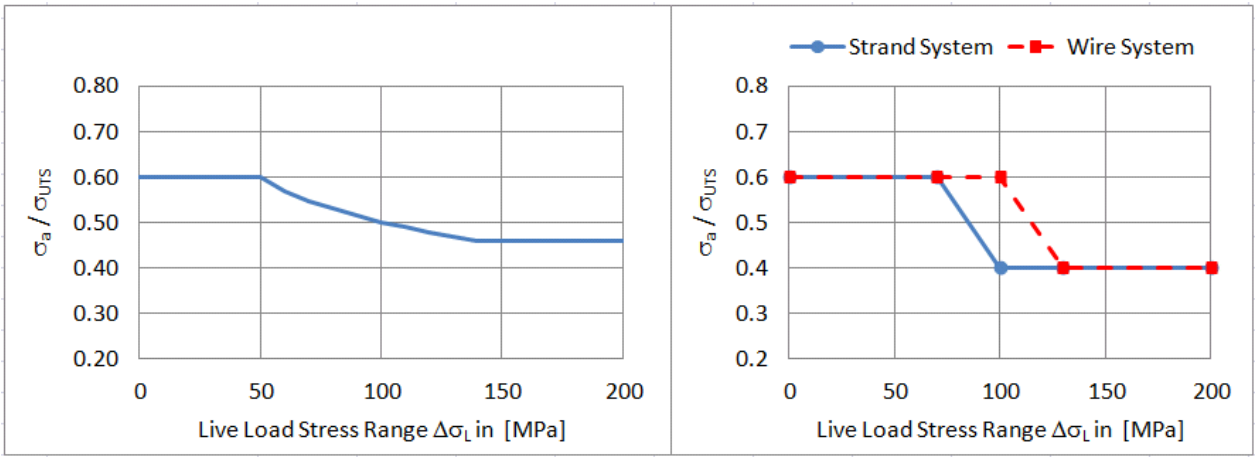

SETRA Recommendations (2001)

Japan Prestressed Concrete Engineering Association's Specifications [Ogawa and Kasuga 1998] [Kasuga 2006]

fig. 5.8: Allowable stresses for stay cables of extradosed bridges versus the stress variation due to live loads

The SLS design method demonstrated above involves implicitly the fatigue consideration for the stay cable system. The explicit fatigue limit state design requires the stay cable system to be tested for two million cycles for specific upper stress limits and specific amplitudes. For cable-stayed bridges, the upper stress limit is taken usually as 45% σ_{UTS}. The amplitude is commonly taken as 160 MPa for strand systems and 200 MPa for wire systems. Upon carrying out the fatigue test, appropriate safety factors should be taken into account to specify the allowable stress

variation. PTI indicates that the allowable stress variation may be taken equal to 69 MPa for the strand system and 105 MPa for the wire system [PTI 2001]. R. Walter [Walter et al. 1999] suggests simplified method for the definition of the permissible stress variation $\Delta\sigma_{per}$ by establishing the Woehler curve (fig. 5-9) from the available test results then deducing the allowable stress variation $\Delta\sigma_{per}$ by using the following equation:

$$\Delta\sigma_{per} = \frac{\Delta\sigma_{test}}{\gamma_1 \gamma_2 \gamma_3} \approx \frac{\Delta\sigma_{test}}{1.5} \tag{5.6}$$

where:

$\gamma_1 \approx 1.15$ is the assumed basic partial coefficient for steel

$\gamma_2 \approx 1.15$ is the partial coefficient taking into account the effect of grouping (tests carried out on separated wires or strands or the full size of the stay cable). γ_2 may be set to 1, if the test is carried out on the full size of the stay cable

$\gamma_3 \approx 1.15$ is the partial coefficient taking into account the conversion of the test values into characteristic values (may be reduced if sufficient numbers of test results are available)

[SETRA 2002] indicates that $\Delta\sigma_{test}$ may be taken equal to the $\Delta\sigma_0$ shown in fig. 5.9

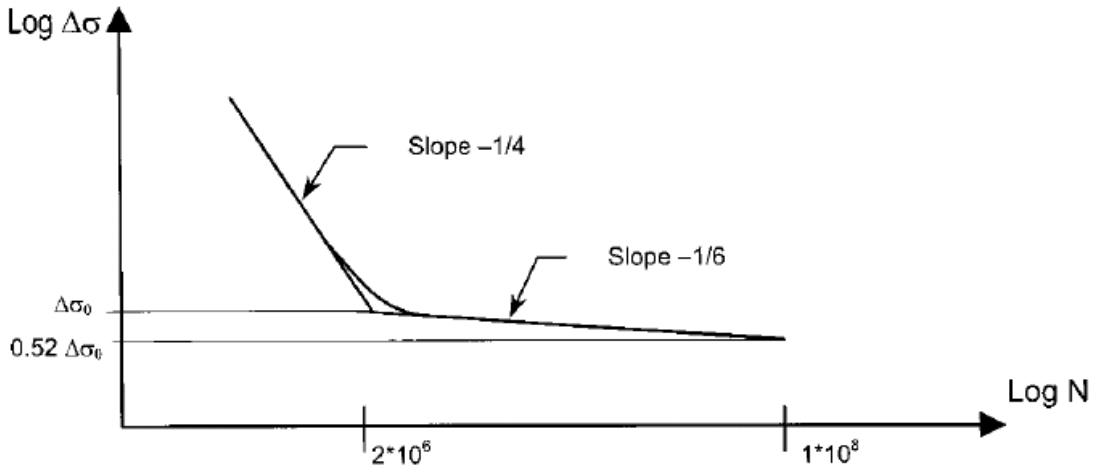

fig. 5.9: Typical fatigue curve of a cable stay [SETRA 2002]

Upon the determination of $\Delta\sigma_{test}$, the stress variation due to the fatigue load should be calculated (using a structural computer model) and should be less than $(0.52\Delta\sigma_0/1.5)$. For a stay cable system with $\Delta\sigma_0$ = 200MPa for example, the allowable stress variation due to the fatigue load = (0.52 x 200/1.5) ≈ 70MPa. The fatigue load for road bridges as per the Eurocode EN 1991-2-2003, for example, is shown in fig. 5.10.

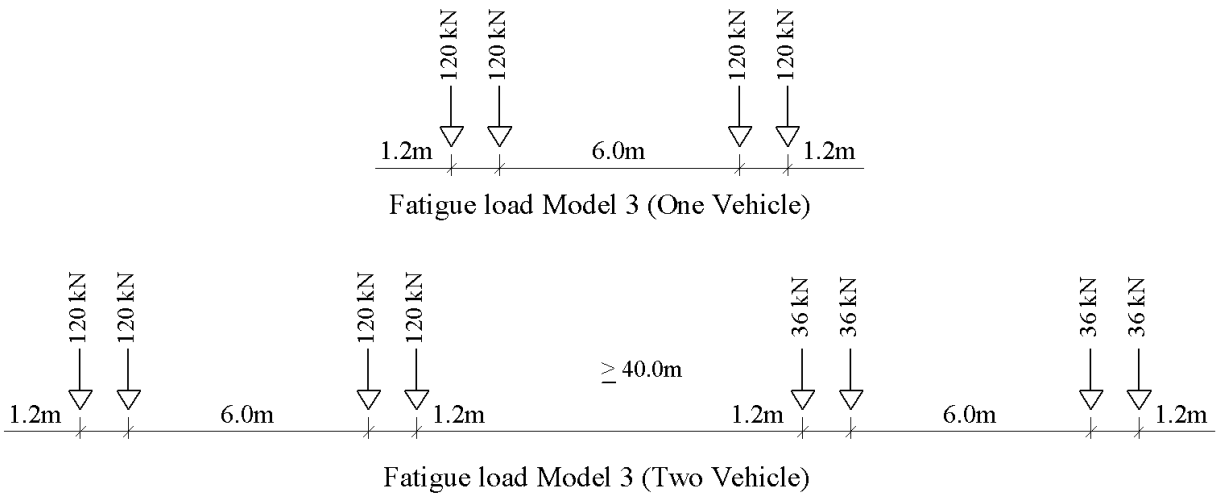

fig. 5.10: Fatigue load Model 3 as defined within Eurocode EN 1991-2-2003 + AC:2010

Based on the previous experience with the design of cable-stayed bridges with concrete decks, the stress variations due to fatigue loads similar to that of the Model 3 of Eurocode EN 1991-2-2003, are often far below 70MPa. The SLS design governs therefore the required size of the stay cables. For extradosed bridges, where the stress variations due to live loads are less than the corresponding stress variations for the cable-stayed bridges, the SLS design is expected to govern also the size of the stay cables even in the case the permissible stress at SLS is increased as allowed for by SETRA Recommendations (2001) and the Japan Prestressed Concrete Engineering Association's Specifications (fig. 5.8).

It should be further noted that the allowable stress of the ultimate limit state strength is specified by several international specification as being equal to $\sigma_{UTS}/1.5$ ($\approx 1.5 \times 0.45\ \sigma_{UTS}$). As such the SLS design requirements, remain governing the selected size of stay cables (in case $\sigma_a = 0.45\sigma_{UTS}$ at SLS) owing to the fact that the combined ULS load factor for the dead and the live loads, is normally less than 1.5.

5-3 Structural system for extradosed bridges

As it is the case for conventional cable-stayed bridges it is generally preferred, if practically possible, to connect the piers rigidly to the deck. From the survey of the extradosed bridges built so far, it is noted that the designers were in some cases unable to connect the deck to the piers rigidly on both sides of the main span. This case occurs when the piers are too short as it is the case of the Ibi River bridge in Japan (fig. 5.11) [Kasuga 2006]. Connecting the deck rigidly to

short piers would lead to undesired restraining forces between the deck and the piers due to shrinkage, creep and thermal effects.

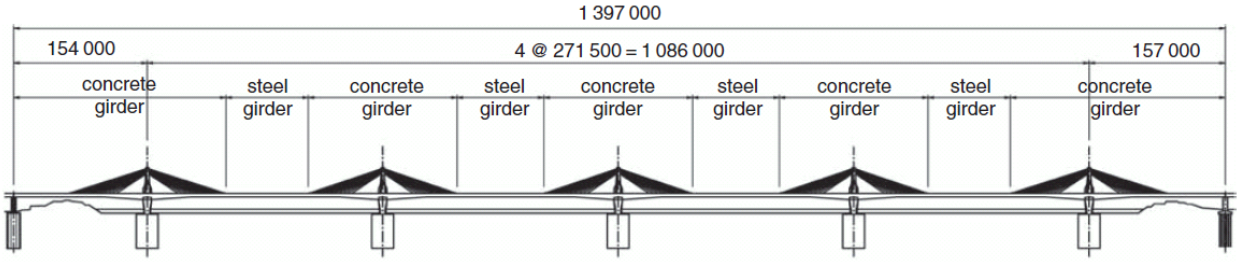

fig. 5.11: Ibi River bridge/bridge with short piers [Kasuga 2006]

The rigid connection between the deck and the piers are only recommended in case of tall/flexible piers as shown in fig. 5.12 (a) and the case of Himi bridge in Japan (fig. 5.13).
To avoid the restraining forces in the piers, they may be designed as two slender walls "leaves" as shown within fig. 5.12 (b). This approach was adopted by Dar Al-Handasah Consultants for the second Manama-Muharraq crossing in Bahrain (fig. 5.14). Selecting the pier cross sections as two leaves may be found ideal solution for pier heights more than 15m under the deck level. Such types of pier cross sections should however be examined of being able to carry the possible high torsion moment during construction in case the deck is planned to be constructed with the balanced cantilever method. The maximum torsion takes place when the two cantilevers on both sides of the tower are loaded with different transverse wind loads. For the case of short piers under the deck level, some bridge designers prefer to connect the deck rigidly only to one of the two piers and to design the deck on sliding bearings at the second pier as shown in fig. 5.12 (c).

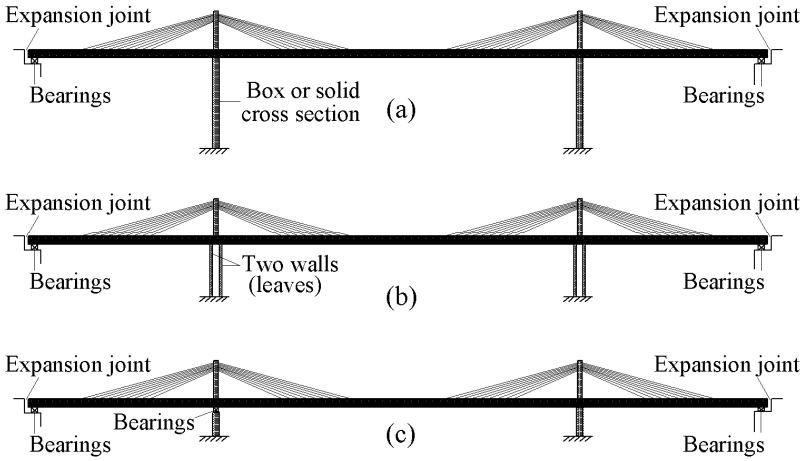

fig. 5.12: Supporting system between the deck and the piers

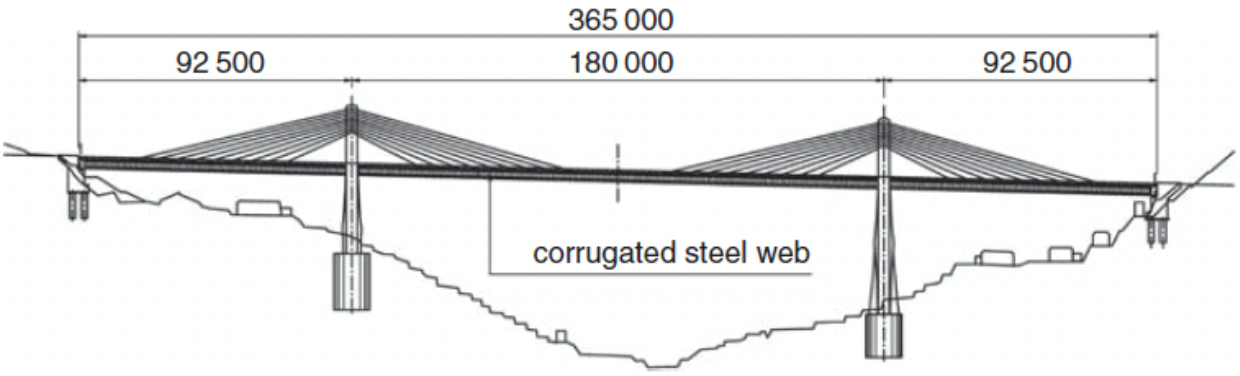

fig. 5.13: Himi bridge in Japan with high piers [Kasuga 2006]

fig. 5.14: Second Manama-Muharraq crossing in Bahrain during construction [www.archirodon.net]

Similar to the conventional cable-stayed bridges, the extradosed bridges are normally constructed with the balanced cantilever method. The ends of the two cantilevers at the middle of the main span are preferred to be connected rigidly to avoid possible future damages/kinks of connections similar to that shown within fig. 5.15 (a) to (c).

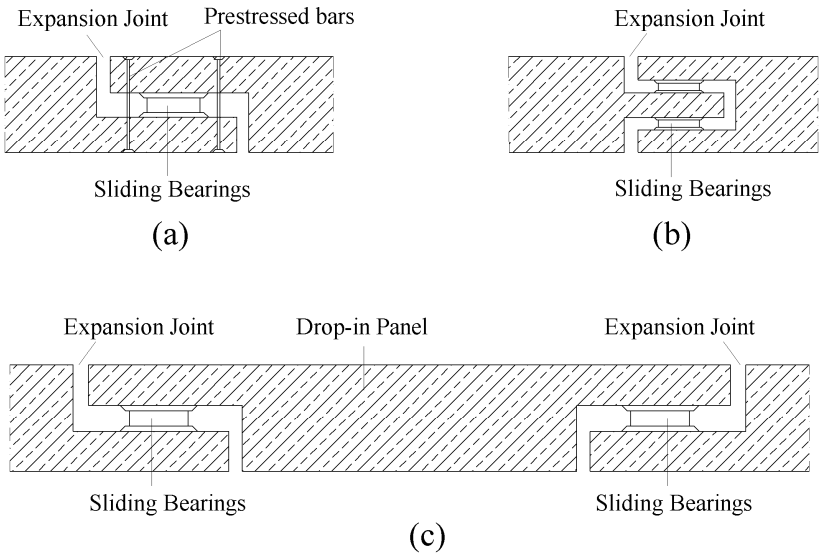

fig. 5.15: Sliding connections at the middle of the main spans

CHAPTER 6

6- PROPOSED METHOD FOR THE DETERMINATION OF THE STAY CABLE FORCES UNDER DEAD LOAD FOR EXTRADOSED BRIDGES

The stay cables of conventional cable-stayed bridges are often designed to carry nearly 100% of the dead load of the deck as shown in fig. 6.1 (a). As explained previously in (Chapter 3) the stay cable forces in fig. 6.1 (a) can be calculated by the continuous beam method assuming imaginary rigid supports at the anchorage points of each stay cable at the deck level. For extradosed bridges the continuous beam method cannot be used by assuming a rigid imaginary support at the anchorage point of each stay cable as such an assumption would mean that some stay cables would have to carry compression forces as can be easily understood from fig. 6.1 (b). Due to the unequal spans between the imaginary rigid supports, the imaginary vertical reaction forces would act upwards and downwards. Consequently, the stay cables where the reaction forces act downwards, would have to carry compression forces. The method of the continuous beam has ,therefore, to be modified as will be explained hereafter.

As shown in fig. 6.1 (c) it is proposed not to assume imaginary rigid supports at the end of each cable anchorage at the deck level, as it is the case of cable-stayed bridges but rather at the middle of each of the four groups of the stay cables. The reaction force at each of the four imaginary supports represents the corresponding sum of the vertical components of each of the four groups of the stay cables. Assuming that the stay cables and the dead load are symmetrical around the vertical axis of the pylon, the vertical component of the individual stay cables may be selected to be equal. Accordingly, the vertical components of the stay cable forces may be replaced by an equivalent uniformly distributed load W_C and the resulting bending moment distribution (BMD) under the combination of the dead load W and the equivalent vertical stay cable forces W_C, will be as shown in fig. 6.1 (c). It is important to note that equal/symmetrical stay cable forces on both sides of the pylon are needed to avoid bending or rotation of the pylon under dead load.

The method of determination of the desired value of the equivalent stay cable forces W_C in relation to the total dead load of the deck W, which in turn leads to the desired stay cable force under dead load, will be explained in Section 6-1.

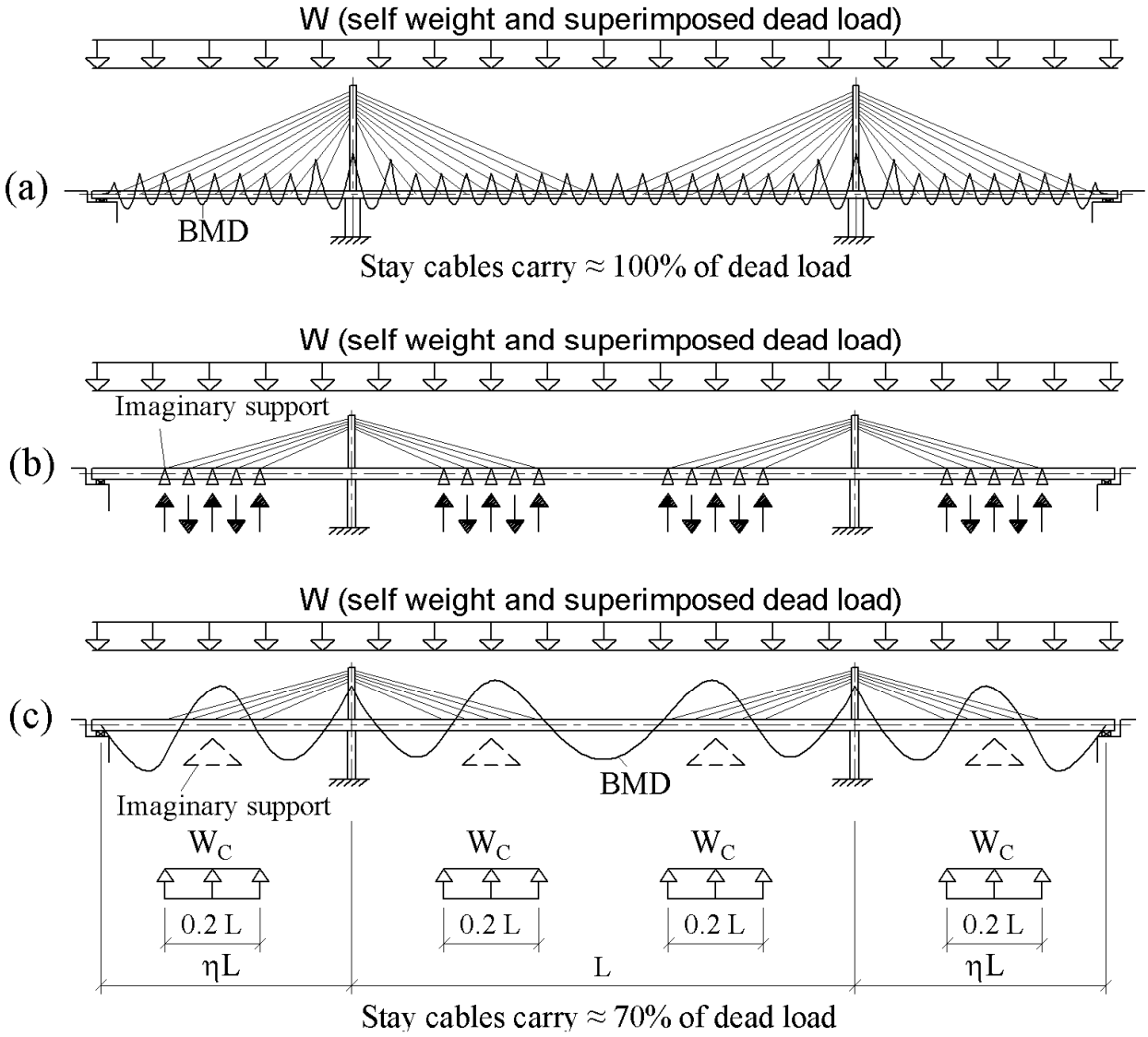

fig. 6.1: The BMD for cable-stayed bridges along the deck elements under dead load in comparison with the proposed BMD of an extradosed bridge

6-1 Method of the calculation of the desired equivalent vertical stay cable forces W_C

The general configuration of an extradosed bridge with a deck of variable depth under the variable dead load W(x) and the equivalent vertical stay cable forces W_C is shown in fig. 6.2 (a) In this research work it is proposed to select the equivalent vertical components of the stay cable forces W_C in such a way that the deflection of the deck at the points s_1, m_1, m_3 and s_2 are equal to zero (this means that the deck under dead load will behave as a continuous beam on 8-supports at the points s_1, m_1,m_3 and s_2, in addition to the already existing rigid supports at points 1 to 4. The

benefit for this is that for the pertinent moment distribution shown in fig. 6.1 (c) , the effect of creep due to bending will be eliminated at the points s_1, m_1, m_3 and s_2.

Accordingly, using the virtual work method, the following two equations may be written for the structure shown in fig. 6.2 (b):

$$\Delta Z_{s1} = \int_{-\eta\, x\, L}^{(1+\eta)\, x\, L} \frac{M(x)\ M_{s1}(x)}{E\, I(x)} dx = 0 \qquad (6.1)$$

$$\Delta Z_{m1} = \int_{-\eta\, x\, L}^{(1+\eta)\, x\, L} \frac{M(x)\ M_{m1}(x)}{E\, I(x)} dx = 0 \qquad (6.2)$$

where:

x = x-coordinate measured from support no. 2

M(x) = the bending moment at any point, along the entire length of the deck, due to the combination of W(x) and W_C

ΔZ_{s1} = the vertical deflection of deck at s_1 due to the combination of W(x) and W_C

ΔZ_{m1} = the vertical deflection of deck at m_1 due to the combination of W(x) and W_C

$M_{s1}(x)$ = the bending moment at any point, along the entire length of the deck, due to a vertical unit load F=1 acting at s_1

$M_{m1}(x)$ = the bending moment at any point, along the entire length of the deck, due to a vertical unit load F=1 acting at m_1

I(x) = the moment of inertia of the deck cross section at any point along the entire length of the deck

η = the ratio between the side span and the main span length

For a bridge with a given main span length L, dead load W(x) and moment of inertia of its deck cross section I(x), the bending moments M(x), $M_{s1}(x)$ and $M_{m1}(x)$ along the entire length of the deck will be dependant only on the unknown parameters W_C and η. Therefore, each of the two equations (6.1) and (6.2) will have only the two unknowns W_C and η. Accordingly, the solution of the two equations (6.1) and (6.2) will deliver the values of the two unknowns W_C and η which are necessary to obtain a bending moment distribution as if there were rigid supports at the points s_1, m_1, m_3 and s_2. In case such bending moment distribution is achieved, the effect of creep due to the time dependent effect "type I" at the points s_1, m_1, m_3 and s_2, can be eliminated.

For ease of understanding the method described above for the determination of W_C and η, the dead load and the moment of inertia of the deck cross section will be considered hereafter to be constant along the entire length of the deck and they will be assumed to be equal to W and I respectively. Accordingly the equations (6.3), (6.4) and (6.5) for M(x), $M_{s1}(x)$ and $M_{m1}(x)$ can be written. From fig. 6.2(b), it can be understood that equation (6.3) for the bending moment M(x) shown in fig. 6.2(d) is required to be written for 11-zones. Similarly, each of the equations (6.4) and (6.5) is written for 4-zones [refer to figs 6.2(e) and 6.2(f)]. By substituting from equations (6.3), (6.4) and (6.5) in equations (6.1) and (6.2), equations (6.1) and (6.2) can be solved for W_C and η either graphically or numerically using a mathematical software for engineering calculations [Maxfield, 2006]. Fig. 6.3 shows the graphical solution of equations (6.1) and (6.2). Each point on the curve representing equation (6.1), provides two values of η and W_C leading to a vertical deflection ΔZ_{s1} at node s_1 equal to zero independent of the vertical deflection ΔZ_{m1} at point m_1. Similarly, each point on the curve representing equation 6.2, provides two values of η and W_C leading to a vertical deflection ΔZ_{m1} at node m_1 equal to zero independent of the vertical deflection ΔZ_{s1} at point s_1. Accordingly, the intersection point of the two curves representing equations (6.1) and (6.2), is the point at which the two values η and W_C lead to simultaneous vertical deflection at the points s_1 and m_1 equal to zero. Due to the structure/loads symmetry, the deflection at the points m_3 and s_2 will be also equal to zero. It can, therefore, be concluded from fig. 6.3 that the vertical deflection at the points s_1, m_1, m_3 and s_2 (for the case of constant dead load W and constant moment of inertia I) may be achieved in case the equivalent vertical component of the stay cable forces W_C is approximately equal to 1.9 W and the side span to the main span ratio η is equal to 0.615. Accordingly, the bending moment distribution shown in fig 6.2(b) will take the desired diagram shown in fig. 6.2 (g).

Based on the above described approach, it can be also concluded that the stay cables will carry approximately 70 % of the dead load:

$$\frac{4\, W_C \text{ x } (0.2\, L)}{W\,(2\,\eta\, L + L)} = \frac{4 \text{ x } 1.9\, W \text{ x } 0.2\, L}{W\,(2 \text{ x } 0.615\, L + L)} \approx 70\%$$

As expected, the contribution of the stay cables for carrying the dead load of extradosed bridges is less than the corresponding contribution of the stay cables in case of conventional cable-stayed bridges which reaches nearly 100% [refer to fig. 6.1 (a)].

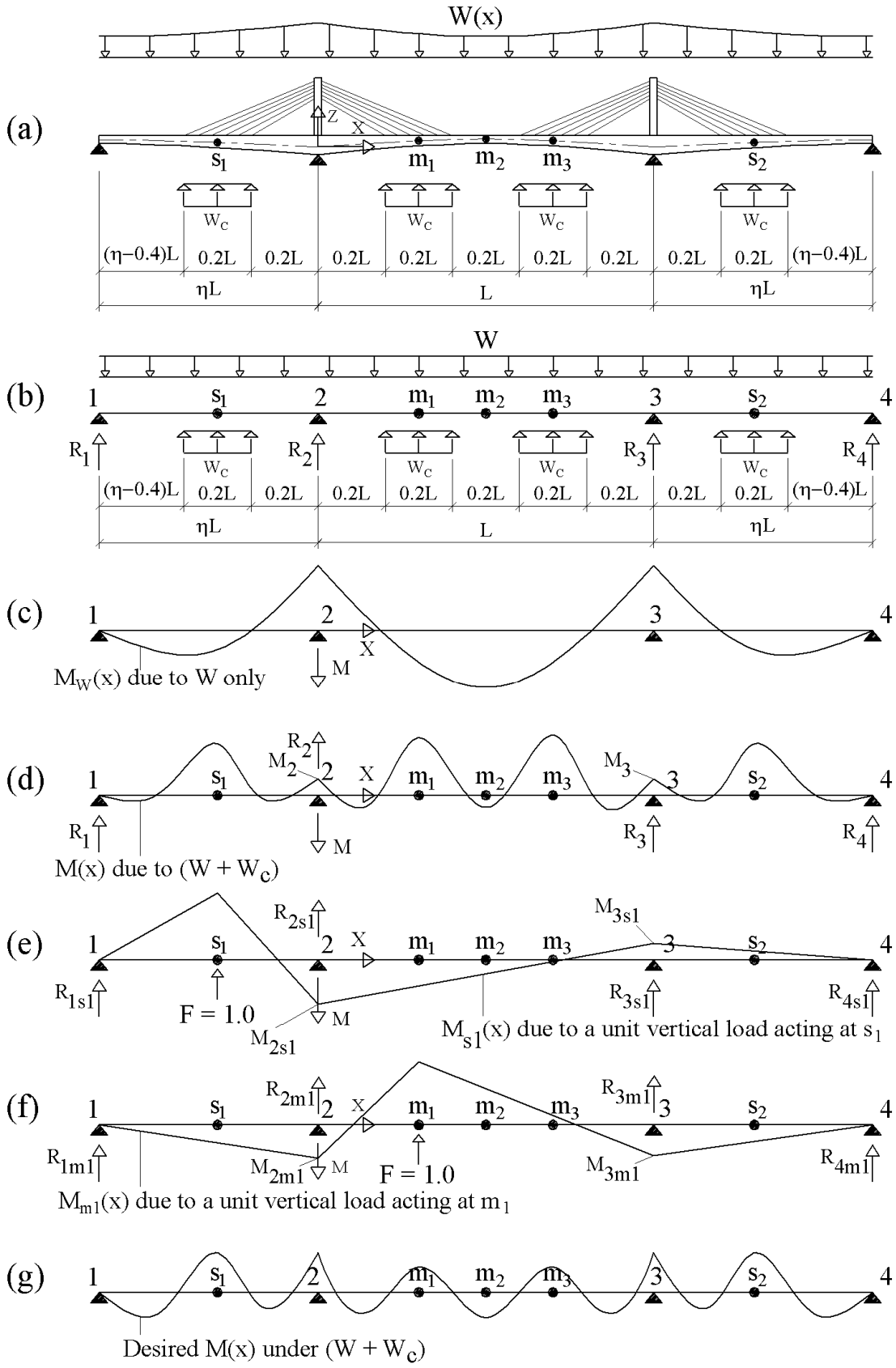

fig. 6. 2: Method for the calculation of the desired equivalent stay cable forces W_C

From fig. 6.2(b), M(x) in fig. 6.2(d) may be written for 11-zones as follows:

$$M(x)=\begin{cases} R_1(\eta L+x)-W\dfrac{(\eta L+x)^2}{2} & \text{if } -\eta L\le x\le 0.4L \\ R_1(\eta L+x)-W\dfrac{(\eta\ L+x)^2}{2}+W_C\ \dfrac{(0.4L+x)^2}{2} & \text{if } -0.4L<x\le 0.2L \\ R_1(\eta L+x)-W\dfrac{(\eta L+x)^2}{2}+0.2L\,W_C\ (0.3L+x) & \text{if } -0.2L<x\le 0 \\ M_2-W\dfrac{x^2}{2}-Q_{2r}\,x & \text{if } 0<x\le 0.2L \\ M_2-W\dfrac{x^2}{2}-Q_{2r}\,x+W_C\ \dfrac{(x-0.2L)^2}{2} & \text{if } 0.2L<x\le 0.4L \\ M_2-W\dfrac{x^2}{2}-Q_{2r}\,x+0.2L\,W_C\ (x-0.3L) & \text{if } 0.4L<x\le 0.6L \\ M_2-W\dfrac{x^2}{2}-Q_{2r}\,x+0.2L\,W_C\ (x-0.3L)+W_C\ \dfrac{(x-0.6L)^2}{2} & \text{if } 0.6L<x\le 0.8L \\ M_2-W\dfrac{x^2}{2}-Q_{2r}\,x+0.4L\,W_C\ (x-0.5L) & \text{if } 0.8L<x\le L \\ M_3-W\dfrac{(x-L)^2}{2}-Q_{3r}\ (x-L) & \text{if } L<x\le 1.2L \\ M_3-W\dfrac{(x-L)^2}{2}-Q_{3r}\,(x-L)+W_C\ \dfrac{(x-1.2L)^2}{2} & \text{if } 1.2L<x\le 1.4L \\ M_3-W\dfrac{(x-L)^2}{2}-Q_{3r}\,(x-L)+0.2L\,W_C\ (x-1.3L) & \text{if } 1.4L<x\le (1+\eta \end{cases} \tag{6.3}$$

From fig. 6.2(e), $M_{sl}(x)$ may be written for 4-zones as follows:

$$M_{sl}(x)=\begin{cases} R_{lsl}(\eta L+x) & \text{if } -\eta L\le x\le 0.3L \\ R_{lsl}(\eta L+x)+(0.3L+x) & \text{if } -3L<x\le 0 \\ M_{2sl}-Q_{2rsl}\,x & \text{if } 0<x\le 0.3L \\ M_{3sl}-Q_{3rsl}\,(x-L) & \text{if } L<x\le (1+\eta)L \end{cases} \tag{6.4}$$

From fig. 6.2(f), $M_{ml}(x)$ may be written for 4-zones as follows:

$$M_{ml}(x)=\begin{cases} R_{lml}(\eta L+x) & \text{if } -\eta L\le x\le 0 \\ M_{2ml}-Q_{2rml}\,x & \text{if } 0<x\le 0.3L \\ M_{2ml}-Q_{2rml}\,x+(x-0.3L) & \text{if } 0.3L<x\le L \\ M_{3ml}-Q_{3rml}\,(x-L) & \text{if } L<x\le (1+\eta)\ x\ L \end{cases} \tag{6.5}$$

where R_1 is the reaction force at the support (1) for the structure shown in fig. 6.2 (b) and it can be calculated by using equations (6.6), (6.7) and (6.8), noting that M_2 is the bending moment at the support (2) for the structure shown in fig. 6.2 (b) [refer also to fig. 6.2 (d)] and f_η is an unknown factor depending only on the parameter η.

$$R_1 = \frac{M_2 + \frac{W\,(\eta\,L)^2}{2} - \frac{6\,W_C\,L^2}{100}}{\eta\,L} \tag{6.6}$$

$$M_2 = \frac{-W\,L^2\left(1+\eta^3\right) + W_C\,L^2\left(\frac{62}{125} + 24\,f_\eta\right)}{8\,\eta + 12} = M_3 \tag{6.7}$$

$$f_\eta = \left(\frac{1}{50}\,\eta - \frac{7}{750} + \frac{1}{1000}\,\frac{1}{\eta}\right) \tag{6.8}$$

R_2 is the reaction force at the support (2) for the structure shown in fig. 6.2 (b) and it can be calculated by using equation (6.9)

$$R_2 = \frac{W\,(L + 2\,\eta\,L) - 0.8\,L\,W_C - 2\,R_1}{2} \tag{6.9}$$

R_3 is the reaction force at the support (3) for the structure shown in fig. 6.2 (b) and it is equal to R_2 due to the structure symmetry.

Q_{2r} is the shear force on the right hand side of the support (2) for the structure shown in fig. 6.2 (b) and it can be calculated by using equation (6.10)

$$Q_{2r} = -R_1 + W\,\eta\,L - 0.2\,L\,W_C - R_2 \tag{6.10}$$

Q_{3r} is the shear force on the right hand side of the support (3) for the structure shown in fig. 6.2 (b) and it can be calculated by using equation (6.11)

$$Q_{3r} = Q_{2r} + W\,L - 0.4\,L\,W_C - R_3 \tag{6.11}$$

R_{1s1} is the reaction force at the support (1) for the structure shown in fig. 6.2 (e) and it can be calculated by using equations (6.12), (6.13) and (6.14) noting that M_{2s1} and M_{3s1} are the bending moments at the supports (2) and (3) respectively for the structure shown in fig. 6.2 (e).

$$R_{1s1} = \frac{M_{2s1} - 0.3\,L}{\eta\,L} \tag{6.12}$$

$$M_{2s1} = -2\,(\eta+1)\,M_{3s1} \tag{6.13}$$

$$M_{3s1} = \frac{6\,\frac{L}{\eta}\left(0.1\,\eta^2 - 0.045\,\eta + 0.0045\right)}{1-4\,(\eta+1)^2} \tag{6.14}$$

R_{4s1} , R_{3s1} , R_{2s1} are the reaction forces at the support (4), (3) and (2) for the structure shown in fig. 6.2 (e) and they can be calculated by using equations (6.15), (6.16) and (6.17)

$$R_{4s1} = \frac{M_{3s1}}{\eta\,L} \tag{6.15}$$

$$R_{3s1} = \frac{M_{2s1} - R_{4s1}\,(\eta+1)\,L}{L} \tag{6.16}$$

$$R_{2s1} = \frac{M_{3s1} - R_{1s1}\,(\eta+1)\,L - 1.3\,L}{L} \tag{6.17}$$

Q_{2rs1} is the shear force on the right hand side of the support (2) for the structure shown in fig. 6.2 (e) and it can be calculated by using equation (6.18)

$$Q_{2rs1} = -R_{1s1} - R_{2s1} - 1 \tag{6.18}$$

Q_{3rs1} is the shear force on the right hand side of the support (3) for the structure shown in fig. 6.2 (e) and it can be calculated by using equation (6.19)

$$Q_{3rs1} = -R_{1s1} - R_{2s1} - 1 - R_{3s1} \tag{6.19}$$

R_{1m1} is the reaction force at the support (1) for the structure shown in fig. 6.2 (f) and it can be calculated by using equations (6.20), (6.21) and (6.22) noting that M_{2m1} and M_{3m1} are the bending moments at the supports (2) and (3) respectively for the structure shown in fig. 6.2 (f).

$$R_{1m1} = \frac{M_{2m1}}{\eta L} \tag{6.20}$$

$$M_{2m1} = \frac{0.714(\eta+1) - 0.273}{4(\eta+1)^2 - 1} \text{ x } L \tag{6.21}$$

$$M_{3m1} = 0.357\,L - 2\,(\eta+1)\,M_{2m1} \tag{6.22}$$

R_{4m1} , R_{3m1} and R_{2m1} are the reaction forces at the support (4), (3) and (2) for the structure shown in fig. 6.2 (f) and they can be calculated by using equations (6.23), (6.24) and (6.25)

$$R_{4m1} = \frac{M_{3m1}}{\eta\ L} \tag{6.23}$$

$$R_{2m1} = \frac{M_{3m1} - R_{1m1}(\eta+1)\ L - 0.7\,L}{L} \tag{6.24}$$

$$R_{3m1} = \frac{M_{2m1} - R_{4m1}(\eta+1)\ L - 0.3\,L}{L} \tag{6.25}$$

Q_{2rm1} is the shear force on the right hand side of the support (2) for the structure shown in fig. 6.2 (f) and it can be calculated by using equation (6.26)

$$Q_{2m1} = -R_{1m1} - R_{2m1} \tag{6.26}$$

Q_{3rm1} is the shear force on the right hand side of the support (3) for the structure shown in fig. 6.2 (f) and it can be calculated by using equation (6.27)

$$Q_{3m1} = -R_{1m1} - R_{2m1} - 1 - R_{3m1} \tag{6.27}$$

fig. 6.3: Determination of the ideal values of η and W_C / W

Upon the determination of the desired equivalent stay cable forces W_C and the corresponding desired bending moment distribution as explained above, the desired stay cable force for each stay cable F_{Di} under dead load may be determined, by hand calculatin, by using the following equation (refer also to fig. 6.4):

$$F_{Di} = \frac{0.20\, W_C\, L}{n' \sin(\theta_i)} = \frac{0.38\, WL}{n' \sin(\theta_i)} \qquad (6.28)$$

where:

n' = the nos. of the stay cables within the length 0.2 L

θ_i = the angle of stay cable i as shown in fig. 6.4 (a)

For the achievement of the desired stay cable forces F_{Di} under dead load in the computer model, during the design stage, each stay cable will be required to be shortened/re-stressed by a force equal to ΔF_i . The re-stressing force ΔF_i for each stay cable may be determined by using equation (29) (refer to Section 3-3). For the installation of the stay cables during construction, the un-stressed length for stay cable no. i, should be determined from the force F_{Di} and the stressed length L_i calculated from the deformed bridge structure shown in fig. 6.4 (c). In case the deck elements are fabricated with a precamber profile [= the mirror profile of the deck deflection line shown in fig. 6.4 (c)], the un-stressed length of the stay cable no. i, is to be determined by using the force F_{Di} and the stressed length L_i calculated from the un-deformed structure.

$$\begin{pmatrix} f_{11} & f_{12} & \cdots & f_{1i} & \cdots & f_{1(n-1)} & f_{1n} \\ f_{21} & f_{22} & \cdots & f_{2i} & \cdots & f_{2(n-1)} & f_{2n} \\ \cdots & \cdots & \cdots & \cdots & \cdots & \cdots & \cdots \\ f_{j1} & f_{j2} & \cdots & f_{ji} & \cdots & f_{j(n-1)} & f_{jn} \\ \cdots & \cdots & \cdots & \cdots & \cdots & \cdots & \cdots \\ f_{(n-1)1} & f_{(n-1)2} & \cdots & f_{(n-1)i} & \cdots & f_{(n-1)(n-1)} & f_{(n-1)n} \\ f_{n1} & f_{n2} & \cdots & f_{nj} & \cdots & f_{n(n-1)} & f_{nn} \end{pmatrix} \begin{pmatrix} \Delta F_1 \\ \Delta F_2 \\ \cdots \\ \Delta F_j \\ \cdots \\ \Delta F_{(n-1)} \\ \Delta F_n \end{pmatrix} = \begin{pmatrix} F_{D1} - F_1 \\ F_{D2} - F_2 \\ \cdots \\ F_{Dj} - F_j \\ \cdots \\ F_{D(n-1)} - F_{(n-1)} \\ F_{Dn} - F_n \end{pmatrix} \qquad (6.29)$$

where (refer also to fig. 6.4) :

n = total nos. of stay cables

F_{Di} = desired stay cable force for the cable no. i as per equation (6.28)

F_i = stay cable force of the cable no. i under the effect of the dead load prior to the shortening/re-stressing of any stay cable by the forces ΔF_i

F_{ji} = force in stay cable no. j due to tensioning the stay cable no. i by a force equal to 1

Note: Upon the re-stressing of all stay cables by the respective force ΔF_i, the stay cable force F_i and the bending moment distribution shown in fig. 6.4 (a) will be changed to the desired stay cable force F_{Di} and the desired bending moment distribution shown in fig. 6.4(b).

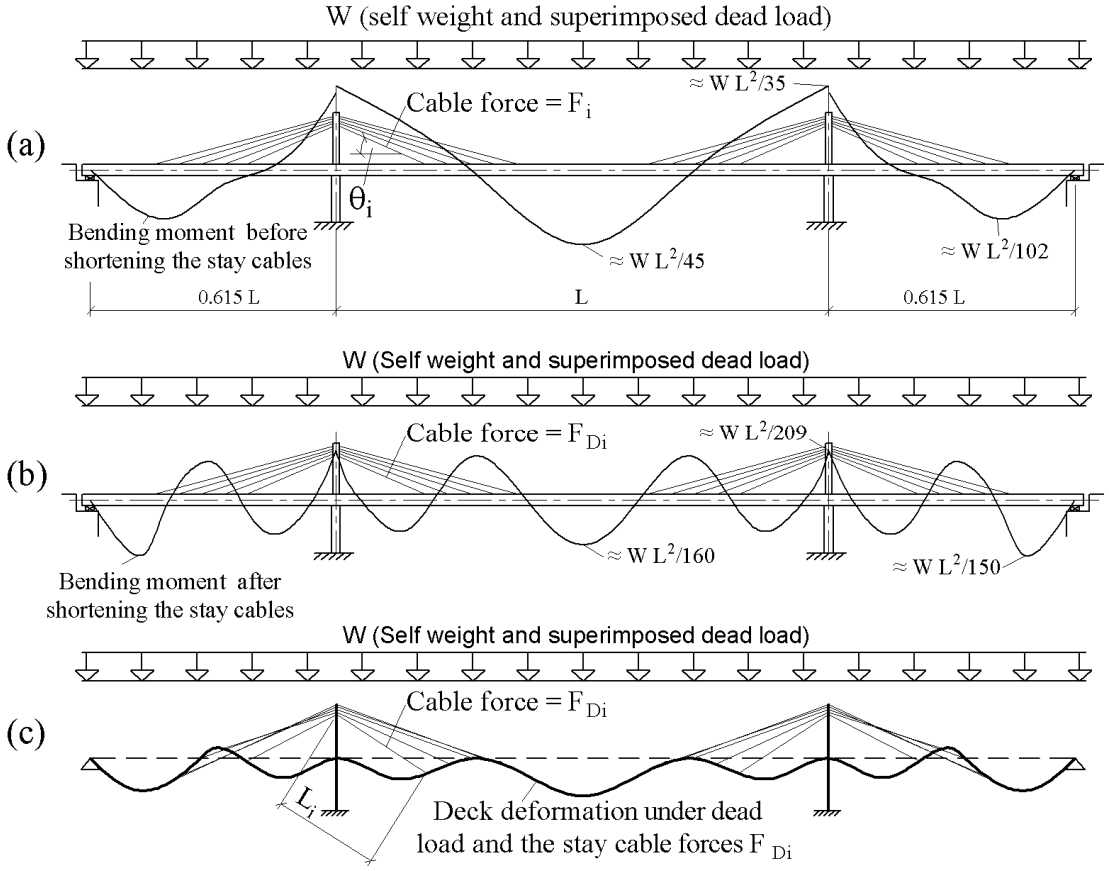

fig. 6.4: Method for the calculation of the desired stay cable force F_{Di} as per equation (6.29)

6-2 Proposed method for handling the prestressing forces for extradosed bridges

As explained under Section 6-1, equation (6.29) can be used to achieve the bending moment distribution shown in fig. 6.4(b). Equation (6.29) is suitable for use for extradosed bridges with steel deck or steel/concrete composite deck. For extradosed bridges with concrete deck section, the bending moment distribution shown in fig.6.4(b), can be further reduced by using prestressing tendons as will be explained. The use of prestressing tendons for extradosed bridges is helpful during erection and also for the completed structure, noting that the stay cables do not support the entire deck length contrary to the configuration of conventional cable-stayed bridge.

6-2-1 Use of concordant prestressing cable profiles for continuous beams [Lin and Burns 1989] [Leonhardt 2004]

To ease the understanding of the possible use of concordant prestressing profiles within the deck of extradosed bridges, such prestressing arrangement will be first briefly explained for continuous beams resting on rigid and flexible supports. Fig. 6.5 (a) shows a continuous beam on rigid supports under the effect of uniform load W and the related reaction forces R_i. The typical bending moment distribution resulting from W is shown in fig. 6.5 (b). The prestressing tendons which may be used for such a continuous beam can be grouped and represented by a cable profile affine with the bending moment distribution shown in fig. 6.5 (b). This means that the ordinate of the cable profile at any point z(x), measured from the neutral axis of the continuous beam, will be equal to M(x) divided by a constant value C (=the affinity factor) [refer to fig. 6.5 (c)].

$$z(x) = \frac{M(x)}{C} \tag{6.30}$$

Assuming that the prestressing force of the concordant cable is equal to F_P and by ignoring the friction prestressing losses, the prestressing forces of the concordant cable may be replaced by an equivalent uniform load W_{eq} and equivalent nodal loads $P_{eq\text{-}i}$ acting at the support no. i.

where:

$$W_{eq} = F_P \frac{d^2 z(x)}{dx^2} = \frac{F_P}{C} \frac{d^2 M(x)}{dx^2} = W \frac{F_P}{C} \tag{6.31}$$

$$P_{eq-i} = R_i \frac{F_P}{C} \tag{6.32}$$

From equations (6.31) and (6.32), it can be seen that the ratio between the equivalent uniform load W_{eq} and W is equal to the ratio between the equivalent nodal load P_{eq-i} and the reaction force R_i. Accordingly, the vertical reaction forces R'_i at the rigid supports due to the concordant prestressing forces will be equal to zero [refer to fig. 6.5 (d)] regardless of the selected prestressing force F_P. It can be further understood that in case the prestressing force F_P is selected to be equal to the affinity factor C in equation (6.30), the equivalent uniform and nodal loads W_{eq} and P_{eq-i} will be equal to W and R_i respectively. Accordingly, the resultant bending moment due to the combination of the external load W and the prestressing forces will be equal to zero.

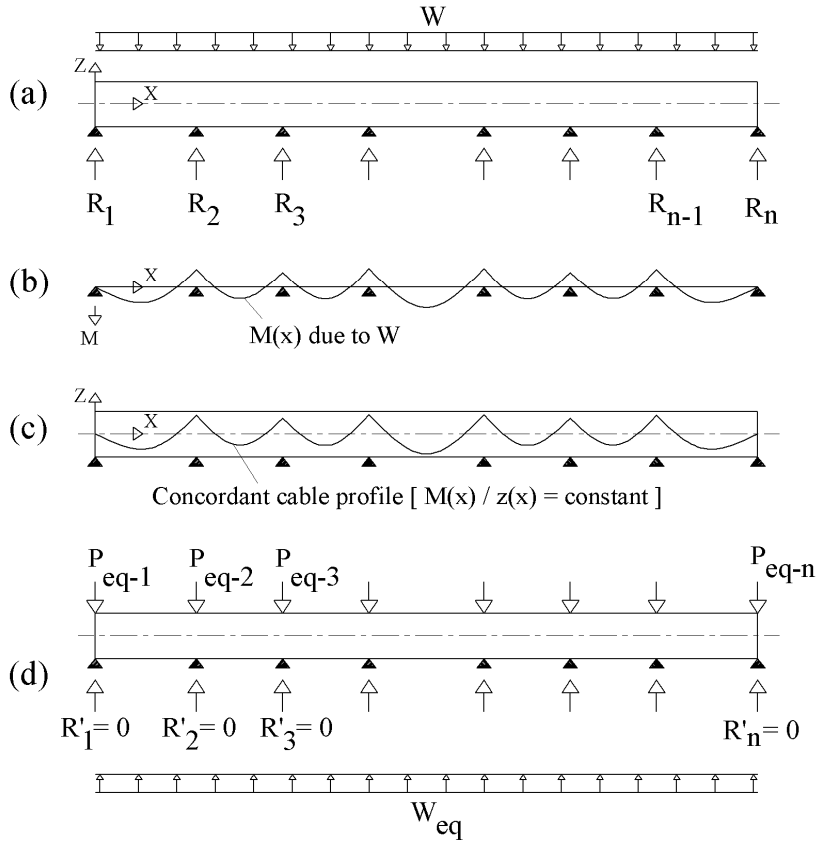

fig. 6.5: Use of a concordant prestressing cable profile for continuous beams

As the deck of the extradosed bridges is carried by rigid supports (piers and abutments) and elastic supports (stay cables), the use of the concordant prestressing for continuous beams resting on flexible supports will be also explained. Fig. 6.6 shows the application of the concordant cable profile on a continuous beam resting on internal flexible springs in addition to the end rigid supports. The reaction forces of the internal springs S_i due to the external uniform load W, are shown in fig. 6.6 (a). The reaction forces of the springs and the corresponding bending moment distribution M(x) shown in fig. 6.6 (b) will be dependent on both of the stiffness of the springs

and the bending stiffness of the beam. In case the used prestressing tendons are represented by a concordant cable profile fig. 6.6 (c), the ordinate z(x) of such a cable profile will be equal to the value of M(x) shown in fig. 6.6 (b) divided by the affinity factor C (refer to equation 6.30). Assuming further that the prestressing force F_P, is selected equal to C, the prestressing forces can be replaced by the equivalent uniform and nodal loads W_{eq} and P_{eq-i} as shown in fig. 6.6 (d). The values of the equivalent loads W_{eq} and P_{eq-i} will be equal to W and S_i shown in fig. 6.6 (a) but in opposite direction. By comparing figs. 6.6 (d) and 6.6 (a), the reaction forces at the springs due to the upward equivalent uniform load W_{eq} (= W) alone, will be equal to downward reaction forces S_i having the same values shown in fig. 6.6 (a). As the upward reaction forces due to the equivalent nodal loads P_{eq-i} shown in fig. 6.6 (d), would be equal to S_i only in case the springs are very stiff, the final reaction forces R'_i of the internal springs will not be equal to zero as it would have been in the case of internal rigid supports. Accordingly, the resultant bending moment due to the combination of the external load W and the concordant prestressing forces, will not be equal to zero.

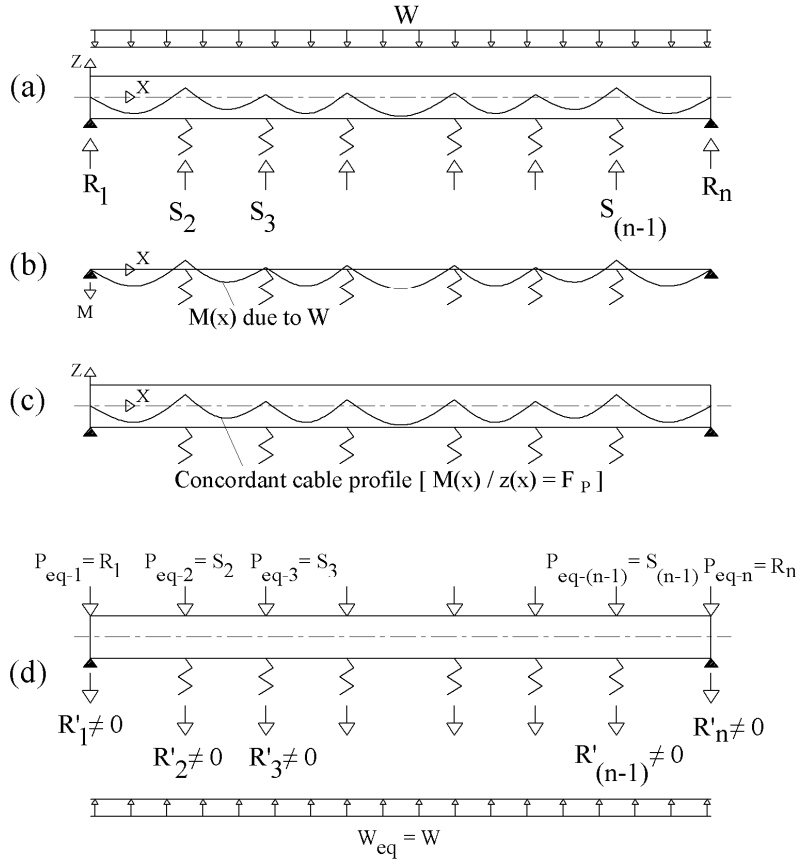

fig. 6.6: Behavior of continuous beam on springs under the effect of the equivalent prestressing forces

6-2-2 Possible use of concordant cable profiles for the extradosed bridges

The typical prestressing configuration for extradosed bridges follows in general the arrangement shown in fig. 6.7 (a). Similar prestressing configuration was adopted for the design of Odawara extradosed bridge in Japan (completed in 1994) and the Second Vivekananda extradosed bridge in India (completed in 2007). As explained under 6.1, it is possible to select the stay cable forces for the completed bridge to achieve bending moment distribution under dead load similar to that shown in fig. 6.4 (b). The achievement of such bending moment distribution allows the possible use of draped tendons within the side and main spans of extradosed bridges. A study has been made to investigate the possible arrangement of concordant cable profile as that shown in fig. 6.7(b) which is affine with the bending moment distribution of fig. 6.4 (b). As explained under 6.2.1, the use of concordant prestressing profile within a continuous beam on flexible supports, does not lead to zero reaction forces at the flexible supports. Similarly, the use of concordant cable profiles within the deck elements of the extradosed bridge [(fig. 6.7 (b)] leads to a change of the stay cable forces. Fig. 6.8 (a) shows the bending moment distribution for extradosed bridge under dead load before re-stressing the stay cables [which is similar to fig. 6.4 (a)]. Under the effect of the concordant prestressing alone, the change of the force in stay cable "i" is assumed to be equal to F_{PTi} [refer to fig. 6.8 (b)]. Due to the existence of the stay cable forces F_{PTi} , resulting from the prestressing forces, the bending moment distribution shown in fig. 6.8 (b) is not exactly equal to the mirror of the bending moment distributions shown in fig 6.8 (c) or 6.4 (b) which are based on the calculation made under 6.1. If however, each stay cable force is re-stressed by a force ΔF_i in accordance with equation 6.33 (compare it with equation 6.29), the desired stay cable forces F_{Di} (as calculated under 6.1) will be kept unchanged and the final bending moment distribution due to dead load, stay cable forces and prestressing forces will be equal to zero.

$$\begin{pmatrix} f_{11} & f_{12} & \cdots & f_{1i} & \cdots & f_{1(n-1)} & f_{1n} \\ f_{21} & f_{22} & \cdots & f_{2i} & \cdots & f_{2(n-1)} & f_{2n} \\ \cdots & \cdots & \cdots & \cdots & \cdots & \cdots & \cdots \\ f_{j1} & f_{j2} & \cdots & f_{ji} & \cdots & f_{j(n-1)} & f_{jn} \\ \cdots & \cdots & \cdots & \cdots & \cdots & \cdots & \cdots \\ f_{(n-1)1} & f_{(n-1)2} & \cdots & f_{(n-1)i} & \cdots & f_{(n-1)(n-1)} & f_{(n-1)n} \\ f_{n1} & f_{n2} & \cdots & f_{nj} & \cdots & f_{n(n-1)} & f_{nn} \end{pmatrix} \begin{pmatrix} \Delta F_1 \\ \Delta F_2 \\ \cdots \\ \Delta F_j \\ \cdots \\ \Delta F_{(n-1)} \\ \Delta F_n \end{pmatrix} = \begin{pmatrix} F_{D1} - F_1 - F_{PT1} \\ F_{D2} - F_2 - F_{PT2} \\ \cdots \\ F_{Dj} - F_j - F_{PTj} \\ \cdots \\ F_{D(n-1)} - F_{(n-1)} - F_{PT_{(n-1)}} \\ F_{Dn} - F_n - F_{PTn} \end{pmatrix} \quad (6.33)$$

In reality the prestressing cables will be installed as polygonal lines and not exactly affine with the bending moment curve shown in fig. 6.8 (c). However, the closer the real polygonal prestressing profile to the concordant profile, the closer to zero will be the final bending moment under the combinations of the dead load, the stay cable forces and the prestressing forces.

It should also be understood that in case it is not possible to arrange many tendons within the selected deck cross section (i.e. if it is not possible to get the prestressing force F_P to be equal to the affinity factor C in equation 6.30), the concordant cable profile can still be used with a prestressing force less than the affinity factor C in equation 6.30. Equation (6.33) remains also valid provided that the stay cable forces F_{PTi} are based on the actual selected prestressing force. The resultant bending moment due to dead load, stay cable forces and the selected prestressing force will be as shown in fig 6.8 (c) in dotted line.

Naturally, the bridge elements should be checked for all possible service and ultimate load case combinations and if necessary additional prestressing tendons may be added in such a way that the center of gravity of the additional tendons coincide with the center of gravity of the deck cross section and, therefore, only axial prestressing forces would be introduced and will not affect the desired stay cable forces F_{Di}.

Further to the above explanation it is self evident that the effect of the prestressing losses should be taken into consideration (the prestressing losses due to elastic shortening of the deck cross section, friction losses, slippage of wedges, shrinkage and creep of the concrete material and relaxation of the prestressing steel material).

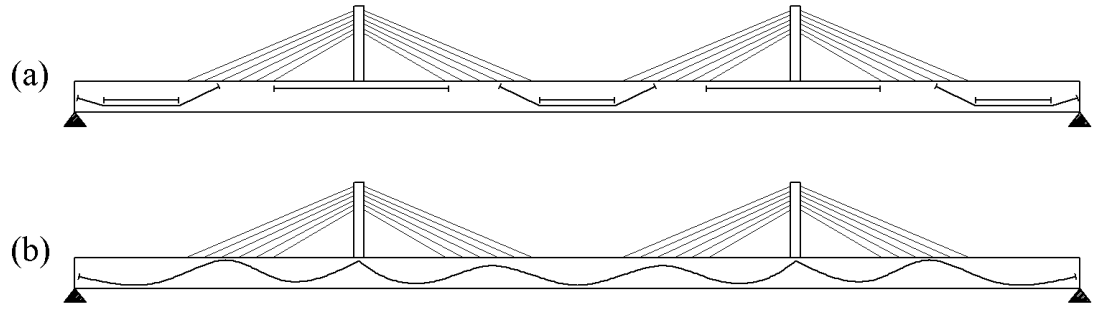

fig. 6.7: Prestressing configurations for extradosed bridges

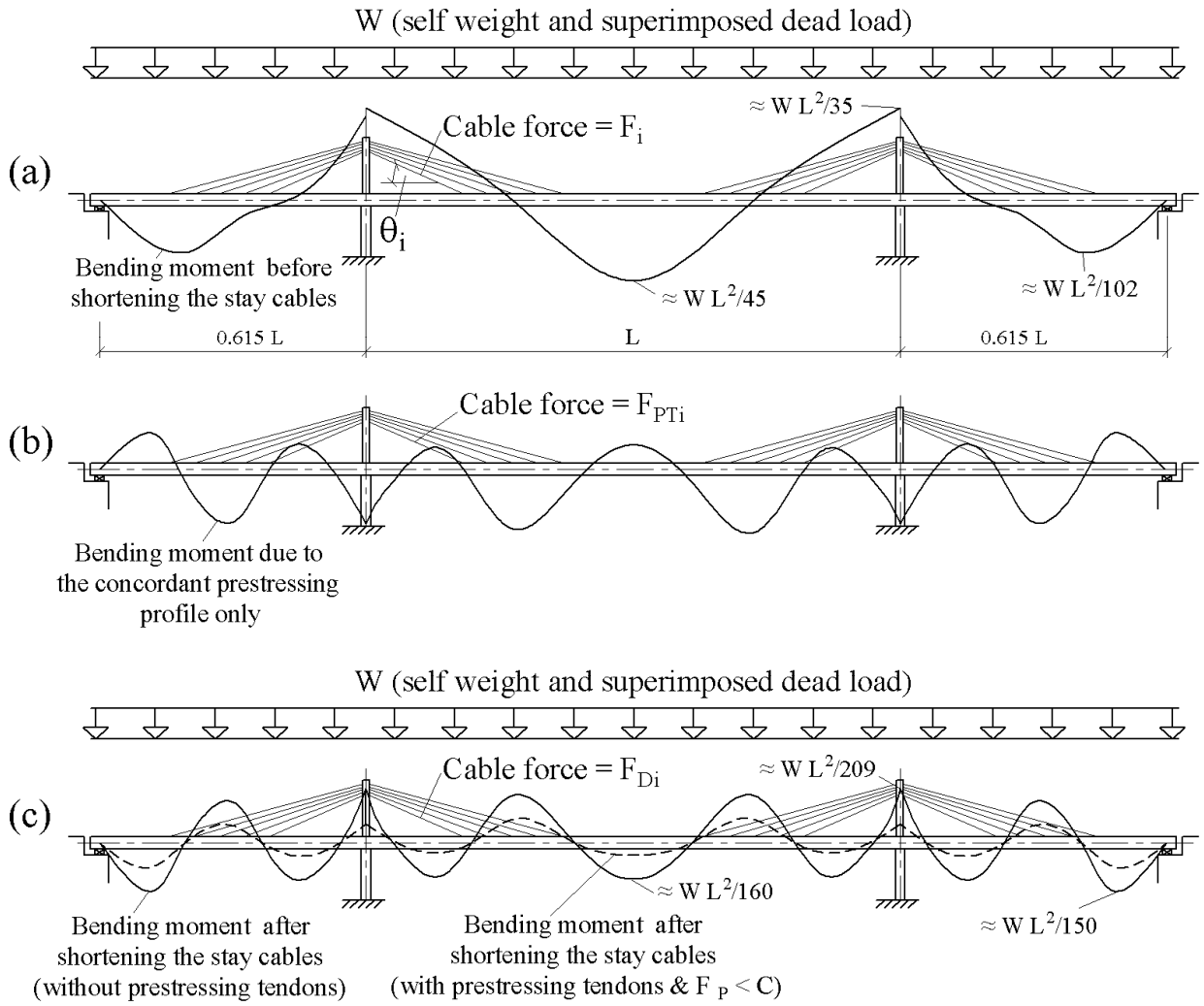

fig. 6.8: Method for the calculation of the desired stay cable force F_{Di} taking into account the effect of the prestressing forces as per equation (6.33)

6-2-3 Handling prestressing configurations other than concordant profiles

The advantage of the possible use of concordant cable profile within the deck elements of the extradosed bridges is explained under 6.2.2. Bridge designers may, however, opt to use external straight tendons as that shown in figs. 6.9 to 6.11, noting that the external tendons have the advantage of being replaceable. In case the deck is to be constructed with the balanced cantilever method, the use of permanent top straight tendons similar to that shown in fig. 6.10, may be found as the preferred option rather than using temporary stressing bars.

Such arrangement of prestressing cables (internal or external) may affect the desired stay cable forces F_{Di} calculated under 6.1 by up to nearly 15%. The use of equation (6.33) may however serve to handle both of the stay cable forces and the prestressing forces separately as far as the

bending moment distributions due to both of them are concerned. By using equation (6.33), the change of the stay cable forces due to any selected prestressing configuration can be eliminated. Accordingly, the bending moment distribution resulting from any selected scheme of the prestressing can be determined as if the stay cables were not existing. Based on this approach the bending moments resulting from the prestressing configurations shown in figs. 6.9 to 6.13, may be calculated with the help of equations (6.34) to (6.60) noting that these equations were derived assuming that the moment of inertia of the deck cross section is constant along the entire bridge length and noting also that the prestressing losses have been ignored (Note: the reaction forces at the supports nos. 1 and 2 and the bending moment at the support no. 2 are sufficient to draw the bending moment diagram BMD along the entire deck length). These equations are considered to be very useful during the initial design stage where simple hand calculations are normally preferred to be carried out. Using the same equations, the plausibility of the computer results during the detailed design stage may be examined as well.

In fig. 6.12, it is useful to understand that the function of the draped tendons as per the equations 6.43 to 6.49 along with equation 6.33, is to counterbalance part or the full uniform dead load W from the central span, where there are no stay cables, without affecting the stay cable forces. The extent of the said counterbalancing of the uniform dead load W, will depend on the selected nos. of prestressing tendons and/or the prestressing force F_P. The same is valid for the draped tendons in the side spans shown in fig. 6.13 (refer also to equations 6.50 to 6.60.

The forces resulting from the bottom straight tendons at the middle of the main span (fig. 6-9):

$$M_f = -F_P\, e_b \tag{6.34}$$

$$M_2 = -3\, M_f \frac{L_f}{L} \frac{1}{3+2\eta} \tag{6.35}$$

$$R_{1f} = -R_{2f} = \frac{M_2}{\eta L} = -3\, M_f \frac{L_f}{\eta L^2} \frac{1}{3+2\eta} \tag{6.36}$$

The forces resulting from the top straight tendons at the pylons (fig. 6-10)

$$M_s = F_P\, e_t \tag{6.37}$$

$$M_2 = M_s \left(1 - \frac{24\, L_s\, \eta L - 3\, L_s^2}{12\, \eta L^2\, (\eta + 1) - 4\, \eta^2\, L^2} \right) \tag{6.38}$$

$$R_{1s} = -R_{2s} = -M_s \left(\frac{24\, L_s\, \eta\, L - 3\, L_s^2}{12\, \eta^2\, L^3\, (\eta + 1) - 4\, \eta^3\, L^3} \right) \tag{6.39}$$

The forces resulting from the bottom straight tendons in the side spans (fig. 6-11)

$$M_o = -F_P\, e_b \tag{6.40}$$

$$M_2 = \frac{-6\, M_o\, L_o \left(\lambda\, L + \frac{L_o}{2} \right)}{3\, \eta\, L^2\, (\eta + 1) - \eta^2\, L^2} = R_{1o} \eta\, L \tag{6.41}$$

$$R_{1o} = -R_{2o} = \frac{M_2}{\eta\, L} \tag{6.42}$$

The forces resulting from draped tendons at the middle of the main span (fig. 6-12)

$$W_{eq} = \frac{8\, e_b}{L_f^2} F_P \quad , \quad P = \frac{-4\, e_b}{L_f} F_P \tag{6.43}$$

$$M_{2w} = \frac{\frac{W_{eq}\, L_f}{48} \left(3\, (L - L_f)^2 + 6\, L_f\, (L - L_f) + 2\, L_f^2 \right)}{L \left(\frac{\eta}{3} + \frac{1}{2} \right)} \tag{6.44}$$

$$R_{1w} = \frac{M_{2w}}{\eta\, L} \quad , \quad R_{2w} = \frac{-W_{eq}\, L_f}{2} - R_{1w} \tag{6.45}$$

$$R_{2p} = \frac{3\, P\, \eta\, L\, (2\, \eta\, L + L + L_f) \left(\eta\, L + \frac{L - L_f}{2} \right) - 2\, P\, \eta^3\, L^3}{6\, \eta^2\, L^3\, (\eta + 1) - 2\, \eta^3\, L^3} \tag{6.46}$$

$$R_{1p} = -(R_{2p} + P) \tag{6.47}$$

$$M_{2p} = R_{1p}\, \eta\, L \tag{6.48}$$

$$M_2 = M_{2w} + M_{2p} \tag{6.49}$$

The forces resulting from draped tendons in the side spans (fig. 6-13)

The forces due to the equivalent uniform load W_{eq} alone, can be determined by using the equations (6.50) to (6.55)

$$W_{eq} = \frac{8\, e_b}{L_o^2} F_P \tag{6.50}$$

$$r_1 = W_{eq}\, L_o \frac{\left(\eta L - \lambda L - \frac{L_o}{2}\right)}{\eta L} \quad , \quad r_2 = W_{eq}\, L_o \frac{\left(\lambda L + \frac{L_o}{2}\right)}{\eta L} \tag{6.51}$$

where r_1 and r_2 are supplementary variables and will be used below to determine M_{2w} in equation (6.52)

$$\begin{aligned} &\frac{1}{3}\frac{\lambda^3}{\eta} L^2 r_1 + L_o\, r_2 \left(\eta L - \lambda L - L_o\right) \frac{\lambda L + \frac{L_o}{2}}{\eta L} + \frac{1}{2} L_o \left(r_1 \lambda L - r_2 \left(\eta L - \lambda L - L_o\right)\right) \frac{\lambda L + \frac{L_o}{3}}{\eta L} \\ &+ \frac{1}{12} W_{eq}\, L_o^3 \frac{\lambda L + \frac{L_o}{2}}{\eta L} + \frac{1}{2} r_2 \left(\eta L - \lambda L - L_o\right)^2 \frac{\eta L - \frac{2}{3}\left(\eta L - \lambda L - L_o\right)}{\eta L} = M_{2w}\, L \left(\frac{1}{2} + \frac{\eta}{3}\right) \end{aligned} \tag{6.52}$$

$$R_{1w} = -\frac{W_{eq}\, L_o \left(\eta L - \lambda L - \frac{L_o}{2}\right) - M_{2w}}{\eta L} \tag{6.53}$$

$$R_{2w} = -\left(W_{eq}\, L_o + R_{1w}\right) \tag{6.54}$$

The forces due to each two symmetrical nodal loads P, may be calculated by using equations (6.55) to (6.60). L_{si} in equation (6.56) should be substituted by (ηL - λL - L_o) and (ηL - λL) for the first and the second two symmetrical nodal loads respectively as per equation (6.57) The final forces resulting from the equivalent uniform loads W_{eq} and the 2x2 vertical nodal loads P, can be determined then by superposition.

$$P = \frac{-4\, e_b}{L_f} F_P \tag{6.55}$$

$$R_{2p} = \sum_{i=1}^{2} \frac{-P\left(3\,\eta L\left(\eta L + L + L_{si}\right)\left(\eta L - L_{si}\right) - \left(\eta L - L_{si}\right)^2 \left(\eta L + 2\, L_{si}\right) - 3\, L_{si}^2 \left(\eta L - L_{si}\right)\right)}{3\,\eta^2 L^3 \left(\eta + 1\right) - \eta^3 L^3} \tag{6.56}$$

$$L_{s1} = \eta L - \lambda L - L_o \quad , \quad L_{s2} = \eta L - \lambda L \tag{6.57}$$

$$R_{1p} = -2P - R_{2p} \tag{6.58}$$

$$M_{2p} = R_{1p}\, \eta L + P\left(L_{s1} + L_{s2}\right) \tag{6.59}$$

$$M_2 = M_{2w} + M_{2p} \tag{6.60}$$

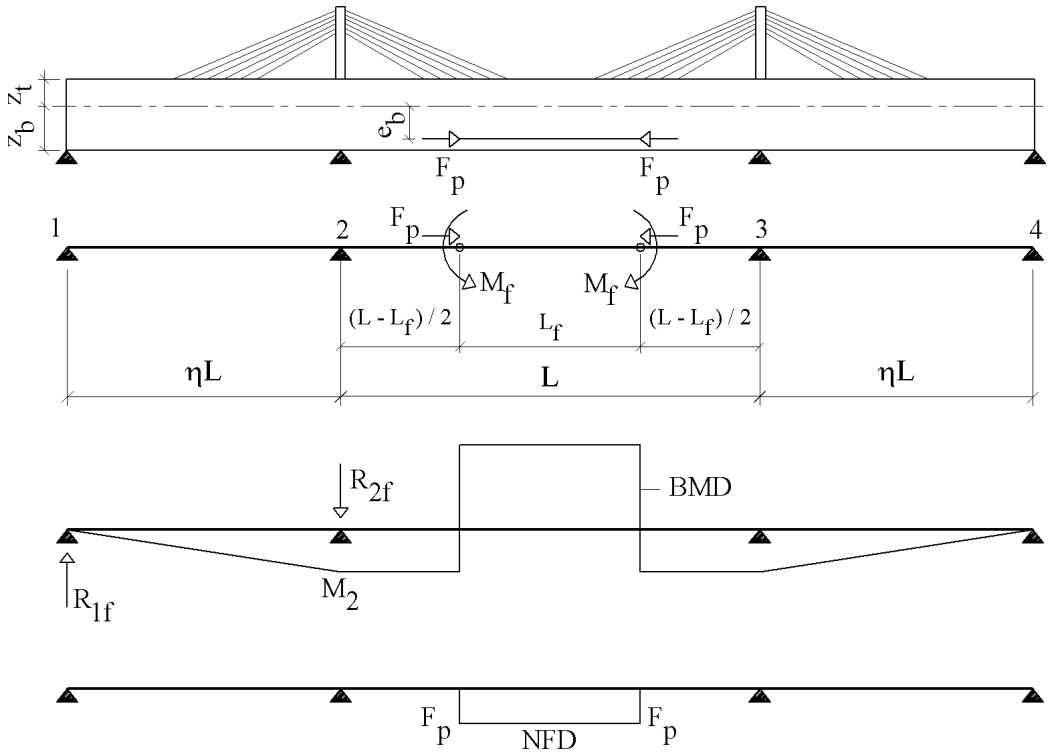

fig. 6.9: BMD and NFD due to bottom straight tendons at the middle of the main span

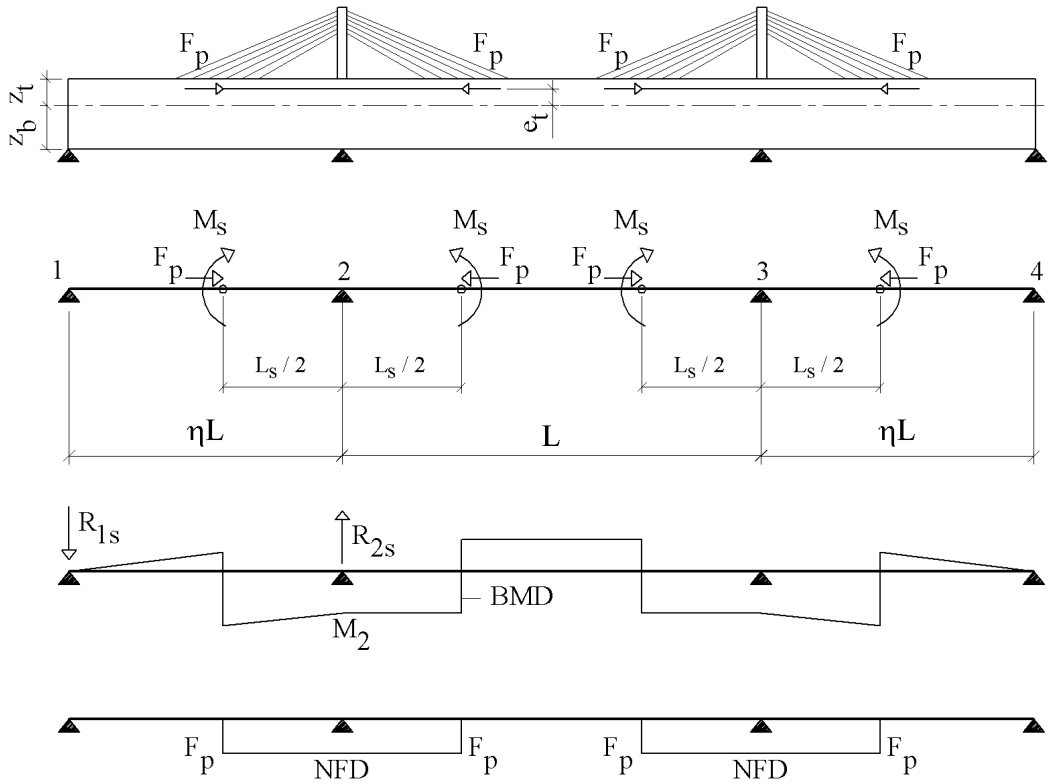

fig. 6.10: BMD and NFD due to top straight tendons at the pylons

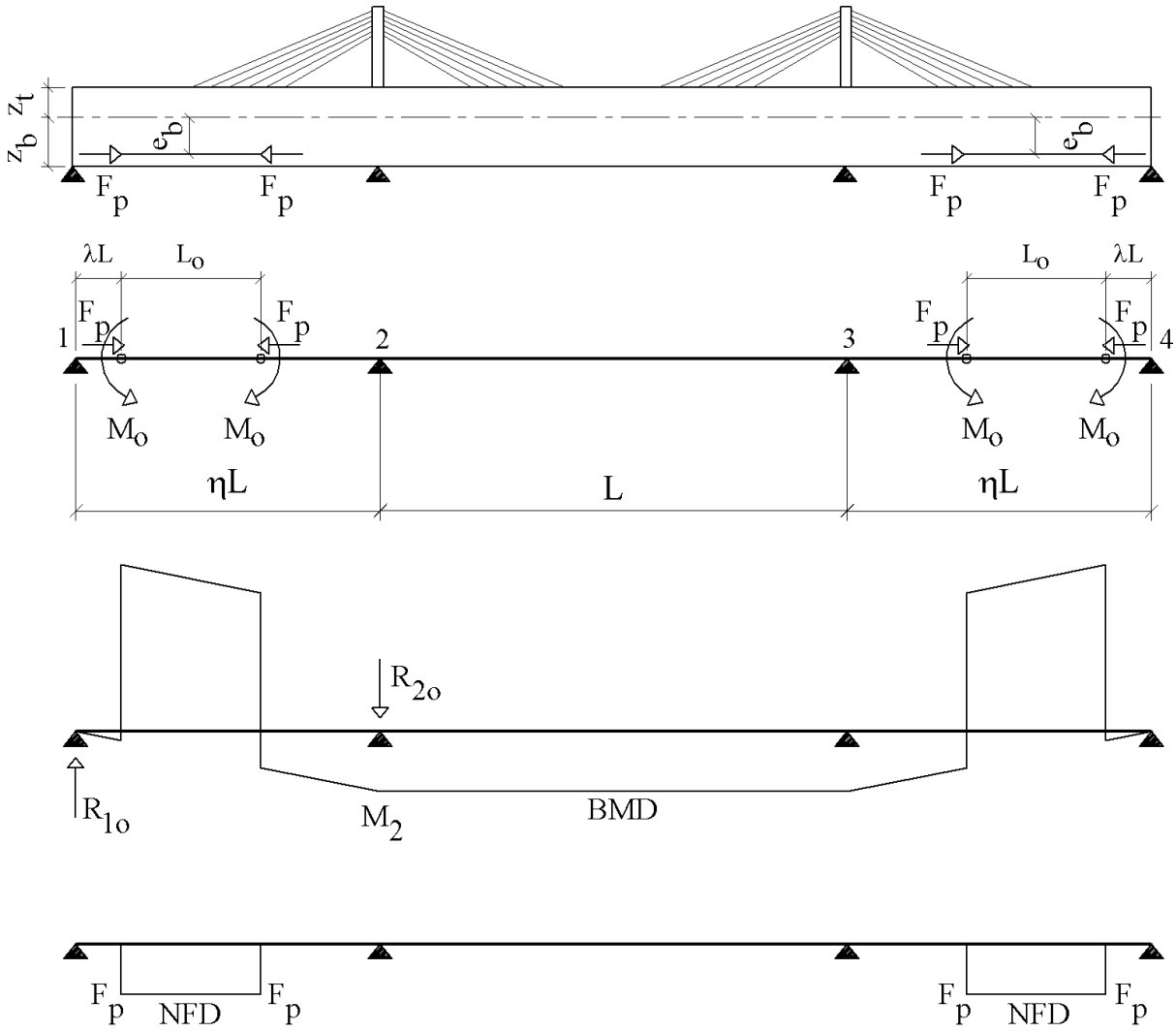

fig. 6.11: BMD and NFD due to bottom straight tendons in the side spans

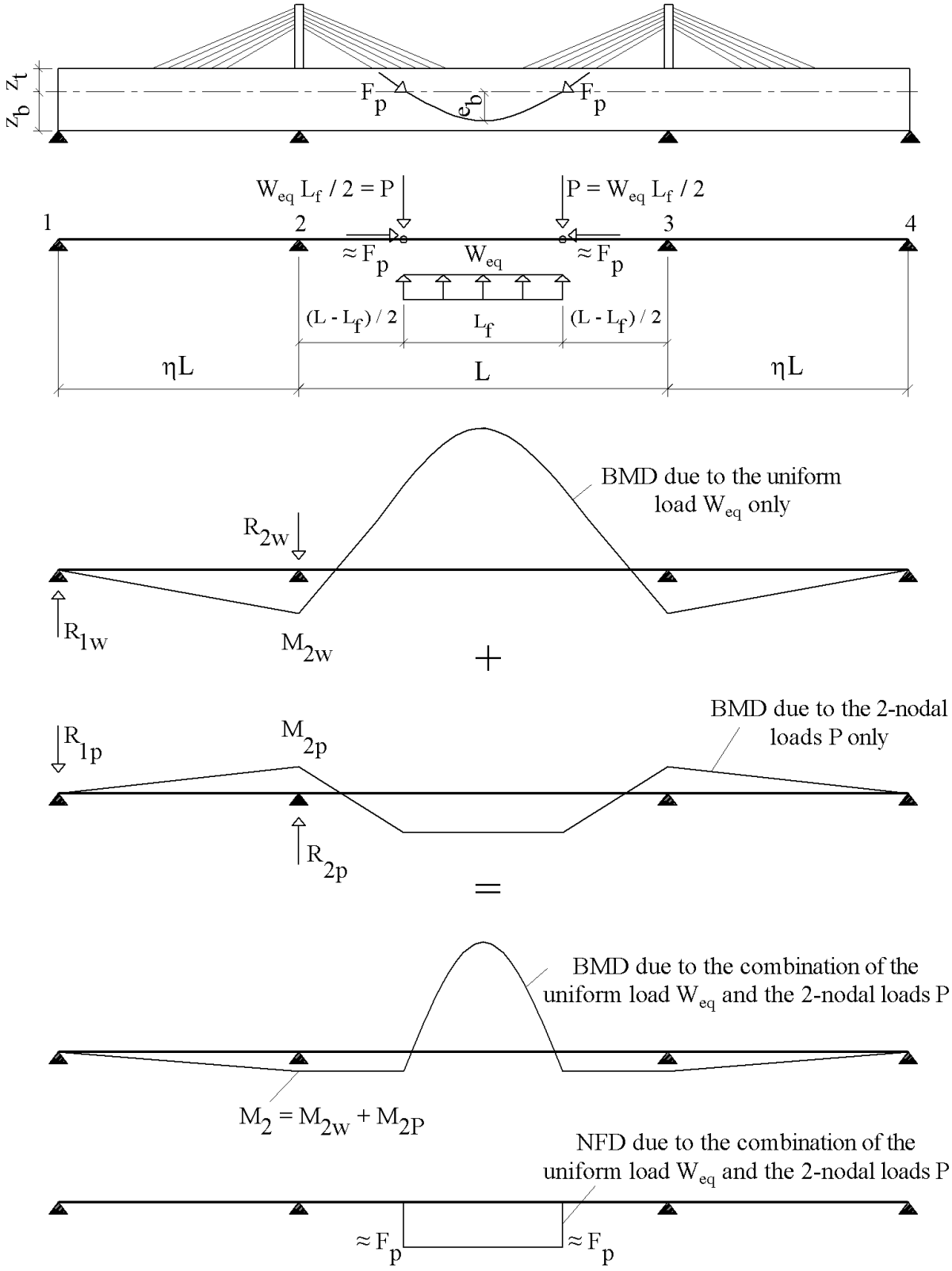

fig. 6.12: BMD and NFD due to draped tendons at the middle of the main span

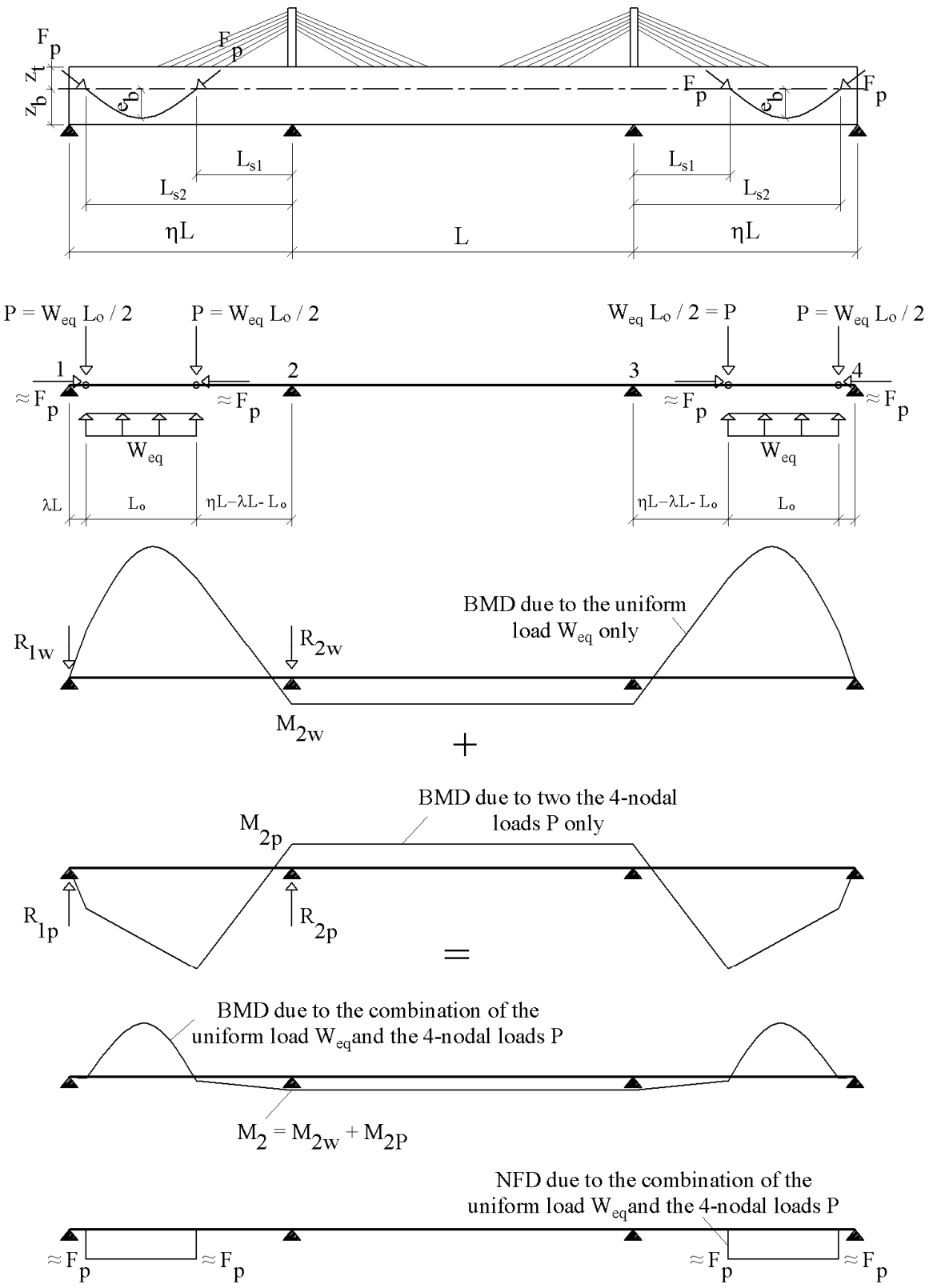

fig. 6.13: BMD and NFD due to draped tendons in the side spans

6-2-4 Preliminary design

For the preliminary design of extradosed bridges with concrete decks, the deck cross section should be first estimated based on the record/survey of the previously constructed bridges. As a first trial a section with a uniform height equal to L/50 for example may be assumed. The dead load W (self weight of the assumed section plus the superimposed dead load) should then be determined accordingly. As explained under Section 6-1, the bending moment distribution shown in fig. 6.4 (b) will be obtained under the conditions that the dead load W is uniform, the stiffness of the deck is uniform along the entire length of the bridge, the ratio between the side span and the main span length η is equal to 0.615 and in addition the ratio between the equivalent stay cable forces W_C and the dead load W is equal to 1.9 (refer to fig. 6.3). By hand calculations, the force in each stay cable F_{Di} may be determined using equation (6.28) and the normal force distribution due to the horizontal components of the stay cable forces may be drawn along the entire deck length accordingly.

By substituting η by 0.615 and W_C by 1.9W in equations (6.6) to (6.10), the following results will be obtained:

$$M_2 = \frac{-W L^2}{209.5} \quad , \quad R_1 = \frac{W L}{8.744} \quad , \quad R_2 = \frac{W L}{4.156} \quad \text{and} \quad Q_{2r} = \frac{-W L}{8.334} \tag{6.61}$$

Substituting from (6.61) in equation (6.3), the bending moment at the middle of the main span M_{m2} can be calculated from the following equation:

$$M_{m2} = \frac{W L^2}{160.7} \tag{6.62}$$

The values of the critical bending moment M_2 at the pier and M_{m2} at the middle of the main span (due to the effect of dead load and the stay cable forces F_{Di}) can be used to estimate the required prestressing tendons. Equations (6.34) to (6.60) may be used if non concordant prestressing tendons are planned to be used. In case concordant prestressing profiles are selected, the required prestressing force F_P may be estimated using the values of the critical bending moments M_2 and M_{m2} and the distances z_t and z_b (= the distances between the center of gravity of the deck section and the top and bottom fibres of the deck section respectively). It is also necessary to check that the dimensions of the selected deck section are adequate to contain all the prestressing tendons

required to produce the estimated prestressing force F_P. Accordingly, the bending moments and the normal force distribution due to the selected prestressing may be calculated/drawn.

The critical sections of the deck (at the middle of the main span and at the pier) should then be checked under the combination of the dead load, stay cable forces, prestressing forces and live loads taking into account the instantaneous and long term prestressing losses.

The envelope of the bending moments resulting from a uniform live load q is shown in fig. 6.14.

The values of the bending moments shown in fig. 6.14 are based on the following assumptions:

- The moment of inertia of the deck cross section is constant along the entire length of the bridge.
- The ratio between the side span length and the main span length is equal to 0.615.

Based on the nos. of traffic lanes and the live load acting on each lane as required by the project specification, the value of the load q and the corresponding maximum and minimum bending moments may be determined accordingly. The normal forces associated with the maximum bending moments due to live loads (due to the presence of the stay cables) may be ignored. Such assumption is normally on the safe side.

The calculation process described above may be required to be repeated to increase the prestressing forces or the dimensions of the selected deck cross section until satisfactory results, to carry safely the combination of dead and live loads, are reached.

The method of calculation described above may be also used to check the plausibility of the computer results in the detailed design stage.

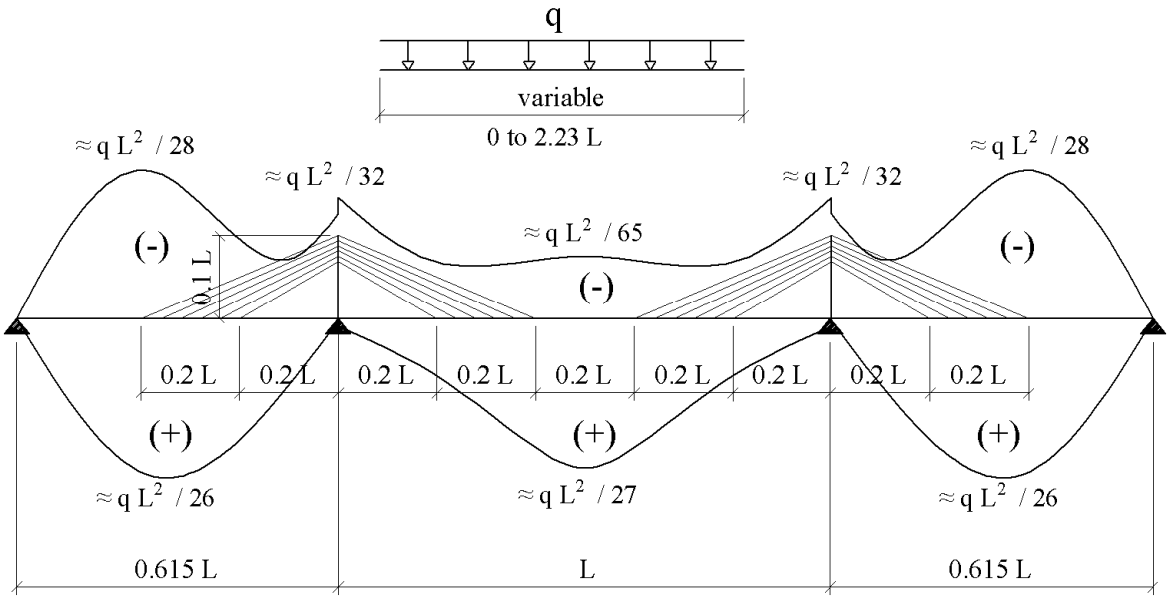

fig. 6-14: Envelope of the bending moments due to uniform live load q

6-3 Commercial consideration related to the use of the stay cables and the concordant prestressing cables

As explained under sections 6-1 and 6-2, a combination of stay cable forces and prestressing forces may be targeted to nearly eliminate the bending moments under dead load. Based on the contribution of the stay cables and the prestressing in reducing the bending moments at the critical sections of the deck, the use of the stay cables and prestressing materials may be evaluated commercially as will be explained in this Section, taking into account the prevailing unit weight costs for both materials.

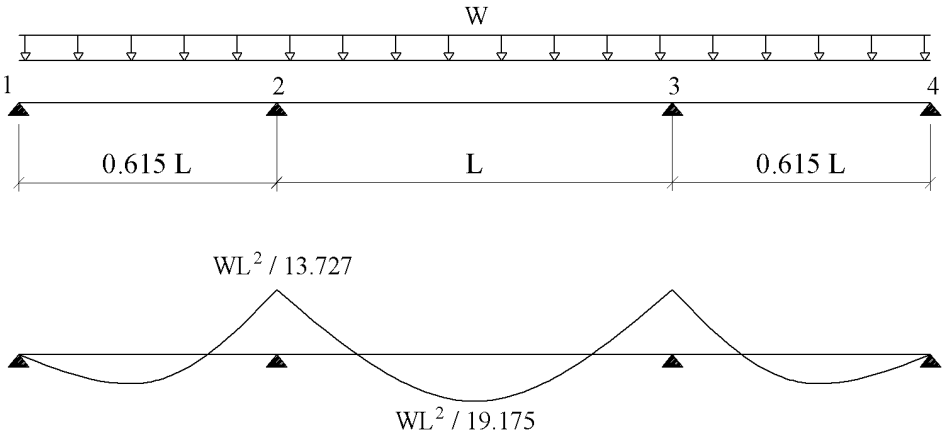

fig. 6.15: Bending moment distribution under the dead load W in the absence of the stay cables and the prestressing forces

fig. 6.15 shows the bending moment distribution along the entire deck length due to the dead load W in the absence of the stay cables and the prestressing. From figs. 6.4(b) and 6.15, it may be understood that the stay cables contribute to reduce the bending moments at the critical deck sections at the pylon and the middle of the main span from $WL^2/13.727$ and $WL^2/19.175$ to $WL^2/209$ and $WL^2/160$ respectively (refer also to equations (6.61) and (6.62). This means that the stay cables serve to reduce the bending moments at the pylon and the middle of the main span by 93% and 88% respectively. In average it may be approximately stated that the stay cables reduce the critical bending moments due to dead load by 90%.

Further, it was concluded under section 6-2-2 that the bending moment along the entire length of the extradosed bridge may be eliminated by the use of concordant prestressing profiles. Accordingly, it may be stated that the concordant prestressing contributes to reduce the critical bending moments by 10%.

To evaluate the use of the stay cables commercially in comparison with the use of the prestressing inside the deck section, the unit weight cost of the stay cable material is assumed to be equal to "S" and the total weight of the stay cables material required to reduce the critical bending moments under dead load by 90% will be referred to as "W_{sc}". This means that the cost of reducing the critical bending moments under dead load by 1% by the stay cables is equal to: $\frac{S\, W_{sc}}{90} = 0.01\, S\, W_{sc}$.

On the other hand, it has been found from the detailed analysis of the bridge shown in Appendix E that the weight of the concordant cable prestressing required to reduce the critical bending moments under dead load by 10% is equal to ≈ 1.5 W_{sc}. By assuming that the unit weight cost of the stay cables material is approximately equal to 3.0 times the unit weight cost of the prestressing material, the cost of reducing the critical bending moments under dead load by 1% by the prestressing material will be equal to: $\frac{S \text{ x } (1.5 W_{sc})}{3.0 \text{ x } 10} = 0.05\ S\, W_{sc}$.

Based on the above calculation's approach, it may be concluded that the cost of the stay cables material required to reduce the critical bending moments in the deck under dead load by 1% is equal to about 20% of the cost of the prestressing material required to reduce the critical bending moments by the same amount (1%). The above conclusion is valid only for a bridge with uniform dead load W, uniform moment of inertia of the deck section I and side span to main span ratio η equal to 0.615.

CHAPTER 7

7- POSSIBLE CONSTRUCTION METHODS FOR THE EXTRADOSED BRIDGES

As explained in Chapter 5, the extradosed bridges are usually built with main spans of 100 to 200m and side spans of 50 to 150m. For such types of spans the precast segmental construction method are considered to be most suitable. The precast segmental construction for both of the side and main spans may be implemented by the balanced cantilever erection method. Alternatively, the side span may be constructed by the "span by span" erection method, by using temporary trestles if necessary and the segmental construction of the main span may follow using the free cantilevering method.

In this Chapter, the fabrication methods for the precast segments will be briefly explained under Section 7-1 and the common erection methods of the precast segments will be presented in Section 7-2. Further, a proposal for the construction of extradosed bridges, using a concrete/ concrete composite deck section, will be explained in Section 7-3.

Bridges with precast concrete deck segments gained popularity among bridge designers in the last twenty years. The precast segmental construction has been found suitable for use for approach viaduct bridges, conventional cable-stayed bridges and in addition extradosed bridges. The precast deck segments were used for the Ibi river extradosed bridge in Japan (completed in 2001), the second Vivekananda extradosed bridge in India (completed in 2007) and the Canada line extradosed LRT bridge in Canada (completed in 2009).

The deck segments can be fabricated under controlled conditions at the same time of the construction of the bridge foundations and the substructure. As such not only the tight construction time schedule, imposed often by the bridge owner authorities, can be met but outstanding finishing quality for the bridge elements can be achieved as well.

The erection of deck by the use of the precast segments started in the 1960s and the first pre-stressed concrete bridge consisting of precast segments with match cast epoxy joints was Choisy-Le-Roi bridge over Seine River/France (fig. 7.1). The bridge was designed by Jean Muller and constructed by the French Contractor "Campenon Bernard" in the time period 1962-1964. The total length is equal to 131m (=37.5+55+37.5) and its deck width is equal to 28.40m [Podolny and Muller 1992]. Precast segments were then used worldwide for conventional elevated bridges

and cable supported bridges. The 4.5 km Bandra Worli sea link bridge in Mumbai India (completed in 2009) is considered to be a good example for precast segmental construction (fig. 7.2).

fig. 7.1: Choisy-Le-Roi bridge over Seine River/France [http://en.structurae.de]

fig. 7.2: Erection of precast segments for Bandra Worli Sea Link in Mumbai/India

7-1 Fabrication of Precast Segments

The concrete precast segments are fabricated normally with the "match-cast" technique which means that every segment is cast against the preceding segment creating a matching which permits the re-establishment of the casting geometry configuration at the erection time. The "match casting" can be carried out either by the "short line" or the "long line" casting method (figs. 7.3 to 7.5). It can be understood from these figures that in the "short line" method, a fixed in place "bulkhead" and form works for two segments only are sufficient. For the "long line method", movable "bulkheads" and form works for several segments are normally used.

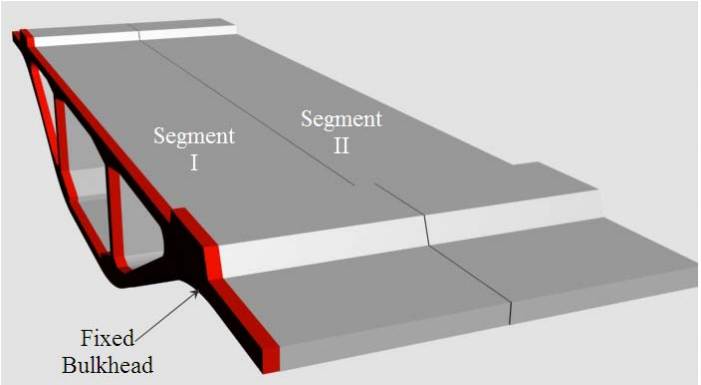

fig. 7.3: Pre-casting the segments using the short line method

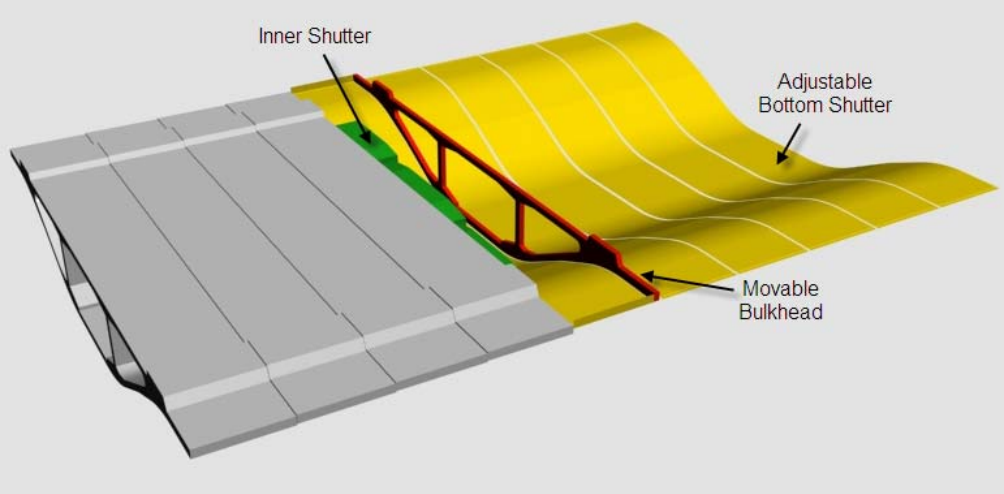

fig. 7.4: Pre-casting the segments using the long line method

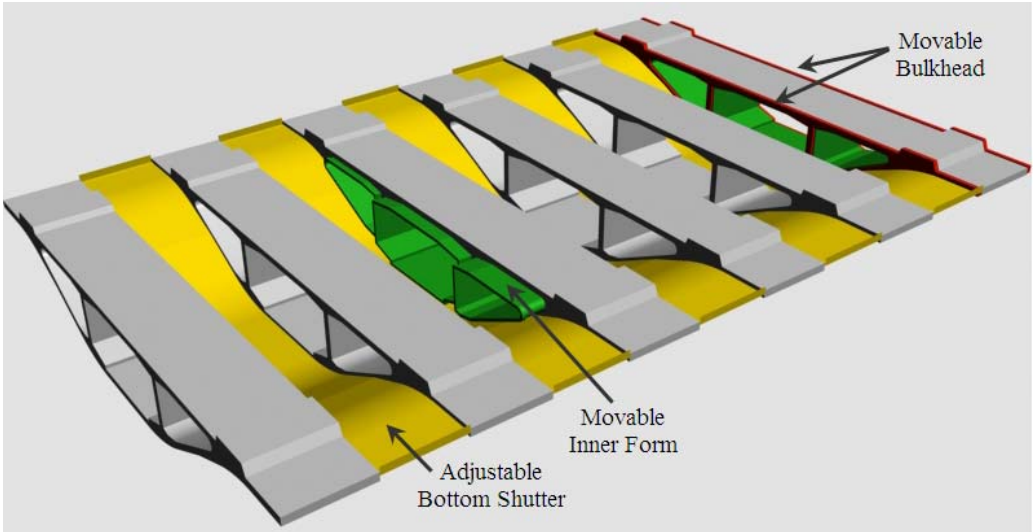

fig. 7.5: Alternative casting scheme for the long line method

7-2 Methods of erection of precast segments

Since the advent of the precast segments for bridges construction in the 1960s, the following erection methods used to be followed:

- Erection of precast segments on Scaffolding.
- Erection by the balanced cantilever method.
- Span by span erection method.
- Incremental launching method.

Erection of the precast segments on scaffolding is considered normally to be the right choice in case the bridge deck is constructed on the land and the deck is not too high (fig. 7.6). Erection of precast segments on scaffolding may be carried out in the sea also. The precast segments in the vicinity of the tower of Bandra cable-stayed bridge in Mumbai were erected on scaffolding as shown in (fig. 7.7). Every segment is placed usually on a steel trolley as that shown in fig. 7.6. The scaffolding should be provided by hydraulic and mechanical jack systems to allow the trolley along with the precast segment to be moved in the longitudinal and transverse directions to reach the required alignment in plan. The trolley itself should be provided with hydraulic and mechanical jacks to allow the segment to move upwards or downwards, relative to the trolley, to take the required alignment vertically. The precast segments may be also erected by the "span by span erection method" as shown in fig. 7.2 or by the balanced cantilever method as shown in fig. 7. 8. The incremental launching method as developed by VSL [VSL 1977] is shown in figs. 7.9 and 7.10. In this erection method, the concrete deck is cast in segments behind the abutment. Each segment is cast directly behind the preceding one. The segment is subsequently prestressed and pushed forward along with the previously cast segments by a segment's length which ranges between 15 to 25m, using hydraulic jacks. It can be understood from fig. 7.9 that the tendons used for launching the deck segments are connected to the rear end of the deck segments and the horizontal jacks are bearing on the abutment. During launching the superstructure, the cross section of the deck segment will have to carry alternating bending moments. Each cross section moves from regions of positive bending moment into regions of negative bending moment, so that tensile stresses occur alternately at the bottom and top fiber of the deck section. The use of axial pre-stressing is therefore necessary to reduce the tensile stresses to the permissible value. If the deck segments are simply launched to the first pier with no special provision to reduce the bending moment, the hog bending moment in the first span will be in the order of six times the

typical hog bending moment over the pier (the ratio between $WL^2/2$ and $WL^2/12$). The method used most frequently to overcome this problem is to use a light structural steel nose attached to the leading cantilever fig. 7.10. The nose must be light to reduce the hog bending moment and stiff enough to withstand safely the forces it has to carry. Fig. 7.10 and table 7.1 show also that the maximum hog bending moment in the deck during construction, depends on the ratio between the length of the nose and the span length and depends also on the unit weight of the nose relative to the standard unit weight of the deck which normally varies between 0.10 to 0.15 [Podolny and Muller 1992].

fig. 7.6: Erection of precast segments on scaffolding by mobile crane

fig. 7.7: Erection of precast segments on scaffolding- All precast segments are lifted at one location by a lifting frame and slid on top of the scaffolding longitudinally (used by HCC-Contractor in India)

fig. 7.8: Erection of the precast segments for Bandra cable-stayed bridge with the balanced cantilever method

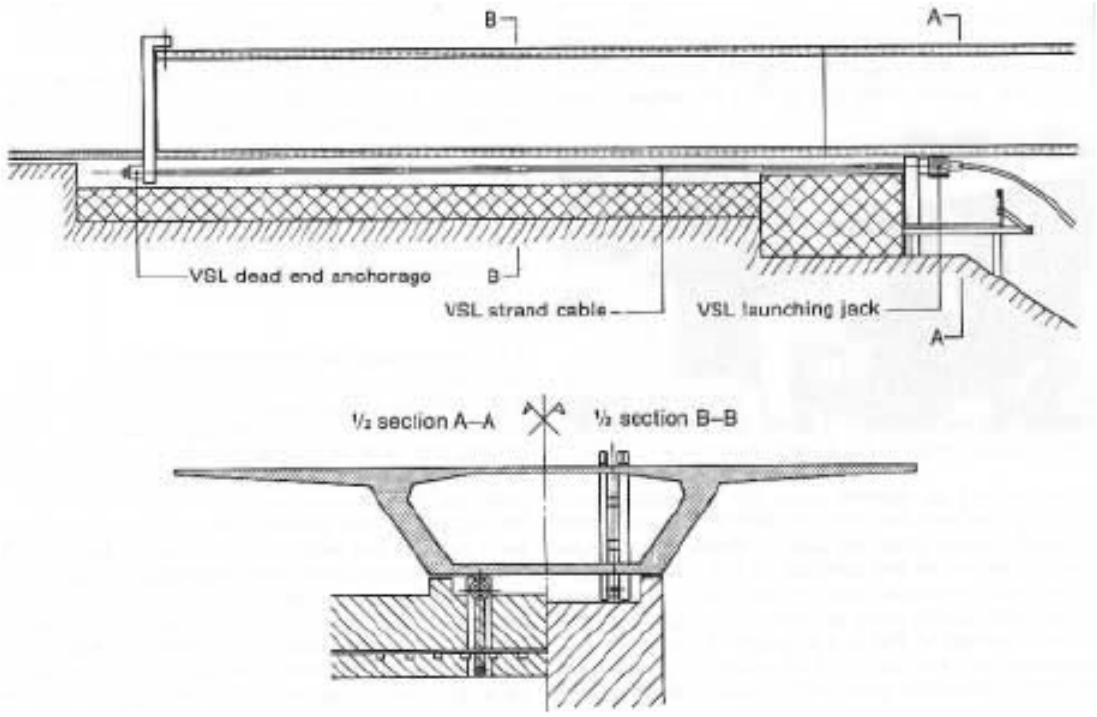

fig. 7.9 Method used by "VSL" to launch the deck segments [VSL 1977]

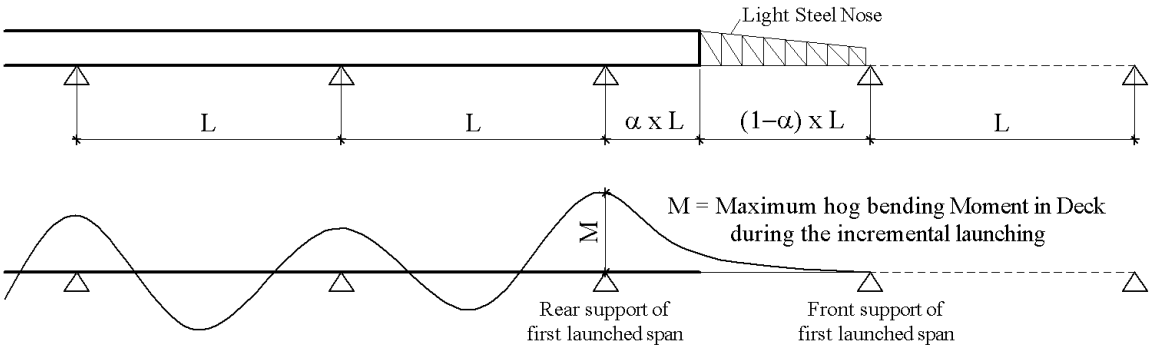

$$M = w \times \frac{(\alpha \times L)^2}{2} + 0.13 \times w \times (1-\alpha) \times L \times \left[\alpha + \frac{(1-\alpha)}{2}\right] \times L$$

fig. 7.10: Critical hog bending moment during the incremental launching of precast segments [Podolny and Muller 1992]

α	M	$M/(w \times L^2/12)$
0.2	$0.082\ w\ L^2$	0.99
0.3	$0.104\ w\ L^2$	1.25
0.4	$0.135\ w\ L^2$	1.62
0.5	$0.174\ w\ L^2$	2.09
0.6	$0.222\ w\ L^2$	2.66
0.8	$0.343\ w\ L^2$	4.12
1.0	$0.500\ w\ L^2$	6.00

Table 7.1: Effect of the steel nose length on M during the incremental launching of precast segments [Podolny and Muller 1992]

7-2-1 Erection of deck with cross section consisting of three precast segments

The deck cross section may be fabricated out of three precast segments as shown within fig. 7.11. The central spine precast segments can be erected on scaffolding, by the "balanced cantilever method", by "the span by span method or by the incremental launching method. The erected spine segments may then be used as a platform to erect the side frame precast segments on both sides of the previously erected spine segment. The separation of the cross section into three lighter segments enables the use of lighter erection machines. Such type of cross section is considered therefore to be an effective choice for the construction of extradosed bridges where the stay cables are not arranged over the full length of the deck. Each individual side frame segment may be lifted by a mobile crane, running on the ground or on the previously erected spine segments. Fig. 7.12 shows the forces acting on the side frame segment during erection. The self weight W of the side frame segment should not be transferred from the mobile crane to the

spine segment until the side frame has been placed properly on the nib of the spine segment and the tensioning of the temporary stressing bars has been carried out. The proper placement of the side frame on the nib of the spine segment and the temporary stressing leads to the balance of the forces W, T, R_v and R_h acting on the side frame segment. Accordingly the mobile crane may be released and the erection of a new side frame segment may start. Upon the erection of the side frame segments on both sides of the spine segments, fixing the reinforcement bars within the longitudinal joints between the spine and side frame precast segments and also the transverse joints between the side frame precast segments, may start and the joints can be subsequently concreted. Upon the hardening of the stitching concrete, the stressing of the permanent transverse tendons in the top slab may start (fig. 7.13). The temporary stressing may be removed upon tensioning the permanent transverse tendons.

Fig. 7.14 shows the temporary stressing and reinforcements of the joints between the side frame and spine precast segments. Fig. 7.15 shows the erection of the side frame segments for Sungai Prai cable-stayed bridge by the JV contractors Züblin/IJM/Freyssinet. The erection of the side frame segments were carried out by mobile cranes running on the previously erected spine segments or by mobile cranes running on the ground [Freyssinet 2005]. Fig. 7.16 shows an additional possible alternative erection method of the side frame segments by a gantry running on the spine segments.

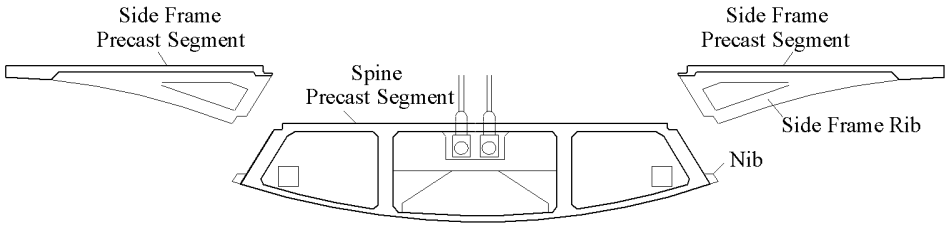

fig. 7.11: Deck cross section composed of one spine precast segment and two side frame segments

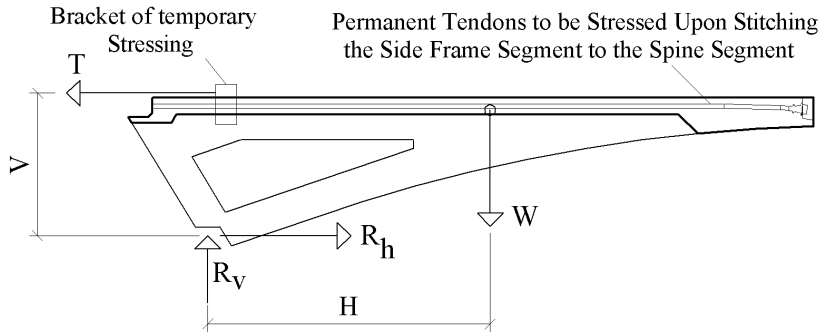

fig. 7.12: Forces acting on the side frame segment during erection

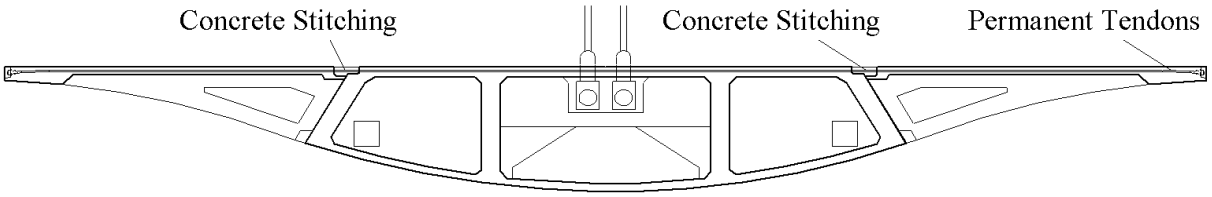

fig. 7.13: Deck cross section upon the achievement of the composite action between the spine and side frame precast segments

fig. 7.14: Temporary stressing of the side frame segments to the previously erected spine Segments

fig. 7.15: Erection of the side frame segments by mobile cranes running on the previously erected spine segments or by mobile cranes running on the ground

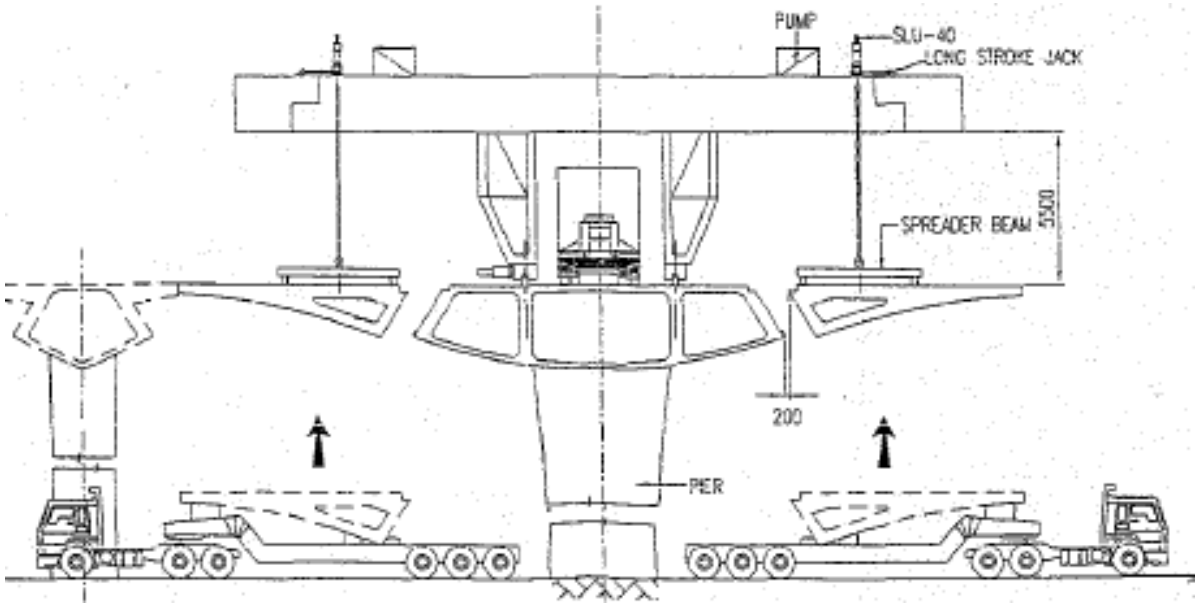

fig. 7.16: Erection of the Side frame segments by a gantry running on the spine segments

Noting the flexibility and varieties of the construction methods described above for the spine and the side frame segments of a concrete/concrete composite section, such type of section should be a competitive solution for extradosed bridges. The efficient and successful use of this composite deck cross sections for cable-stayed bridges, should lead to an equal success for extradosed bridges.

7-3 Proposal for the construction of extradosed bridges

Taking into account the method explained in Chapter 6 for the determination of the stay cable forces under dead load, the construction of extradosed bridges with a concrete/concrete composite section similar to that shown in fig. 7.11, can be carried out by following these steps:

a- The equivalent stay cable forces W_C (fig. 7.17), under the dead load W (including the superimposed dead load), should be determined as explained in Chapter 6.

b- The first part of the composite section (the spine precast segments) may be constructed for the full length of the bridge. The construction of the spine segments may be carried out by the balanced cantilever method [fig. 7.18 (a)]. Alternatively and in case the ground conditions in the side spans are easily accessible and temporary foundations can be constructed with low costs, the spine segments of the side spans may be erected by the "span by the span erection method" using temporary piers [fig. 7.18 (b)]. The spine segments may also be erected on

scaffolding if practically possible. Upon the erection of the spine segments in the side spans, the spine segments of the main span segments may be erected by the progressive placement method (free cantilevering method from one side only). The stay cables may be installed in two stages. The first stage installation forces may be made to carry the concrete weight W' only of the composite section (self weight of the spine + side frame segments) without the superimposed dead load.

c- The side frame segments on both sides of the spine segments can be erected as shown in figs. 7.14 to 7.16.

Upon the erection of all side frame segments, the longitudinal and transverse joints between the spine segments and the side frame segments can be concreted. Accordingly, the stay cables forces at this stage, will be equal to the corresponding stay cable forces under 100% of the dead load (including the superimposed dead load) multiplied by a factor equal to W'/W (i.e. W'_C / W_C = W' / W). Similarly, the "frozen" bending moment distribution in the spine segments at this stage (shown with dotted line in fig. 7.17) will be equal to the bending moment distribution under 100% of the dead load multiplied by a factor equal to W'/W.

It is also to note that the "frozen" bending moment, carried by the spine segment alone, can be reduced considerably in case concordant prestressing cable profiles are used within the spine segments, as explained in Section 6-2-2, and stressed prior to casting the in-situ concrete stitching between the spine and side frame segments (i.e. prior to the achievement of the composite section properties).

d- Upon the hardening of the in-situ concrete in the joints between the precast segments, the permanent transverse stressing between the side frames and the spine segments, may be carried out (refer to fig. 7.13). Subsequently, the superimposed loads may be placed.

e - The stay cable forces are to be re-stressed to the final desired forces.

It is also important to note that temporary stay cables may be feasible to erect the segments in the central part of the main span where there are normally no permanent stay cables available (fig. 7.18). The use of the temporary stay cables may be found easier and more economical as compared to the use of excessive numbers of temporary prestressing bars between the deck segments. The anchorage of the temporary stay cables at the deck and the pylon head levels may be arranged as shown in figs. 7.19 and 7.20. The stressing of the temporary stay cables may be

carried out at the deck level by using stressing bars [fig 7.19 (a)] and floating steel anchor beams. The anchorage of the temporary stay cable at the pylon head should be provided with two independent pen assemblies allowing the anchor to rotate vertically and horizontally to orient the temporary stay cable to different anchorage locations at the deck level. Such arrangements was used by "Larsen & Toubro and VSL" for the construction of Wadi Abdound bridge in Amman/Jordan (fig. 7.20).

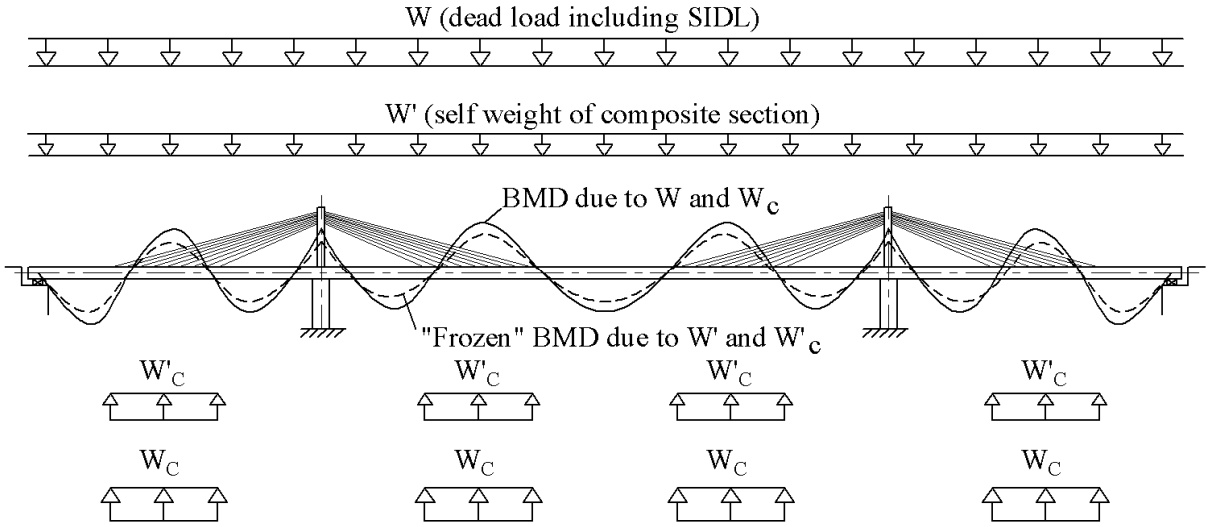

fig. 7.17: Proposed stay cable forces and bending moment distribution during the construction of extradosed bridges with concrete/concrete composite deck

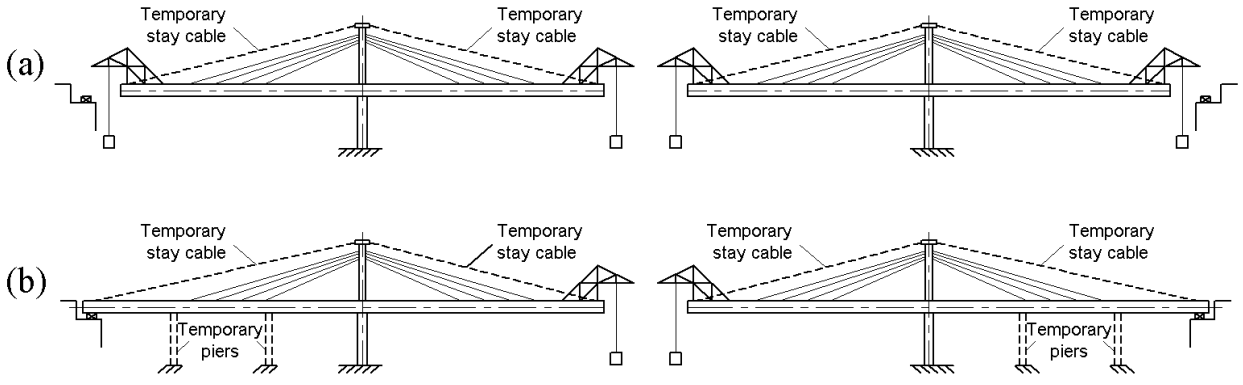

fig. 7.18: Possible construction method of extradosed bridges using temporary stay cables

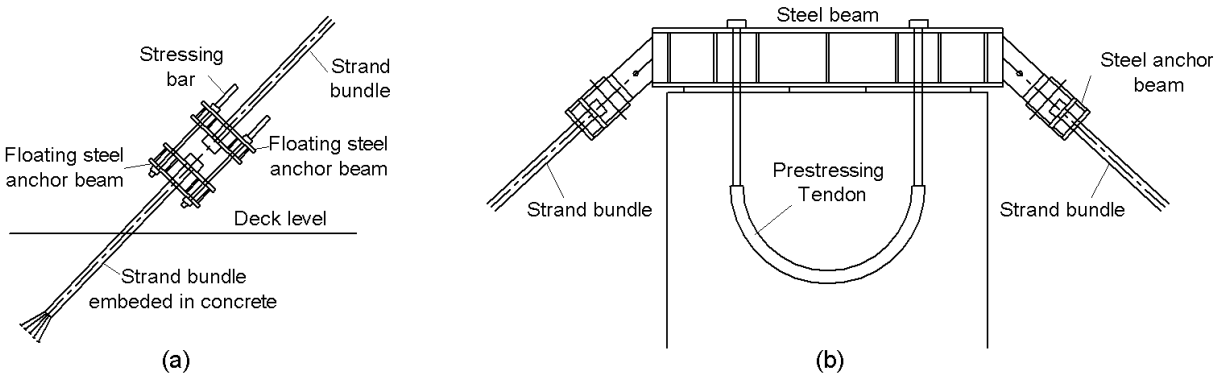

fig. 7.19: Anchorage of the temporary stay cable at the deck and pylon head levels

fig. 7.20: Use of temporary stay cables for the construction of Wadi Abdoun bridge in Jordan

CHAPTER 8

8- CONCLUSIONS AND RECOMMENDATIONS

8-1 Conclusions

The determination of the desired stay cable forces under dead load for cable-stayed bridges with composite decks (steel/concrete) or (concrete/concrete) may be carried out by the continuous beam method, similar to the conventional cable-stayed bridges with concrete-only deck sections. The stay cables should be installed in such a way that the vertical components of the stay cable forces will be equal to the vertical reaction forces of an imaginary continuous beam with rigid supports at the anchorage points of the stay cables at the deck level. The "step by step construction stage analysis" for cable-stayed bridges with composite decks, has however shown that the installation of the stay cables "to length", using the stay cable forces obtained from the continuous beam method, will not lead to the desired end results. The deviation between the resulting and the desired stay cable forces will depend mainly on the ratio between the moment of inertia of the first part of the composite section to moment of inertia of the total composite section "I_s/I_{comp}". The deviation will be also affected by the vertical shift between the center of gravity of the first part of the composite section to the center of gravity of the total composite section "e". The lower the ratio "I_s/I_{comp}" and the higher the value of "e", the higher the deviation will be between the resulting and the desired stay cable forces. The end results will be further affected by the time dependent forces due to creep and shrinkage of the concrete components of the composite section. A new construction method for cable-stayed bridges with composite decks is therefore proposed in this research work to achieve the desired forces and bridge alignment taking into account the effects of "I_s/I_{comp}" , "e" and the time dependant forces due to creep and shrinkage of the concrete material.

Further and based on a survey and a study of the previously constructed extradosed bridges, it was found out that there is a need to establish a method for the determination of the stay cable forces under dead load for this type of bridges. In this research work a proposal has been made for this purpose including recommended methods for the determination and handling the required internal and/or external prestressing within the deck cross section. The proposed method for the form finding of the extradosed bridges, is suitable for use for bridges with concrete, steel or composite deck sections. For extradosed bridges with concrete decks, a combination of the stay

cable forces and the prestressing forces inside the deck section may be selected to eliminate the bending moment due to dead load along the entire length of the deck.

8-2 Recommendations

The method established in this research work to determine the stay cable forces under dead load for extradosed bridges is based on the following assumptions:

A- The dead load and the moment of inertia of the deck section are constant along the entire length of the deck.

B- The pylon's height above the deck level is equal to 1/10 of the main span L.

C- The stay cables support 4 x 0.2 L of the entire deck length.

The effects of changing the above assumptions on the results obtained in this research work may be investigated. A feasibility study may be further carried out to quantify the possible savings, if any, in case varying deck depths are used taking into consideration the related costs of the necessary prestressing quantities.

Finally, reference is made to the "active macrosystem" and the "active microsystem" described within [Schlaich and Korvink 2000]. In the "active macrosystem" computer controlled jacks are located at the end of each stay cable. These computer controlled jacks are thought to continuously and automatically re-stress or de-stress the stay cables to reduce the deck deflection due to live loads. The live loads and the re-stressing/de-stressing operations, are sensed by small sensors and the final action is thought to be carried out by conventional "large" hydraulic jacks (hence the name "macrosystem"). The "active microsystem" is a further enhancement to the "active macrosystem" to allow the bridges to be more "autonomous", where the final action is to be executed also by "small" tools. As suggested, the "active microsystem" would require the stay cables to be fabricated out of lightweight multifunctional layer materials, consisting of load bearing carbon fibers combined with "active" materials such as piezo-ceramics or polymer gels. The achievement of a real progress towards the implementation of the above mentioned "active macrosystem" or the "active microsystem", would lead to a considerable reduction of the deck stresses due to live loads and, therefore, lighter deck cross sections may be achieved.

LIST OF FIGURES

fig. 1.1: Desired bending moment distribution under dead load for conventional cable-stayed bridges (1)
fig. 1.2: Composite deck steel/concrete used for the design of Ting Kau bridge in Hong Kong by“schlaich bergermann und partner” (1)
fig. 1.3: Composite deck concrete/concrete used for the design of Sungai Prai cable-stayed bridge in Penang/Malaysia by “Dar Consultants” (2)
fig. 1.4: Common configuration of extradosed bridges (2)
fig. 1.5: Proposed bending moment distribution under dead load for extradosed bridges (3)
fig. 2.1: Parallel bar cables [Walter et al. 1999] (6)
fig. 2.2: Locked coil strand (7)
fig. 2.3: Stay Cables with Parallel Wires cables/ BBR-HiAm system [www.bbrnetwoork.com] (8)
fig. 2.4: Swaging the wires prior to grouting the stay cable head (9)
fig. 2.5: Anchorage of the wires at the stay cable head (9)
fig. 2.6: Testing of the fabricated stay cable with its full length prior to its delivery to the erection site (9)
fig. 2.7: Uncoiling and pulling the stay cable ends to the tower head and along the deck level (10)
fig. 2.8: Pulling the Stay cable to the deck soffit using pulling rods and temporary strands anchored at the pulling rod head (10)
fig. 2.9: Equipments used for installation and stressing of stay cables (parallel wire cables system) (10)
fig. 2.10: Components of Freyssinet parallel strand cables [www.freyssinetusa.com] (11)
fig. 2.11: Cross sections through the strand bundle and the mono-strand used for Freyssinet stay cable system [Freyssinet 1999] (12)
fig. 2.12: Anchorage components of Freyssinet parallel strand stay cable system [www.freyssinetusa.com] (13)
fig. 2.13: Anchorage block used for Freyssinet stay cable system (13)
fig. 2.14: Installation of the parallel strand cables with the isotension method (schematic) (14)
fig. 2.15: Isotension principle diagram [Freyssinet 1999] (14)
fig. 2.16: Threading the strands from the anchorage location on the side span side to the anchorage location on the main span side through the deviator saddle (schematic) (15)
fig. 2.17: Threading the stay cables strands for Sungai Prai cable-stayed bridge in Penang/Malaysia (15)
fig. 2.18: Installation of the parallel strand cable by the "strand by strand" method (16)
fig. 2.19: Passive Anchorage at deck level (16)
fig. 2.20: Active anchorage at deck level [Leonhardt and Zellner 1980] (16)
fig. 2.21: Stay cable anchorages inside the tower head (19)
fig. 2:22: Anchorage of stay cables using external steel box (19)
fig. 2.23: Tower Head of Ting Kau Bridge (19)
fig. 2.24: Overcrossing of stay cables [Leonhardt and Zellner 1980] (19)
fig. 2.25: Anchorage of the stay cables at the tower head of Worli cable-stayed bridge in Mumbai/India (20)

fig. 2.26: Anchorage of stay cable at the tower head by the use of steel saddle and rigid cement grout (20)
fig. 2.27: Placement of steel saddles within the tower head prior to concreting (21)
fig.2.28: The prefabricated saddles used for Sungai Muar cable-stayed Bridge in Johor /Malaysia [Lecinq et al. 2005] (21)
fig. 2.29: Sungai Muar Cable-stayed Bridge in Johor/Malaysia [Lecinq et al. 2005] (21)
fig. 2.30: Possible structural systems for conventional cable-stayed bridges (24)
fig. 2.31: Load case for maximum back stay forces (26)
fig. 2.32: Load case for minimum back stay forces (26)
fig. 2.33: Relationship between the ratio of the side span and the main span η & the ratio between the live load and the dead load λ [Gimsing and Georgakis 2011] (26)
fig. 2.34: Effect of the stay cable sag on its effective elastic modulus [Walter et al. 1999] [Freyssinet 1999] (28)
fig. 3.1: Desired bending moments, shear and normal force distributions under dead load, for cable-stayed bridges with concrete deck cross sections (30)
fig. 3.2: Creep effect on a simple concrete beam (33)
fig. 3.3: Creep effect on a continuous concrete beam (40)
fig. 3.4: Common construction methods for cable-stayed bridges (42)
fig. 3.5: Effect of the live load on the selection of the stay cable forces under dead load [Svensson 2012] (43)
fig 3.6: Application of the "influence matrix for stay cable forces" method to achieve specific desired stay cable forces under dead load (45)
fig 3.7: Application of the "influence matrix for stay cable forces" method to achieve a specific desired bending moment distribution along the deck length under dead load (48)
fig 3.8: Application of the "influence matrix for stay cable forces" method to achieve a specific desired vertical profile for the deck under dead load (49)
fig. 4.1: Time dependent effect due to vertical loads (Type I) (55)
fig. 4.2: Additional time dependent effect in case of composite deck (Type II) (56)
fig. 4.3: Installation of stay cables to "length" (57)
fig. 4.4: Rion Antirion bridge in Greece (completed in 2004) [http://en.wikipedia.org] (58)
fig. 4.5: Rion Antirion bridge during construction [http://en.structurae.de] (58)
fig. 4.6: Construction methods for composite section in two stages (schematic) [Schlaich 2001] (59)
fig. 4.7: Bending moment distribution along the deck segment under erection prior to the achievement of the composite section properties [Schlaich 2001] (61)
fig. 4.8: Comparison between the erection cycle of construction methods nos. (1) and (4) (63)
fig. 4.9: Cable supported beam with a rectangular cross section constructed in two stages (66)
fig. 4.10: Application of the construction methods nos. 2 and 3 on a cables supported beam (69)
fig. 4.11: Effect of the ratio I_s/ I_{comp} on the vertical deflection profile of the completed structure in case the cables are installed "to length" with construction method no. 4 (71)
fig.4.12: Effect of the ratio I_s/ I_{comp} on the bending moment distribution of the completed

structure in case the cables are installed "to length" with construction method no. 4 (71)
fig. 4.13: Comparison between construction methods 4 or 5 with construction method 1 (75)
fig. 5.1: Common configuration of prestressed box girder bridges and conventional cable-stayed bridges (77)
fig. 5.2: Common configuration of extradosed bridges (78)
fig. 5.3**:** Arrêt-Darré viaduct as proposed by J. Mathivat in 1988 [Mermigas 2008] (79)
fig. 5.4: Ganter bridge, Switzerland completed in 1980 (completed in 1980) [www.highestbridges.com] (79)
fig. 5.5: Cables configuration for extradosed bridges (80)
fig. 5.6: Strength criterion and fatigue criterion for the design of stay cables (81)
fig. 5.7: Relationship between the dead load permissible stress σ_w and the ratio q/w [Walter et al. 1999] (82)
fig. 5.8: Allowable stresses for stay cables of extradosed bridges versus the stress variation due to live loads (83)
fig. 5.9: Typical fatigue curve of a cable stay [SETRA 2002] (84)
fig. 5.10: Fatigue load Model 3 as defined within Eurocode EN 1991-2-2003 + AC:2010 (85)
fig. 5.11: Ibi River bridge/bridge with short piers [Kasuga 2006] (86)
fig. 5.12: Supporting system between the deck and the piers (86)
fig. 5.13: Himi bridge in Japan with high piers [Kasuga 2006] (87)
fig. 5.14: Second Manama-Muharraq crossing in Bahrain during construction [www.archirodon.net] (87)
fig. 5.15: Sliding connections at the middle of the main spans (87)
fig. 6.1: The BMD for cable-stayed bridges along the deck elements under dead load in comparison with the proposed BMD of an extradosed bridge (90)
fig. 6.2: Method for the calculation of the desired equivalent stay cable forces W_C (93)
fig. 6.3: Determination of the ideal values of η and W_C / W (95)
fig. 6.4: Method for the calculation of the desired stay cable force F_{Di} as per equation (6.29) (99)
fig. 6.5: Use of a concordant prestressing cable profile for continuous beams (101)
fig. 6.6: Behavior of continuous beam on springs under the effect of the equivalent prestressing forces (102)
fig. 6.7: Prestressing configurations for extradosed bridges (104)
fig. 6.8: Method for the calculation of the desired stay cable force F_{Di} taking into account the effect of the prestressing forces as per equation (6.33) (105)
fig. 6.9: BMD and NFD due to bottom straight tendons at the middle of the main span (109)
fig. 6.10: BMD and NFD due to top straight tendons at the pylons (109)
fig. 6.11: BMD and NFD due to bottom straight tendons in the side spans (110)
fig. 6.12: BMD and NFD due to draped tendons at the middle of the main span (111)
fig. 6.13: BMD and NFD due to draped tendons in the side spans (112)
fig. 6.14: Envelope of the bending moments due to uniform live load q (114)
fig. 6.15: BMD under the dead load W in the absence of the stay cables and the prestressing forces (118)
fig. 7.1: Choisy-Le-Roi bridge over Seine River/France [http://en.structurae.de] (118)
fig. 7.2: Erection of precast segments for Bandra Worli Sea Link in Mumbai/Indi (118)
fig. 7.3: Pre-casting the segments using the short line method (119)

fig. 7.4: Pre-casting the segments using the long line method (119)
fig. 7.5: Alternative casting scheme for the long line method (119)
fig. 7.6: Erection of precast segments on scaffolding by mobile crane (121)
fig. 7.7: Erection of precast segments on scaffolding- All precast segments are lifted at one location by a lifting frame and slid on top of the scaffolding longitudinally (used by HCC- Contractor in India) (121)
fig. 7.8: Erection of the precast segments for Bandra cable-stayed bridge with the balanced cantilever method (122)
fig. 7.9: Method used by "VSL" to launch the deck segments [VSL 1977] (119)
fig. 7.10: Critical hog bending moment during the incremental launching of precast segments [Podolny and Muller 1992] (123)
fig. 7.11: Deck cross section composed of one spine precast segment and two side frame segments (124)
fig. 7.12: Forces acting on the side frame segment during erection (124)
fig. 7.13: Deck cross section upon the achievement of the composite action between the spine and side frame precast segments (125)
fig. 7.14: Temporary stressing of the side frame segments to the previously erected spine Segments (125)
fig. 7.15: Erection of the side frame segments by mobile cranes running on the previously erected spine segments or by mobile cranes running on the ground (125)
fig. 7.16: Erection of the side frame segments by a gantry running on the spine segments (126)
fig. 7.17: Proposed stay cable forces and bending moment distribution during the construction of extradosed bridges with concrete/concrete composite deck (128)
fig. 7.18: Possible construction methods of extradosed bridges using temporary stay cables (128)
fig. 7.19: Anchorage of the temporary stay cable at the deck and pylon head levels (129)
fig. 7.20: Use of temporary stay cables for the construction of Wadi Abdoun bridge in Jordan (129)

REFERENCES

BBR: HiAm CONA Strand Stay Cable System, Elegance and Strength, the extended HiAm CONA family. www.bbrnetwork.com, 2011.

Bergermann, R.; Schlaich M.: Die Ting Kau Schrägkabelbrücke in Hong Kong. Bauingenieur, BD. 74, Nr. 10- Oktober, 1999.

Bergermann, R.; Schlaich M.: Ting Kau Bridge, Hong Kong. Structural Engineering International 3/96, PP. 152-154,1996.

Benaim, R.: The Design of Prestressed Concrete Bridges, concepts and principles. Taylor & Francis, London and New York, 2008.

Eurocode 1: Einwirkungen auf Tragwerke, Teil 2, Verkehrslasten auf Brücken, Deutsche Fassung. EN 1991-2:2003, AC 2010, Beuth Verlag, GmbH, 10772, Berlin, 2011.

Freyssinet: Segmental bridge construction methods and survey procedures. Association of Consulting Engineer Malaysia Seminar, Kuala Lumpur, Malaysia 21st – 22nd June, 2005.

Freyssinet: Stay Cables, Freyssinet catalogue for stay cable system. September, 1999.

Gabrow, M.: Construction Stage Analysis of Cable-Stayed Bridges. Thesis at the faculty of the technical university of Hamburg-Harburg, Hamburg, Germany, June, 2004.

Gimsing, N.; Georgakis, C.: Cable Supported Bridges, concept and design (Third Edition). John Wiley & Sons, Chichester, UK, 2011.

Ghali, A.; Favre, A.: Concrete Structures, Stresses and Deformations (Second edition). E & FN Spon, London, UK, 1994.

Herzog, M.: Beispiele prüffähiger Festigkeitsnachweise mit Baupraktischen Näherungen. ISBN 3-8041-2034-2, Werner-Verlag, Düsseldorf, Germany, 1994.

Hurst, M.: Prestressed Concrete Design, (Second Edition). E & FN SPON, London and New York, 1998.

Iles, D.: Design Guide for Continuous Composite Bridges, 1 – Compact Sections. The Steel Construction Institute, UK, 1989.

Kasuga, A.: Extradosed bridges in Japan. Structural Concrete, 7(3), 91-103, 2006.

Kasuga, A.: Construction of extradosed bridges in Japan. PWD Malaysia/JICA, Kuala Lumpur, August, 2002.

Lecinq, B.; Petit, S.; Zivanovic, I.: Cohestrand stay cables and suspension cables for an extended durability. *fib* Symposium “Keep Concrete Attractive”, Budapest, 2005.

Leonhardt, F.: Vorlesungen über Massivbau, Teil 5, Spannbeton. Springer-Verlag, Berlin, Heidelberg, New York, 6. Nachdruck, 2004.

Leonhardt, F.; Zelner, W.: Cable-Stayed Bridges. IABSE SURVEYS, S-13/80, 1980.

Lin, T. Y.; Burns, N: Design of prestressed concrete structures (3nd Edition). John Wiley & Sons, 1989.

Mathivat, J.: The Cantilever Construction of Prestressed Concrete Bridges. English translation by C. J. Emberson, John Wiley & Sons, 1983.

Maxfield, B.: Engineering With Mathcad, Using Mathcad to Create and Organize your Engineering Calculations. Butterworth-Heinemann, Oxford, UK, 2006.

Mermigas, K.: Behavior and Design of Extradosed Bridges. Thesis at Graduate Department of Civil Engineering, University of Toronto, 2008.

Meiss, K.: Anwendung von Strukturoptimierungsmethoden auf den Entwurf mehrfeldriger Schrägseilbrücken und Extradosed Bridges. Dissertation Universität Stuttgart, Institut für Leichtbau Entwerfen und Konstruieren, 2007.

Menn C.: Stahlbeton Brücken. Springer Verlag, 1990.

Midas: Civil Software, Integrated Solution System for Bridge and Civil Engineering. http://en.midasuser.com, 2011.

Mosley, B.; Bungey, J.; and Hulse, R.: Reinforced concrete design to Eurocode 2, (Sixth Edition). Palgrave Macmilian, New York, 2007.

Mutsuyoshi, H.; Hai, N.; Kasuga, A.: Recent technology of prestressed concrete bridges in Japan. IABSE-JSCE Joint Conference on Advances in Bridge Engineering-II, Dhaka, Bangladesh, August 8-10, 2010.

Ogawa, A.; Kasuga, A.: Extradosed bridges in Japan. FIP notes, 2, 11-15, 1998.

Pedrozzi, P.: A Software Tool for the Analysis, Design and Monitoring of Cable-stayed Bridges. Institut für Baustatik und Konstruction (ibk), ETH Zürich, August, 2004.

PFEIFER: PFEIFER-Zugglieder/PFEIFER-Tension Members. www.pfeifer.de, 2010.

Podolny, W.; Muller, J.: Construction And Design of Prestressed Concrete Segmental Bridges. Krieger Publishing Company, 1992.

Post-Tensioning Institute (PTI): PTI Guide Specifications, Recommendations for Stay Cable Design, Testing and Installation. 2001.

Rombach, G.: Precast segmental box girder bridges with external prestressing, design and construction. Technical university Hamburg-Harburg, 2002.

Schlaich, J.: Conceptual Design of bridges, More Variety. Bridge Engineering Conference, Sharm El-Sheikh, Egypt, Egyptian Society of Engineers, organized by ESE, IABSE and fib, 2000.

Schlaich, M.; Abdalsamad, A.; Annan, R.: Großversuche zur Ermüdung von Litzenseilen auf Umlenksätteln für Schrägseilbrücken. Bautechnik 89 (11), S. 777–785, 2012.

Schlaich, M.: Erection of Cable-stayed Bridges Having Composite Decks With Precast Concrete Slabs. Journal of Bridge Engineering, PP. 333-339, September / October, 2001.

Schlaich, M.; Korvink J.: Autonomous bridges. Bridge Engineering Conference, Sharm El-Sheikh, Egypt. Egyptian Society of Engineers, organized by ESE, IABSE and fib, 2000.

SETRA: Cable stays- Recommendations of French interministerial commission on Prestressing. Service d'Etudes Techniques des Routes et Autoroutes, Juin, 2002.

SOFISTIK: Finite Element Software, Bridge Design. www.sofistik.com, 2012.

Srinivasan, G.: Design for construction, economy and elegance in concrete bridges. Structural Concrete, 8. No. 4, PP. 213-217, 2007.

Srinivasan, S.: Design and Construction of Modern Concrete Bridges. The Structural Engineer, PP. 31-36, May, 2004.

Srinivasan, S.: Award-winning design for two bridges in the middle east, Concrete Engineering international, PP. 20-23, May, 2004.

Srinivasan, S.: The philosophy of Design and Construction of Concrete Bridges. 13th Shri. S. B. Joshi Memorial Award Function, Alumni Association of College of Engineering, Pune 411005, India, October, 2007.

Svensson, H.: Cable-Stayed Bridges / 40 Years Experience Worldwide. Ernst & Sohn, 2012.

VSL: Stay Cable Systems, VSL in the Saddle, Flower Anchorage, LRT Dubai. VSL International LTD. Berne/Switzerland, The VSL news magazine, issue one, 2008.

VSL: The Incremental Launching Method in Prestressed Concrete Bridge Construction. VSL International LTD, Berne/Switzerland, Gerber A.G Schwarzenburg, April, 1977.

Walther, R.; Houriet, B.; Isler, W.; Moia, P.; Klein, J.: Cable-stayed Bridges (2nd Edition). Thomas Telford Publishing, London, 1999.

APPENDIX A

Application of the continuous beam method for the determination of the stay cable forces under dead load

(refer to Section 3-1)

Software used: [SOFISTK 2012] & [Midas 2011]

Elastic modulus of the concrete beam E_c = 35000 MPa

Elastic modulus for the cable material E_s = 200000 MPa

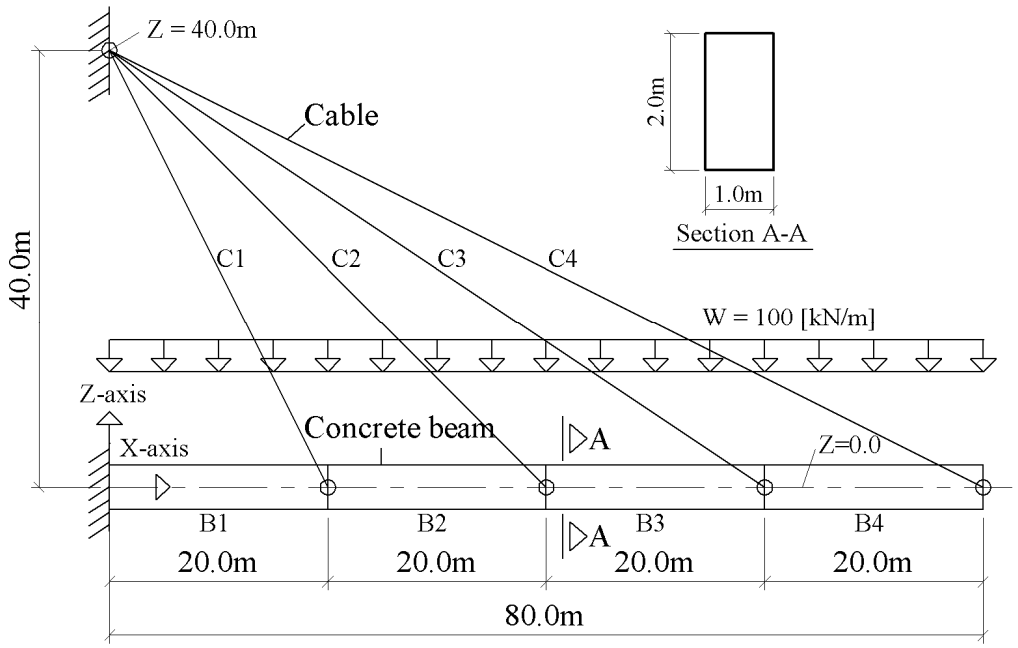

fig. A.1: Geometry of a simple cable-supported structure

Objective:

The desired cable forces at time infinity should have vertical components equal to the reaction forces of an equivalent continuous beam (fig. A.2).

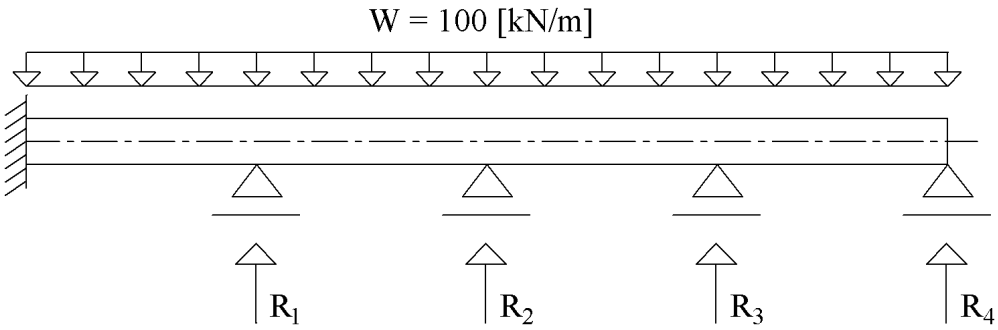

fig. A.2: Imaginary continuous beam equivalent to the cable-supported structure

Steps for the determination of the cable forces for the completed structure:

- The desired cable forces for the completed structure are determined using the imaginary continuous beam structure shown in fig. A.2 above and as per the table A.1 below.

  Notes:

  The reaction forces R_i are calculated taking into account the shear stiffness of the beam cross section.

  The desired cable force F_{Di} (refer to table A.1) = R_i x L_i / ΔZ_i

Cable no.	ΔX [m]	ΔY [m]	ΔZ [m]	L_i [m]	Reaction R_i [kN]	C-Force F_{Di} [kN]
C1	20.0	0.0	40.0	44.721	2019.3	2257.6
C2	40.0	0.0	40.0	56.569	1930.4	2730.0
C3	60.0	0.0	40.0	72.111	2265.2	4083.6
C4	80.0	0.0	40.0	89.443	789.8	1766.0

table A.1: Desired cable forces F_{Di} for the completed structure

- The desired bending moment and normal force distributions at time infinity, corresponding to the desired cable forces in table A.1, are shown in fig. A.3 below.

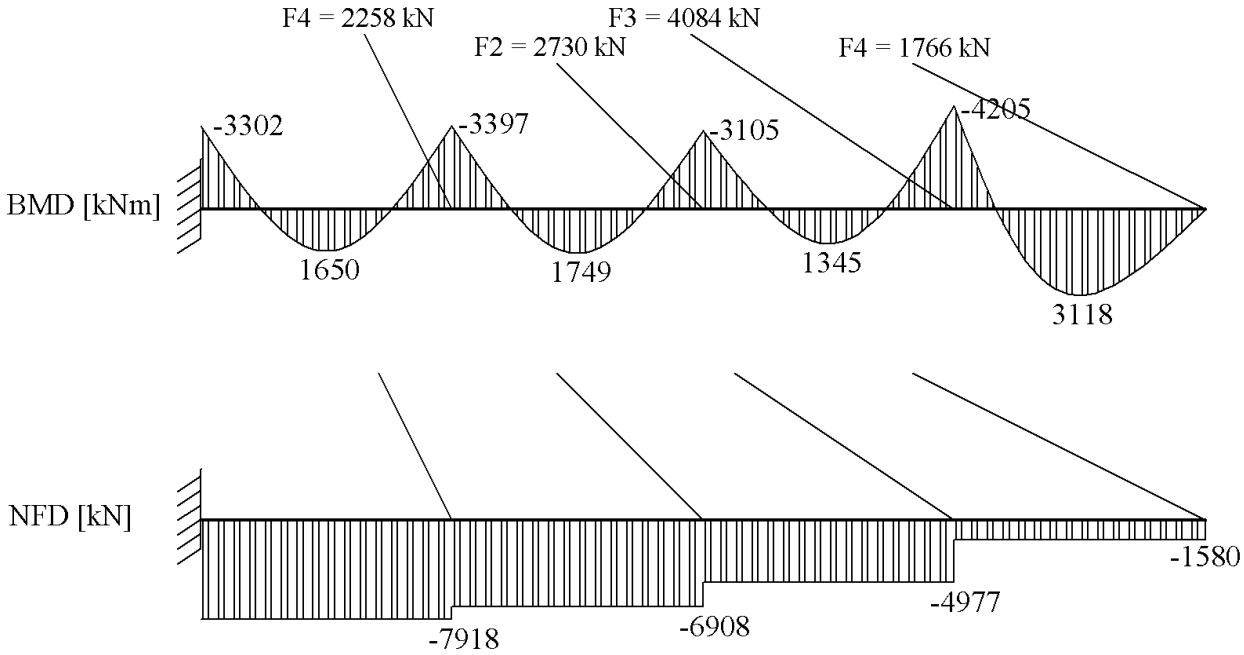

fig. A.3: Desired cable forces, bending moment and normal force distribution under dead load

- The cross section of each cable may be calculated as shown in table A.2 below based on the forces F_{Di} in table 1, assuming that the cables are fabricated from 7-wire strands and that each strand has a cross sectional area A = 150 mm^2. It is also assumed that the maximum stress in the cable material due to the dead load W is equal to, say, 300 MPa.
- The beam segments B1 to B4 are defined in the computer model with the rectangular cross section A-A shown in fig. A.1 and the cables are defined with the cross sectional areas A_{si} calculated in table A.2.

  The unstressed lengths L_{ui} of the cables C1 to C4 are calculated in table A.2 below by using the following formula:

$$L_{ui} = \frac{L_i}{(1+\varepsilon_i)} = \frac{L_i}{\left(1+\frac{F_{Di}}{E_s A_{si}}\right)}$$

where :

L_i = the stressed length of the cable

ε_{si} = elastic strain of the cable due to the desired stay cable force F_{Di}

A_{si} = the cross sectional area of each cable (refer to table A.2).

E_s = the elastic modulus for the cable material.

Cable no.	C-Force F_i [kN]	no. of Strands	Area A_{si} [mm^2]	ε_{si} [m/m]	ΔL_i [mm]	L_i [m]	L_{ui} [m]
C1	2257.6	50	7500	0.001505	67.3	44.7214	44.6540
C2	2730.0	61	9150	0.001492	84.4	56.5685	56.4842
C3	4083.6	91	13650	0.001496	107.9	72.1110	72.0032
C4	1766.0	39	5850	0.001509	135.0	89.4427	89.3077

table A.2: Un-stressed lengths L_{ui} of the cables C1 to C4

- For the beam segments: to counterbalance the elastic shortenings $\varepsilon_{C\text{-}el}$ (resulting from the normal force N_i in fig. A.3), the expected shortening due to creep $\varepsilon_{C\text{-}cr}$ and the expected shortening due to shrinkage $\varepsilon_{C\text{-}sh}$, each beam segment is to be assigned an "elongation strain" ε_{Ci} equal to :

$$\varepsilon_{Ci} = \varepsilon_{C-el} + \varepsilon_{C-cr} + \varepsilon_{C-sh} = \frac{N_i}{E_C\ A_C} + \phi\frac{N_i}{E_C\ A_C} + \frac{0.1}{1000}$$

where ϕ is equal to the creep coefficient (assumed in this example equal to 1.5), N_i is equal to the normal force acting on each beam segment as per fig. A.3, A_c is equal to the beam cross sectional area (A_c = 2 m^2), $\varepsilon_{C\text{-}cr}$ is equal to the creep strain due to the normal force N_i and $\varepsilon_{C\text{-}sh}$ is equal to the estimated shrinkage strain of the beam segments (assumed in this example equal to 0.1mm/m). E_C is the elastic modulus for the concrete material = 35000 MPa.

B-Segment no.	N-force N_i [kN]	Area A_c [mm^2]	$\varepsilon_{C\text{-}el}$ [m/m]	$\varepsilon_{C\text{-}cr}$ [m/m]	$\varepsilon_{C\text{-}sh}$ [m/m]	ε_C [m/m]	ΔL_c [mm]
B1	-7917.5	2000000	-0.00011	-0.00017	-0.00010	-0.00038	-7.7
B2	-6907.8	2000000	-0.00010	-0.00015	-0.00010	-0.00035	-6.9
B3	-4977.4	2000000	-0.00007	-0.00011	-0.00010	-0.00028	-5.6
B4	-1579.6	2000000	-0.00002	-0.00003	-0.00010	-0.00016	-3.1

table A.3: Initial elastic, creep and shrinkage strains of the beam segments

2- Erection Stages

The cables C1 to C4 are introduced in the "Construction Stage Analysis Model" with the un-stressed lengths calculated in table A.2.

The beam segments (B1 to B4) are introduced in the model in 4-stages with 4-equal lengths (each =20m). Each new beam segment is introduced tangential to the previously erected segment and with longer lengths as per the values ΔL_c calculated in table A.3.

Figs. A.4 and A.5 show, for example, the computer results after the installation of the cable C2.

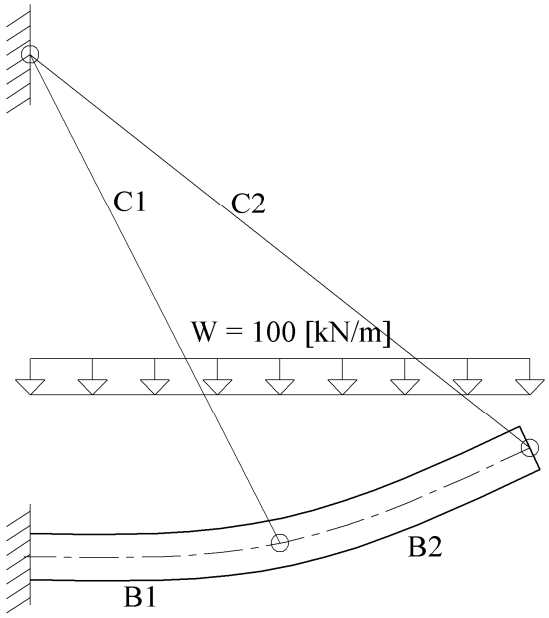

fig. A.4: The "Construction Stage Analysis Model" after the introduction of the beam segments B1 & B2 and the cables C1 & C2

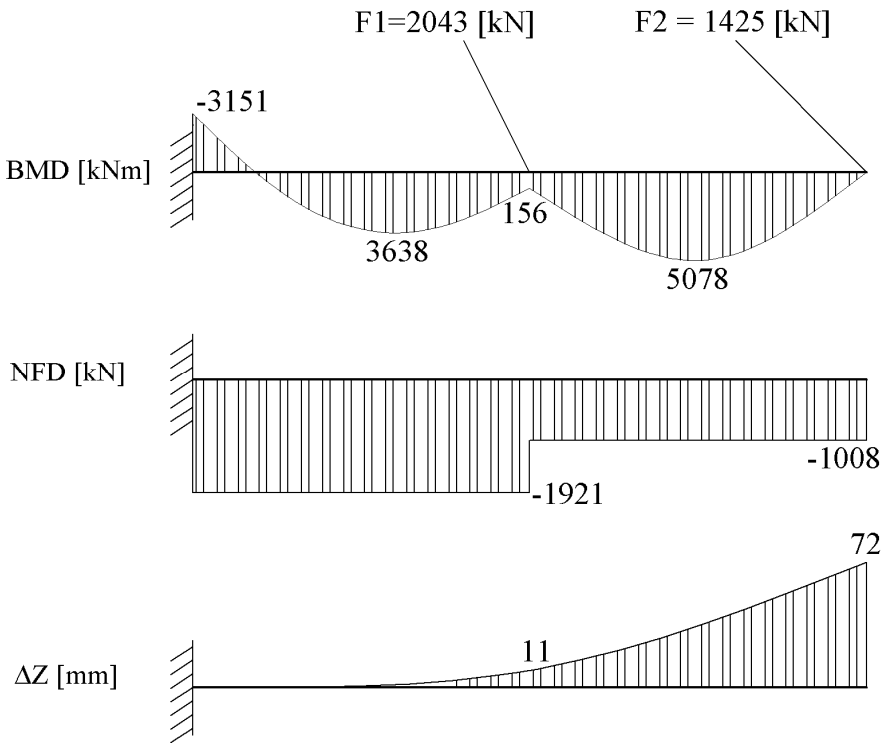

fig. A.5: Cable forces, BMD, NFD and deflection line in Z-direction after the installation of the cables C1 and C2 to the unstressed lengths L_{u1} and L_{u2} shown in table A.2

Note:

After introducing the cables C3 & C4 with their calculated un-stressed lengths and introducing the beam segments B3 and B4 with their extra lengths, the cable forces, the bending moment distribution and the normal force distribution shown in fig. A.3 will be obtained at time infinity when all of the creep and shrinkage have taken place.

APPENDIX B

Application of the proposed construction method no. (5) on a simple cable supported beam with composite cross section

(refer to Section 4-3-4)

Software used: [SOFISTK 2012] & [Midas 2011]

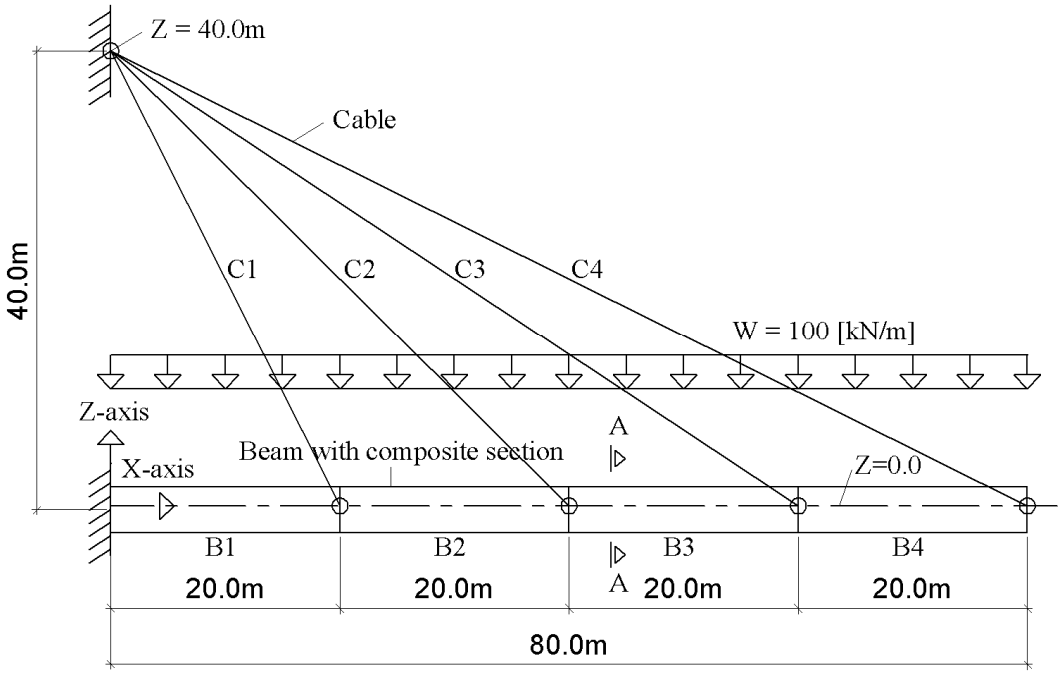

fig. B.1: Geometry of a cable-supported beam with a composite cross section

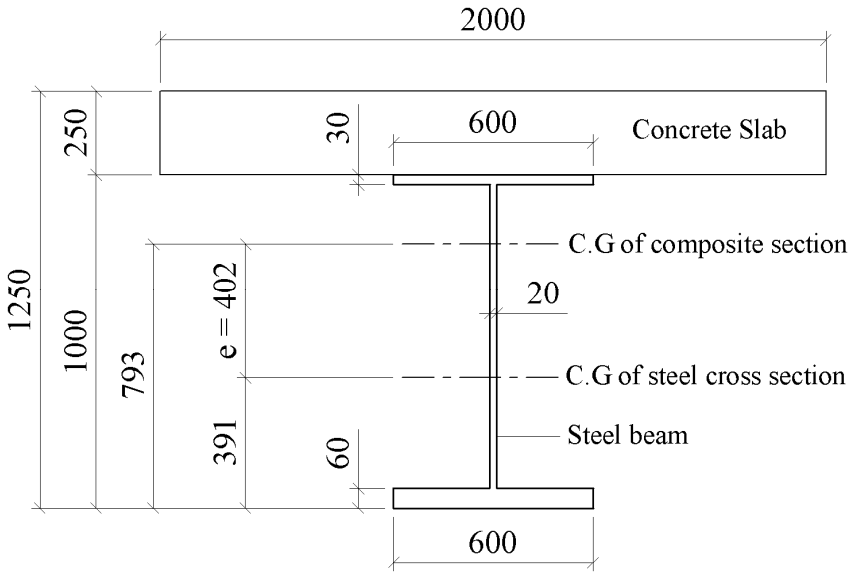

fig. B.2: Cross section A-A

	A	A_i	z	$A_i \times z$	I_i	$I_i + A_i \times (z - z_{C.G})^2$
Element	[mm^2]	[mm^2]	[mm]	[mm^3]	[mm^4]	[mm^4]
Steel	72200	72200	391	28230200	13000000000	24677115911
Concrete	500000	87500	1125	98437500	455729167	10091017952
Sum		159700		126667700		34768133863

A = Cross sectional area

A_i = Cross sectional area converted to steel units = A (concrete) x E_c / E_s

= Idealized cross sectional area

$Z_{C.G}$ = Distance from the C.G of the composite section to soffit of steel section = $\Sigma (A_i \times z) / \Sigma A_i$

= 793 [mm]

I_i = Moment of Intertia of the idealized cross section of each element

Table B.1: Properties of the composite cross section shown in fig. B.2 above

The desired cable forces, bending moment distribution and normal force distribution, at time infinity under dead load, are similar to that shown in fig. A.3 in Appendix A.

If the elements of the composite section (steel + concrete) of each beam segment are planned to be erected in two stages, each stay cable should be installed in two stages. The first stage installation force should be determined in such a way that the "frozen" bending moment distribution in the steel-only section will be as that shown in fig. B.3 (refer to section 4-3-2).

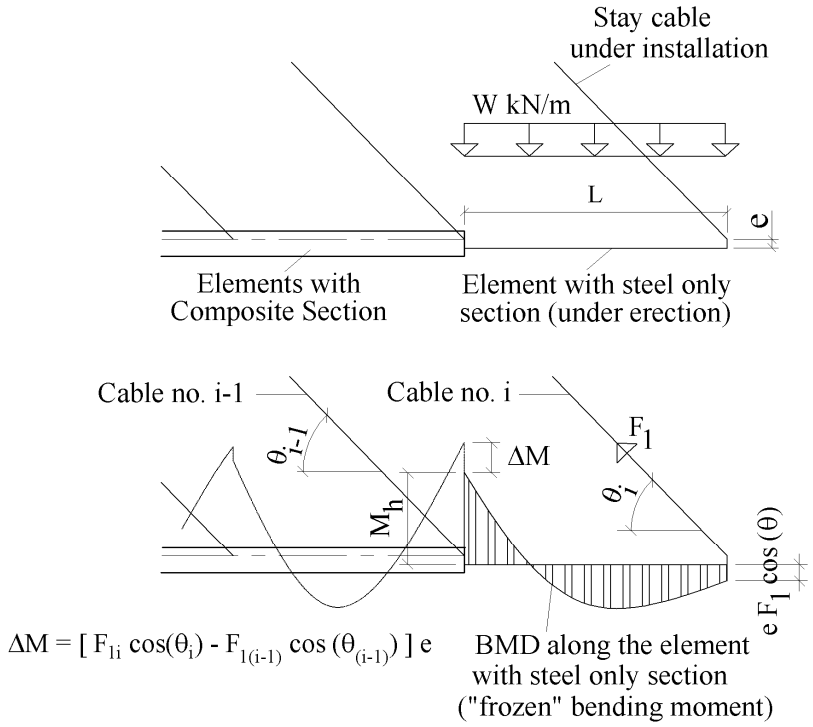

fig. B.3: "frozen" bending moment distribution after the first stage installation of the cable

The first stage installation force F_1 of the cable may be calculated by using the following equation:

$$F_1 = \frac{3}{8}\frac{W\,L}{\sin(\theta)}\left(\frac{1}{1+\frac{3}{2}\frac{e}{L}\cot(\theta)}\right) \qquad \text{(B.1)}$$

Accordingly, the first stage installation forces for the cables C1 to C4 will be equal to 826, 1030, 1294 and 1582kN respectively.

The beam segments B1 to B4 may be initially introduced in the "Construction Stage Analysis" model, longer, as per table B.2, to counterbalance the sum of the shortening due to elastic strains noting that the effect of creep and shrinkage will be dealt with separately later below.

Beam segment no.	Desired cable force F_{Di} at t_∞ [kN]	N at t_∞ [kN]	$A_{comp\text{-}beam}$ [mm^2]	Initial Strain ε [m/m]	ΔL [mm]
B1	2258	7918	159700	0.0002479	5
B2	2730	6908	159700	0.0002163	4
B3	4084	4977	159700	0.0001558	3
B4	1766	1580	159700	0.0000495	1

Table B.2 Initial elongation of the beam segments B1 to B4 in the computer model

After the first stage installation of the cable, the composite action between the steel section and the concrete slab shown in fig. B.2 can be achieved and the cable can be shortened further to the unstressed lengths L_{ui} shown in table A.2 in Appendix A. Figs.

B.4 and B.5 show the bending moment distribution along the beam segments after the first and the second stage installation forces of cable no. C2.

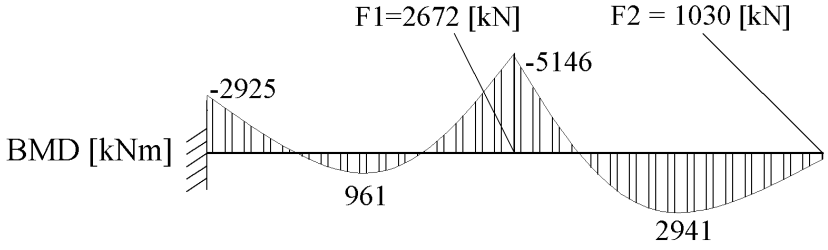

fig. B.4: Cable forces and BMD after the first stage installation of cable C2

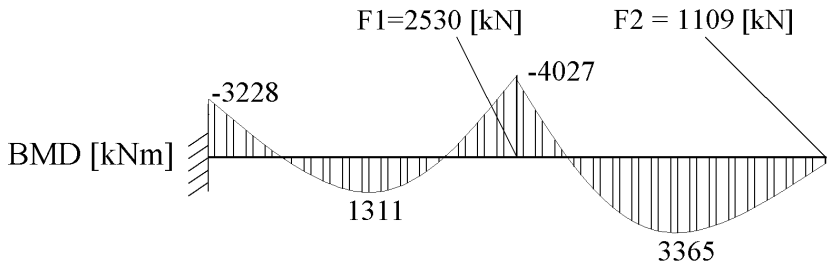

fig. B.5: Cable forces and BMD after the second stage installation of cable C2 to the unstressed length L_{u2}

Elastic longitudinal strains of the beam segments

Beam segment no.	First stage installation force [kN]	$N_{s\text{-}beam}$ [kN]	$A_{s\text{-}beam}$ [mm^2]	elastic $\varepsilon_{s\text{-}beam}$ [m/m]
B1	826	369	72200	-0.000026
B2	1030	728	72200	-0.000050
B3	1294	1076	72200	-0.000075
B4	1582	1415	72200	-0.000098

Beam segment no.	Desired cable force at t_∞ [kN]	N at t_∞ [kN]	$N_{comp\text{-}beam}$ [kN]	$A_{comp\text{-}beam}$ [mm^2]	elastic $\varepsilon_{comp\text{-}beam}$ [m/m]	ε_{el} [m/m]
B1	2258	7918	7549	159700	-0.000236	-0.000262
B2	2730	6908	6180	159700	-0.000193	-0.000244
B3	4084	4977	3901	159700	-0.000122	-0.000197
B4	1766	1580	165	159700	-0.000005	-0.000103

$N_{s\text{-}beam}$ = The normal force which will be carried alone by the steel beam

$A_{s\text{-}beam}$ = The cross sectional area of the steel beam

$\varepsilon_{s\text{-}beam}$ = The elastic strain under the effect of the normal force which will be caried alone by the steel beam

$N_{comp\text{-}beam}$ = The normal force which will be carried by the composite section

$A_{comp\text{-}beam}$ = The cross sectional area of the composite section

$\varepsilon_{comp\text{-}beam}$ = The elastic strain under the effect of the normal force which will be carried by the composite section

ε_{el} = The sum of the elastic strain for the steel only section and the composite section

Table B.3 Elastic longitudinal strains of the beam segments (calculated at the C.G of the steel only section and the C.G of the composite section)

Note: For the calculation of $\varepsilon_{s\text{-}beam}$ (steel beam elastic strain) in table B.3, the normal force is taken from the stage of the loading configuration shown in fig. B.3. As for $\varepsilon_{comp\text{-}beam}$ (composite beam

elastic strain), the normal force is taken as the difference between the normal force shown in fig. A.3 in Appendix A and the normal force used for the calculation of $\varepsilon_{s\text{-}beam}$.

By following the method described above (construction method no. 4 as per Section 4-3-2), the bending moment distribution along the full length of the beam, after the second stage stressing of cable C4, will be as shown in fig. B.6.

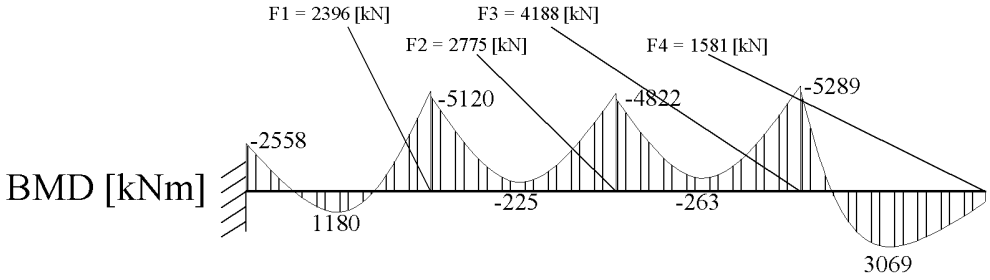

fig. B.6 Cable forces and BMD after the second stage installation of cable C4

It should be noted that although all cables have been installed to "length" (i.e. the cables have been installed to the unstressed lengths L_{ui} shown in table A.2 in Appendix A), the desired cable forces and the bending moment diagrams have not been achieved (compare fig. B.6 with fig. A.3). The desired bending moment diagram (fig. 3.A) can however be achieved by re-stressing or de-stressing the cables C1 to C4 from 2396, 2775, 4188 and 1581 kN to 2258, 2730, 4084 and 1766 kN respectively provided that the effect of creep and shrinkage of the top slab [time dependent effect type (II) explained in Chapter 4] can be ignored .

Effect of creep and shrinkage of the top slab on the bending moment distribution along the beam segments [time dependent effect type (II)]:

As shown in table B.4, the creep strain of the concrete slab $\varepsilon_{c\text{-}cr}$ is calculated based on the assumption that it will be equal to the elastic strain of the composite section $\varepsilon_{comp\text{-}beam}$ shown in table B.3 (i.e. the creep coefficient is assumed equal to 1.0). Further, the shrinkage strain $\varepsilon_{c\text{-}sh}$ is assumed equal to 0.1mm/m.

Beam segment no.	$\varepsilon_{C\text{-}cr}$ [m/m]	$\varepsilon_{C\text{-}sh}$ [m/m]	$\varepsilon_{C\text{-}cr\text{-}sh}$ [mm/mm]
B1	-0.000236	-0.0001	-0.000336
B2	-0.000193	-0.0001	-0.000293
B3	-0.000122	-0.0001	-0.000222
B4	-0.000005	-0.0001	-0.000105

Table B.4: Assumed creep and shrinkage strains of the concrete slab of the composite section

The effect of the creep and shrinkage of the concrete slab on the bending moment distribution along the beam segments may be calculated by using the model shown in fig. B.7. It is assumed further, for simplicity of the calculations, that the creep and shrinkage effects will start to take place after carrying out the second stage stressing of cable C4.

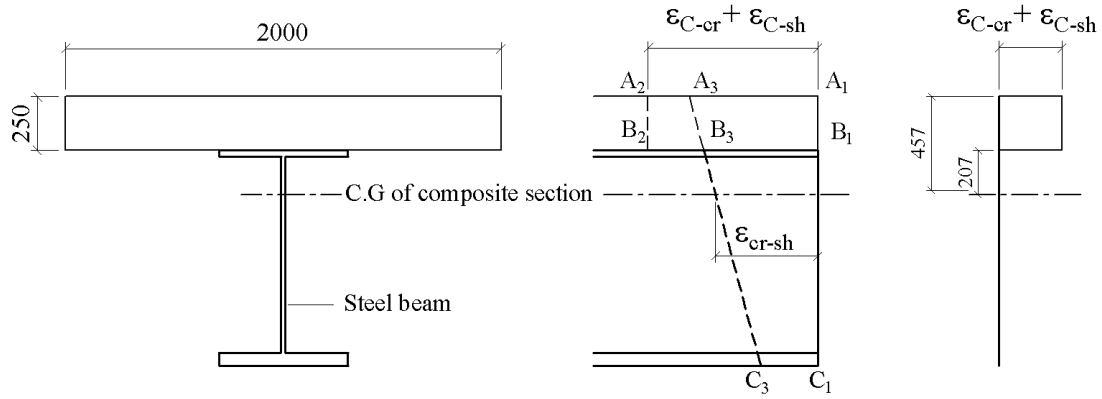

fig. B.7: Creep and shrinkage effect on the composite cross section

- $\varepsilon_{C\text{-}cr}$ = the "unrestrained" creep strain of the concrete slab.
- $\varepsilon_{C\text{-}sh}$ = the "unrestrained" shrinkage strain of the concrete slab.
- $\varepsilon_{C\text{-}cr\text{-}sh} = \varepsilon_{C\text{-}cr} + \varepsilon_{C\text{-}sh}$
- $\varepsilon_{cr\text{-}sh}$ = the resultant effect of creep and shrinkage on the composite section at the level of the centre of gravity of the composite section as shown in the above sketch.
- A_1-B_1 would move to A_2-B_2 under the effect of creep and shrinkage, in case the concrete slab is not restrained by the steel section. Due to the restraining action of the steel beam, the line A1-B1-C1 will move to A3-B3-C3.

In the computer model, the strain $\varepsilon_{C\text{-}cr\text{-}sh}$ ($= \varepsilon_{C\text{-}cr} + \varepsilon_{C\text{-}sh}$) may be defined for each beam segment with the values shown in table B.3 as a rectangular block at distances of 207 and 457mm from the C.G of the composite section as shown in fig. B.7. Accordingly, the effect of the creep and shrinkage on the cable forces and bending moment distribution is shown in fig. B.8.

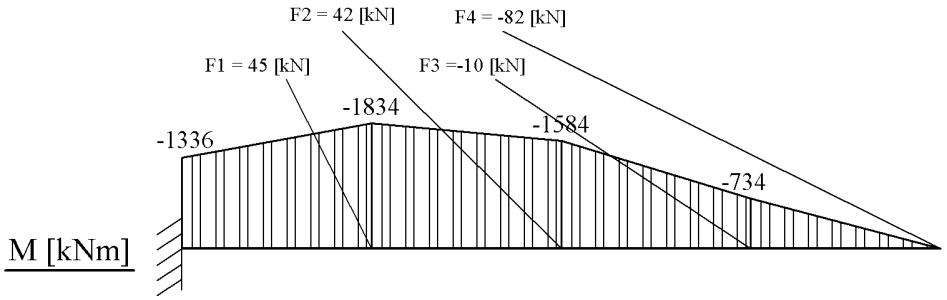

fig. B.8: Net effect of creep and shrinkage of the concrete slab on the cable forces and bending moment distribution

Note:

More accurate results for the bending moment distribution due to creep and shrinkage, can be obtained if the calculations are performed in small time intervals with partial creep and shrinkage coefficients.

Referring to figs. B.6, B.8 and A.3, the desired bending moment distribution shown in fig. A.3 can be achieved by re-stressing or de-stressing the cables C1 to C4 from (2396+45), (2775+42), (4188-10) and (1581-82) to 2258, 2730, 4084 and 1766 kN respectively

After carrying out the above mentioned re-stressing or de-stressing of the cables, the deflection line of the beam segments is shown in fig. B.9.

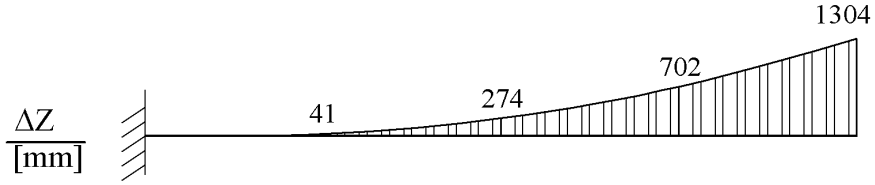

fig. B.9: Deflection line in Z-direction after re-stressing/de-stressing to the desired final cable forces

The beam segments should therefore be built with a pre-camber curve defined as the mirror curve of the deflection line shown in fig. B.9.

Fig. B.10 shows the deflection in X-direction of the C.G of the composite section which is not only due to the creep and shrinkage effect of the concrete slab but it is also due to the deflection of the C.G of the composite section relative to the C.G of the steel section due to the “frozen” bending moment distribution M_f resulting from the load configuration shown in fig. B.3. The shortening for each beam segment ΔL, measured at the C.G of the composite section, in the

longitudinal direction due to the "frozen" bending moment M_f is calculated automatically by the computer model and may be examined by hand calculation using the following equation:

$$\Delta L = \frac{1}{E_s} \int_0^L \frac{M_f}{I_s} e \, dx = \frac{e}{E_s I_s} \int_0^L M_f \, dx$$

where:

E_s = Elastic modulus of the steel material = 200000000 kN/m^2

I_s = moment of inertia of the composite section in steel units = 0.013m^4 (refer to table B.1)

M_f = "frozen" bending moment (refer to fig. B.3)

e = the vertical shift between the C.G of the composite section and the C.G of the steel section = 0.402m (refer to fig. B.2)

L = Length of each beam segment = 20m

$$\int_0^L M_f \, dx = \text{Area of the "frozen" bending moment diagram along the length L of the beam segment under erection} \left(\text{refer to fig. B.3}\right)$$

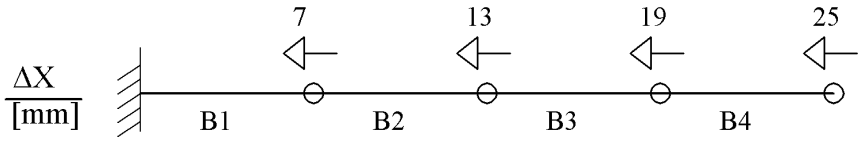

fig. B.10: Deflection in X-direction after re-stressing/de-stressing to the desired final cable forces

From fig. B.10 and table B.2, the fabrication length of the beam segments B1 to B4 may be calculated as follows:

Fabrication length of beam segment B1 =

20.0m + 0.005 + 0.007 = 20.012m

Fabrication length of beam segment B2 =

20.0m + 0.004 + (0.013-0.007) = 20.010m

Fabrication length of beam segment B3 =

20.0m + 0.003 + (0.019-0.013) = 20.009m

Fabrication length of beam segment B4 =

20.0m + 0.001 + (0.025-0.019) = 20.007m

APPENDIX C

Application of the proposed construction method no. (5) on a cable-stayed bridge with a composite deck cross section (steel/concrete)

(refer to Section 4-3-4)

Software used: [SOFISTK 2012] & [Midas 2011]

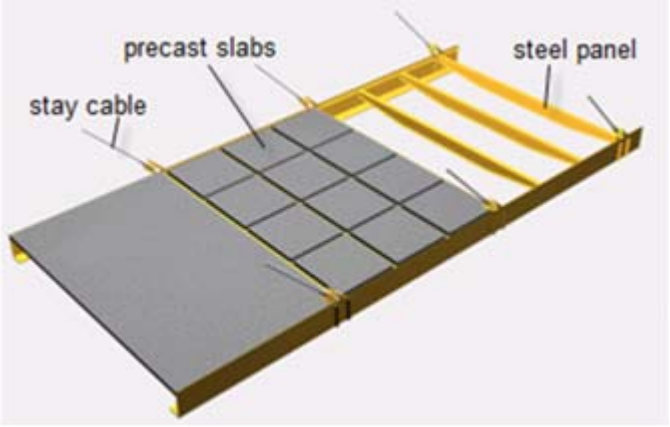

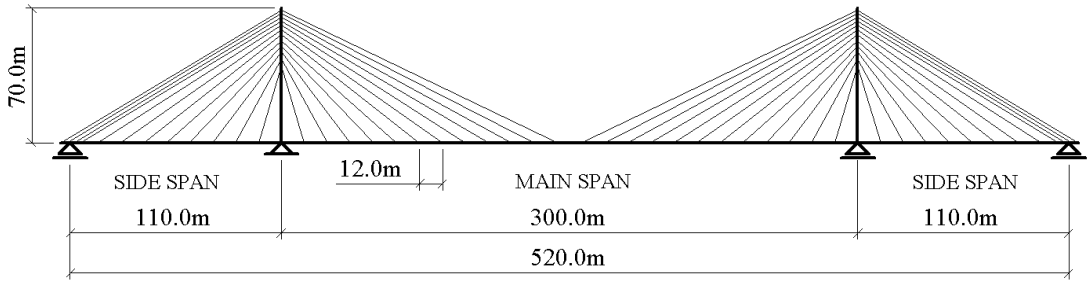

ELEVATION

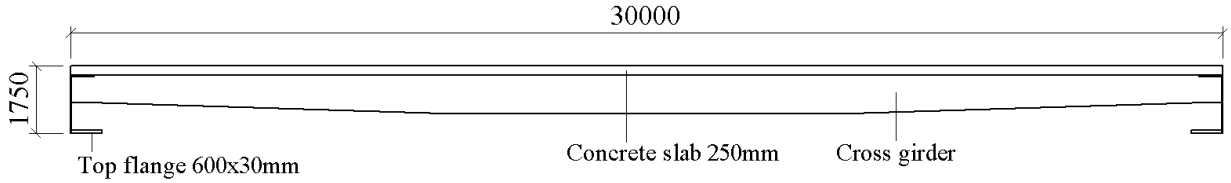

CROSS SECTION OF DECK

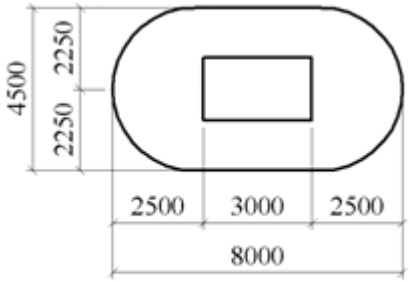

PYLON SECTION

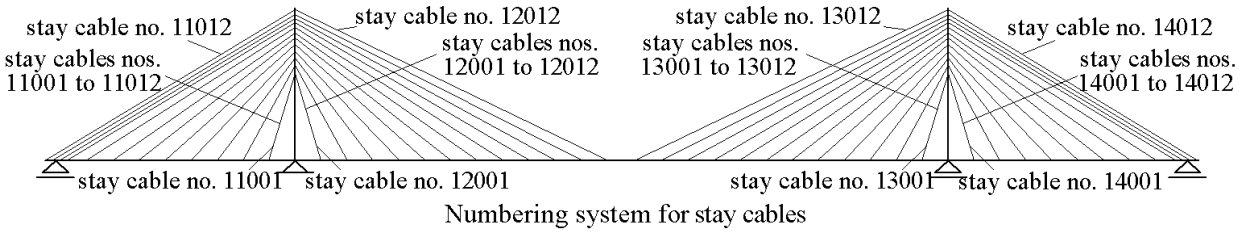

Numbering system for stay cables

fig. C.1: Geometrical data for the cable-stayed bridge with a composite deck (steel/concrete)

Material:

Elastic modulus of concrete = 35000 MPa

Elastic modulus of the construction steel and the stay cables material = 200000 MPa

Properties of the deck cross section

Steel + Concrete

Element	B	h	Area	A	z to soffit	A x z	Iy	Iy + A x ($Z_{CG-comp}$ - z)
				S-units				
	[m]	[m]	[m^2]	[m^2]	[m]	[m^3]	[m^4]	[m^4]
Concrete	30.000	0.2500	7.5000	1.3125	1.6250	2.132813	0.00683594	0.044539540
Top flange	1.2000	0.0300	0.0360	0.0360	1.4850	0.053460	0.00000270	0.000034006
Web	0.0400	1.5000	0.0600	0.0600	0.7500	0.045000	0.01125000	0.041114738
Bottom flange	1.6000	0.0800	0.1280	0.1280	0.0400	0.005120	0.00006827	0.256538169
			Sum_{COMP}=	1.5365		2.2364		0.342226453
			Sum_{STEEL}=	0.2240				
$Z_{C.G}$=	1.4555	[m]						

Steel Only

	B	h	Area	A	z to soffit	A x z	Iy	Iy + A x ($Z_{CG-comp}$ - z)
				S-units				
	[m]	[m]	[m^2]	[m^2]	[m]	[m^3]	[m^4]	[m^4]
Concrete	0.000	0.0000	0.0000	0.0000	1.6250	0.000000	0.00000000	0.000000000
Top flange	1.2000	0.0300	0.0360	0.0360	1.4850	0.053460	0.00000270	0.037647499
Web	0.0400	1.5000	0.0600	0.0600	0.7500	0.045000	0.01125000	0.016212456
Bottom flange	1.6000	0.0800	0.1280	0.1280	0.0400	0.005120	0.00006827	0.022907411
			Sum_{STEEL}=	0.2240		0.1036		0.076767365
$Z_{C.G}$=	0.4624	[m]						

Table C.1: Properties of the deck composite section and the steel only section.

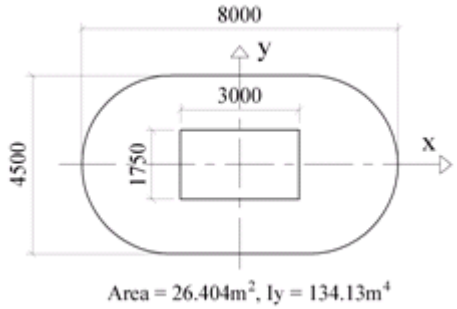

fig. C.2: Properties of the pylon section

Loads

Weight of the steel main girders and cross girders = 55 kN/m

Weight of concrete slab = 190 kN/m

Weight of wearing course, barriers, utilities, ..etc. = 105 kN/m

W (dead load) = 55 + 190 + 105 = 350 kN/m

Based on the above data and using the continuous beam method (Chapter 3/Section 3.1), the desired cable forces at time infinity F_{Di} are calculated (refer to table C.2). The first stage installation forces F_1 of the stay cables 11001 to 11009, 12001 to 12012, 13001 to 13012 and 14001 to 14009, are calculated by using equation (4.4) (refer also to fig. 4.7). The nos. of strands are calculated based on the assumption that the cable forces due to live loads are equal to 50% of the forces due to dead load. Further, the capacity of one strand under SLS is assumed equal to 115 kN. The data for cables 13001 to 13012 and 14001 to 140012 are similar to that of the cables 12001 to 12012 and 11001 to 11012 respectively.

Cable no.	Coordinates at deck level			Coordinates at pylon head			L_i	F_{Di}	nos. of 150 mm^2	L_{ui}	F_1
	X [m]	Y [m]	Z [m]	X [m]	Y [m]	Z [m]	[m]	[kN]	strands	[m]	[kN]
11001	-162.000	0.000	0.000	-150.000	0.000	40.000	41.7612	4385.3	57	41.6544	1109.7
11002	-174.000	0.000	0.000	-150.000	0.000	43.500	49.6815	4797.2	63	49.5557	1178.5
11003	-186.000	0.000	0.000	-150.000	0.000	47.000	59.2030	5288.4	69	59.0522	1268.2
11004	-198.000	0.000	0.000	-150.000	0.000	50.000	69.3109	5830.9	76	69.1341	1365.6
11005	-210.000	0.000	0.000	-150.000	0.000	53.000	80.0562	6308.1	82	79.8515	1460.1
11006	-222.000	0.000	0.000	-150.000	0.000	56.000	91.2140	6986.4	91	90.9812	1548.6
11007	-234.000	0.000	0.000	-150.000	0.000	58.500	102.3633	6764.1	88	102.1017	1637.3
11008	-246.000	0.000	0.000	-150.000	0.000	61.000	113.7409	9868.6	129	113.4516	1719.8
11009	-260.000	0.000	0.000	-150.000	0.000	63.000	126.7636	6334.0	83	126.4419	2182.6
11010	-260.000	0.000	0.000	-150.000	0.000	65.000	127.7693	9175.1	120	127.4445	-
11011	-260.000	0.000	0.000	-150.000	0.000	67.000	128.7983	9757.9	127	128.4693	-
11012	-260.000	0.000	0.000	-150.000	0.000	69.000	129.8499	10550.3	138	129.5198	-

Cable no.	Coordinates at deck level			Coordinates at pylon head			L_i	F_{Di}	nos. of 150 mm^2	L_{ui}	F_1
	X [m]	Y [m]	Z [m]	X [m]	Y [m]	Z [m]	[m]	[kN]	strands	[m]	[kN]
12001	-138.000	0.000	0.000	-150.000	0.000	40.000	41.7612	4384.3	57	41.6544	1109.7
12002	-126.000	0.000	0.000	-150.000	0.000	43.500	49.6815	4797.1	63	49.5557	1178.5
12003	-114.000	0.000	0.000	-150.000	0.000	47.000	59.2030	5290.3	69	59.0521	1268.2
12004	-102.000	0.000	0.000	-150.000	0.000	50.000	69.3109	5822.3	76	69.1343	1365.6
12005	-90.000	0.000	0.000	-150.000	0.000	53.000	80.0562	6343.5	83	79.8528	1460.1
12006	-78.000	0.000	0.000	-150.000	0.000	56.000	91.2140	6843.0	89	90.9809	1548.6
12007	-66.000	0.000	0.000	-150.000	0.000	58.500	102.3633	7343.9	96	102.1030	1637.3
12008	-54.000	0.000	0.000	-150.000	0.000	61.000	113.7409	7840.6	102	113.4502	1719.8
12009	-42.000	0.000	0.000	-150.000	0.000	63.000	125.0320	8326.4	109	124.7144	1804.1
12010	-30.000	0.000	0.000	-150.000	0.000	65.000	136.4734	8822.9	115	136.1253	1883.21
12011	-18.000	0.000	0.000	-150.000	0.000	67.000	148.0304	9278.2	121	147.6530	1957.2
12012	-6.000	0.000	0.000	-150.000	0.000	69.000	159.6778	9719.8	127	159.2715	2026.4

Table C.2: Stay cables geometry, stressed lengthdesired cable forces for the completed structure at time infinity F_{Di}, and the first stage installation forces F_1

Notes:

L_{ui} in table C.2 is the unstressed length of the stay cable and can be calculated from the following formula:

$$L_{ui} = \frac{L_i}{(1+\varepsilon_i)} = \frac{L_i}{\left(1+\frac{F_{Di}}{E_s A_{si}}\right)}$$

where :

L_i = the stressed length of the cable

ε_{si} = elastic strain of the cable due to the desired stay cable force F_{Di}

A_{si} = the cross sectional area of each cable = nos. of strands x 150mm^2

E_s = the elastic modulus for the cable material (assumed = 200000MPa)

Each of the back stays nos. 11010 to 11014 is installed to the unstressed length L_{ui} in one stage. Upon the installation of all stay cables to the unstressed lengths L_{ui} and the subsequent re-stressing/de-stressing of the stay cable forces to the desired forces F_{Di}, the bending moment distribution and the vertical deflection of the deck elements under dead load for the completed bridge at time infinity, will be as that shown in figs. C.3 and C.4. As explained in Section 4-3-4, the deck elements are to be pre-cambered to achieve the desired geometry. The pre-camber profile is the mirror line of the deflection line shown in fig. C.4.

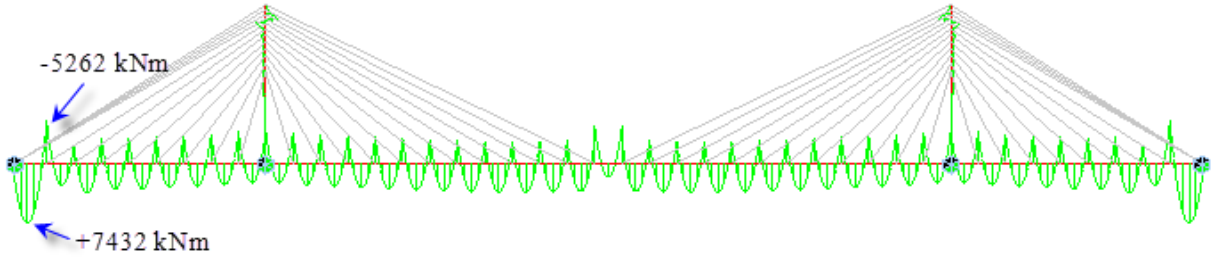

fig. C.3: Bending moment distribution for the completed bridge at time infinity under dead load and the stay cable force F_{Di}

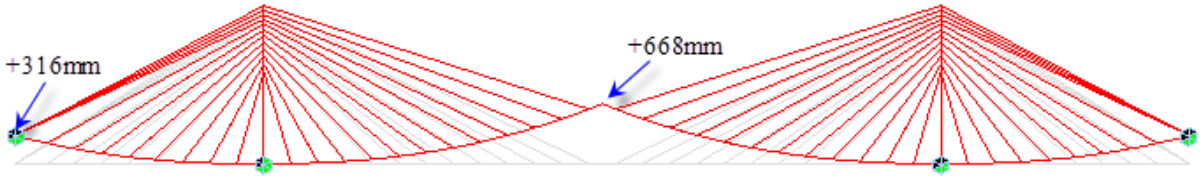

fig. C.4: Theoretical vertical deflection of the deck elements for the completed bridge at time infinity under dead load and the stay cable force F_{Di}, as calculated by the computer model

APPENDIX D

Application of the proposed construction method no. (5) on a cable-stayed bridge with a composite deck cross section (concrete/concrete)

(refer to Section 4-3-4)

Software used: [SOFISTK 2012] & [Midas 2011]

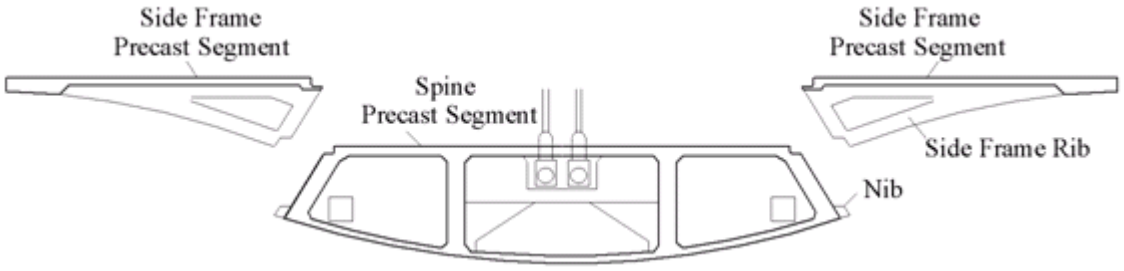

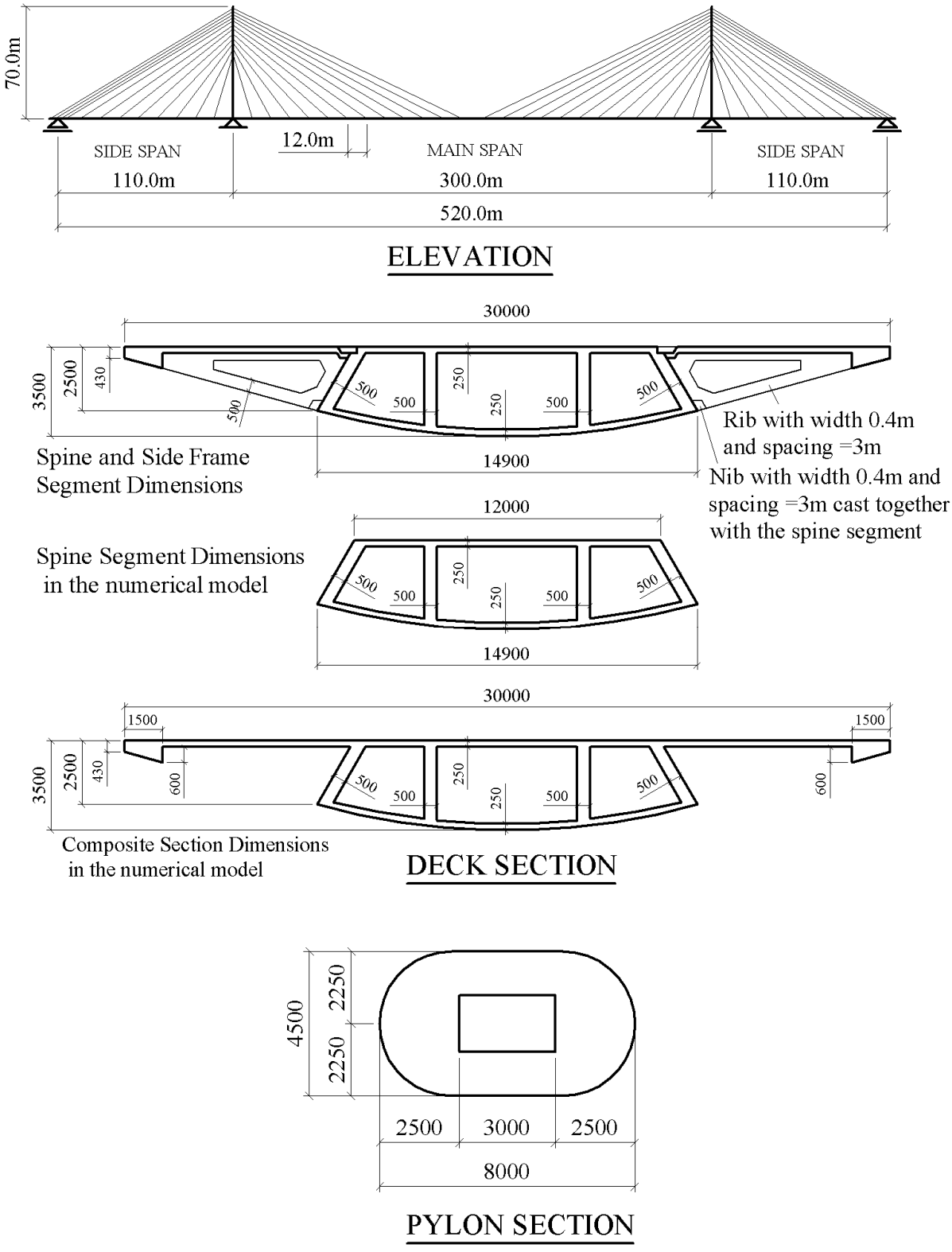

fig. D.1: Geometrical data for the cable-stayed bridge with a composite deck (concrete/concrete)

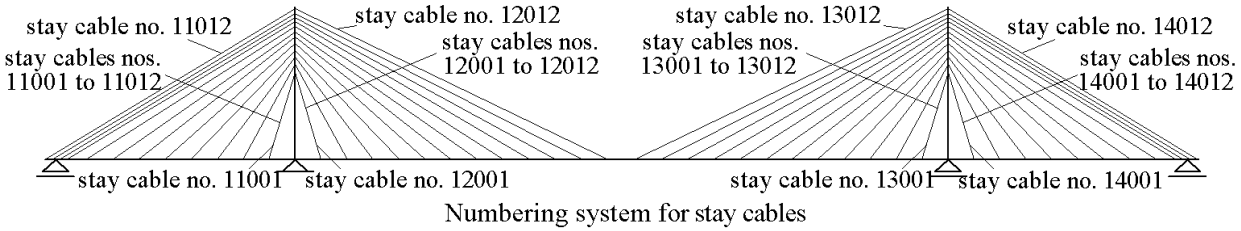

fig. D.2: Numbering system for stay cables

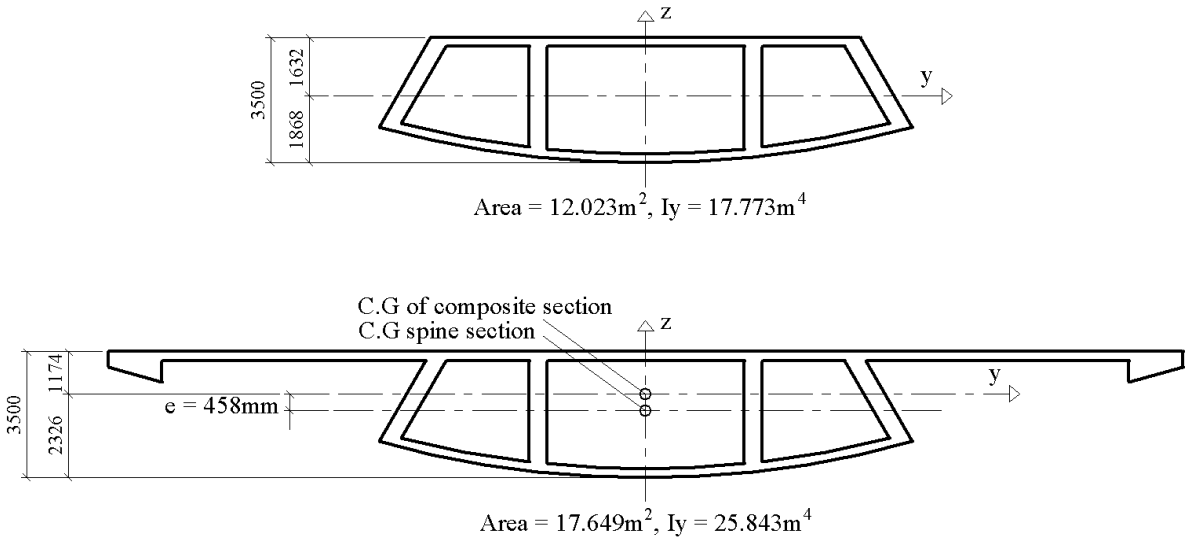

fig. D.3: Properties of the components of the composite deck section

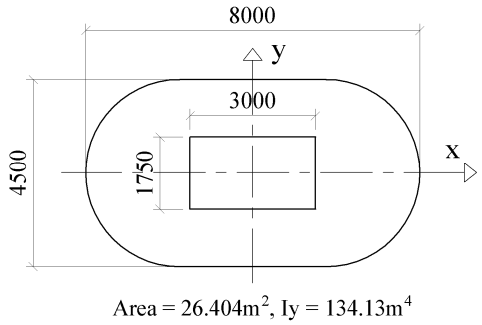

fig. D.4: Properties of the pylon section

Material:

Elastic modulus of concrete = 35000 MPa

Elastic modulus of the stay cables material = 200000 MPa

Loads

Weight of the spine segment (central part of the composite section) = 305 kN/m

Weight of the side frame segments = 190 kN/m

Weight of wearing course, barriers, utilities, ..etc. = 105 kN/m

W (dead load) = 305 + 190 + 105 = 600 kN/m

Based on the above data and using the continuous beam method (Chapter 3/ paragraph 3.1), the desired stay cable forces at end of construction F_{Di} are calculated (refer to table D.1). The first stage installation forces F_1 of the stay cables 11001 to 11009, 12001 to 12012, 13001 to 13012 and 14001 to 14009, are calculated by using equation (4.4) (refer also to fig. 4.7). The nos. of strands are calculated based on the assumption that the cable forces due to live loads are equal to 50% of the forces due to dead load. Further, the capacity of one strand under SLS is assumed equal to 115 kN. The data for cables 13001 to 13012 and 14001 to 140012 are similar to that of the cables 12001 to 12012 and 11001 to 11012 respectively.

Cable no.	Coordinates at deck level			Coordinates at pylon head			L_i	F_{Di}	nos. of 150 mm2	L_{ui}	F_1
	X	Y	Z	X	Y	Z					
	[m]	[m]	[m]	[m]	[m]	[m]	[m]	[kN]	strands	[m]	[kN]
11001	-162.000	0.000	0.000	-150.000	0.000	40.000	41.7612	7520.9	98	41.6547	2286.3
11002	-174.000	0.000	0.000	-150.000	0.000	43.500	49.6815	8222.0	107	49.5546	2466.1
11003	-186.000	0.000	0.000	-150.000	0.000	47.000	59.2030	9067.9	118	59.0518	2688.0
11004	-198.000	0.000	0.000	-150.000	0.000	50.000	69.3109	9992.9	130	69.1338	2926.9
11005	-210.000	0.000	0.000	-150.000	0.000	53.000	80.0562	10821.2	141	79.8520	3159.8
11006	-222.000	0.000	0.000	-150.000	0.000	56.000	91.2140	11950.9	156	90.9817	3379.4
11007	-234.000	0.000	0.000	-150.000	0.000	58.500	102.3633	11660.4	152	102.1022	3601.6
11008	-246.000	0.000	0.000	-150.000	0.000	61.000	113.7409	16844.4	220	113.4514	3810.1
11009	-260.000	0.000	0.000	-150.000	0.000	63.000	126.7636	10835.7	141	126.4397	4816.3
11010	-260.000	0.000	0.000	-150.000	0.000	65.000	127.7693	15814.1	206	127.4432	-
11011	-260.000	0.000	0.000	-150.000	0.000	67.000	128.7983	16698.1	218	128.4703	-
11012	-260.000	0.000	0.000	-150.000	0.000	69.000	129.8499	18081.6	236	129.5191	-

Cable no.	Coordinates at deck level			Coordinates at pylon head			L_i	F_{Di}	nos. of 150 mm2	L_{ui}	F_1
	X	Y	Z	X	Y	Z					
	[m]	[m]	[m]	[m]	[m]	[m]	[m]	[kN]	strands	[m]	[kN]
12001	-138.000	0.000	0.000	-150.000	0.000	40.000	41.7612	7510.6	98	41.6548	2286.3
12002	-126.000	0.000	0.000	-150.000	0.000	43.500	49.6815	8226.3	107	49.5545	2466.1
12003	-114.000	0.000	0.000	-150.000	0.000	47.000	59.2030	9066.7	118	59.0518	2688.0
12004	-102.000	0.000	0.000	-150.000	0.000	50.000	69.3109	9984.7	130	69.1339	2926.9
12005	-90.000	0.000	0.000	-150.000	0.000	53.000	80.0562	10865.2	142	79.8526	3159.8
12006	-78.000	0.000	0.000	-150.000	0.000	56.000	91.2140	11764.6	153	90.9808	3379.4
12007	-66.000	0.000	0.000	-150.000	0.000	58.500	102.3633	12492.3	163	102.1025	3601.6
12008	-54.000	0.000	0.000	-150.000	0.000	61.000	113.7409	13618.1	178	113.4516	3810.1
12009	-42.000	0.000	0.000	-150.000	0.000	63.000	125.0320	14095.4	184	124.7135	4025.7
12010	-30.000	0.000	0.000	-150.000	0.000	65.000	136.4734	15216.5	198	136.1247	4229.8
12011	-18.000	0.000	0.000	-150.000	0.000	67.000	148.0304	15880.4	207	147.6528	4422.6
12012	-6.000	0.000	0.000	-150.000	0.000	69.000	159.6778	16667.6	217	159.2700	4604.7

Table D.1: Stay cables geometry, desired cable forces for the completed bridge at time infinity F_{Di}, and first stage installation forces F_1

Note:

L_{ui} in table D.1 is calculated in the same way as that of table C.2 in Appendix C.

Each of the back stays nos. 11010 to 11014 is installed to the unstressed length L_{ui} in one stage.

Upon the installation of all stay cables to the unstressed lengths L_{ui} and the subsequent re-stressing/de-stressing of the stay cable forces to the desired forces F_{Di}, the bending moment distribution and the vertical deflection of the deck elements under dead load for the completed bridge, will be as that shown in figs. D.5 and D.6. As explained in Section 4-3-4, the deck elements are to be pre-cambered to achieve the desired geometry. The pre-camber profile is the mirror line of the deflection line shown in fig. D.6. It is also to be noted that the final vertical deflection of the deck elements in this example is small when compared with the corresponding vertical deflection in the example shown in Appendix C. This is attributed to the different value of the ratio between the moment of inertia of the first part of the composite section I_s to the moment of inertia of the total composite section I_{comp} (refer to Section 4-3-3). The ratios I_s / I_{comp} in the examples of appendices C and D are equal to 23% and 69% respectively. Further the vertical shift of the eccentricity "e" between the center of gravity of the first part of the composite section and the center of gravity of the total composite section, are equal to 993mm in Appendix C and 458mm in Appendix D. It is also to be noted that the time dependent effect (type II) has been ignored in both of the examples in appendices C and D. This effect may be dealt with in the same way as explained in Appendix B.

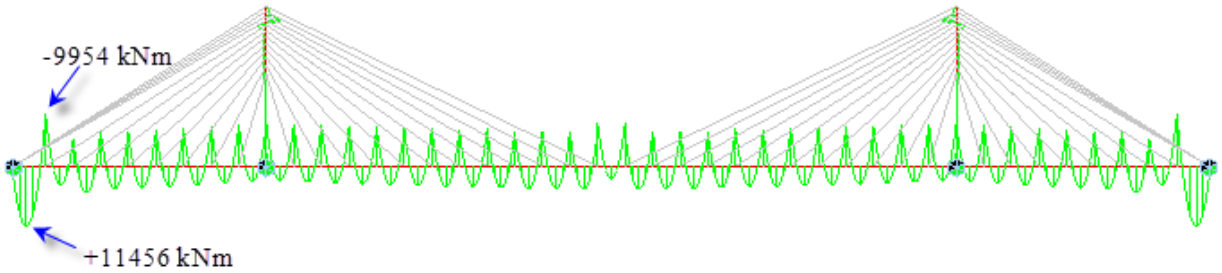

fig. D.5 Bending moment distribution for the completed bridge at time infinity under dead load and the stay cable forces F_{Di}

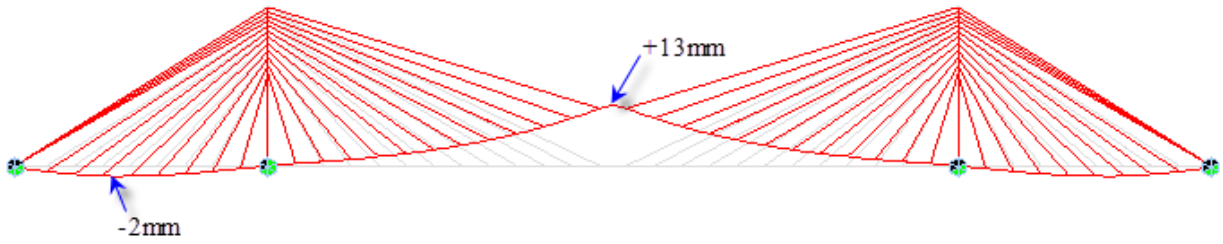

fig. D.6: Vertical deflection of the deck elements for the completed bridge at time infinity under dead load and the sta cable forces F_{Di}, as calculated by the computer model.

APPENDIX E

Stay cable forces under dead load for extradosed bridges

(refer to Chapter 6)

Software used: [SOFISTK 2012] & [Midas 2011]

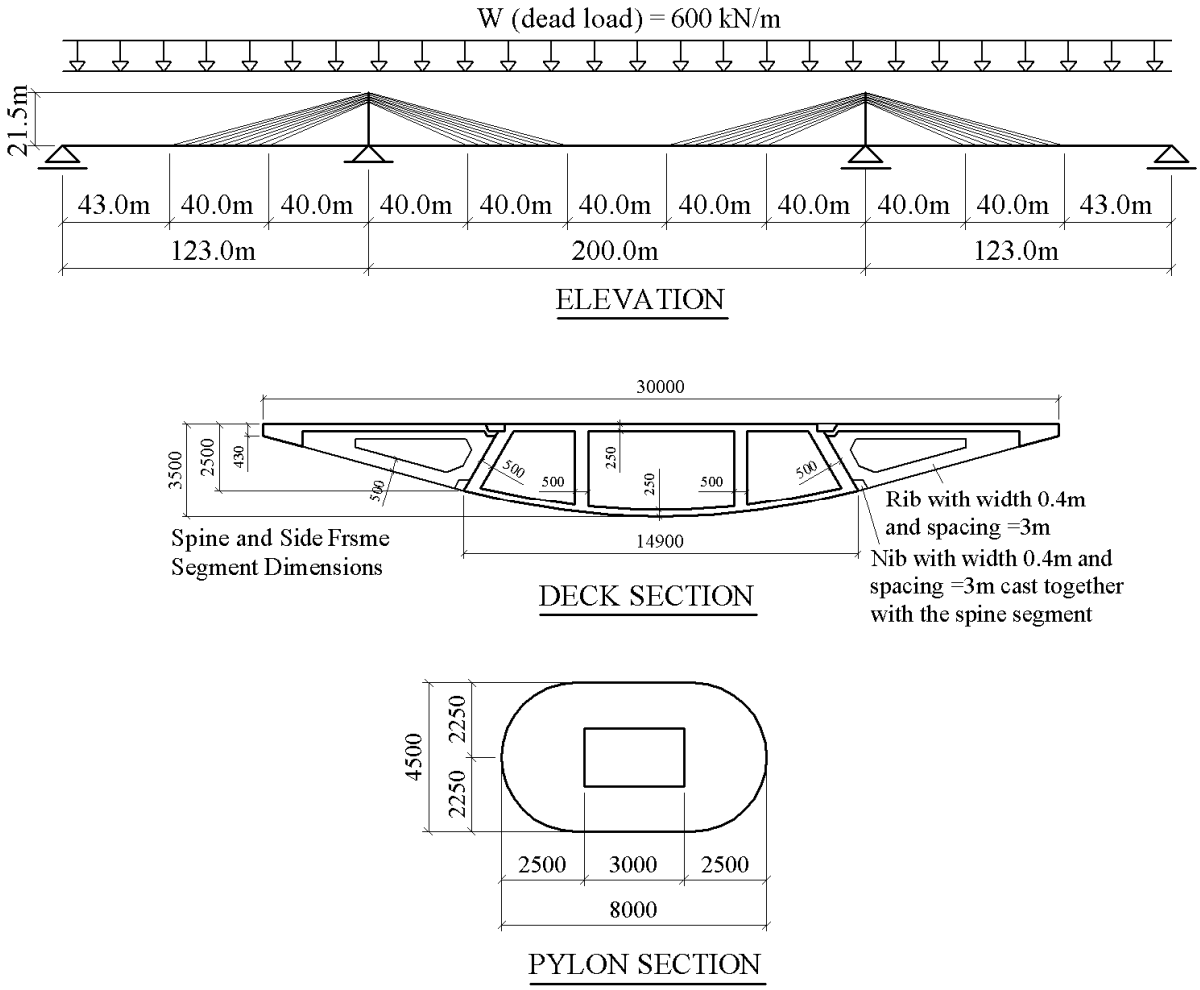

fig. E.1: Geometrical data for the extradosed bridge

Note:

The properties of the deck and pylon cross sections are the same as that shown in figs. D.3 and D.4 in Appendix D.

Material:

Elastic modulus of concrete = 35000 MPa

Loads

Weight of the spine segment (central part of the composite section) = 305 kN/m

Weight of the side frame segments = 190 kN/m

Weight of wearing course, barriers, utilities, ..etc. = 105 kN/m

W (dead load) = 305 + 190 + 105 = 600 kN/m

Cable no.	Coordinates at deck level			Coordinates at pylon head			Cable length	F_{Di}	nos. of 150 mm2 strands
	X [m]	Y [m]	Z [m]	X [m]	Y [m]	Z [m]	[m]	[kN]	
11001	-40.000	0.000	0.000	0.000	0.000	16.000	43.081	13642.4	130
11002	-45.000	0.000	0.000	0.000	0.000	16.500	47.930	14717.8	141
11003	-50.000	0.000	0.000	0.000	0.000	17.000	52.811	15739.7	151
11004	-55.000	0.000	0.000	0.000	0.000	17.500	57.717	16710.4	160
11005	-60.000	0.000	0.000	0.000	0.000	18.000	62.642	17632.5	169
11006	-65.000	0.000	0.000	0.000	0.000	18.500	67.581	18508.8	177
11007	-70.000	0.000	0.000	0.000	0.000	19.000	72.533	19342.1	185
11008	-75.000	0.000	0.000	0.000	0.000	19.500	77.494	20135.1	193
11009	-80.000	0.000	0.000	0.000	0.000	20.000	82.462	20890.4	200

Cable no.	Coordinates at deck level			Coordinates at pylon head			Cable length	F_{Di}	nos. of 150 mm2 strands
	X [m]	Y [m]	Z [m]	X [m]	Y [m]	Z [m]	[m]	[kN]	
12001	40.000	0.000	0.000	0.000	0.000	16.000	43.081	13642.4	130
12002	45.000	0.000	0.000	0.000	0.000	16.500	47.930	14717.8	141
12003	50.000	0.000	0.000	0.000	0.000	17.000	52.811	15739.7	151
12004	55.000	0.000	0.000	0.000	0.000	17.500	57.717	16710.4	160
12005	60.000	0.000	0.000	0.000	0.000	18.000	62.642	17632.5	169
12006	65.000	0.000	0.000	0.000	0.000	18.500	67.581	18508.8	177
12007	70.000	0.000	0.000	0.000	0.000	19.000	72.533	19342.1	185
12008	75.000	0.000	0.000	0.000	0.000	19.500	77.494	20135.1	193
12009	80.000	0.000	0.000	0.000	0.000	20.000	82.462	20890.4	200

Table E.1: Stay cables geometry, desired cable forces under dead load
(the stay cables may be arranged in pair as shown in fig. 1.3)

Note:

The desired stay cable forces under dead load F_{Di} are calculated based on the assumption that the equivalent uniform vertical load of the stay cable forces W_C is equal to 1.9 W (refer to Chapter 6 and fig. 6.3). Accordingly, the sum of the vertical components of each 9-stay cables acting on 40m of the deck length = 1.9 x 600kN/m x 40m = 45600 kN. The vertical component of each stay cable = 45600 / 9 = 5067kN and the desired stay cable force for cable no. 11005 (for example) F_{D5} = 5067 x (62.642m / 18.0m) = 17633kN.

The cross sectional area of each stay cable (nos. of 150mm^2 strands) is defined in the computer model based on the assumption that the stay cable forces due to live loads are equal to 10% of the stay cable forces due to dead loads. It is also assumed that the capacity of each strand under the service load (dead + live load) = 115 kN.

Figs. E.2 and E.3 show the bending moment distribution and the stay cable forces due to the dead load W (= 600 kN/m) before re-stressing the stay cables. By re-stressing the stay cables by the forces ΔF_i in accordance with equation 6.29 (in Chapter 6), the bending moment distribution

shown in fig. E.2 will be changed to the bending moment distribution shown in fig. E.4. Further, the stay cable forces F_i shown in fig. E.3 will be changed to the desired stay cable forces F_{Di} shown in table E.1 or in fig. E.5.

As explained in Chapter 6, the bending moment distribution shown in fig. E.4 can be further reduced or eliminated by selecting concordant prestressing tendon forces/ profile affine with the bending moment distribution of fig. E.4. The bending moment distribution resulting from the concordant prestressing forces alone, is shown in fig. E.6, noting that the prestressing force F_p is equal to 200000 kN.

The final desired stay cable forces shown in table E.1 should however be kept unchanged. The stay cable forces resulting from the tendon forces (shown in fig. E.7) may be added to the forces shown in fig. E.3 and equation 6.33 (in Chapter 6) can be used to determine the related required re-stressing forces ΔF_i of the individual stay cables to achieve the desired stay cable forces in table E.1 upon the application of the selected concordant prestressing forces. Accordingly, the final bending moment distribution due to dead load, stay cable forces F_{Di} and the concordant prestressing forces will be as that shown in fig. E.8. The final bending moment is not exactly equal to zero because the prestressing profile is defined in the computer model as a polygonal line and not exactly affine with the bending moment shown in fig. E.4.

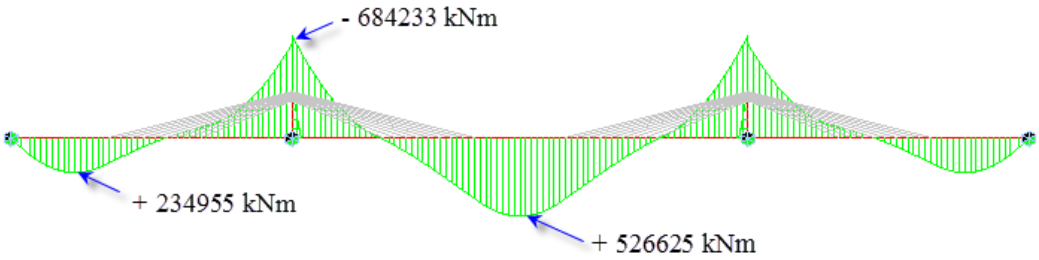

fig. E.2: Bending moment distribution due to the dead load W = 600 kN/m before shortening/re-stressing the stay cables

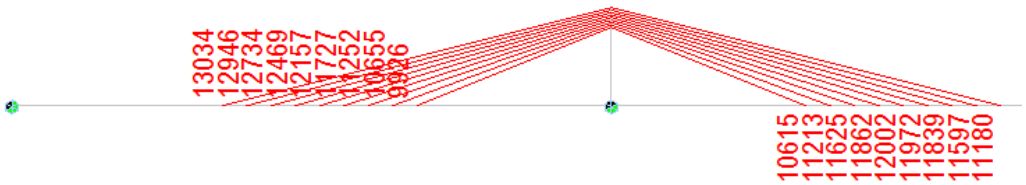

fig. E.3: Stay cable forces F_i in kN due to the dead load W = 600 kN/m before shortening/re-stressing the stay cables

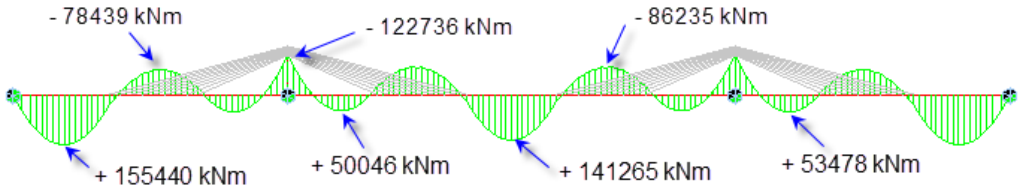

fig. E.4: Bending moment distribution due to the dead load W = 600 kN/m after shortening the stay cables (this diagram is used for the definition of the concordant prestressing cable profile)

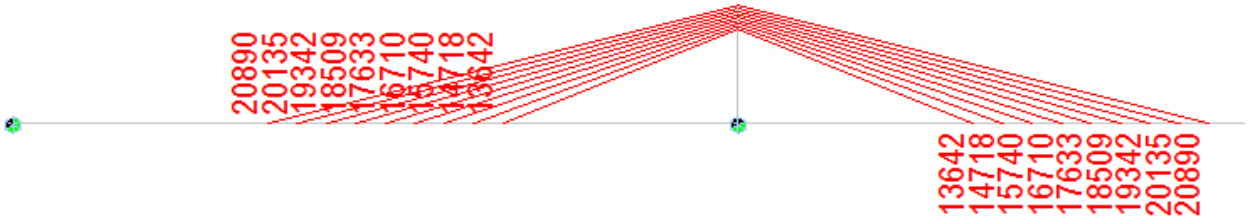

fig. E.5: Desired Stay cable forces F_{Di} in kN

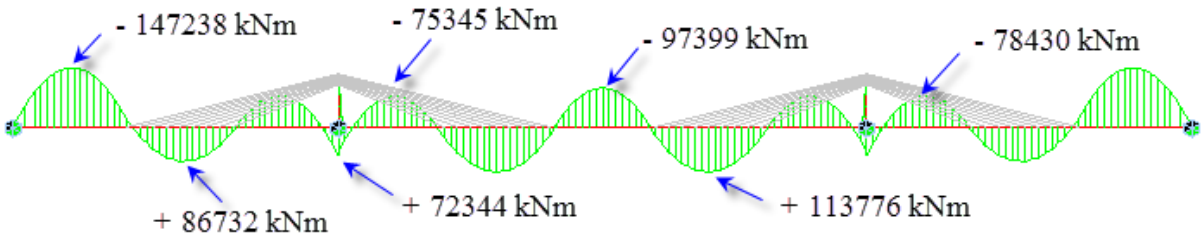

fig. E.6: Bending moment distribution due to the "concordant" prestressing forces alone (F_P = 200000 kN)

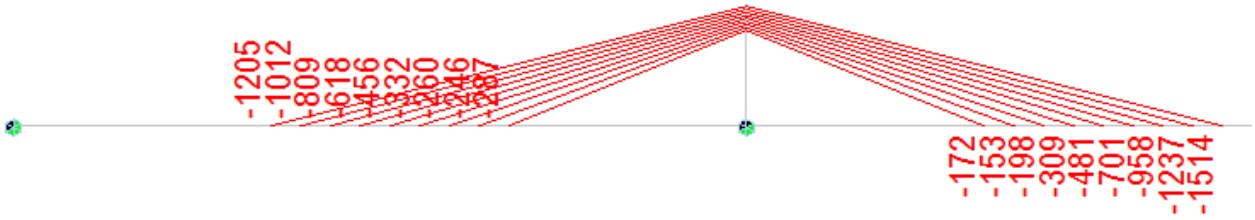

fig. E.7: Stay cable forces due F_{PTi} due to the prestressing forces alone

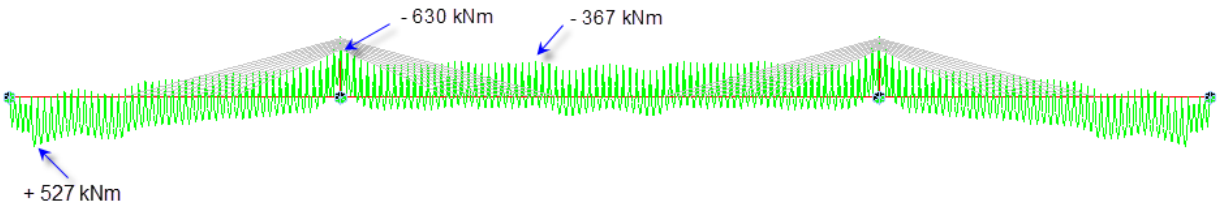

fig. E.8: Bending moment distribution due to the dead load W, the desired stay cable forces F_{Di} and the concordant prestressing forces

Note:

The next tables include the influence matrix for stay cable forces and the data used for solving the equations (6.29) and (6.33) for the determination of the re-stressing forces ΔF_i as described in Chapter 6.

Influence Matrix for stay cable forces

	C1	C2	C3	C4	C5	C6	C7	C8	C9
R1	0.9240266	-0.0759373	-0.0741972	-0.0715029	-0.0683329	-0.0649904	-0.0616623	-0.0584558	-0.0554225
R2	-0.0740304	0.9229140	-0.0772942	-0.0760894	-0.0740799	-0.0716620	-0.0690891	-0.0665163	-0.0640285
R3	-0.0703044	-0.0751255	0.9216610	-0.0790750	-0.0786180	-0.0774678	-0.0759531	-0.0742838	-0.0725842
R4	-0.0656893	-0.0717034	-0.0766681	0.9196678	-0.0818076	-0.0822591	-0.0820987	-0.0815975	-0.0809246
R5	-0.0610956	-0.0679400	-0.0741835	-0.0796165	0.9160249	-0.0863642	-0.0878534	-0.0887827	-0.0893722
R6	-0.0564077	-0.0638003	-0.0709602	-0.0777145	-0.0838383	0.9109365	-0.0924958	-0.0951196	-0.0972104
R7	-0.0521200	-0.0599017	-0.0677540	-0.0755354	-0.0830545	-0.0900778	0.9036669	-0.1009260	-0.1047658
R8	-0.0482460	-0.0563127	-0.0647042	-0.0733060	-0.0819562	-0.0904513	-0.0985489	0.8940293	-0.1118184
R9	-0.0445452	-0.0527877	-0.0615689	-0.0707985	-0.0803409	-0.0900198	-0.0996206	-0.1088915	0.8824549
R10	0.0043478	0.0045792	0.0049344	0.0054207	0.0060399	0.0067896	0.0076641	0.0086545	0.0097489
R11	0.0045067	0.0050987	0.0057239	0.0065160	0.0074768	0.0086036	0.0098893	0.0113228	0.0128890
R12	0.0047712	0.0056192	0.0066709	0.0078045	0.0091475	0.0106968	0.0124436	0.0143747	0.0164712
R13	0.0051390	0.0062639	0.0076380	0.0092682	0.0110288	0.0130401	0.0152918	0.0177680	0.0204459
R14	0.0056334	0.0070606	0.0087874	0.0108221	0.0131651	0.0156859	0.0184952	0.0215738	0.0248946
R15	0.0062095	0.0079541	0.0100519	0.0125122	0.0153360	0.0185159	0.0219148	0.0256305	0.0296315
R16	0.0068884	0.0089716	0.0114659	0.0143818	0.0177207	0.0214744	0.0256252	0.0300259	0.0347582
R17	0.0076573	0.0100984	0.0130126	0.0164115	0.0202968	0.0246593	0.0294793	0.0347250	0.0402351
R18	0.0084611	0.0112630	0.0146007	0.0184872	0.0229241	0.0279014	0.0333969	0.0393751	0.0457866
R19	-0.0013489	-0.0018527	-0.0024467	-0.0031327	-0.0039106	-0.0047787	-0.0057327	-0.0067666	-0.0078718
R20	-0.0015257	-0.0020997	-0.0027761	-0.0035571	-0.0044427	-0.0054306	-0.0065163	-0.0076927	-0.0089503
R21	-0.0016932	-0.0023347	-0.0030906	-0.0039630	-0.0049520	-0.0060552	-0.0072674	-0.0085810	-0.0099850
R22	-0.0018477	-0.0025528	-0.0033833	-0.0043417	-0.0054279	-0.0066393	-0.0079703	-0.0094124	-0.0109539
R23	-0.0019965	-0.0027640	-0.0036677	-0.0047103	-0.0058917	-0.0072090	-0.0086564	-0.0102244	-0.0119003
R24	-0.0021232	-0.0029457	-0.0039139	-0.0050305	-0.0062954	-0.0077058	-0.0092551	-0.0109335	-0.0127273
R25	-0.0022348	-0.0031077	-0.0041347	-0.0053188	-0.0066599	-0.0081549	-0.0097971	-0.0115760	-0.0134771
R26	-0.0023261	-0.0032426	-0.0043205	-0.0055628	-0.0069696	-0.0085375	-0.0102595	-0.0121247	-0.0141181
R27	-0.0023794	-0.0033259	-0.0044386	-0.0057206	-0.0071719	-0.0087892	-0.0105652	-0.0124888	-0.0145444
R28	-0.0008040	-0.0011125	-0.0014757	-0.0018947	-0.0023696	-0.0028991	-0.0034809	-0.0041112	-0.0047849
R29	-0.0010846	-0.0015003	-0.0019898	-0.0025547	-0.0031948	-0.0039086	-0.0046928	-0.0055425	-0.0064507
R30	-0.0013983	-0.0019340	-0.0025649	-0.0032928	-0.0041177	-0.0050376	-0.0060483	-0.0071434	-0.0083138
R31	-0.0017407	-0.0024074	-0.0031926	-0.0040985	-0.0051252	-0.0062700	-0.0075279	-0.0088908	-0.0103475
R32	-0.0021186	-0.0029300	-0.0038855	-0.0049879	-0.0062372	-0.0076305	-0.0091613	-0.0108198	-0.0125924
R33	-0.0025163	-0.0034798	-0.0046144	-0.0059236	-0.0074073	-0.0090618	-0.0108797	-0.0128493	-0.0149545
R34	-0.0029422	-0.0040688	-0.0053954	-0.0069261	-0.0086608	-0.0105953	-0.0127208	-0.0150237	-0.0174850
R35	-0.0033932	-0.0046923	-0.0062222	-0.0079874	-0.0099878	-0.0122187	-0.0146698	-0.0173255	-0.0201639
R36	-0.0038458	-0.0053182	-0.0070521	-0.0090527	-0.0113199	-0.0138483	-0.0166263	-0.0196361	-0.0228530

Influence Matrix for stay cable forces (continuation)

	C10	C11	C12	C13	C14	C15	C16	C17	C18
R1	0.0043478	0.0046228	0.0050354	0.0055938	0.0063007	0.0071543	0.0081496	0.0092777	0.0105271
R2	0.0044642	0.0050987	0.0057814	0.0066471	0.0076987	0.0089343	0.0103476	0.0119282	0.0136614
R3	0.0046755	0.0055633	0.0066709	0.0078778	0.0093127	0.0109738	0.0128534	0.0149391	0.0172129
R4	0.0049800	0.0061404	0.0075669	0.0092682	0.0111199	0.0132439	0.0156315	0.0182678	0.0211313
R5	0.0054002	0.0068571	0.0086316	0.0107334	0.0131651	0.0157980	0.0187446	0.0219874	0.0255010
R6	0.0058930	0.0076598	0.0097982	0.0123196	0.0152272	0.0185159	0.0220508	0.0259321	0.0301301
R7	0.0064781	0.0085742	0.0111004	0.0140693	0.0174849	0.0213419	0.0256252	0.0301903	0.0351218
R8	0.0071430	0.0095859	0.0125209	0.0159625	0.0199150	0.0243726	0.0293187	0.0347250	0.0404335
R9	0.0078356	0.0106262	0.0139715	0.0178875	0.0223790	0.0274397	0.0330511	0.0391819	0.0457866
R10	0.9241237	-0.0759002	-0.0742427	-0.0716553	-0.0686180	-0.0654359	-0.0622969	-0.0593095	-0.0565260
R11	-0.0739942	0.9229088	-0.0773553	-0.0762218	-0.0743001	-0.0719874	-0.0695377	-0.0671068	-0.0647797
R12	-0.0703475	-0.0751848	0.9215817	-0.0791779	-0.0787484	-0.0776294	-0.0761497	-0.0745189	-0.0728612
R13	-0.0658293	-0.0718283	-0.0767679	0.9196038	-0.0818237	-0.0822144	-0.0819791	-0.0813878	-0.0806087
R14	-0.0613505	-0.0681420	-0.0743065	-0.0796322	0.9161473	-0.0860705	-0.0873529	-0.0880380	-0.0883439
R15	-0.0567943	-0.0640900	-0.0711083	-0.0776723	-0.0835532	0.9115210	-0.0915517	-0.0937525	-0.0953542
R16	-0.0526564	-0.0602907	-0.0679294	-0.0754253	-0.0825814	-0.0891584	0.9051211	-0.0988439	-0.1019591
R17	-0.0489506	-0.0568126	-0.0649090	-0.0731176	-0.0812687	-0.0891512	-0.0965159	0.8969219	-0.1079347
R18	-0.0454321	-0.0534071	-0.0618038	-0.0705222	-0.0794165	-0.0883009	-0.0969517	-0.1051095	0.8875196
R19	-0.0016919	-0.0021376	-0.0026427	-0.0032060	-0.0038246	-0.0044935	-0.0052057	-0.0059525	-0.0067229
R20	-0.0020839	-0.0025633	-0.0030950	-0.0036765	-0.0043027	-0.0049666	-0.0056588	-0.0063681	-0.0070809
R21	-0.0025040	-0.0030082	-0.0035538	-0.0041364	-0.0047487	-0.0053812	-0.0060220	-0.0066569	-0.0072697
R22	-0.0029454	-0.0034646	-0.0040105	-0.0045764	-0.0051526	-0.0057268	-0.0062842	-0.0068077	-0.0072779
R23	-0.0034195	-0.0039461	-0.0044808	-0.0050146	-0.0055348	-0.0060261	-0.0064704	-0.0068474	-0.0071345
R24	-0.0039001	-0.0044217	-0.0049292	-0.0054104	-0.0058498	-0.0062286	-0.0065255	-0.0067168	-0.0067766
R25	-0.0044001	-0.0049063	-0.0053719	-0.0057818	-0.0061169	-0.0063550	-0.0064709	-0.0064376	-0.0062256
R26	-0.0049128	-0.0053913	-0.0057985	-0.0061159	-0.0063209	-0.0063871	-0.0062860	-0.0059863	-0.0054553
R27	-0.0054034	-0.0058378	-0.0061665	-0.0063672	-0.0064136	-0.0062753	-0.0059199	-0.0053125	-0.0044170
R28	-0.0013489	-0.0015650	-0.0017870	-0.0020112	-0.0022330	-0.0024462	-0.0026440	-0.0028183	-0.0029604
R29	-0.0018061	-0.0020997	-0.0024021	-0.0027090	-0.0030138	-0.0033087	-0.0035844	-0.0038302	-0.0040342
R30	-0.0023183	-0.0026982	-0.0030906	-0.0034895	-0.0038870	-0.0042728	-0.0046351	-0.0049601	-0.0052327
R31	-0.0028780	-0.0033521	-0.0038424	-0.0043417	-0.0048399	-0.0053246	-0.0057809	-0.0061920	-0.0065388
R32	-0.0034965	-0.0040745	-0.0046727	-0.0052825	-0.0058917	-0.0064851	-0.0070447	-0.0075501	-0.0079781
R33	-0.0041476	-0.0048348	-0.0055465	-0.0062725	-0.0069982	-0.0077058	-0.0083738	-0.0089781	-0.0094913
R34	-0.0048456	-0.0056497	-0.0064829	-0.0073331	-0.0081835	-0.0090131	-0.0097971	-0.0105070	-0.0111109
R35	-0.0055848	-0.0065127	-0.0074744	-0.0084560	-0.0094382	-0.0103969	-0.0113033	-0.0121247	-0.0128245
R36	-0.0063268	-0.0073790	-0.0084696	-0.0095832	-0.0106977	-0.0117859	-0.0128152	-0.0137486	-0.0145444

Influence Matrix for stay cable forces (continuation)

	C19	C20	C21	C22	C23	C24	C25	C26	C27
R1	-0.0013489	-0.0015650	-0.0017870	-0.0020112	-0.0022330	-0.0024462	-0.0026440	-0.0028183	-0.0029604
R2	-0.0018061	-0.0020997	-0.0024021	-0.0027090	-0.0030138	-0.0033087	-0.0035844	-0.0038302	-0.0040342
R3	-0.0023183	-0.0026982	-0.0030906	-0.0034895	-0.0038870	-0.0042728	-0.0046351	-0.0049601	-0.0052327
R4	-0.0028780	-0.0033521	-0.0038424	-0.0043417	-0.0048399	-0.0053246	-0.0057809	-0.0061920	-0.0065388
R5	-0.0034965	-0.0040745	-0.0046727	-0.0052825	-0.0058917	-0.0064851	-0.0070447	-0.0075501	-0.0079781
R6	-0.0041476	-0.0048348	-0.0055465	-0.0062725	-0.0069982	-0.0077058	-0.0083738	-0.0089781	-0.0094913
R7	-0.0048456	-0.0056497	-0.0064829	-0.0073331	-0.0081835	-0.0090131	-0.0097971	-0.0105070	-0.0111109
R8	-0.0055848	-0.0065127	-0.0074744	-0.0084560	-0.0094382	-0.0103969	-0.0113033	-0.0121247	-0.0128245
R9	-0.0063268	-0.0073790	-0.0084696	-0.0095832	-0.0106977	-0.0117859	-0.0128152	-0.0137486	-0.0145444
R10	-0.0016919	-0.0021376	-0.0026427	-0.0032060	-0.0038246	-0.0044935	-0.0052057	-0.0059525	-0.0067229
R11	-0.0020839	-0.0025633	-0.0030950	-0.0036765	-0.0043027	-0.0049666	-0.0056588	-0.0063681	-0.0070809
R12	-0.0025040	-0.0030082	-0.0035538	-0.0041364	-0.0047487	-0.0053812	-0.0060220	-0.0066569	-0.0072697
R13	-0.0029454	-0.0034646	-0.0040105	-0.0045764	-0.0051526	-0.0057268	-0.0062842	-0.0068077	-0.0072779
R14	-0.0034195	-0.0039461	-0.0044808	-0.0050146	-0.0055348	-0.0060261	-0.0064704	-0.0068474	-0.0071345
R15	-0.0039001	-0.0044217	-0.0049292	-0.0054104	-0.0058498	-0.0062286	-0.0065255	-0.0067168	-0.0067766
R16	-0.0044001	-0.0049063	-0.0053719	-0.0057818	-0.0061169	-0.0063550	-0.0064709	-0.0064376	-0.0062256
R17	-0.0049128	-0.0053913	-0.0057985	-0.0061159	-0.0063209	-0.0063871	-0.0062860	-0.0059863	-0.0054553
R18	-0.0054034	-0.0058378	-0.0061665	-0.0063672	-0.0064136	-0.0062753	-0.0059199	-0.0053125	-0.0044170
R19	0.9241237	-0.0759002	-0.0742427	-0.0716553	-0.0686180	-0.0654359	-0.0622969	-0.0593095	-0.0565260
R20	-0.0739942	0.9229088	-0.0773553	-0.0762218	-0.0743001	-0.0719874	-0.0695377	-0.0671068	-0.0647797
R21	-0.0703475	-0.0751848	0.9215817	-0.0791779	-0.0787484	-0.0776294	-0.0761497	-0.0745189	-0.0728612
R22	-0.0658293	-0.0718283	-0.0767679	0.9196038	-0.0818237	-0.0822144	-0.0819791	-0.0813878	-0.0806087
R23	-0.0613505	-0.0681420	-0.0743065	-0.0796322	0.9161473	-0.0860705	-0.0873529	-0.0880380	-0.0883439
R24	-0.0567943	-0.0640900	-0.0711083	-0.0776723	-0.0835532	0.9115210	-0.0915517	-0.0937525	-0.0953542
R25	-0.0526564	-0.0602907	-0.0679294	-0.0754253	-0.0825814	-0.0891584	0.9051211	-0.0988439	-0.1019591
R26	-0.0489506	-0.0568126	-0.0649090	-0.0731176	-0.0812687	-0.0891512	-0.0965159	0.8969219	-0.1079347
R27	-0.0454321	-0.0534071	-0.0618038	-0.0705222	-0.0794165	-0.0883009	-0.0969517	-0.1051095	0.8875196
R28	0.0043478	0.0046228	0.0050354	0.0055938	0.0063007	0.0071543	0.0081496	0.0092777	0.0105271
R29	0.0044642	0.0050987	0.0057814	0.0066471	0.0076987	0.0089343	0.0103476	0.0119282	0.0136614
R30	0.0046755	0.0055633	0.0066709	0.0078778	0.0093127	0.0109738	0.0128534	0.0149391	0.0172129
R31	0.0049800	0.0061404	0.0075669	0.0092682	0.0111199	0.0132439	0.0156315	0.0182678	0.0211313
R32	0.0054002	0.0068571	0.0086316	0.0107334	0.0131651	0.0157980	0.0187446	0.0219874	0.0255010
R33	0.0058930	0.0076598	0.0097982	0.0123196	0.0152272	0.0185159	0.0220508	0.0259321	0.0301301
R34	0.0064781	0.0085742	0.0111004	0.0140693	0.0174849	0.0213419	0.0256252	0.0301903	0.0351218
R35	0.0071430	0.0095859	0.0125209	0.0159625	0.0199150	0.0243726	0.0293187	0.0347250	0.0404335
R36	0.0078356	0.0106262	0.0139715	0.0178875	0.0223790	0.0274397	0.0330511	0.0391819	0.0457866

Influence Matrix for stay cable forces (continuation)

	C28	C29	C30	C31	C32	C33	C34	C35	C36
R1	-0.0008040	-0.0011125	-0.0014757	-0.0018947	-0.0023696	-0.0028991	-0.0034809	-0.0041112	-0.0047849
R2	-0.0010846	-0.0015003	-0.0019898	-0.0025547	-0.0031948	-0.0039086	-0.0046928	-0.0055425	-0.0064507
R3	-0.0013983	-0.0019340	-0.0025649	-0.0032928	-0.0041177	-0.0050376	-0.0060483	-0.0071434	-0.0083138
R4	-0.0017407	-0.0024074	-0.0031926	-0.0040985	-0.0051252	-0.0062700	-0.0075279	-0.0088908	-0.0103475
R5	-0.0021186	-0.0029300	-0.0038855	-0.0049879	-0.0062372	-0.0076305	-0.0091613	-0.0108198	-0.0125924
R6	-0.0025163	-0.0034798	-0.0046144	-0.0059236	-0.0074073	-0.0090618	-0.0108797	-0.0128493	-0.0149545
R7	-0.0029422	-0.0040688	-0.0053954	-0.0069261	-0.0086608	-0.0105953	-0.0127208	-0.0150237	-0.0174850
R8	-0.0033932	-0.0046923	-0.0062222	-0.0079874	-0.0099878	-0.0122187	-0.0146698	-0.0173255	-0.0201639
R9	-0.0038458	-0.0053182	-0.0070521	-0.0090527	-0.0113199	-0.0138483	-0.0166263	-0.0196361	-0.0228530
R10	-0.0013489	-0.0018527	-0.0024467	-0.0031327	-0.0039106	-0.0047787	-0.0057327	-0.0067666	-0.0078718
R11	-0.0015257	-0.0020997	-0.0027761	-0.0035571	-0.0044427	-0.0054306	-0.0065163	-0.0076927	-0.0089503
R12	-0.0016932	-0.0023347	-0.0030906	-0.0039630	-0.0049520	-0.0060552	-0.0072674	-0.0085810	-0.0099850
R13	-0.0018477	-0.0025528	-0.0033833	-0.0043417	-0.0054279	-0.0066393	-0.0079703	-0.0094124	-0.0109539
R14	-0.0019965	-0.0027640	-0.0036677	-0.0047103	-0.0058917	-0.0072090	-0.0086564	-0.0102244	-0.0119003
R15	-0.0021232	-0.0029457	-0.0039139	-0.0050305	-0.0062954	-0.0077058	-0.0092551	-0.0109335	-0.0127273
R16	-0.0022348	-0.0031077	-0.0041347	-0.0053188	-0.0066599	-0.0081549	-0.0097971	-0.0115760	-0.0134771
R17	-0.0023261	-0.0032426	-0.0043205	-0.0055628	-0.0069696	-0.0085375	-0.0102595	-0.0121247	-0.0141181
R18	-0.0023794	-0.0033259	-0.0044386	-0.0057206	-0.0071719	-0.0087892	-0.0105652	-0.0124888	-0.0145444
R19	0.0043478	0.0045792	0.0049344	0.0054207	0.0060399	0.0067896	0.0076641	0.0086545	0.0097489
R20	0.0045067	0.0050987	0.0057239	0.0065160	0.0074768	0.0086036	0.0098893	0.0113228	0.0128890
R21	0.0047712	0.0056192	0.0066709	0.0078045	0.0091475	0.0106968	0.0124436	0.0143747	0.0164712
R22	0.0051390	0.0062639	0.0076380	0.0092682	0.0110288	0.0130401	0.0152918	0.0177680	0.0204459
R23	0.0056334	0.0070606	0.0087874	0.0108221	0.0131651	0.0156859	0.0184952	0.0215738	0.0248946
R24	0.0062095	0.0079541	0.0100519	0.0125122	0.0153360	0.0185159	0.0219148	0.0256305	0.0296315
R25	0.0068884	0.0089716	0.0114659	0.0143818	0.0177207	0.0214744	0.0256252	0.0300259	0.0347582
R26	0.0076573	0.0100984	0.0130126	0.0164115	0.0202968	0.0246593	0.0294793	0.0347250	0.0402351
R27	0.0084611	0.0112630	0.0146007	0.0184872	0.0229241	0.0279014	0.0333969	0.0393751	0.0457866
R28	0.9240266	-0.0759373	-0.0741972	-0.0715029	-0.0683329	-0.0649904	-0.0616623	-0.0584558	-0.0554225
R29	-0.0740304	0.9229140	-0.0772942	-0.0760894	-0.0740799	-0.0716620	-0.0690891	-0.0665163	-0.0640285
R30	-0.0703044	-0.0751255	0.9216610	-0.0790750	-0.0786180	-0.0774678	-0.0759531	-0.0742838	-0.0725842
R31	-0.0656893	-0.0717034	-0.0766681	0.9196678	-0.0818076	-0.0822591	-0.0820987	-0.0815975	-0.0809246
R32	-0.0610956	-0.0679400	-0.0741835	-0.0796165	0.9160249	-0.0863642	-0.0878534	-0.0887827	-0.0893722
R33	-0.0564077	-0.0638003	-0.0709602	-0.0777145	-0.0838383	0.9109365	-0.0924958	-0.0951196	-0.0972104
R34	-0.0521200	-0.0599017	-0.0677540	-0.0755354	-0.0830545	-0.0900778	0.9036669	-0.1009260	-0.1047658
R35	-0.0482460	-0.0563127	-0.0647042	-0.0733060	-0.0819562	-0.0904513	-0.0985489	0.8940293	-0.1118184
R36	-0.0445452	-0.0527877	-0.0615689	-0.0707985	-0.0803409	-0.0900198	-0.0996206	-0.1088915	0.8824549

Data related to the use of equations (6.29) and (6.33)

Cable no.	F_i	F_{Di}	F_{PTi}	ΔF_i in equation (6.29)	ΔF_i in equation (6.33)
	[kN]	[kN]	[kN]	[kN]	[kN]
11001	9926	13642	-287	14251	15600
11002	10655	14718	-246	15471	16871
11003	11252	15740	-260	16573	18061
11004	11727	16710	-332	17557	19172
11005	12157	17633	-456	18439	20223
11006	12469	18509	-618	19227	21201
11007	12734	19342	-809	19943	22127
11008	12946	20135	-1012	20602	23001
11009	13034	20890	-1205	21224	23813
12001	10615	13642	-172	14195	15599
12002	11213	14718	-153	15399	16870
12003	11625	15740	-198	16483	18059
12004	11862	16710	-309	17448	19170
12005	12002	17633	-481	18308	20221
12006	11972	18509	-701	19073	21199
12007	11839	19342	-958	19763	22123
12008	11597	20135	-1237	20395	22998
12009	11180	20890	-1514	20988	23809

Note: The forces for stay cables nos. 14001 to 14009 are equal to that of 11001 to 11009

The forces for stay cables nos. 13001 to 13009 are equal to that of 12001 to 12009